University of Nottingham
UK | CHINA | MALAYSIA

Molecular and in-silico approaches to understanding intracellular allosteric modulation at the CXC chemokine receptor 2

Bianca Maria Casella, MSc

Thesis submitted to the University of Nottingham for the degree of Doctor of Philosophy

July 2023

Declaration of own work

This thesis is entirely the candidate's own work. The experiments described in this thesis were performed by the author between February 2019 and February 2023 at the University of Nottingham at the Division of Biomolecular Sciences and Medicinal Chemistry in Nottingham, UK. No part of the material has been submitted previously for a degree or any other qualification at any university.

Publication arising from this Thesis:

Casella, B.M.; Farmer, J.P.; Nesheva, D.N.; Williams, H.E.L.; Charlton, S.J.; Holliday, N.D.; Laughton, C.A. and Mistry, S.N. Design, Synthesis, and Application of Fluorescent Ligands Targeting the Intracellular Allosteric Binding Site of the CXC Chemokine Receptor 2. *J. Med. Chem.* **2023**, 66, 12911-12930.

i.Abstract

The CXC chemokine receptor 2 (CXCR2) is a key mediator of the inflammation response, for example it regulates neutrophil migration and activation in a number of inflammatory-based disorders. CXCR2 inhibition is a potential strategy for the treatment of several pulmonary diseases, such as chronic obstructive pulmonary disorder (COPD) and asthma, and through its expression on various tumour cell types CXCR2 is also a candidate cancer target. The interaction of large endogenous chemokine peptides (including CXCL8 / interleukin 8 (IL8)) at the orthosteric binding site is a complex, multi-step process which presents significant challenges when designing small molecule competitive orthosteric antagonists. This has led to the development of CXCR2 allosteric modulators targeting an intracellular pocket near the *C*-terminal of the receptor, formed by the transmembrane domains overlapping the G-protein binding site. Navarixin (**2**) is an intracellular negative allosteric modulator (NAM) belonging to the 3,4-diamino-3-cyclobutene-1,2-dione class and it exhibits sub-nanomolar potency and selectivity for CXCR2 over the related CXCR1 subtype. Our understanding of the binding and mode of action of navarixin and other CXCR2 NAMs has been limited by the availability of suitable tracer ligands for competition studies, that allow convenient direct measurements of ligand binding. Here we report the rational design, synthesis and pharmacological evaluation of a series of fluorescent NAMs, based on navarixin (**2**), which are the first examples of ligands able to bind to intracellular binding sites of CXCR1 and CXCR2. These novel fluorescent ligands display high affinity and selectivity for CXCR2 over CXCR1, and, notably, they can be applied in both NanoBRET assay formats in whole cells or membranes and in fluorescence imaging. We also demonstrate that the NanoBRET binding assay using these fluorescence probes is capable of direct measurement of the affinity of unlabelled NAMs acting at the intracellular site, thus providing a platform to screen for alternative chemophores targeting these receptors.

ii. Acknowledgements

"Non temete i momenti difficili. Il meglio viene da lì"
"Don't fear difficult moments. The best comes from them"
(Rita Levi Montalcini)

First, I would like to thank my PhD supervisors Dr Shailesh Mistry, Prof Charles Laughton and Dr Nicholas Holliday. I am extremely grateful to all of you for your guidance, support and help during these years. I have learned so much from you and I have discovered the amazing worlds of medicinal chemistry, computational chemistry and pharmacology through your eyes and expertise, and it has been a truly incredible journey. You have pushed me to become better, you have challenged me every time with precious questions, and you have taught me not to ever settle, because there is always something more to learn, even when the experiments do not go as planned. You have supported me when I was losing confidence in myself, and you have helped me focus on the progress and achievements made rather than on the difficulties and this is an important approach that I am learning to apply to everything in life.
Shailesh, thank you for dealing even with the occasional moments of discouragement during these years. You have patiently taught me to not give up, not to lose hope, to have the courage of making decisions without being scared and you truly have supported me during some very difficult moments.

I would like to thank Dr Huw Williams for all the incredibly precious help provided in solving my "NMR problems". You have guided me through the NMR world which, thanks to you, has become less scary and much much more fascinating.

I would like to thank all the members of the staff in the chemistry labs in BDI and in Cell Signalling research group, all the NMR technicians in the School of Chemistry and all the present and past members of C-floor and Cell

Signalling research group for all the practical (and non) help during this journey. I am grateful to have had the chance to work with a lot of amazing scientists and human beings. A special thank you goes to Dr Nicholas Kindon, Dr Sarah Mistry, Dr Eleonora Comeo, Dr Scott Grossman, Dr Jack Ayre, Dr Ryan Gangloff, Matt, Rebecca, Jaffer, Rhianna, George, James and Dr Desislava Nesheva. I am grateful to have found not only great scientists but also great friends.

Nick, I cannot even begin to thank you for everything you have taught me and for all the incredible support you've given me during these years. I've learned so much from you. You truly are an incredible chemist and an even more wonderful person, and I am lucky to have had you beside me all the time and I could not have arrived here without you. Thank you for dealing with my (multiple) crisis with your exceptional patience and kindness and thank you for giving me confidence when I really needed it.

Eleonora, you have been with me from the beginning, literally from before my PhD application, and you have been so amazingly kind to me since then. You have always been the person to turn to: in the nice times you were always ready to celebrate with me and every time something went not as planned you were there to help me find a solution or just to hug me. Thank you for everything, thank you for being there for me, always.

James, not only you've taught me how to be a pharmacologist (there's still a long way to go…but I did my best) with your patience and your competence, but you have also supported me when I was going through some very difficult moments. I thank you for your help, for your kindness and for your friendship during these years.

Desi, thank you for the help right at the start of my pharmacology experience, you've been very patient with me. And thank you for all our stress relieving squash sessions, they were definitely super helpful.

I would like to thank my housemates, Letizia, Sarah and Alessio. Thank you for all the times you have taken care of me and for all the moments we have shared. Your presence really helped me during these years, through beautiful and less beautiful moments.
Lorenzo, thank you for the time we spent together and for the support you gave me during these years.

Family is a real treasure, and I've been blessed with an amazing one. Thank you to my beautiful big family. You always supported and encouraged me.

Mum and dad, you have truly been my biggest supporters this whole time. I could not have done this without you, without your support and without your unconditional and endless love. Thank you for pushing me, for always believing in me and for supporting me even if you did not totally agree with my decisions. I know I am difficult to deal with sometimes and I have my bad moments and I truly thank you for having been there for me throughout them. Thank you for everything you do for me, always.

I would like to thank my grandmas Natalia and Franca, always ready to warmly welcome me home but also supportive when I had to leave, even if leaving your loved ones is always difficult.
Aunt Mari, you are always with me, and I know that you have been looking out for me from up there. I have felt your presence and guidance in every step, and I am certain that you are proud of me.
Auntie Ceci, thank you for always being by my side. No matter what happened, you have always trusted me without a single doubt and that gave me strength throughout the difficulties.
Uncle Nic, thank you for the encouragement you gave me when I needed it the most.
Thank you to all my amazing cousins, always ready to brighten up my day.

I would like to thank all my friends from home. You have been with me always and, even far from home, I have never felt alone, thanks to you. Thank you, Eleonora and Giorgia for your constant presence in these 30 years (literally), not always physical of course but always felt.

I would like to thank the University of Nottingham for funding this PhD project.

iii. List of Abbreviations

AI	Artificial intelligence
ANC	Absolute neutrophil count
β2AR	β2 Adrenergic receptor
AT2	Angiotensin 2 receptor
BAL	Broncoalveolar lavage
BLAST	Basic local alignment search tool
Boc	*tert*-Butyloxycarbonyl protecting group
BODIPY	4,4-difluoro-4-bora-3a,4a-diaza-s-indacene
BRET	Bioluminescence resonance energy transfer
BSA	Bovine serum albumin
cAMP	Cyclic adenosine monophosphate
CCR	CC chemokine receptor
CF	Cystic fibrosis
CFTR	Cystic fibrosis transmembrane conductance regulator
CLSM	Confocal laser scanning miscroscopy
COPD	Chronic obstructive pulmonary disease
COSY	Correlation spectroscopy
CRS	Chemokine-recognition site
CX_3CR	CX_3C Chemokine receptor
CXCR	CXC Chemokines receptor
CXCR2	CXC Chemokine receptor 2
Cryo-EM	Cryonelectron microscopy
D2	Dopamine receptor 2
DAG	Diacylglycerol
DIPEA	*N*,*N*-Diisopropylethylamine
DMEM	Dulbecco's modified eagle's medium
DMF	*N,N*-Dimethylformamide
E-COPD	Exacerbated-chronic obstructive pulmonary disease
EDC	1-Ethyl-3-(3-dimethylaminopropyl)carbodiimide
ECL	Extracellular loop
ERK	Extracellular signal-regulated kinase
FACS	Fluorescence activated cell sorting

FCS	Foetal calf bovine serum
FCS	Fluorescence correlation spectroscopy
Fmoc	Fluorenylmethoxycarbonyl protecting group
FRET	Fluorescence-resonance energy transfer
GDP	Guanosine diphosphate
GPCR	G-protein-coupled receptor
GRKS	GPCR kinases
GTP	Guanosine trisphosphate
Gpp(NH)p	Guanosine-5'-(βγimino)trisphosphate
HBS	HEPES-buffered saline
HEK	Human embryonic kidney
HMBC	Heteronuclear multiple-bond correlation spectroscopy
HOBt	Hydroxybenzotriazole
HRMS	High resolution mass spectrometry
HSQC	Heteronuclear single-quantum correlation spectroscopy
ICL	Intracellular loop
IL8	Interleukin 8
IP_3	Inositol trisphosphate
JNK	c-Jun N-terminal kinase
LC-MS	Liquid chromatography-mass spectrometry
LgBiT	Large BiT
M2	Muscarinic receptor 2
M3	Muscarinic receptor 3
Mp	Melting point
MAPK	Mitogen-activated protein kinase
MPLC	Medium pressure liquid chromatography
NAM	Negative allosteric modulator
NanoBiT	NanoLuc binary technology
NanoLuc	Nanoluciferase
NFkB	Nuclear factor kappa B
NMR	Nuclear magnetic resonance
NSB	Non-specific binding
NSCLC	Non-small cell lung cancer

PCA	Protein-fragment complementation assay
PDB	Protein data bank
PI3K	Phospatidylinositol-3-kinase
PKC	Protein kinase C
PLC	Phospholipase C
Prep	Preparative
Raf	Rapid accelerated fibrosarcoma kinase
RAS	Rat sarcoma kinase
ROESY	Rotating-frame nuclear Overhauser effect spectroscopy
RT	Room temperature
RTK	Tyrosine kinase receptor
SAR	Structure activity relationship
SEM	Standard error of the mean
SmBiT	Small BiT
TLC	Thin layer chromatography
TM	Transmembrane
TMS	Tetramethylsilane
TNF-α	Tumour necrosis factor α
Tr-FRET	Time-resolved fluorescent energy transfer
UV	Ultraviolet
VT	Variable temperature

iv. Table of contents

Chapter 1. General Introduction

1.1 Chemokines

Chemokines are small 8–12 kDa proteins[1,2] containing 1–3 (usually 2) disulfide bridges.[3] They all share very similar tertiary structures[4] although their sequence homology is highly variable (20–90%)[4]. Around 50 chemokines have been identified in humans[5] and they are subdivided into families, according to the position of the first two closely paired and highly conserved cysteine residues.[1,6] The C-C family, where the first two cysteines are adjacent, the C-X-C family, in which the two first cysteines are separated by one amino acid and the C-X_3-C family, where there are 3 amino acids between the first two cysteines.[7,8] CXC chemokines are further grouped in two classes according to the presence of the motif glutamic acid-leucine-arginine (ELR) in the *N*-terminal region: ELR^+ chemokines, specific for myeloid cells and ELR^- chemokines, which attract a variety of leukocytes[4]. Chemokines are chemotactive cytokines[9], responsible for inducing chemotaxis, a cell movement in response to a chemical gradient. They are secreted by cells that are involved in the regulation of the inflammatory response.[6,8] In addition, they are involved in lymphoid organ development, T-cell differentiation and tumor cells metastasis.[4,6,8]

1.2 Chemokine receptors

1.2.1 G-protein coupled receptors (GPCRs)

Chemokine receptors belong to the G-protein-coupled receptors (GPCRs) family, the largest family of protein targets of approved drugs.[10] In fact, approximately 35% of marketed drugs act at a GPCR[10] since these receptors are involved in the modulation of almost all aspects of human physiology, including having significant roles within the cardiovascular and central nervous system, and therefor are involved in a variety of pathological

conditions. GPCRs within the human genome can be classified into five families, based on sequence homology and functional similarities: class A (rhodopsin-like family), class B (secretin family), class C (metabotropic glutamate family), adhesion family and frizzled family.[11,12]

GPCRs are integral membrane proteins that contain seven transmembrane (TM) α-helices[13] connected by three extracellular loops (ECL1-3) and three intracellular loops (ICL1-3), an extracellular amino *N*-terminus and an intracellular carboxyl *C*-terminus of different lengths.[11] Upon stimulation, GPCRs activate heterotrimeric guanine nucleotide-binding G proteins consisting of an α-subunit and a βγ-complex subunit.[13] The natural ligand binding to the GPCR leads to the recruitment of the partner heterotrimeric G-protein and promotes the exchange of guanosine diphosphate (GDP) for guanosine trisphosphate (GTP) on the alpha subunit leading to the dissociation of the G-protein into the Gα subunit bound to GTP and the Gβγ-complex[8,13,14] which can then modulate various downstream effector proteins.[15]

Chemokine receptors belong to the rhodopsin-like family of G-protein-coupled receptors (GPCRs).[8] They are predominantly coupled to the G_i class of G proteins, the most important G protein subfamily expressed in neutrophils.[8] The natural ligand binding to the GPCR leads to the recruitment of the partner heterotrimeric G_i-protein and promotes the exchange of GDP for GTP on the alpha subunit leading to the dissociation of the G-protein into the Gα subunit bound to GTP and the Gβγ-complex.[8,13,14] The dissociated α-subunit inhibits the enzyme adenylyl cyclase, resulting in a decrease of intracellular cyclic adenosine monophosphate (cAMP) levels and cAMP-dependent protein kinase activity.[8,16] The βγ-complex may have its own signalling functions. The most notable of these is its role in activation of the RAS-Raf-MEK-ERK pathway which facilitates extracellular signal related kinases (ERK) and phosphatidylinositol-3-kinase γ (PI3Kγ) phosphorylation and activation.[8,14,17,18] ERK is a key component of the Ras-Raf-MEK signalling pathway and, along with PI3K, appears to play roles in promoting chemotaxis (towards areas of high chemokine concentration), proliferation, inflammation and cell survival.[8,14,17,18] Additionally, G_i coupled receptors can

regulate calcium levels through βγ-mediated activation of phospholipase C β (PLCβ), since PLC generates inositol trisphospate (IP_3), which mobilizes calcium from intracellular, non-mitochondrial stores, and diacylglycerol (DAG) which acts in conjugation with calcium to activate various isoforms of protein kinase C (PKC). Subsequently this leads to a series of additional signalling events and subsequent cellular responses[1,8] (Figure 1.1).

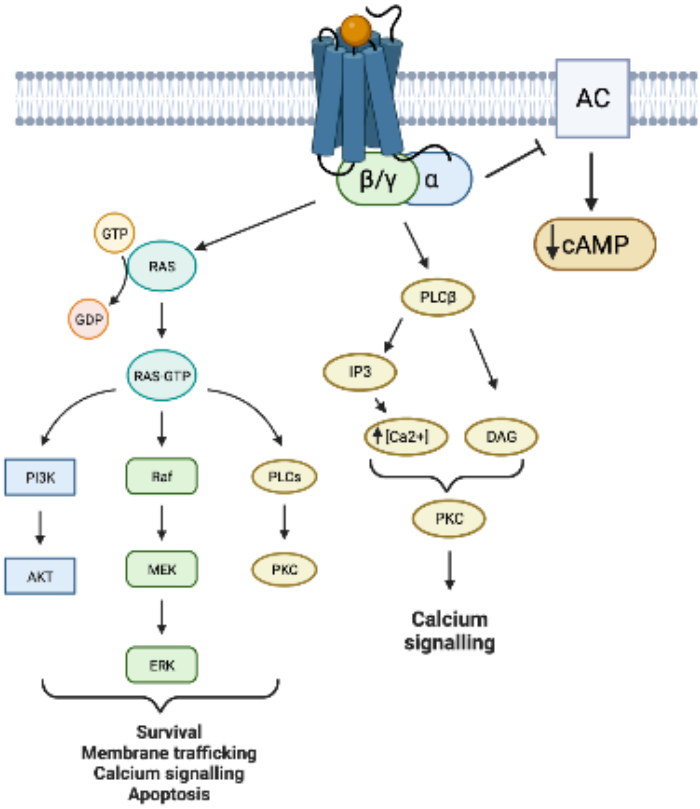

Figure 1.1: $G_{\alpha i}$-GPCR Chemokine receptor signalling. Image modified after Stadtmann *et al.* 2012.[8] AC, adenylyl cyclase; AKT, protein kinase B; Ca^{2+}, calcium; cAMP, cyclic adenine monophosphate; DAG, diacylglycerol; ERK, extracellular signal-regulated kinase; IP3, inositol triphosphate; MEK, mitogen-activated protein kinase; PI3K, phosphatidylinositol-3-kinase; PKC, protein kinase C; PLCβ, phospholipase C beta; Raf, rapid accelerated fibrosarcoma kinase; RAS, rat sarcoma kinase. RAS-Raf-MEK-ERK pathway known as mitogen-activated protein kinase (MAPK)/ERK pathway. Image created with BioRender.com.

GPCR signalling is also controlled by GPCR kinases (GRKs) and β-arrestins 1 and 2 which mediate receptor desensitisation.[13,19,20] The chemokine agonist binding to the receptor induces GRKs to phosphorylate the intracellular loops and/or carboxy terminal of the receptor[15] which promotes the binding of arrestins which sterically inhibits the interaction of the receptor with the G-protein.[19] This leads to reduction or prevention of the receptor signalling.[19] Furthermore, the GRK-arrestin system triggers the clathrin-mediated internalization of inactivated receptors and their subsequent degradation or resensitisation.[19,21] The desensitisation via arrestin binding and removal of the receptor from the membrane causes the continue agonist presence to no longer produce a functional response[22]. β-arrestins not only possess a role in receptor desensitisation and inactivation but can also activate signalling proteins such as mitogen activated protein kinase (MAPK), extracellular signal-regulated kinase (ERK)1/2 and Janus kinase (JNK)[19,23–25] (Figure 1.2).

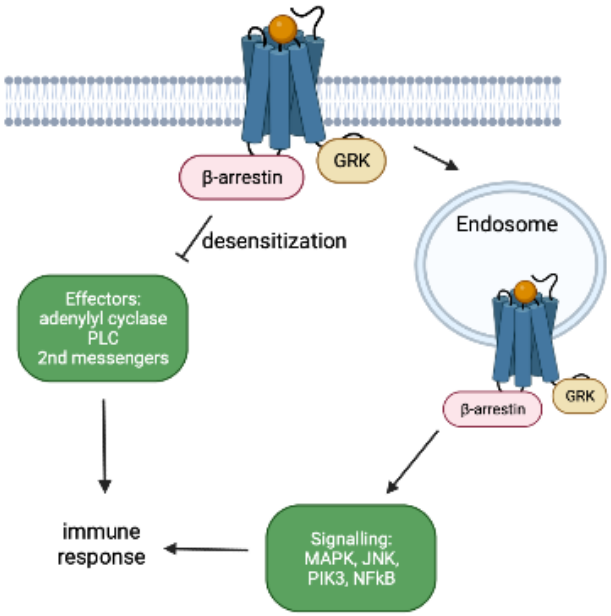

Figure 1.2: Schematic summary of the role of GRKs/arrestins in activation, signalling, and desensitisation of GPCRs in the immune system. Image modified after Vroon *et al.* 2006.[19] GRK, GPCR kinase; JNK, Janus Kinase; MAPK, mitogen-activated protein kinase; NFkB, nuclear factor kappa B; PLC, phospholipase C; PI3K, phosphatidylinositol-3-kinase. Image created with BioRender.com.

1.2.2 Pharmacological analysis of ligand action at GPCRs

GPCRs act as molecular switches as the receptor (R) and the drug (D) exist in a dynamic equilibrium between unbound, inactive and active state (equation below where R is the unoccupied receptor, DR is the occupied but inactive receptor and DR* is the active receptor).

$$D + R \rightleftharpoons DR \rightleftharpoons DR^*$$

The ligands binding the GPCR are defined according to where they bind the receptor. They can be orthosteric ligands, binding the receptor at the orthosteric binding site, typically where the native ligand binds, or allosteric ligands, which bind the receptor in a site distinct from the orthosteric site. The affinity of a ligand consists in its ability to bind the receptor ($D + R \rightleftharpoons DR$),

while the efficacy is the ability of a bound ligand to activate the receptor ($DR \rightleftharpoons DR^*$)[26,27] and, in the case of a GPCR, to activate the secondary effector proteins such as G-protein and arrestins. The affinity is dependent on these forward and reverse rates of interaction: $D + R \rightleftharpoons DR$. They are described by the law of mass action as association rate constant (k_{on}) and dissociation rate constant (k_{off}). At equilibrium, the forward and reverse binding rates are equal and the receptor affinity of a ligand is represented by the equilibrium dissociation constant (K_D) which is defined by the ratio of dissociation rate constant and association rate constant (k_{off}/ k_{on}). Moreover, as described by the Hill-Langmuir equation[28,29], K_D is related to the proportional receptor occupancy alpha (α) and to the drug concentration by: $\alpha = \frac{[D]}{[D]+K_D}$.

K_D can also be defined as the concentration of the drug to occupy 50% of the receptors, where K_D is equal to the concentration of the drug when $\alpha = 0.5$. The equilibrium dissociation constant is a fundamental measure for the affinity of a drug, but the binding kinetics constants (k_{off} and k_{on}) have been increasingly recognized as important indicators of drug properties. In particular, the binding kinetics of a drug can influence the duration of action, and in the case of a slow dissociation rate from the receptor, can change the observed mode of action.[30,31]

GPCRs ligands are also categorised by the effect that they exert on the receptor. Agonists are ligands that bind at the orthosteric binding site and activate the receptor. They can be full agonists, producing a maximal signal response, or partial agonists, producing a lower maximal response compared to a full agonist.[32] Antagonists are ligands that bind the receptor either on the orthosteric binding site or on an allosteric site and block agonist signalling. Inverse agonists exert the opposite effect with respect to the agonist by stabilizing the inactive conformation of the receptor and suppressing spontaneous constitutive (agonist-independent) signalling.[33] Differently from binding affinity, the efficacy of a drug is more challenging to define experimentally and is often measured from functional downstreaming signalling.[32,34] The two-state model[34] simply describes the activation of DR complexes by modelling the receptor as a switch transitioning between active

and inactive states upon agonist binding, but it is experimentally challenging to estimate individual affinity and intrinsic efficacy parameters for most receptors.[32] The relative maximal response of a drug is influenced by its intrinsic efficacy but is not a direct measure of it due to variations in experimental measures of maximal response, introducing a system dependent factor. Additionally, the derivation of agonist efficacy is further complicated as the functional response arising from drug-receptor activation may not require full receptor occupancy to reach the maximal functional response. In this case, the concentration of drug required for 50% maximal response (EC_{50}), or potency of the agonist, will be lower than the measured K_D, with the presence of receptor reserve in the system. Downstream signal amplification can further complicate things as a response from a partial agonist can be amplified to a maximal response, causing it to appear as full agonist.[35]

The activation of the drug-receptor (DR) complex relies on a conformational change of the complex itself.[34] When this theory is applied to GPCRs it is necessary to incorporate the agonist-mediated recruitment of intracellular effectors to the receptor. The agonist bound GPCRs stabilises effector binding allosterically. This model, built on the classical two state model[34], is described as the 'ternary complex model'[36] and it takes into consideration the three-way interaction happening at GPCRs. When a ligand binds to the GPCR it causes a conformational change of the receptor which allow an active state to be stabilized and the coupling with the G-protein, with the formation of the ternary complex.[36] This model was evolved further due to the presence of an effector bound to the receptor promoting an increase of agonist binding affinity through formation of a "high-affinity state". Additionally, this evolution incorporated the ability of GPCR constitutively active, meaning that it can adopt an active conformation even in the absence of an agonist as a result of effector coupling[37] leading to the generation of the 'extended ternary complex model'.[38] This model was further modified into the 'cubic ternary complex model' which incorporates the thermodynamic interactions between the receptor and the G-protein in the absence of an agonist[39]. Although this final model is the most complete theoretically, its complexity limits the possibilities of experimental applications and it is not a complete

model of GPCRs interactions since the activated receptor can exist in several active conformational states[13] and the model does not consider this observation. Ternary complex models consider the influence of the effector binding to the receptor on ligand binding and vice versa. These effects can be defined as "cooperativity" factors and they can be either positive or negative whether the effector increases or decreases the affinity of the ligand for the receptor complex.[40]

A. $A + R \rightleftharpoons AR^{*} + G \rightleftharpoons ARG$

B.
$$\begin{array}{ccccc} A+R & \rightleftharpoons & AR^{*}+G & \rightleftharpoons & AR^{*}G \\ \Updownarrow & & \Updownarrow & & \Updownarrow \\ A+R+G & \rightleftharpoons & A+R^{*}+G & \rightleftharpoons & A+R^{*}G \end{array}$$

C.

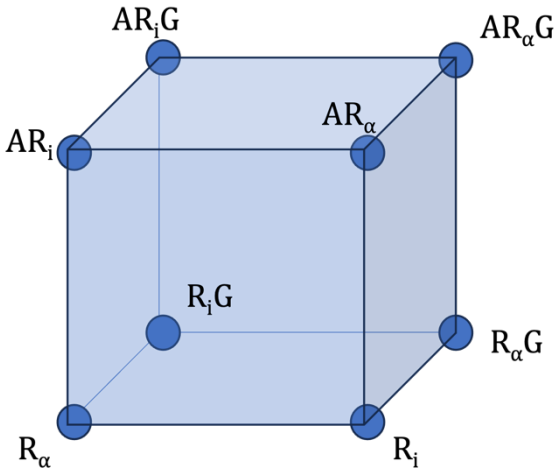

Figure 1.3: Ternary complex models describing interactions between receptors (R), agonists (A) and G-proteins (G). **A**) Original ternary complex model[36]. **B**) Extended ternary complex model incorporating constitutively active receptors (R*)[37,38]. **C**) Cubic tertiary complex model. Receptor exists either bound to a ligand (A) and/or a G-protein (G) and existing in an active (R_α) or inactive state (R_i).[39] Image adapted from Weiss *et al.* 1996.[39]

Chemokine receptors bind chemokine ligands, which results in a downstream cellular response. Chemokine receptors are composed of 340–370 amino acid residues and they share 25–80% homology.[4,8] They all share several structural

characteristics: the *N*-terminal domain (where the chemokines bind), a conserved sequence of 10 amino acids in the second intracellular loop, a characteristic cysteine within each extracellular domain, and a short basic third intracellular loop.[4,8] Similarly to chemokines, chemokine receptors are grouped into three families: ten receptors belong to the CC-chemokine receptors (CCRs), seven belong to the CXC chemokine receptors (CXCRs) and one to the CX_3C chemokine receptor family (CX_3CR).[8] CCRs are expressed on cells involved in allergic reactions including basophils, eosinophils, lymphocytes, macrophages and dendritic cells while CXCRs are mainly present on neutrophils and lymphocytes.[8]

1.2.3 CXC Chemokine receptor 2

CXC receptor 2 is a $G\alpha_i$-coupled receptor expressed on neutrophils, lymphocytes, mast cells, monocytes, alveolar macrophages[41], keratinocytes, eosinophils, endothelial and epithelial cells.[8,42] CXCR2 mediates several effects including neutrophil chemotaxis, integrin expression and activation, which leads to cell motility, polarization, respiratory burst, phagocytosis, proliferation and apoptosis[8], calcium mobilization and angiogenesis.[42]
Several chemokines bind CXCR2, CXCL8 (or IL8) is the most potent ligand that binds this receptor in humans and other ligands are CXCL1, CXCL2, CXCL3, CXCL5, CXCL6 and CXCL7[43] (Figure 1.4). CXCL8 is part of the ELR^+ CXC chemokines family.

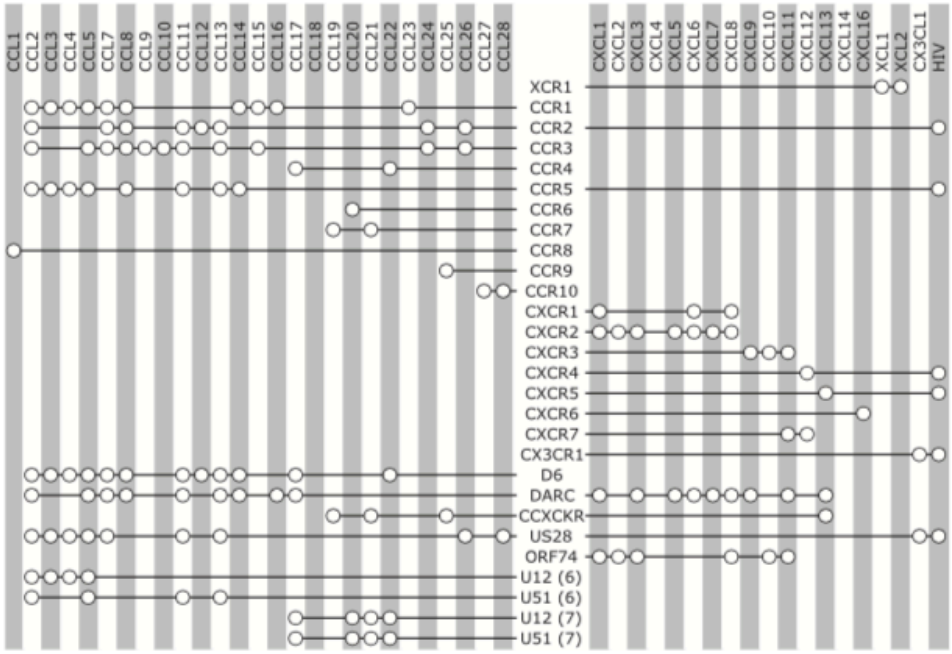

Figure 1.4: Overview of chemokine receptors (vertical) and their ligands (horizontal). An open circle indicates the specific ligand binds to the receptor connected to it by a black line.[43] Human chemokine receptors (XCR1 to CX3CR1), chemokine decoy receptors (D6 to CCX CKR) and viral chemokine receptors (US28 to U51).[43] Image taken from Scholten *et al*. 2012.[43]

The interaction between CXCL8 and CXCR2 is complex.[44] Chemokine-receptor binding occurs in a two-step process.[2,43] First, the chemokine binds to the *N*-terminus and extracellular loops (ELs) of the receptor.[43] In the second step, the flexible *N*-terminus (triggering domain) of the chemokine is positioned in a way that it interacts with a second site of the receptor, formed by parts of the ELs and/or TM domains, resulting in receptor activation.[43] This complex two-step CXCR2-CXCL8 binding has been elucidated through the release of two cryo-electron microscopy structures (PDB: 6LFO and 6LFM)[45] by Liu *et al.* in 2020. The chemokine initially interacts with the *N*-terminal of CXCR2 through the chemokine-recognition site 1 (CRS1).[45] The *N*-terminal of the chemokine interacts with the transmembrane pocket and extracellular loop (ECL) domains of the receptor.[45] The first 25 residues of

the receptor *N*-terminus therefore have a crucial role in the initial recruitment and binding of CXCL8.[45] This was confirmed by the different activities in effector recruitment by CXCL8 in a β-arrestin 2 recruitment assays employing *N*-terminally truncated variants of CXCR2.[45] At first, CRS1 is responsible for CXCL8 recruitment, then the interaction with CRS2 activates the receptor.[45–47] The main interactions are formed between the Gly-Pro (GP) motif in the 30s-loop of CXCR2 and the ELR motif from the CXCL8 N-terminus.[45] The ELR motif from the CXCL8 N-terminus interacts with chemokine-recognition site 2 (CRS2): Arg6 and Leu5 establish hydrophobic interactions and hydrogen bonds that function as anchor points to stabilize the N-terminus of CXCL8.[45] The hydrogen bonds formed by the carbonyl oxygens of Leu5 and Glu4 of CXCL8 and Tyr197^{ECL2} of CXCR2 induce a conformational change of ECL2 that initiates the activation.[45] The driving force for activation, consisting of the inward movement of the extracellular portion of TM5, are the electrostatic interactions and H-bonds between Glu4 of the ELR motif and Arg208$^{5.35}$ (superscript indicate Ballesteros-Weinstein numbering for GPCRs[48]), Arg212$^{5.39}$ and Arg278$^{6.62}$ in the major subpocket of CXCR2.[45] The conformational change of TM5 induces the rotation of Pro223$^{5.50}$ and the rearrangement of the proline-isoleucine-phenyalanine (PIF) motif and the outward swing of TM6.[45] The activation of CXCR2 also includes conformational changes of the aspartic acid-arginine-tyrosine (DRY) and asparagine-proline-x-x-tyrosine (NPxxY) motifs, a common characteristic of class A GPCRs activation.[45]

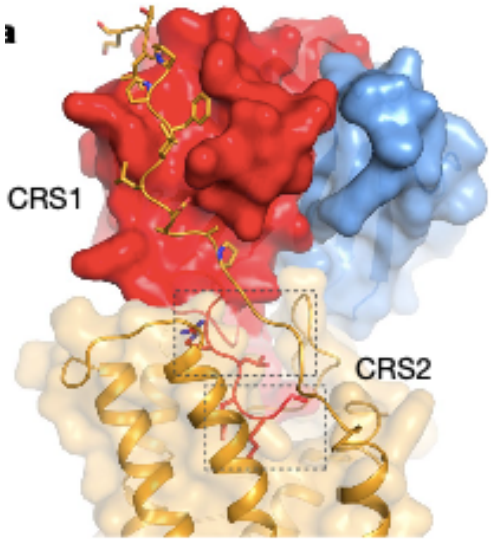

Figure 1.5: The *N*-terminal region of CXCR2 forms a large contact surface with CXCL8 (red) in CRS1. The *N*-terminus of CXCL8 forms extensive interactions with the CXCR2 helix bundles in CRS2. Image taken from Liu *et al.* 2020.[45]

1.3 The role of CXCR2 in pathological conditions

CXCR2 plays a critical role in the regulation of neutrophil homeostasis[8,49] and in their release from the bone marrow.[49,50] The excessive extravasation of leukocyte is associated with a worsening of acute and chronic inflammatory diseases and the deterioration of the integrity of the organism[8,9,50], therefore the regulation of leukocyte recruitment is crucial. In addition, CXCR2 activation is involved in angiogenesis and plays a vital role in the tumour microenvironment and growth.[51,52,53] For these reasons, CXCR2 and its ligands are implicated in a variety of diseases with inflammatory components[8,42] including lung diseases, cystic fibrosis and cancer.

1.3.1 Pulmonary diseases

CXCR2 is expressed on many structural (epithelial and endothelial cells) and inflammatory cells in the lungs, it mediates several pulmonary responses and

it is involved in a series of pulmonary diseases.[9]

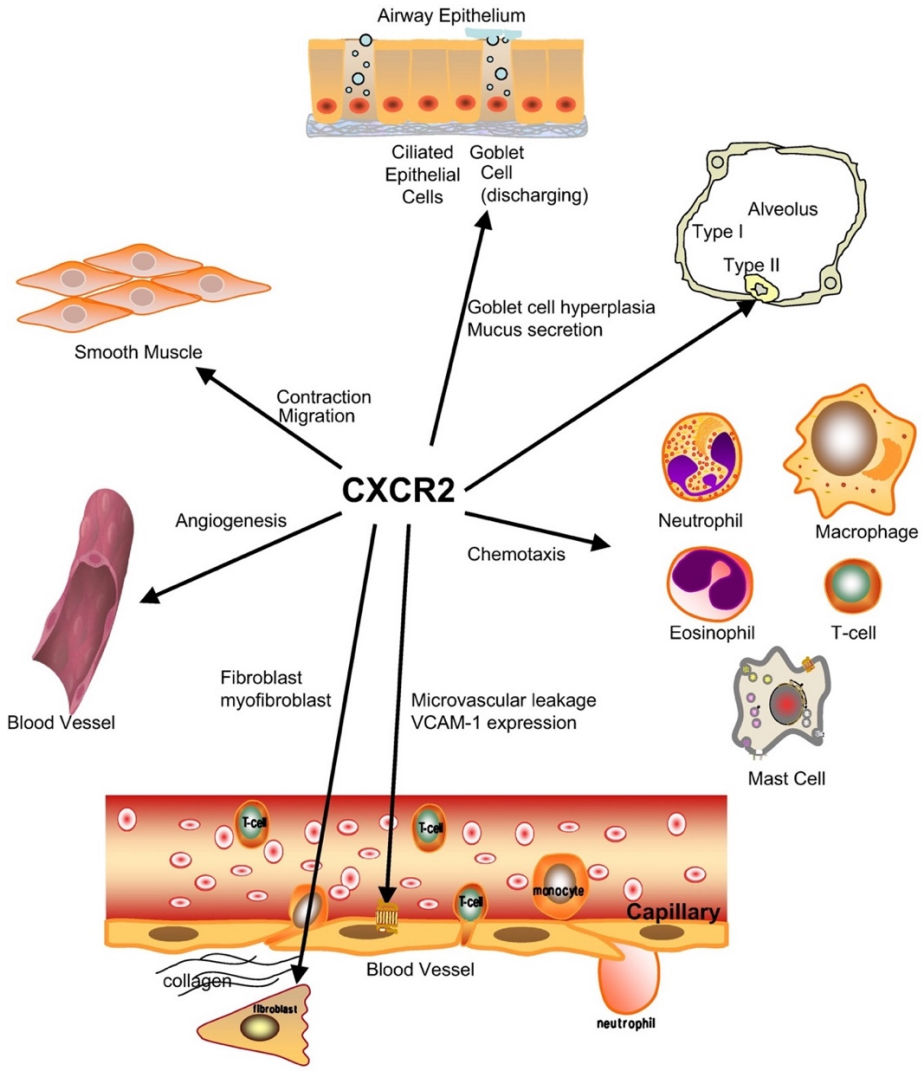

Figure 1.6: Functional role of CXCR2 receptors on structural and inflammatory cells in the lung. Image taken from Chapman *et al.* 2009[9].

1.3.1.1 Chronic obstructive pulmonary disease (COPD)

Chronic obstructive pulmonary disease (COPD) is one of the largest causes of death in most countries[54] and it is considered a major incurable global health burden.[55] It is a progressive, irreversible disease characterised by chronic airway inflammation and structural remodelling. The airflow limitation is progressive and associated with an abnormal inflammatory

response.[8,54,56] The characteristic symptoms of COPD are chronic and progressive dyspnea, cough, and sputum production.[54] The primary cause of COPD is cigarette smoking[8,56–58] which acts as a trigger in stimulating damage of epithelial cells and tumour necrosis factor-α (TNF-α) production, leading to sustained lung inflammation and proteolysis of the extracellular matrix.[59,60] TNF-α causes the migration of monocytes, macrophages and neutrophils to the airway epithelium.[56] Macrophages and epithelial cells produce CXCL8 which causes neutrophil degranulation, respiratory burst and free radical release, causing epithelial damage.[56,61]

As chronic bronchitis is associated with an increased recruitment of leukocytes and excess mucus secretion in the airways, it is not surprising that elevated levels of C-X-C and C-C chemokines have been detected in the bronchoalveolar lavage (BAL) fluids of COPD patients.[8,57] It has also been noticed that patient exposure to cigarette smoke increases CXCR2 expression.[57] In addition, patients with severe acute exacerbations (AECOPD), mostly associated to bacterial or viral infections which enhance lung neutrophil inflammation[59], have significantly increased numbers of neutrophils and this is associated with increases in CXCL5, CXCL8, and CXCR2 but not in CXCR1 expression.[62,63] No disease-modifying medications for COPD exist at the present time. Current therapy consists of inhaled anticholinergics, β-adrenergic bronchodilators and corticosteroids[8], used to treat the symptoms and exacerbation of the disease.[9] AECOPD is correlated to significant morbidity and mortality and the treatment with inhaled glucocorticoids fails to avoid disease progression.[59,60,64] Since CXCR2 is involved in the inflammatory events occurring in the disease[8], its inhibition may be a possible therapeutic approach for COPD.[65] Receptor blockage could result in the reduction of neutrophil-mediated lung tissue destruction.[66] CXCR2 blockage has been tested in animal studies using different COPD models and this approach resulted in mucus hypersecretion inhibition.[8,66] Small molecule CXCR2 antagonists are currently under evaluation for COPD treatment (compounds **2** and **3** [Figure 1.7] and compound **7** [Figure 1.8]).[9,59,67–72] They show promising anti-inflammatory effect in mice models of COPD[59,67], reduced leukocyte and neutrophil

numbers and CXCL8 concentration in sputum.[69,73] Additionally, they show reduced neutrophil migration and activation in the lung.[70,74] Unfortunately dose-related discontinuations were observed for some drugs due to absolute neutrophil count (ANC) decrease.[67,71]

1.3.1.2 Asthma

Asthma is a common inflammatory lung disease characterized by recurring episodes of acute, reversible airflow obstruction, bronchial hyperresponsiveness, bronchospasm, mucus overproduction and chronic eosinophilic lung inflammation.[8,9,75] The standard therapy for mild to moderate asthma consists of treatment with inhaled corticosteroids and β-adrenergic bronchodilators.[8,9] On the other hand, severe asthma, occurring in approximately 10% of patients[76–78], mainly characterized by a predominantly neutrophilic inflammation of the lungs with airway remodeling[8,9,62], poorly responds to this therapy.[8,9,76–78] It has been reported that an increase in sputum CXCL8 precedes the exacerbations of acute asthma[8,9,79,80] and that in severe asthmatic patients there is a positive correlation between ELR^+ CXC chemokines and the presence of neutrophils in the lungs.[8,9,62,79] Moreover, CXCR2 plays an important role in the response to viral and bacterial lung infections which contribute to the frequency of asthma exacerbations.[8,9,81–83] CXC chemokines and CXCR2 also have a role in the formation of new vessels in the lungs[8,9,52], which is linked to the increased vascularization of the airway mucosa, a characteristic of human asthma.[8,9] In addition, CXCR2 expressed on airway smooth muscle cells, may also be involved in development of bronchial hyperresponsiveness in asthmatic patients since there is the possibility that it is involved in the contractile responses of airway smooth muscle.[8,9,84] Considering all the above information, it is clear CXCR2 and CXC chemokines play a relevant role in lung inflammation and in the histopathology of severe asthma.[9] CXCR2 inhibition may therefore have an important therapeutic contribution in this pathology.[59]

1.3.1.3 Cystic fibrosis

Cystic fibrosis (CF) is the most common, life-shortening, genetic disease in Caucasians.[85] It is inherited in an autosomal recessive manner and it is characterized by airway obstruction, infection and progressive bronchiectasis.[86] It is caused by a mutation in the cystic fibrosis transmembrane conductance regulator (CFTR) gene, responsible for the encoding of a cAMP-dependent chloride channel regulating the mucociliary clearance in the airways.[9,87] CTRF absence leads to abnormal transport of chloride and sodium across the epithelium, thick and viscous mucus production, loss in lung mucociliary clearance, recurrent lung infections, hypertrophy and hyperplasia of mucus secreting cells and airways obstruction.[8,9,87] Patients with CF experience declining pulmonary function related to chronic airway inflammation, primarily of neutrophilic nature.[9,88] The degree of inflammation is excessive and this contributes significantly to the pathophysiology of CF.[89] Studies with ibuprofen[90], systemic steroids[91] and azytromycin[92,93] have been performed but no anti-inflammatory therapy has been shown to effectively reduce airway inflammation markers.[85] The inflammation results from epithelial and immune cell secretion of proinflammatory mediators that promote neutrophil influx into the airways.[88] This is confirmed by the presence of high levels of CXCL8 in BAL, sputum and serum of CF patients[9,94] and by the presence of high concentration of neutrophil elastase in CF patients respiratory secretions.[8,9,88] Moreover, studies demonstrated an inverse relationship between lung function and sputum levels of CXCL8, neutrophil counts and neutrophil elastase.[95–97] In addition, it has been shown that the CXCR2 gene is upregulated in neutrophils extracted from the airways and blood of CF patients.[9,98] As previously stated, CXCR2 has a role in mucus hypersecretion and proliferation of mucus secreting cells and, for these reasons, it is likely that this receptor is involved in CF pathophysiology due to the high neutrophil / CXCL8 environment promoting CXCR2 overactivation.[9] It must be taken into consideration that neutrophils are crucial for the antimicrobial response in the lungs but, from recent studies, it has been shown that CXCL8 promotes bacterial killing by neutrophils through CXCR1 but not CXCR2.[9,99] This information and studies

in primates[100], suggest that the blockage of CXCR2 should not affect the innate host defense against pathogens[8,9,100] and consequently, this may be a viable approach for CF treatment.

1.3.2 Cancer

Cancer is one of the leading causes of death worldwide[101] and the carcinogenesis process is extremely complex[102], arising from the accumulation of mutations that develop due to damage to the genome.[103] Our understanding of cancer at the molecular level has progressed over the years, and novel targets for therapeutic intervention and treatment developments have been identified which can lead to an improvement in patient prognosis.[102] CXC chemokines and CXCR1/2 are increasingly recognized to be involved in the process of tumour development process[102] since they activate multiple signalling pathways which regulate cell survival and migration.[51] Furthermore, they play a role in the recruitment of neutrophils to inflammatory sites and the tumour microenvironment since they are implicated in driving angiogenesis in tissue.[51] Chronic inflammation, mainly caused by extensive neutrophil infiltration into the tissue, is considered to be closely correlated with cancer initiation.[51] Increased expression of CXCL8 has been identified in various cancers[104], such as breast cancer[105], lung cancer, especially in non-small cell lung cancer (NSCLC)[106,107], prostate cancer[104], colorectal carcinoma[104], pancreatic cancer[108], renal cell carcinoma, and melanoma.[51,107,109,110] Given that high expression of CXCL8 and its receptors is associated with tumorigenesis and progression of tumours, these factors could be used as biomarkers in screening and in determination of the prognosis.[109] Moreover, CXCR2 effect on migration, invasion and angiogenesis, has been associated with the progression of different cancers such as lung cancer[111,112], melanoma[110,113], prostate cancer[114], breast cancer[115–117], hepatocellular carcinoma[118], laryngeal carcinoma[119], pancreatic cancer[108], colorectal cancer[120] and ovarian cancer.[121,122] CXCR2 has been found to be upregulated in lung cancer[111,112] and its involvement in increased neutrophil infiltration as a result of the immune response is linked to poorer

outcomes in patients.[123,124] Similarly, elevated expression of CXCR2 and CXCL8 has been detected in prostate cancer patients.[125] In breast cancer, CXCR2 expression has been shown to be higher in malignant cells compared to benign cell samples[115] and the receptor has been shown to be implicated in the bone metastasization process.[126] A higher expression of CXCR2 was also observed in patients with advanced colorectal cancer[127] and it has been associated with greater metastatic potential of the tumour cells.[120] Additionally, ovarian cancer cells frequently overexpress CXCR2 which reduces apoptosis and promotes growth through enhanced angiogenesis.[121] The involvement of CXCR2 in tumour progression has been widely assessed and its inhibition could therefore have anti-tumorigenic effects. Small-molecule dual antagonists of CXCR1/2 exerted anti-tumour activity in xenograft models of breast cancer[128], colorectal cancer[129], melanoma[130] and murine models of pancreatic cancer.[131] CXCR2 inhibitors are also in clinical trial studies under evaluation for cancer treatment.[132] Based on all these considerations, targeted inhibition of CXCL8 and CXCR1/2 may be an effective approach to explore in the targeted molecular therapy for tumours[109] but due to the complexity of the tumor microenvironment, it is unlikely that a single CXCR2 inhibitor would be curative.[102]

1.4 CXCR2 antagonists

CXCR2 is an attractive target in therapeutics due to its involvement in several pathologic conditions presented previously in this chapter. As previously introduced, the inhibition of inflammatory cell recruitment may be an appropriate strategy in a number of inflammatory-based diseases[133] such as COPD, asthma, cystic fibrosis and some types of cancers. Inhibition of CXCR2 prevents CXCL8 induced neutrophil chemotaxis *in vitro* and sequestration *in vivo*[133] and, since it is mediated predominantly by CXCR2, this suggests that CXCR1 does not play a crucial role.[133] For this reason, the search for selective antagonists of CXCR2 has been extensive and has led to different classes of antagonists.[58,134–136] Considering that the binding at the

chemokine binding site is complex[45] and difficult to mimic with a small molecule, an alternative allosteric pocket has been discovered and negative allosteric modulators have been develop to block CXCR2 signalling.[137]

1.4.1 CXCR2 intracellular allosteric binding pockets and allosteric antagonists acting at this site

Two different antagonist allosteric binding sites, interacting with different classes of allosteric modulators have been identified on CXCR2. The first site has been identified from mutagenesis studies on CXCR1, the closest homolog to CXCR2 (77%).[138,139] A hydrophobic channel defined by helices 1, 2, 3, 6, and 7 in the TM domain has been characterized[138] as an allosteric binding pocket for imidazolypyrimidine class of CXCR2 antagonists.[140] This class of ligands, which includes Repertaxin (**1**, Figure 1.7), inhibits both CXCR1 and CXCR2 showing lower potency in the inhibition of the latter.[139] The second non-peptide allosteric antagonist binding site is on the intracellular side of CXCR2.[42] 3,4-Diamino-cyclobutenediones compound such as Sch527123 (navarixin, **2**), urea compounds such as SB265610[141] (**3**), and Pteridone-1 (**4**) bind the receptor in this region[42,139] (structures shown in Figure 1.7). Mutagenesis studies have been conducted to clarify the amino acid residues crucial for binding and for selectivity of CXCR2 over CXCR1.[42] These studies suggest that the *C*-terminal region, amino acid residues 302–320, plays a prominent role in the interaction with the allosteric modulators.[42] In particular, lysine $320^{8.49}$ was identified as a key residue for receptor selectivity.[42,139] Other crucial residues for binding are tyrosine $314^{7.53}$ and aspartic acid $84^{2.40}$.[139] Similar allosteric binding sites have since been structurally identified in other GPCRs such as β_2-adrenoceptor, CCR2, CCR9 and CCR7 and EP_2.[142–146] This suggests the existence of a putative intracellular binding site among GPCRs.

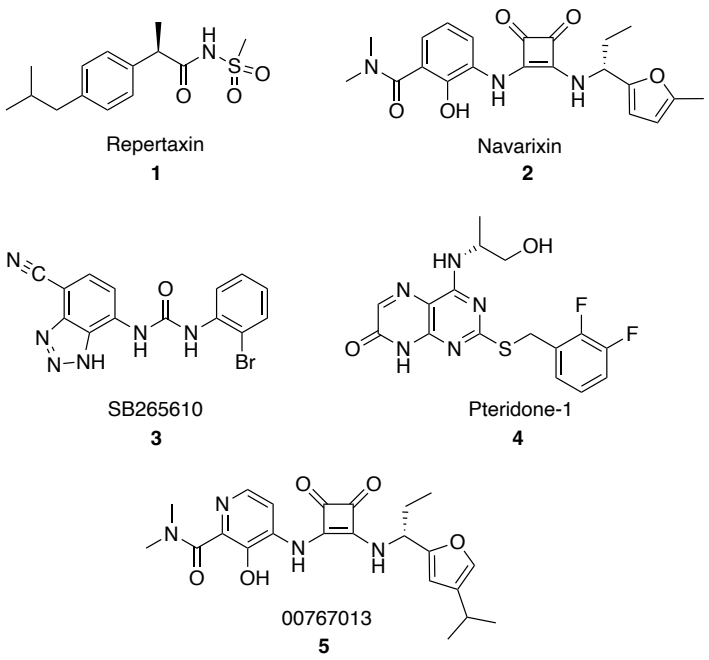

Figure 1.7: Structures of Repertaxin (**1**), Navarixin (Sch527123, **2**), SB265610 (**3**), Pteridone-1 (**4**) and 00767013 (**5**).[45,139–141]

GPCR allosteric modulators are molecules that interact with binding sites that are distinct from the orthosteric site, where the endogenous ligands bind.[147] They can fine-tune the classical response of the receptor because of their ability to modulate its conformation in the presence of the natural ligand[147] and to modulate the binding and/or signalling properties of the orthosteric site.[147] An allosteric antagonist is an allosteric modulator that reduces orthosteric ligand affinity and/or orthosteric agonist efficacy.[147] CXCR2 intracellular allosteric modulators can act in this classical allosteric mode, reducing the receptor affinity of the chemokines, or they can prevent the formation of the ternary complex with the G-protein.[36] Many of the residues crucial for the binding of CXCR2 intracellular allosteric antagonists are located close to the G-protein binding site or to the region of the receptor responsible for the transduction of the signal.[139] In particular, it has been shown that the binding of Sch527123 (**2**) and SB265610 (**3**) were affected by the mutation of Asp84$^{2.40}$, located in the DRY motif of the receptor and by the mutation of Tyr314$^{7.53}$ in the NPXXY motif.[139] These motifs are conserved among GPCRs[148] and they play a role in GPCR activation, G-

protein coupling, receptor internalization and signalling.[148–150] Moreover, the antagonists prevented receptor activation without affecting the agonist binding affinity.[139] These data suggested that their molecular mechanism may be via a competitive interaction with the G-protein as their binding sites overlap. The structural basis of the allosteric mechanism of these modulators has been elucidated by Liu *et al.* with the publication of the X-ray crystal structure of CXCR2 bound to the NAM 00767013 (**5**) (PDB ID: 6LFL).[45] The antagonist is shown to sterically interfere with the binding of the G-protein to CXCR2 since the binding site of the NAM overlaps with that of the G-protein. The hydrophobic side chains of the $G\alpha_i$ subunit are directed towards the hydrophobic pocket of the receptor formed by the cytosolic ends of TM3, TM5, TM6 and TM7, lined by Ile148$^{3.53}$, Leu238$^{5.65}$, Val252$^{6.36}$, Ile253$^{6.37}$ and Ile317$^{7.56}$ [45] with similar interactions to those observed previously in other receptors binding $G\alpha_i$.[151–154] Moreover, the NAM restricts the conformational changes of TM6, TM3 and TM7 required for receptor activation.[45] The small molecules analysed by Salchow *et al.*, acting at this intracellular allosteric site of CXCR2, Pteridone-1 (**4**), SB265610 (**3**) and Sch527123 (**2**) share some common features. An acidic center, able to interact with the basic Lys320$^{8.49}$ residue of the receptor through ionic interactions[139] and an hydrophobic side chain or a combination of H-bonding core and side chain.[139] Moreover, since these molecules require intracellular access, lipophilicity is a key determinant for the diffusion across the cell membrane.[42,139] The partition coefficient (logD) at pH 6.8 was calculated by Salchow *et al.* to be greater than 2.5 for all the three antagonists in the study.[139]

1.4.2 Urea-based CXCR2 receptor antagonists

The first example of small-molecule CXCR2 receptor antagonist was reported in 1998 by SmithKline Beecham (currently GlaxoSmithKline).[133] Since then, there have been considerable efforts to identify additional classes of CXCR2 antagonists throughout the pharmaceutical industry.[137] The first molecule identified by SmithKline Beecham (SB225002, **6**, Figure 1.8) was part of the diaryl urea-based CXCR2 receptor antagonists. SAR on this class of compounds established the phenolic OH and the NH's of the molecule as

key ionizable elements required to retain receptor binding affinity.[155] Another compound belonging to this class is SB265610[141] (**3**, Figure 1.8), where the phenol group of compound **6** was replaced with a bioisostere to improve its pharmacokinetic properties and reduce the rapid glucuronication of the phenolic moiety.[137] Compound **3** possesses selectivity for CXCR2 over CXCR1[156], inhibits CXCL8-induced chemotaxis *in vitro* and significantly inhibits neutrophilia in *in vivo* models of inflammation.[157] To further enhance the pharmacokinetic profile of the compounds, an electron-withdrawing group (e.g. sulfonamide group) was installed in position 3 to retard the glucuronidation of the phenol.[134] Another interesting compound belonging to this sulfonamide-related urea-based class of CXCR2 NAMs is Danirixin (GSK-1325756, **7**, Figure 1.8) showing an improved pharmacokinetic profile in healthy patients[158,159] and the compound is under evaluation for the treatment of COPD.[158] The urea-based compounds bind the intracellular allosteric binding pocket of CXCR2[141] presented previously in this section.

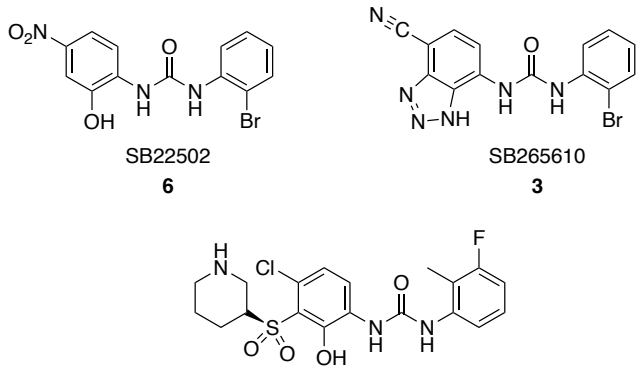

Figure 1.8: Urea-based CXCR2 receptor antagonists.

1.4.3 3,4-Diamino-cyclobutenediones CXCR2 allosteric antagonists

The bioisosteric replacement of the central urea functionality of the previously presented first small molecules series of CXCR2 NAMs[134,160] with

a squarate core gave origin to the 3,4-diaminocyclobut-3-ene-1,2-dione-based series of antagonists of CXCR2.[161,162] SAR studies on these compounds identified the phenolic OH and the two NH's as key groups required for receptor binding, as previously observed for the urea series[162–166], as the removal or substitution of these groups resulted in substantial loss of potency.[162] Similarly to the previously presented series, an electron-withdrawing group was added on the phenolic ring to mask the phenol and reduce glucuronidation.[162] Aniline substituent on the left side of the compounds has been optimised leading to the identification of the dimethylamide moiety as substituent conferring the best potency.[162,166] Further studies focused on the incorporation of an alkyl chain on the right side of the squaramide moiety, resulted in compound **8** (Table 1) which displayed good potency, solubility, absorption and metabolic stability.[162] Replacement of the alkyl chain of compound **8** with a benzyl moiety and its enantiomeric α-substituents derivatives did not show an improvement in the activity but a preferred trend in stereochemistry was observed since there was a significant difference in activity between the *R* and the *S* enantiomers (e.g. compounds **11** and **13** compared to compounds **10** and **12,** Table 1) and also in the length of the chiral side chain (e.g. compound **13** compared to compound **11**, Table 1).[164,166] An α-ethyl sidechain possessing a *R* stereochemistry and the introduction of a 5-methyl furyl ring resulted in the identification of navarixin (Sch527123, **2**, Table 1).[166] In particular, the *R* stereochemistry has been proven to be critical for the potency of these compounds.[166]

Table 1.1 SAR studies results from Dwyer *et al.*[166]

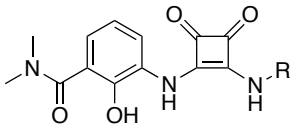

Compound Number	R	IC_{50} for CXCR2 (nM)*	IC_{50} for CXCR1 (nM)*
2	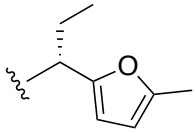	2.6 ± 0.3	36 ± 5
8	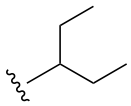	15 ± 1	910 ± 66
9	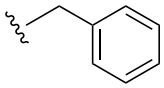	236 ± 10	na**
10	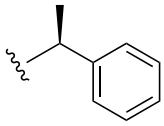	244 ± 19	na**
11	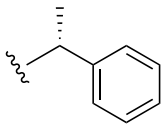	17 ± 1	3058 ± 313
12	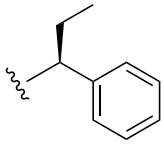	234 ± 20	na**
13	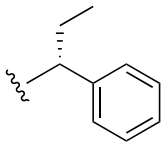	6.8 ± 1.2	254 ± 4
14	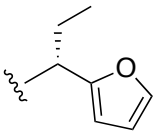	3.8 ± 0.2	26 ± 2

*The *in vitro* affinities were determined by a radioligand binding assay using ^{125}I-hCXCL8 in membranes.[166] Values reported are the mean ± range (n=2) except Navarixin (**2**) (mean ± standard error of the mean (SEM); n=4).

**na = not active at > 10000 nM

Navarixin (**2**) binds both CXCR2 and CXCR1, with higher affinity for CXCR2 compared to CXCR1, probably due to the dissociation rate from the receptor ($t_{1/2} \cong 22$ h), much slower compared to that of CXCR1 ($t_{1/2} \cong 5$ min).[41,139] As will be discussed later (Chapter 5.5.2), the binding kinetics of compound **2** potentially contributes to its selective mode of action. Navarixin (**2**) suppressed neutrophil influx to the lungs and mucus hypersecretion in mouse models of lungs inflammation[167,168] and demonstrated efficacy in numerous inflammation models leading to its advancement from preclinical to clinical studies for inflammatory disorders, such as COPD and asthma, characterised with the presence of underlying neutrophilia. The compound showed inhibition of ozone-induced airway neutrophilia in healthy patients[169,170] and reduction of sputum neutrophils in patients with severe asthma[171], leading to a modest improvement of disease control. Moreover, the chronic oral administration at clinical dose of navarixin (**2**) did not have an effect on cell-mediated immunity or acquired humoral immunity.[172] The clinical evaluation of this compound for the treatment of COPD has been stopped by Merck for undisclosed reasons, presumably due to the reported reduction of peripheral neutrophil counts in healthy patients.[169] Compound **2** has been additionally evaluated for the treatment of cancer. It showed a decrease of cell proliferation and angiogenesis combined with an increase in apoptosis which inhibit the growth of human melanoma tumours in mice[173], decreased liver metastasis in an *in vivo* model of colon carcinoma[174] and an increase sensitivity to oxaliplatin *in vivo* model of colorectal cancer.[129] The anti-metastatic effect of navarixin (**2**) may be due to its effect on CCR7 in addition to CXCR2/CXCR1, since CCR7 has a role during the metastatic process.[129,145,174] Therefore, the silencing of CCR7 may contribute to the anticancer effect of compound **2** since the compound is able to bind the intracellular allosteric pocket of this receptor and to act as a NAM.[145] Additional SAR studies focused on the furan portion of the molecule identified the 4-isopropyl furyl derivatives as compounds with excellent affinity for both CXCR2 and CXCR1[175] displaying efficacy in reducing inflammation in mouse models.[176] Attempts at replacing the furan moiety with other heterocycles without loss in binding affinity and with the maintaining of a similar pharmacokinetic profile, failed[137,163,164] as the

compounds bearing the furan moiety retains the better pharmacodynamic and pharmacokinetic properties.

The mechanism of action of the 3,4-diamino-cyclobutenediones class of intracellular allosteric modulators has been recently elucidated with the release of the X-ray crystal structure of CXCR2 in complex with the antagonist 00767013 (**5**) (PDB: 6LFL).[45] The two vinyligous amides of the compound form hydrogen bonds with Asp84$^{2.40}$ and the carbonyl groups of the cyclobut-3-ene-1,2-dione form hydrogen bonds with Lys320$^{8.49}$ and Phe321$^{8.50}$ at the turn of TM7.[45] The furan isopropyl group forms hydrophobic interactions with Val69$^{1.53}$, Val72$^{1.56}$ and Ile73$^{1.57}$ in TM1, the pyridine-3-ol hydroxyl group and the carbonyl group of the dimethyl-amide side of the molecule form hydrogen bonds with Ser81$^{2.37}$ and Thr83$^{2.39}$.[45] The binding pocket of 00767013 (**5**) is also lined by Arg144$^{3.50}$, belonging to the DRY motif and Tyr314$^{7.53}$ of the NPxxY motif.[45] The binding of the modulator sterically interferes with the binding of the G-protein to CXCR2, preventing the conformational changes of TM3, TM6 and TM7.[45] Moreover, the binding sites of the NAM and the G-protein overlap.[45]

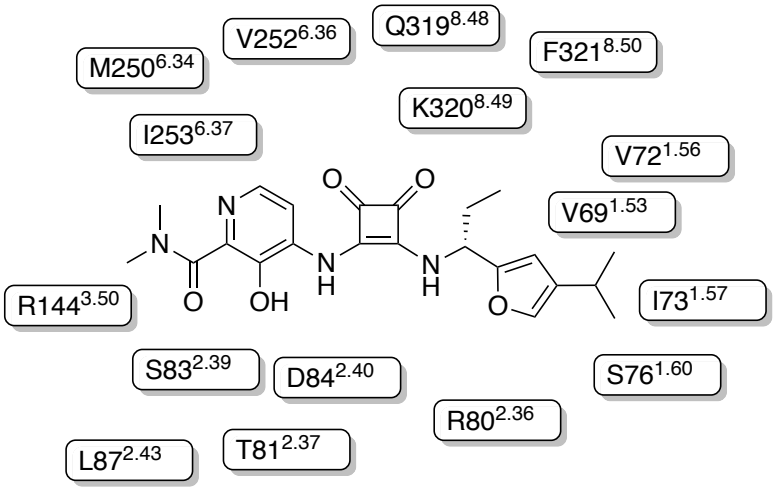

Figure 1.9: Allosteric antagonist 00767013 (**5**) binding CXCR2. Image adapted from Liu et al 2020[45]. Single letter amino acid code: D, aspartate; F, phenylalanine; I, isoleucine; K, lysine; L, leucine; M, methionine; Q, glutamine; R, arginine; S, serine; T, threonine; V, valine.

1.4.4 Modified urea/diaminocyclobutenediones CXCR2 receptor antagonists

There has been a substantial effort to find alternative bioisosteres to replace the urea core. In addition to the 3,4-diaminocyclobut-3-ene-1,2-dione-based compounds presented in the previous section, new classes of CXCR2 NAMs included the incorporation of a cyclic sulfonamide or a cyanoguanidine in place of the urea core. The introduction of a cyclic sulfonamide (e.g. compound **15**, Figure 1.10)[177] did not improve binding affinity or potency, compared to the urea series, and the compounds showed poor oral bioavailability.[177] The *N*-*N*'-diarylcyanoguanidine (e.g. compound **16**, Figure 1.10) displayed good and balanced selectivity between CXCR2 and CXCR1.[178] Moreover, the central urea core of the initial series of CXCR2 NAMs was replaced with 1,2,5-thiadiazole-based cores possessing varying oxidation states. Initially, a functionality similar to the squarate, 3,4-diamino-1,2,5-thiadiazole-1,1-oxide, was introduced, leading to compound **17** (Figure 1.10).[179] This compound showed good binding affinity for CXCR1 and CXCR2 *in vitro* but lacked functional activity[179], probably due to poor cell permeability of these compounds.[179] An alternative related series possessing a 3,4-diamino-2,5-thiadiazole-1-oxide core was evaluated.[179] Compound **18** (Figure 1.10), belonging to this series, displayed excellent binding affinity for CXCR1 and CXCR2, improved solubility compared to the dioxide analogues and potent functional activity.[179] Finally, a series of compounds with a 3,4-diamino-1,2,5-thiadiazole-based core was evaluated. As an example, compound **19** (Figure 1.10), possessed lower binding affinity for both CXCR2 and CXCR1 compared to **17** and **18** and a good functional activity.[180] No compounds belonging to these presented series, possessing modified urea cores, appeared to have moved beyond *in vitro* initial evaluation.[137]

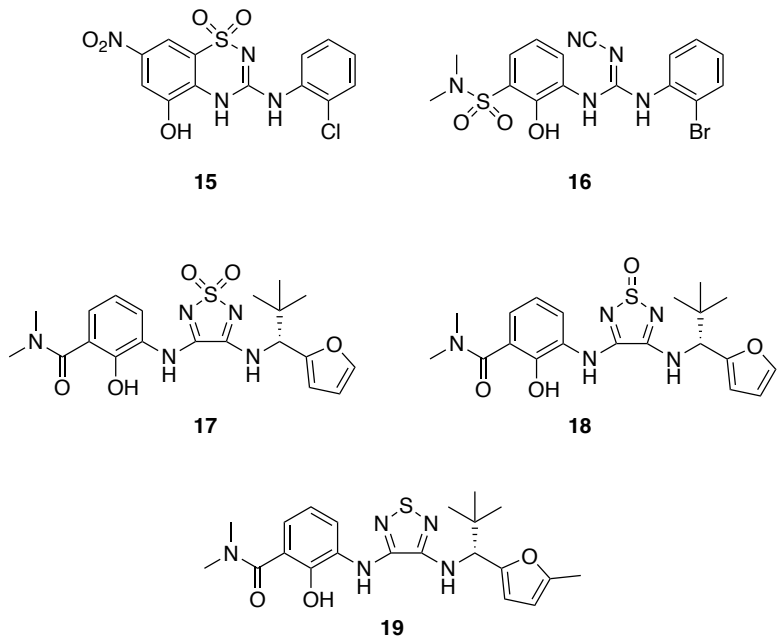

Figure 1.10: Modified urea/diaminocyclobutenediones CXCR2 receptor antagonists.

1.4.5 Pyrimidine-based CXCR2 receptor antagonists

Another class of CXCR2 NAMs binding at the intracellular allosteric site of CXCR2 is represented by the pyrimidine-based series of compounds developed by Astra-Zeneca. This series possess a functionalised pyrimidine ring as core scaffold, that is structurally distinct from the urea, 3,4-diaminocyclobut-3-ene-1,2-dione and modified urea/ diaminocyclobutenediones series presented in the previous sections.[137] An interesting compound belonging to this series is AZD5069 (**20**, Figure 1.11)[181,182], shown to inhibit binding of radiolabelled CXCL8 to CXCR2 with a pIC_{50} of 9.1.[182] Moreover, compound **20** inhibited neutrophils chemotaxis and adhesion molecules expression[83,100,183] and showed a reduction of inflammation in *in vivo* models.[182] Compound **20** is currently under clinical evaluation for the treatment of COPD, asthma[137] and hepatocellular carcinoma.[132] Another compound belonging to this series, AZ10397767 (**21**, Figure 1.11), has been shown to slow tumour growth by significantly reduce neutrophil infiltration into both *in vitro* and *in vivo* tumor models.[124] Other compounds belonging to this series, such as compound **22** (AZD8309, Figure 1.11)[135], displayed good *in vitro* and *in vivo* activity and are under evaluation

for the treatment of COPD.[69,184,185] Recently, novel chemotypes of CXCR2 NAMs have been identified from the modification of this scaffold.[186]

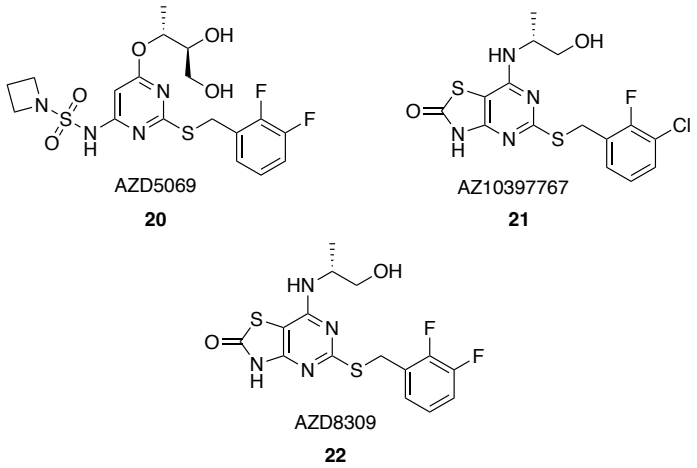

Figure 1.11: Pyrimidine-based CXCR2 receptor antagonists.

1.4.6 2-Arylpropionic acid derived dual CXCR1/CXCR2 receptor antagonists

Based on the observation that *R*-ketoprofen (**23**, Figure 1.12) inhibited CXCL8-mediated human polymorphonuclear neutrophils (PMN) chemotaxis[187], Dompè developed a series of 2-arylpropionic acid analogues.[188] Repertaxin (or reparixin, **1**, Figure 1.12) belongs to this series of compounds and has been generated through the replacement of the aromatic ring coupled with the bioisosteric substitution of the carboxylic acid of *R*-ketoprofen (**23**). Compound **1** allosterically inhibits CXCL8-induced PMN migration, adhesion, degranulation and cytokine expression.[189] It can be considered more selective for CXCR1 as it possesses weaker activity towards CXCR2 compared to CXCR1[138]. Repertaxin (**1**) inhibited neutrophils infiltration, organ dysfunction and tissue damage in preclinical animal models of ischemia/reperfusion injury[190,191] leading to its advancement into phase I clinical trials where it was found to have good exposure and a safe profile.[192] Modification of compound **1** led to the synthesis of new analogues with an improved pharmacokinetic profile and a dual inhibition of CXCR1 and

CXCR2. These series of compound bind a different allosteric pocket, distinct from the one where the previously presented series of NAM bind.[42] In addition to the major classes of CXCR2 NAMs presented, there have been numerous reports describing unique structural series such as nicotinamide *N*-oxide-based compounds[193], 2-amino-3-heteroarylquinoxaline-based compounds[194] and thiazolethiol-based compounds[195]. The discovery and development of CXCR2 antagonists is detailed in several reviews and patent activity reviews.[137,156,161,196,197]

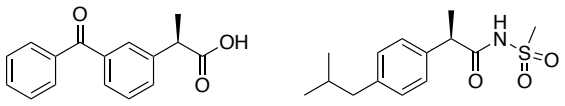

R-Ketoprofen
23

Repertaxin
1

Figure 1.12: 2-Arylpropionic acid derived dual CXCR1/CXCR2 receptor antagonist.

1.5 The use of fluorescent ligands for studying NAMs acting at CXCR2 intracellular allosteric site

The CXCR2 negative allosteric modulators acting at the intracellular binding site of the receptor are interesting molecules for their potential therapeutic applications. A molecular tool which binds competitively with unlabeled ligands to the intracellular binding site is needed to directly determine the affinity and binding kinetics of the NAMs acting at this binding site. Radiolabelled navarixin (**2**) ([^{3}H]Sch527123) has been employed in previous radioligand binding studies to determine binding affinities of unlabelled NAMs acting at the CXCR2 intracellular binding site.[41] However, high affinity fluorescent probes could be used in real-time analysis of ligand binding and can be employed in several GPCR binding techniques such as

bioluminescence resonance energy transfer (BRET) assays.[198–203] These assays present considerable advantages over radioligand binding assays, traditionally used to characterize ligand binding. Radioligands have been copiously used to measure ligand binding affinities and kinetics. They are ligands with a radioisotope ([^{3}H], [^{11}C], [^{25}I] or [^{19}F]) introduced in their core structure whose specific radioactivity (emission of β-particle, positrons) can be detected and monitored.[204] The health hazards and the costs associated to the use of radioligands[204] combined with their insufficient sensitivity and metabolic stability reported for some ligands[205], highlighted fluorescent-based techniques as a valid alternative to radioligands since they display a better safety profile which allows an easier performance of the assay and disposal of waste materials.[206,207] Furthermore, fluorescent ligand-based resonance energy transfer assays have the key capability to monitor specific binding in a homogeneous format, without the need to separate bound from free tracer; and the binding from a single sample can be monitored continuously in real time, enabling kinetic analysis to be performed in a straightforward manner.[199,201]

Fluorescence is a physical process in which the electrons of a molecule (fluorophore), upon exposure to light, are promoted to a higher energy state. After a transient excited state with minimal loss of energy, the molecule returns to its ground state emitting light. The light emission has a longer wavelength than the excitation light.[208] The Stokes shift, crucial to any use of fluorescence-based techniques, is the difference in energy between the excitation and emission wavelengths (Figure 1.13). It allows easy separation of the emitted fluorescence from the excitation light using appropriate optical filters.[208–210]

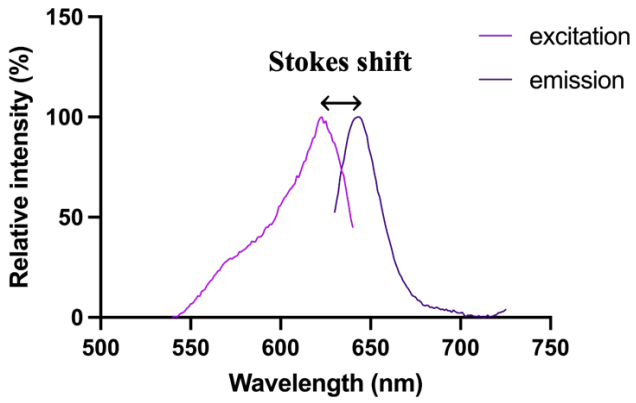

Figure 1.13: Representative excitation and emission spectrum and Stokes shift.

Fluorescence techniques depend on the possibility to fluorescently label the protein of interest. This can be performed through the use of fluorescent proteins or self-labelling protein tags (e.g SNAP-tag)[211], fluorescently labelled antibodies[212] and small-molecules fluorescent ligands.[213] Among these labelling methods, the use of fluorescent ligands has the benefit of being applicable in an unmodified system for the study of receptor in their native state, relevant for the use of these tools in the context of a drug discovery program.[214,215] Examples of fluorescence-based techniques for monitoring of receptor function and dynamics and imaging include: fluorescence-resonance energy transfer (FRET)[216,217], Fluorescence Correlation Spectroscopy (FCS)[218], confocal laser scanning microscopy (CLSM), specialized flow cytometry techniques such as Fluorescence-Activated Cell Sorting (FACS) and super resolution microscopy.[219,220]

1.5.1 Fluorescent ligands design

The development and application of small-molecules fluorescent ligands for GPCRs has increased in the past 20 years due to the increased availability of structural information from X-ray crystallography and cryoelectron microscopy (Cryo-EM) and to the advancements in imaging approaches. These information allowed the rational design of fluorescent probes with high affinity and selectivity for the protein of interest.[221] Fluorescently-labelled ligands are designed by connecting an organic fluorescent dye to a known

agonist or antagonist of the target of interest via a linker.[206,222,223] Fluorescent ligands are composed by three independent units which comprise the parent pharmacophore, the fluorophore and the linker connecting the two parts together (example in Figure 1.14). The addition of linker and fluorophore to the parent pharmacophore could have an influence on its pharmacological profile and it is therefore necessary to consider the novel fluorescent ligand as a separate new pharmacological entity whose profile needs to be evaluated.[224,225] Initially, to design a fluorescent ligand, it is crucial to elucidate the structure-activity relationship of the parent compound. This allows to identify a suitable position for linker attachment without any loss in binding affinity or efficacy of the final ligand. Availability of structural information of the target protein could be of crucial importance during this step. Another crucial step consists in the choice of the fluorophore to employ. This depends on the future application of the fluorescent probe as every technique requires specific spectral properties such as excitation and emission wavelengths, extinction coefficient, quantum yield and fluorescence lifetime.[210] Moreover, the chemical composition of the linker moiety must be evaluated as it has been shown to have an effect on the binding affinity and efficacy of the fluorescent ligand.[224,226]

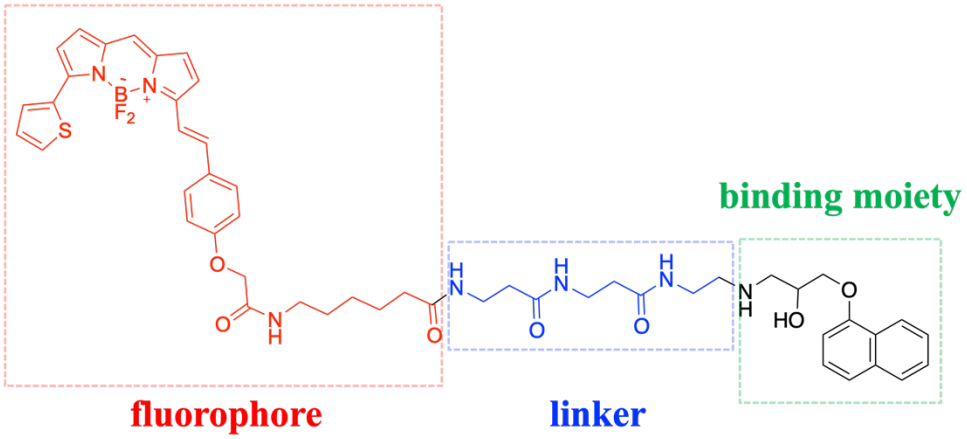

Figure 1.14: Fluorescent analogue of propranolol (BODIPY 630/650-X-β-Ala-β-Ala propranolol) targeting β2 adrenergic receptor, designed by Alcobia *et al.*[223] Example of fluorescent ligand components.

1.5.2 Properties and applications of fluorescent ligands

The first bioimaging studies showing examples of fluorescent ligands use employed molecules conjugated with dyes such as pyrene, dansyl and fluorescein isothiocyanate (FITC) as fluorophores. These dyes possess some disadvantages as they have short excitation and emission wavelengths, they are sensitive to pH, and they show reduced photostability. At present time, there is a number of commercially available fluorophores available able to cover the full range of the visible/electromagnetic spectrum. The scaffolds of the available fluorophores belong to the families of rhodamines, coumarins, fluorescein dyes, cyanin dyes and boron dipyrromethene (BODIPY).[227,228] Moreover, as a result of recent synthetic chemistry, there is the possibility of accessing a broader variety of fluorescent dyes with improved and fine-tuned properties for specific and advanced applications in biological techniques.[229–231] Amongst the fluorophores available for conjugation, BODIPY 630/650 dyes present great stability and spectral properties including high absorption coefficient (ε) and high fluorescence quantum yield (Φ).[232–234] Additionally, BODIPY 630/650 dyes are brighter when located in a lipophilic environment such as the plasma membrane and they are quenched in aqueous environment.[224] Because of their properties, the use of these fluorophores in imaging studies is advantageous since the background fluorescence from the unbound ligand is reduced and BODIPY 630/650 dyes result the be amongst the preferred choice of fluorophores used for conjugation. Conversely, the use of more water-soluble dyes, such as Alexafluor dyes (e.g. AF647) and Cyanine dyes (e.g. Sulfo-Cyanine5)[235], may present more benefits for *in vivo* applications, where a lipophilic dye could present some disadvantages. For *in vivo* applications, fluorophores whose absorption and emission wavelengths are near the IR region of the electromagnetic spectrum (> 600 nm) are preferred. Both BODIPY 630/650 and Cyanine5 dyes absorb and emits in this spectrum. This optical window significantly reduce background autofluorescence resulting from endogenous ligands (aromatic amino acids, collagen, reduced nicotinamide cofactors NADH)[236] and the wavelengths applied are less toxic to the tissues at this lower energy.[223,235]

Fluorescent ligands, combined with advanced fluorescence-based techniques, are a powerful tool to study GPCRs pharmacology and to measure binding affinity and monitor binding kinetics of molecules acting at these receptors.[198,199,201,206,237] Recently, new fluorescent probes targeting the intracellular allosteric binding site of chemokines receptors, such as CCR9[238], CCR2[239] and, more recently, CXCR2 (developed in parallel to this project by Huber *et al*.[240]) have been reported[241] and they have been proven as critically useful tools to have a better understanding of the pharmacology of NAMs targeting the allosteric pockets of these receptors.

1.6 Thesis aims

CXCR2 is an interesting pharmacological target involved in inflammatory-based conditions. Since the interactions at the orthosteric binding site are difficult to mimic with small molecules, allosteric modulators of the receptor, binding an intracellular pocket located near the *C*-terminal of the receptor, have been identified. A particularly interesting class of CXCR2 NAMs is composed by the 3,4-diamino-3-cyclobutene-1,2-dione-based compounds. Their molecular mechanism, elucidated by Liu *et al.*[45], includes the competitive interaction with the G-protein, since its binding site is in close proximity and overlapping with the allosteric binding site of interest. Navarixin (**2**), a compound belonging to this series, possesses excellent potency at CXCR2, which may be related to its particular binding kinetics, since it has been reported to have a slow dissociation rate from the receptor.[41,139] Therefore, kinetics of binding may have an impact on the action of NAMs. The use of high affinity fluorescent ligands in pharmacological binding and functional assays could be valuable to investigate the kinetics of modulators binding at this binding site. The aim of this thesis is to rationally design and synthesize a library of fluorescent ligands to investigate the binding, kinetics and activity of potent and selective 3,4-diamino-3-cyclobutene-1,2-dione CXCR2 receptor allosteric antagonists binding at the

intracellular allosteric site of CXCR2, with a particular interest in navarixin (**2**).

Chapter 2. Synthesis and pharmacological evaluation of a series of compounds belonging to the 3,4-diaminocyclobutenedione class of CXCR2 intracellular allosteric antagonists

2.1 Chemical synthesis of small molecules with a 3,4-diamino-cyclobutenedione core

A series of small molecules belonging to the 3,4-diamino-cyclobutenediones class of CXCR2 intracellular negative allosteric modulators (NAMs) was initially synthesised, in order to validate their previously reported pharmacological activities at the CXCR2 receptor[166] (Table 2.1). The purpose was to confirm a suitable potent compound to be used as a congener to develop a library of fluorescent ligands. Compounds were selected according to their reported potency at CXCR2[166], in addition to specific structural characteristics, such as *R* stereochemistry, linked in general to higher reported potency compared to the corresponding *S*-enantiomers.[166] Moreover, these molecules were also chosen based on expected selectivities for CXCR2 over CXCR1.[166]

Table 2.1 Synthesised compounds belonging to the 3,4-diamino-cyclobutenedione class

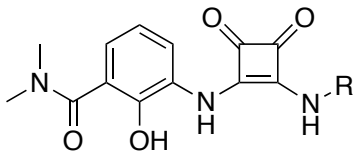

Compound Number	R	IC_{50} for CXCR2 (nM)*	IC_{50} for CXCR1 (nM)*
***R*-Navarixin 2**	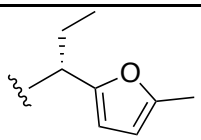	2.6 ± 0.3	36 ± 5
8	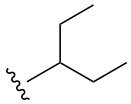	15 ± 1	910 ± 66
11	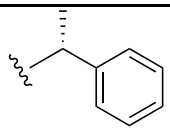	17 ± 1	3058 ± 313
***S*-Navarixin 24**	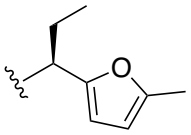	NR**	NR**
Navarixin racemate 25	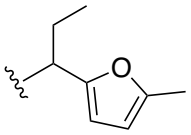	NR**	NR**

* The *in vitro* affinities were determined by a radioligand binding assay using ^{125}I-hCXCL8 in membranes.[166] Values reported are the mean ± range (n=2) except R-navarixin (**2**) (mean ± SEM; n=4). Data reported by Dwyer *et al.*[166]

**NR, not reported.

For the synthesis of the CXCR2 NAMs presented in Table 2.1, the procedure reported by Dwyer *et al.*[166] was followed. The compounds were selected according to their reported IC_{50} values and for their stereochemistry.

Scheme 2.1 Synthesis of compounds 2, 8, 11, 24, 25

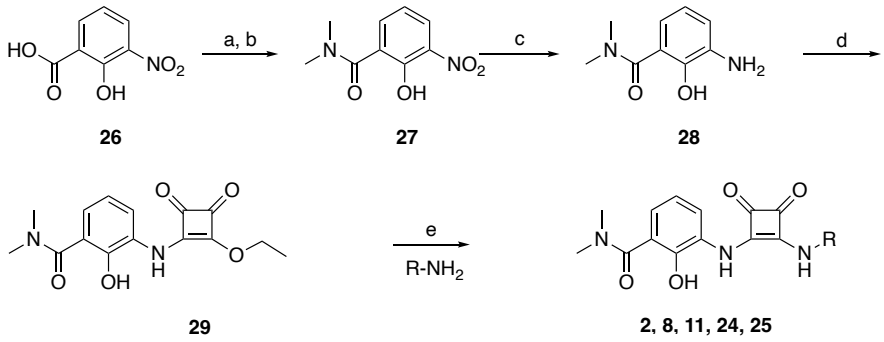

30, 2: R= (*R*)-1-5-methylfuran-2-yl-propan-1-yl.
31, 8: R=3-aminopentyl.
32, 11: R= (*R*)-α-methylbenzyl.
33, 24: R= (*S*)-1-5-methylfuran-2-yl-propan-1-yl.
34, 25: R= 1-5-methylfuran-2-yl-propan-1-yl.

Reagents and conditions: (a) $(COCl)_2$, *N,N*-dimethylformamide (DMF), CH_2Cl_2, room temperature (RT); (b) $HNMe_2$, 0 °C, 65%; (c) 10% Pd/C, H_2, EtOH, RT, 72%; (d) diethyl squarate, EtOH, RT, 45%; (e) R-NH_2 **30-34**, EtOH, RT, 87-30%.

3-Nitrosalicilic acid (**26**) was converted to the corresponding *N,N*-dimethyl amide **27.** This was achieved firstly by the formation of the corresponding acyl chloride via a modified Vilsmeier-Haak reaction, which was then reacted with dimethylamine at 0 °C. The nitro moiety of compound **27** was then reduced, through a Pd/C catalysed hydrogenation, to the corresponding aniline **28**. Compound **28** was subsequently reacted with diethyl squarate in EtOH to afford **29**. Finally, **29** was treated with commercially available or synthesised amines (**30-34**) to afford the final compounds (**2,8,11,24,25**).

The synthesis of the chiral amine **30**, required for the synthesis of *R*-navarixin (**2**), was attempted following several procedures. At first, the diastereoselective addition route proposed by Dwyer *et al.*[166,242] was tried (Scheme 2.2).

Scheme 2.2 Attempted synthesis of amine 30

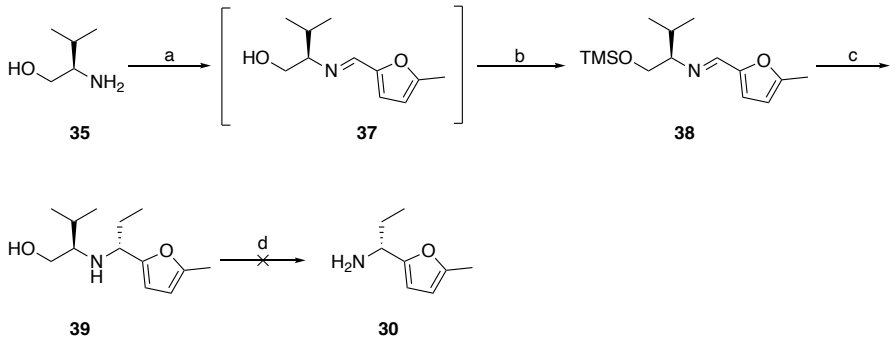

Reagents and conditions: (a) 5-methylfuraldehyde (**36**), $MgSO_4$, CH_2Cl_2, 0 °C; (b) TMSCl, Et_3N (68% two steps); (c) EtI, *t*-BuLi, Et_2O, -40 °C, 52%; (d) H_5IO_6, $MeNH_2$, MeOH, RT or $Pb(OAc)_4$.

This approach employed *R*-Valinol (**35**), which was initially reacted with 5-methylfuraldehyde **(36**) to form imine **37**. This step was then followed by the TMS protection of the alcohol group. The protected imine **38** was subsequently reacted with EtLi, generated in situ from a lithium-halogen exchange between ethyl iodide and *t*-butyllithium, to afford the diastereoselective addition product **39.** The final step in this synthetic procedure consisted of an oxidative cleavage step of compound **39** with periodic acid or lead tetraacetate to obtain amine **30**. Unfortunately, this synthetic route was not successful, and the final chiral amine product was not successfully made and isolated.

It was therefore decided to attempt the synthesis of the racemic mixture of the desired amine, instead of the pure enantiomer, following the procedure described by Blume *et al.*[243] (Scheme 2.3).

Scheme 2.3 Synthesis of amine 34

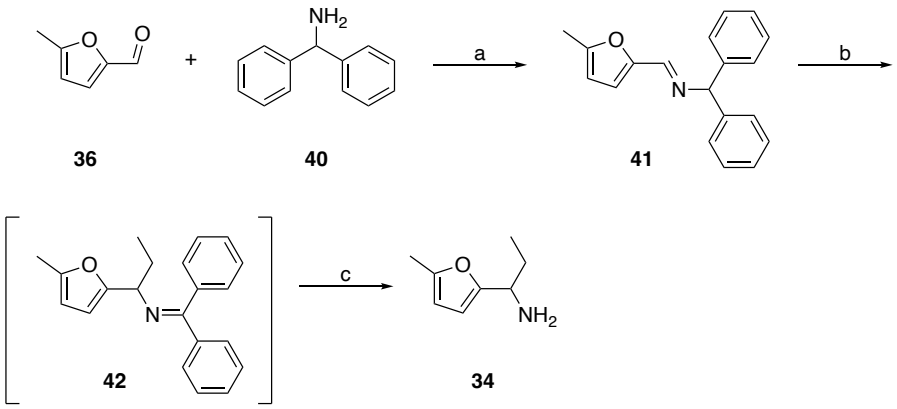

Reagents and conditions: (a) EtOH, RT; (b) *t*-BuOK, EtBr, DMF, 0 °C; (c) 1 M aq HCl, MeOH.

The starting material for this synthetic route was 5-methylfuraldehyde (**36**) which was reacted with benzhydrilamine (**40**) to give furylimine **41**. Deprotonation of **41** with potassium *tert*-butoxide in anhydrous DMF gave a deep red solution of the azaallyl anion to which ethyl bromide was added to afford compound **42**. A final treatment with hydrochloric acid in methanol gave the racemic amine **34** as product.

An additional attempt at synthesizing chiral amine **30** was performed following the procedure present in the *R*-navarixin (**2**) patent (WO 2009/005801) which reports the generation of the tartrate salt of the desired *R*-amine (Scheme 2.4).

Scheme 2.4 Synthesis of tartaric acid salt of amine 30

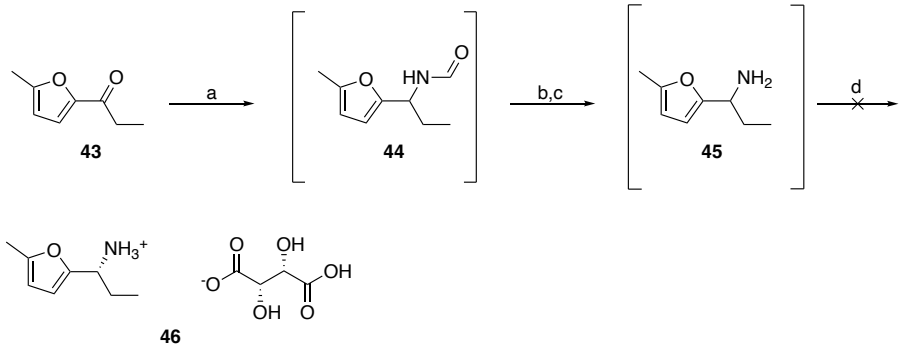

Reagents and conditions: (a) Formamide, formic acid, 140–150 °C; (b) 25% w/w NaOH in H_2O, 70 °C; (c) wash with aq. 10% w/w. NaCl; (d) D-tartaric acid, MeOH, H_2O, 50 °C.

To 2-methyl-5-propionylfuran (**43**) were added formamide and formic acid to afford amide **44** which was then hydrolyzed with sodium hydroxide solution into the amine **45**. Upon treatment with D-tartaric acid, salt **46** of the *R*-enantiomer (**30**) should have been formed. Regrettably, this was found not to be the case and **46** was not isolated.

Several difficulties were encountered during the synthesis of chiral amine **30**. The high volatility of the amine itself was discovered during the synthetic attempts and experimentally confirmed under reduced pressure. The low yields obtained in most of the steps also posed significant challenges which resulted in the unsuccessful synthesis of the desired product. It was therefore decided to purchase the chiral amines **30** and **33** from standard suppliers.
As the optical rotations of the amines **30** and **33** were not reported, it was important to absolutely assign chiral center configuration for each of the enantiomers. Moreover, there appeared to be some discrepancies with the pharmacological results of the tests conducted with compound **2** and **24** (data shown in Figure 2.4). These data initially opposed literature reports in which the *R* enantiomers were reported to be more potent than *S* enantiomers.[166] From experimental optical rotation measurements, it was known that compounds **2** and **24** were enantiomers, since they showed equal and opposite

in sign rotation measurements; **2**: $[\alpha]_D^{32.4\ °C} = +64$ (1; MeOH) and **24**: $[\alpha]_D^{33\ °C} = -76$ (1; MeOH), but the absolute configurations of the compounds were unknown. With this in mind, compound **24** was crystallized from ethanol and its structure was solved by X-ray diffraction in the crystallography department of the university. Analysis of the crystal structure (Figure 2.1) allowed assignment of the absolute configuration of compound **24** as the *S*-enantiomer and to generate previously unreported and unambiguous optical rotation data on compounds **2** and **24** and on the HCl salts of amines **30** and **33** and to explain the discrepancies found with the pharmacological testing.

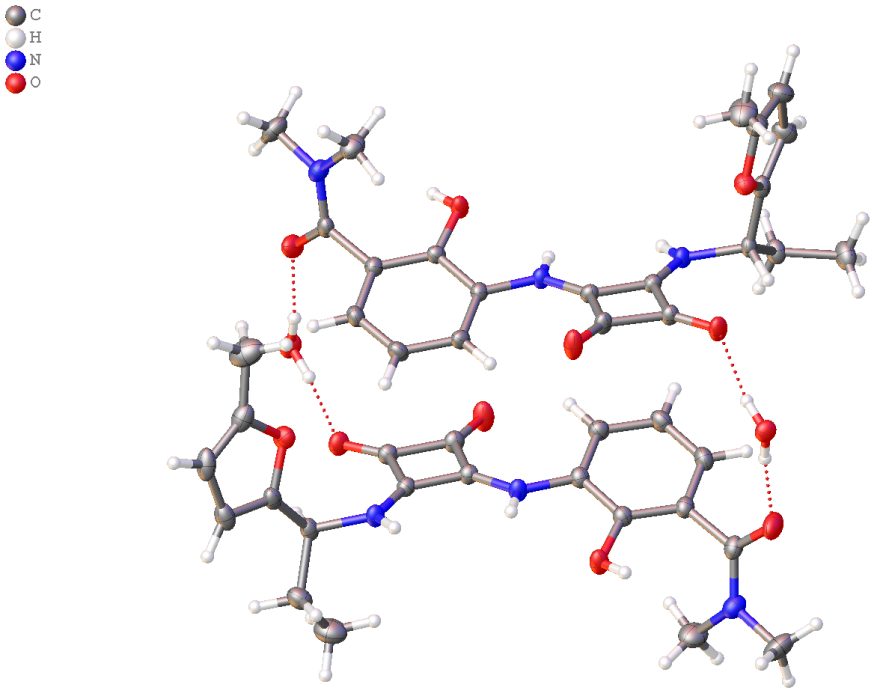

Figure 2.1: Crystal structure of compound **24** (performed by Stephen Argent, Crystallography Service Manager, School of Chemistry, University of Nottingham).

2.2 Pharmacological analysis of compound activities using CXCR2 mini G and arrestin recruitment assays

The pharmacological activities of compounds **2**, **8**, **11** and **24**, needed to be evaluated in order to identify a suitably potent compound to choose as congener for the fluorescent ligand library. For this reason, the compounds were tested in a NanoBiT (NanoLuc Binary Technology) Luciferase complementation assay[244] to report effects on agonist-induced CXCR2 recruitment of a synthetic mini Gα protein[245,246] or β-arrestin2. The Promega NanoBiT complementation methodology is an example protein-fragment complementation assay (PCA), used widely to study protein interactions.[244] This assay employs an engineered luciferase derived from a deep sea luminous shrimp[247], NanoLuc (Nluc), which produces bright and sustained luminescence while being suitably small and stable.[244] These valuable qualities make this enzyme ideal for use in physiologically relevant assays which evaluate protein interactions since the enzyme itself is less likely to sterically affect the fusion partner or influence the affinity and association kinetics of the interacting proteins.[244] In NanoBiT complementation, the interaction between the receptor of interest and an effector protein (mini G protein or β-arrestin2) by the proximity complementation of the two NanoLuc luciferase fragments, Large BiT (LgBiT) and a short Small BiT (SmBiT) peptide. This allows the regeneration of the enzyme which is therefore able to oxidise its substrate and to generate luminescence, which is measured as an indicator of receptor functional activity. In the system that we have used for our assays, stable cell lines in HEK cells have the *C* terminus of human CXCR2 tagged with the Large BiT (LgBiT) of the nanoluciferase and the mini $G_{\alpha}o$ protein or β-arrestin2 N terminally tagged with the Small BiT (SmBiT). Upon agonist ($CXCL8_{28\text{-}99}$) stimulation, the receptor recruits mini $G_{\alpha}o$ proteins or β-arrestin2. This allows reversible complementation of the LgBiT and SmBiT fragments to restore the activity of the luciferase enzyme. Furimazine is present as a substrate and NanoLuc luciferase converts it to furimamide emitting luminescence as an indicator of the response. The CXCR2-LgBiT construct behaves like wild type CXCR2. Based on

comparison with pharmacological assays performed previously, the addition of the NanoLuc luciferase fragment does not modify the potency of CXCL8.[41,182]

In these experiments, mini G proteins were employed instead of full length G proteins. Mini G proteins are the engineered GTPase domains of Gα subunits, originally developed for structural studies.[245,246] They retain the GPCR binding properties because they still contain the Gα binding interface of a normal Gα G protein domain but lack the capacity for guanine nucleotide binding or exchange, or interaction with Gβγ subunits. Mini G_s are small in size, stable and expressed well in cells[246] and, as they are recruited to the receptor from the cytoplasm, they produce less background signal with respect to full length membrane targeted G_α-proteins and can therefore be employed as useful biosensors of receptor activation.

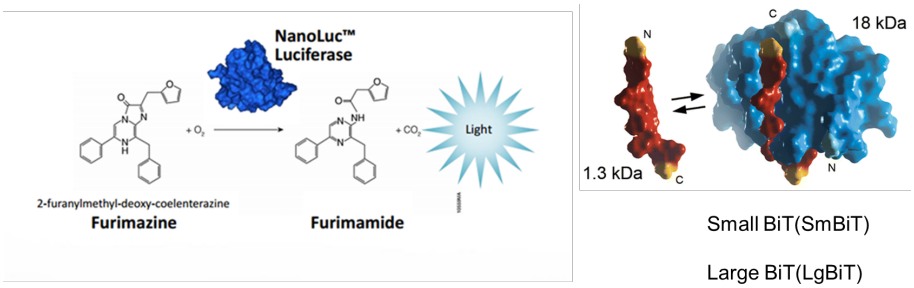

Figure 2.2: Furimazine conversion and NanoLuc complementation (image taken from Dixon *et al.* 2016).[244]

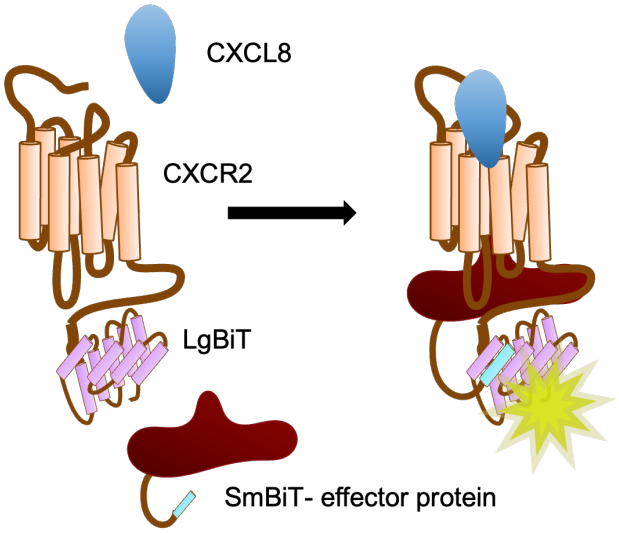

Figure 2.3: Cartoon representation of the NanoBiT complementation assay. CXCR2 tagged with LgBiT and effector protein tagged with SmBiT of NanoLuc luciferase. Stimulation of the receptor with CXCL8 results in β-arrestin2 recruitment, enzyme complementation and luminescence generation in the presence of furimazine as enzyme substrate. Effector protein : β-arrestin2 or mini G protein according to the cell line employed.

2.3 Pharmacological evaluation of the compounds through whole cell CXCR2 NanoBiT complementation assays

Compounds **2**, **8**, **11** and **24** were tested in the NanoBiT complementation assays presented in the previous section, in a whole cell setting, required to fully evaluate the functional activity of the NAMs, which are known to act intracellularly. In our assays, the HEK CXCR2/ mini $G_{\alpha}o$ or CXCR2/β-arrestin2 cell lines cells were pre-treated (1 hour at 37 °C) with the compounds prior to furimazine substrate loading and $CXCL8_{28\text{-}99}$ stimulation at different concentrations for 30 minutes. The pre-treatment time with the modulators was designed to allow equilibrium conditions for cell penetration and receptor binding. The data generated are shown in figure 2.4 and 2.5 (n = 5 for navarixin (**2**) and *S*-navarixin (**24**) and n = 1 for compounds **8** and **11**).

This represents Schild style analysis, in which the activity of the non-competitive NAM is reflected as reductions in CXCL8 potency and maximal response compared to control.

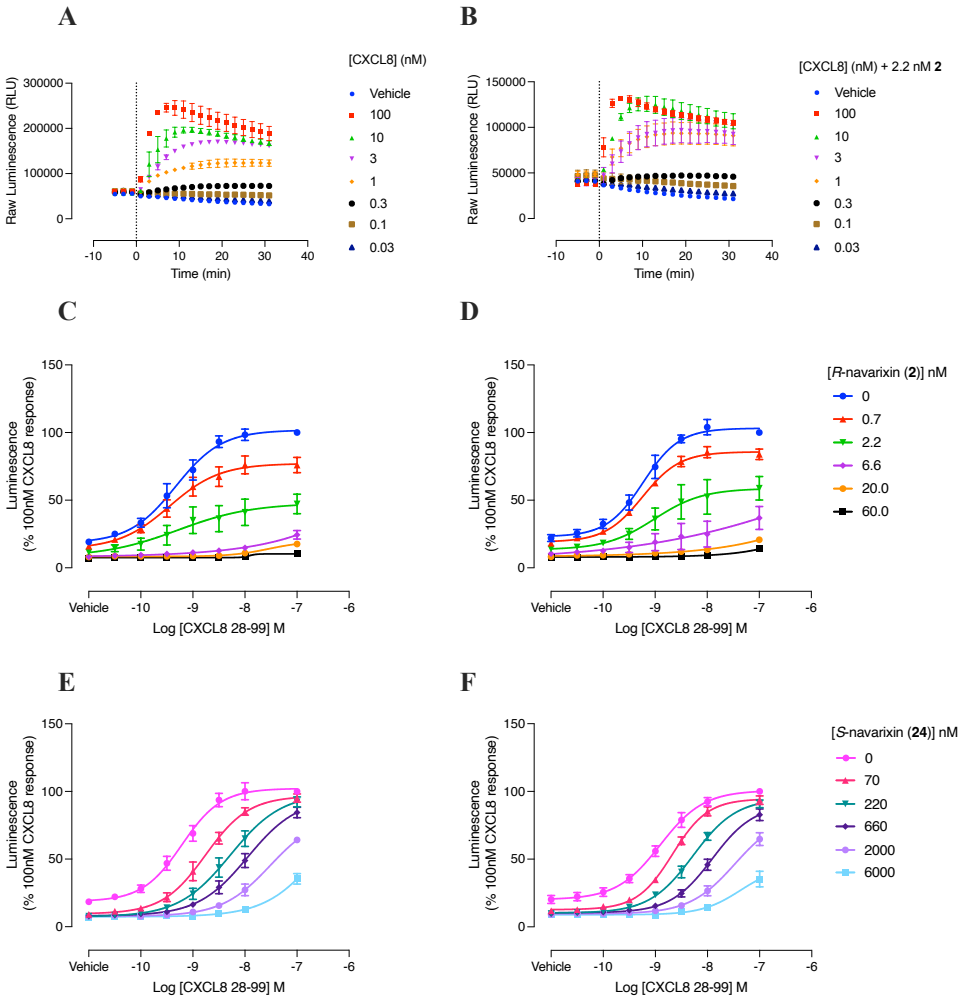

Figure 2.4: (A) $CXCL8_{28-99}$ concentration dependent changes in Nanoluciferase output in mini $G_{\alpha}o$ cell line over time. Data is raw luminescence data from an example experiment from 5 performed. Agonist addition at t = 0. (B) $CXCL8_{28-99}$ concentration dependent changes in Nanoluciferase output in mini $G_{\alpha}o$ cell line past incubation with a single concentration of **2** over time. Data is raw luminescence data from an example experiment from 5 performed. Agonist addition at t = 0. Concentration-response curves for $CXCL8_{28-99}$ in the NanoBiT complementation assay taken at 29-minute time point after agonist addition, with varying concentrations of (C) *R*-navarixin (**2**) in mini $G_{\alpha}o$ cell line, (D) *R*-navarixin (**2**) in β-arrestin2 cell line, (E) *S*-navarixin (**24**) in mini $G_{\alpha}o$ cell line and (F) *S*-navarixin (**24**) in β-arrestin2 cell line. The data shown are pooled from 5 individual experiments (mean ± SEM) which each experiment performed in technical duplicate.

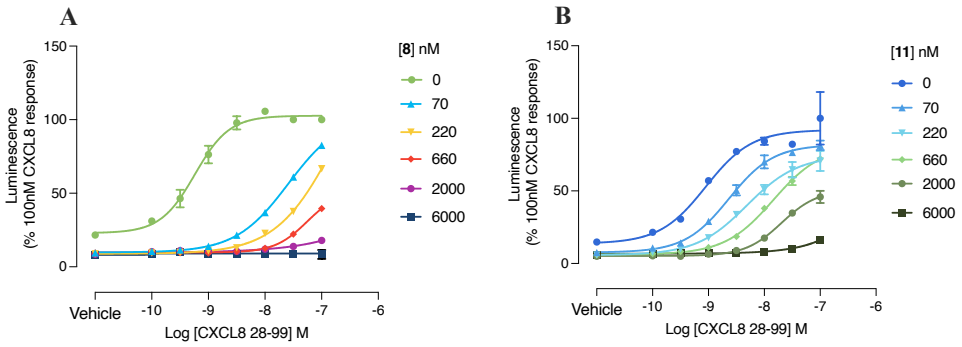

Figure 2.5: Concentration-response curves of $CXCL8_{28-99}$ taken at 29-minute time point of the luminescence read with varying concentrations of (A) compound **8** and (B) compound **11** in mini $G_{\alpha}o$ cell line. Data show a single experiment (mean ± SEM) reflecting duplicate.

Figure 2.4 (A-D) and figure 2.5 (A,B) show the CXCL8 concentration-response curves, taken at the 29-minute time point after agonist addition, in the absence and presence of varying concentrations of the modulators tested. All the compounds (**2, 8, 11, 24**) were tested in the mini $G_{\alpha}o$ cell line and *R*-Navarixin (**2**) and *S*-navarixin (**24**) were additionally tested in the β-arrestin2 cell line.

In the absence of NAM, the CXCL8 control pEC_{50} values were 9.28 ± 0.16 and 9.20 ± 0.09 respectively (n=5) in the mini $G_{\alpha}o$ and β-arrestin2 cell lines. Overall, the pre-treatment with the NAMs inhibited CXCL8 stimulated recruitment of the effector proteins, mini $G_{\alpha}o$ or β-arrestin2. A NAM effect on the basal luminescence response was also observed, consistent with the inhibition of constitutive CXCR2 activity, which is apparent for many GPCRs at high levels of expression in recombinant systems.[37,38,248] The action of each of the tested NAMs on the CXCL8 concentration response curves was characterized both by a rightward shift in agonist potency, and a decrease in the maximal response, characteristic of insurmountable antagonism. These insurmountable properties are consistent with a non-competitive mode of action of intracellular allosteric ligands, and / or a high affinity, slowly

reversible binding mode that prevents CXCL8 overcoming the antagonism within the time frame of its stimulation (non-equilibrium conditions), discussed below.

It should be noted that the *R*-navarixin (**2**) and *S*-navarixin (**24**) effect on the CXCL8 response was similar in both cell lines, detecting mini $G_{\alpha}o$ proteins or β-arrestin2, and therefore the NAM activity of the compounds is not biased towards receptor recruitment for a specific effector protein. This was expected considering the overlap of the G protein and arrestin binding site on the intracellular side of GPCRs[249], in close proximity to the NAM binding site.[45]

It should be also noted that the two navarixin enantiomers present a substantial difference in potency (Figure 2.4), 0.7 – 60 nM for *R*-navarixin (**2**) and 70 – 6000 nM for *S*-navarixin (**24**) respectively, which confirms the importance of the *R*-stereochemistry for the activity, in accordance with previously reported data.[166] The data are unambiguously related to the structure through provision of structure data and optical rotation measurements.

R-navarixin (**2**) was found to be the most potent compound tested, possessing a subnanomolar potency, as expected from literature reports of its affinity (K_D = 0.049 ± 0.004 nM)[41,139] and IC_{50} values in other CXCR2 signalling assays (2.6 ± 0.3 nM)[166]. Furthermore *R*-navarixin (**2**) produced pronounced insurmountable antagonism, as observed previously in other *in vitro* assays[41]. In contrast, effects of *S*-navarixin (**24**) required approximately 100 times the concentrations of **2** to be observed in the NanoBiT assays, consistent with the lower reported activity of the *S* enantiomers at this receptor.[166] In addition, the effect of *S*-navarixin (**24**) on CXCL8 concentration response curves showed a more surmountable profile, with a limited effect on CXCL8 Rmax, and shift in CXCL8 potency (pEC_{50}) with greater concentrations of the NAM. Given both *R*- and *S*-navarixin (**2**, **24**) are likely to target the same, allosteric binding site, dissimilarity in the pharmacological effect between enantiomers suggests a binding kinetic explanation, with non-surmountable behaviour of *R*-navarixin (**2**) arising from its much higher affinity and slower dissociation rate constant (k_{off}). Indeed, this slow k_{off} has been measured and previously proposed.[41,139] As discussed above, in this instance insurmountability in the

assay is generated by non-equilibrium conditions, as CXCL8 is unable to compete and reach a new equilibrium with NAM binding at CXCR2 over the time-frame of agonist stimulation. In order to have a clearer picture, the kinetics of the different NAMs need to be investigated more in depth. This can be achieved with the use of a fluorescent probe that binds in the same site as the NAMs, which will allow the direct measurement of the k_{off} of the compounds using bioluminescence energy transfer assays that follow probe binding kinetics in the presence and absence of unlabelled ligands.[199,250,251] Compounds **11** exerted effects with a similar potency and surmountable profile as *S*-navarixin (**24**) (Figure 2.5). However, compound **8**, in the n=1 test was substantially more potent than **11** or **24** in the assay, though appeared less potent than **2**. These data are supported by literature IC_{50} values for compounds **8** and **11** of 15 ± 1 nM and 17 ± 1 nM respectively.[166] They confirmed that the presence of the alkyl chain in **8** is tolerated (Table 2.1) and its substitution with a benzyl group in compound **11** results in a loss of CXCR2 affinity, also compared to the substitution with a methyl furan ring, present in *R*-navarixin (**2**), which was identified as crucial moiety for binding affinity.

It is conceivable that the compounds generated could interfere directly with the luciferase activity in the assay or have other target effects that for example prevent GPCR-β-arrestin association. They were tested in a similar NanoBiT complementation counter screen measuring β-arrestin2 recruitment by the β_2-adrenergic receptor (β2AR). The host cell line and configuration of the complementation fragments were the same as in the CXCR2 assay; the LgBiT tag was fused to the β2AR and the SmBiT tag was on β-arrestin2. Only limited inhibition of effector recruitment was observed at the highest concentration (60 nM, 6000 nM) of the compounds (**2** and **24**) for isoprenaline-stimulated recruitment of β-arrestin2 by β2AR (Figure 2.6). These results confirmed the CXCR2-related effect of the compounds.

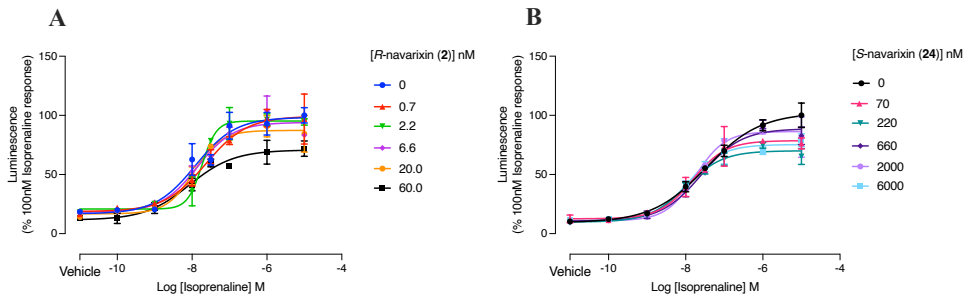

Figure 2.6: Concentration-response curves of isoprenaline-stimulated recruitment of arrestins by β2AR with varying concentrations of (A) *R*-navarixin (**2**) and (B) *S*-navarixin (**24**). Data show a single experiment (mean ± SEM) reflecting duplicate.

The pharmacological testing of the compounds in a functional NanoBiT complementation assay confirmed that the compounds synthesised are NAMs acting as insurmountable CXCR2 antagonists. They decrease the effector protein recruitment mediated by the agonist (CXCL8) in a dose-dependent manner and their effect has been shown to be receptor specific and not mediated by other off-target effects. Moreover, the importance of the *R*-stereochemistry for high affinity antagonism with greater insurmountability has been confirmed through the comparisons between the two navarixin enantiomers. Among the tested compounds, *R*-navarixin (**2**) showed remarkable potency at CXCR2, characteristic that qualifies the compound as an ideal congener for a library of fluorescent ligands. *R*-navarixin (**2**) was therefore chosen as congener and its structure needed to be evaluated for potential linker and fluorophore attachment points through chemical modifications that did not have a negative influence on its binding to the receptor. This led to the computational studies presented in the next chapter of this thesis.

Chapter 3. Computational studies

3.1 Introduction to homology modelling

There were no published CXCR2 crystal structures available via the Protein Data Bank[252–254] at the time of starting this project. Therefore, to perform the docking of the compounds and to visualize their binding poses and their interactions with the amino acid residues lining the binding pocket, it was necessary to build a model of the receptor. Homology modelling was the technique employed to generate a model of CXCR2. It is a computational structure prediction method based on the observation that protein three-dimensional structures are determined by their amino acid sequence and that proteins with a similar amino acid sequence, or homologous proteins, have a very similar three-dimensional (3D) structure.[255,256] Small or medium changes in amino acid sequence generally result in little variation of the 3D structure as the structural conformation of a protein is more highly conserved than its amino acid sequence.[257] On the other hand, proteins that have low sequence homology (<20%), can have a very different structure.[258] Homology modelling therefore constructs a representation of a target protein from its amino acid sequence and a crystal structure of a related homologous protein, called the template.[259] Homology modeling was compared to other 3D structural prediction methods such as threading methods and de novo methods[260] and it was found to be the most accurate between the analysed techniques.[257,260] Threading, similarly to homology modelling, is a template-based method[261] which is based on the principle that protein structures are more conserved than their sequences and therefore proteins can adopt the same fold even if there is no obvious sequence relationship.[262] Consequently, it is possible to generate three-dimensional structures of not evolutionarily related proteins.[260] In this method, the target sequence is assigned to templates with known folds and a set of scoring functions, based on physicochemical parameters, is employed to evaluate the optimal sequence-to-structure alignment for every trial template.[260] The limit of threading methods is that,

through the use of known folds as templates, it could be unable to predict the correct structure of the target if it adopts a novel fold.[260] On the other hand, de novo methods belong to the so called 'free-modelling' or 'template-free' methods[260] which generate 3D protein structures without the use of solved structures but based on the amino acid sequence' s physicochemical and thermodynamic properties. This method uses knowledge-based force fields as scoring functions to search the energy landscape and to find the in-silico protein conformation at the minimum of its potential energy.[260] The scoring functions rely on information on experimentally determined structures deposited in databases.[260] More recently, AlphaFold[263,264], an artificial intelligence (AI) system, has been developed by DeepMind and EMBL's European Bioinformatic Institute (EMBL-EBI). It predicts the 3D structure of a protein from its amino acid sequence with atomic accuracy[264] and the structures are stored in a public database (AlphaFold Protein Structure Database), freely available for the scientific community.[263]

Homology modelling consists of multiple steps: template selection, sequence alignment and correction, model building and optimization. The first step of the process is the identification of the template structure in the Protein Database (PDB)[265] using the target sequence of the desired protein. The Basic Local Alignment Search Tool (BLAST)[266,267] is a commonly employed tool in the search for a template as it provides sequence-sequence alignment between the query sequence and existing PDB sequences. In the selection of eligible templates to use for the next steps, various factors need to be considered: high sequence similarity of the template sequence relative to the target sequence, crucial for generating 3D structures with high accuracy, phylogenetic similarity, environmental factors (pH, solvent type), existence of bound ligand in the structure and the resolution of the experimental structure (R factor and resolution for crystal structures and number of restraints per residue for an NMR structure).[256,261] Additionally, if the purpose of the model generated consists, for example, in ligand docking, a template containing a ligand crystallized in a similar pocket as the target ligand to dock would be preferred. Therefore, the purpose of the model generated would be another criteria for choosing a template over other characteristics.[261] The use

of several templates instead of a single one would increase the accuracy of the model[268], especially when the template-target sequence identity is below 40%[269], but the advantage of using multiple templates disappears above 40% sequence identity.[268] Moreover, most modelling programs do not accept more than one template for model building.[268] Once the template has been identified, the pieces of software used to perform homology modelling produce an alignment of the amino acid sequences of the target and the template proteins which is then used, in combination with the template structure, to generate a structural model of the target protein. The quality of the target-template sequence alignment is crucial to determine the quality of the homology model since most of the errors are generated in this fundamental step and from a poor template selection.[270] The subsequent step consists in the generation of the homology model and this can be achieved through different procedures.[260,271] Rigid-body assembly method (SWISS-MODEL[272]), consists in building the model from the parts of the target structure that align with the template sequence, while de novo methods or a structural database of known protein structures are used to model the fragments that do not align with the template.[260] This method is also used, in combination with stepwise evolutionary mutations on the template until the sequence corresponds to the one of the target protein, in the artificial evolution method.[260] The spatial restraint method builds a model by fulfilling restraints, such as bond angles and lengths, which derive from the template structure.[260] In the segment matching method, the target structure is divided into short segments which are then searched in a database of known structures for matching segments and then selected based on sequence identity, geometrical and energetic considerations. The model is then built through placing these segments on a guiding structure of the target based on the alignment.[260] The generated model then needs to be refined with a particular focus on the correct orientation of the side chains[260] and on loops structures, regions of the target sequence that play crucial structural roles but often do not have homologous regions in the template.[260] Loops are generally modelled using a combination of database-search and de novo conformational-search approaches.[260,273] Finally, the quality of the model is assessed and this can be achieved through the use of specialized programs[274–

[276], through reference to experimental data present in the literature, such as mutagenesis studies, and through the use of computational methods, for example docking studies, which could assess the binding of a known ligand in the binding site of the model.[260]

3.2 CXCR2 homology model

3.2.1 Homology model generation

The aim of this project, as introduced before, consists in the synthesis of fluorescent probes and this is achieved through the modification, via linker and fluorophore attachment, of a known CXCR2 NAM. In order to be able to understand the point of attachment of the new fluorescent moiety in the congener NAM, it is crucial to visualize how such allosteric modulator bind the receptor of interest and which group of the modulator are actively involved in the interaction with the receptor and therefore essential for binding and which parts, on the contrary, can be modified by linker and fluorophore addition without a loss in binding affinity. The absence of a crystal structure made necessary to build a model of the receptor of interest making use of the homology modelling technique. The initial step in the generation of a model of CXCR2 was the template identification through a BLAST (Basic Local Alignment Search Tool) search of protein structures in the Protein Data Bank. This sequence similarity search program, used to search a sequence database for matches to a query sequence[267], found several potential templates with a reasonable sequence similarity to CXCR2. CXCR1 (PDB: 2LNL), CCR9 (PDB: 5LWE), CXCR4 (PDB: 3OE8), CCR5 (PDB: 6AKY) and AT2 (PDB: 6DO1) were selected as templates according to their relatively high homology with the query sequence (Table 3.1). Homology is used to define common structural characteristics and common spatial distribution of proteins with a common evolutionary origin. Sequence identity, on the other hand, is the number of characters which match exactly between two sequences.

Table 3.1

Template receptor (PDB)	% Homology with CXCR2	Experiment type
CXCR1 (2LNL)	86	NMR
CCR9 (5LWE)	39	X-ray diffraction (resolution:2.80 Å)
CXCR4 (3OE8)	38	X-ray diffraction (resolution:3.10 Å)
CCR5 (6AKY)	34	X-ray diffraction (resolution:2.80 Å)
AT2 (6DO1)	33	X-ray diffraction (resolution:2.90 Å)

The percentage homology should not be the only property considered during the selection of the template as other properties of the templates could be crucial for a better homology model generation. In our case, CCR2 (PDB: 5T1A) and β2AR (PDB: 6N48) were included as well in the template list, since they possess a similar intracellular allosteric binding pocket, even though their overall sequence similarity to CXCR2 is below 30%. Moreover, it should be specified that the structure of CXCR1 is NMR based, therefore there were 10 conformations present, each of them used to generate a different homology model. Once the list of templates was generated, 37 homology models of CXCR2 were built using its amino acid sequence and the crystal structures of the template proteins previously selected employing two different homology modelling programs, Swiss Model[272,273,277] and Prime[278] from the Schrödinger suite. The generation of a large variety of models and their comparative analysis allowed outliers/errors, that may arise from an inaccurate target-template alignment, to be spotted more easily.

The subsequent step was the performance of a clustering analysis of the homology models generated. Cluster analysis a statistical data mining tool

whose use is to divide data into groups or 'clusters' that share similar properties and characteristics.[279–281] A particular algorithm sorts the object in the dataset into separate groups according to a metric of similarity between them.[279] In the generated groups or clusters, the degree of similarity between the objects belonging to the same cluster will be greater than the similarity between two objects found in two different clusters.[279] This analysis allowed us to understand the similarities and differences between the CXCR2 homology models generated and to eliminate unnecessary duplicates before performing the docking of the compounds. The clustering analysis conducted, is based on the superposition of the α-carbons of selected amino acid residues of the models and the measure of their average distance through the Root Mean Square Deviation (RMSD).[279,282,283] This was achieved with the use of an in-house python script utilizing mdtraj that generated a graph where the models are positioned according to their similarity: the lower the RMSD the more similar the models are. Two superposed points on the graph therefore represent two identical models and points that are close to each other on the graph represent models that can be considered duplicates. From the emergence of actual clusters of points in the graph, it is possible to select one model that could represent all the models present in the same cluster that will subsequently be employed for the following docking step. The amino acid residues taken into consideration in the clustering analysis were the ones considered crucial for the binding of the negative allosteric modulators (NAMs), previously reported in mutagenesis studies.[139] These comprised the residues present in the region near the *C*-terminal between Glu300$^{8.29}$ and Lys320$^{8.49}$, in the ICL3-TM6 between Gly244$^{6.28}$ and Val256$^{6.40}$ and in the ICL1-TM2 between Val78$^{2.34}$ and Leu90$^{2.46}$.

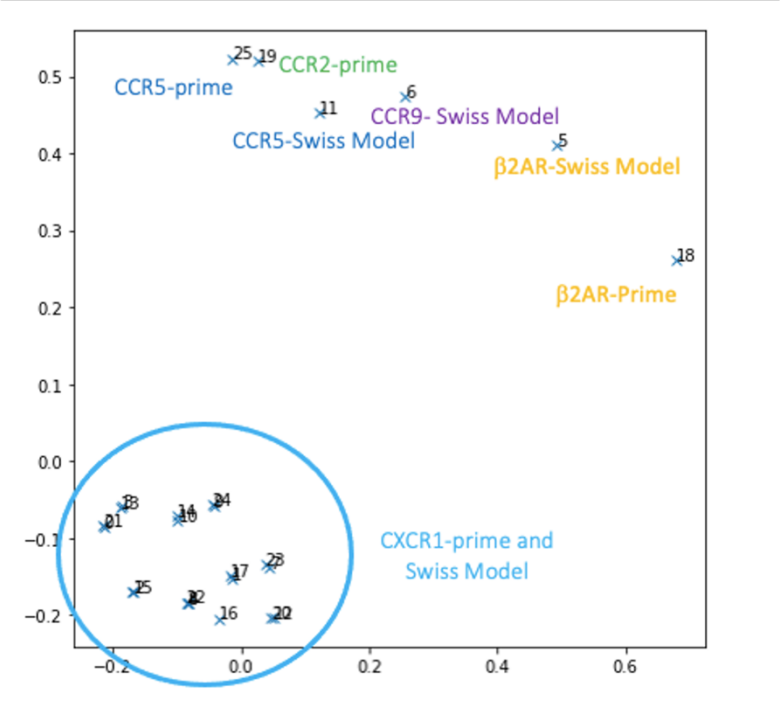

Figure 3.1: Clustering analyses of CXCR2 homology models. X-axis: embedding dimesion1. Y-axis: embedding dimension 2. Each model is identified with a number and the distance between the models represents the RMSD. The templates and the pieces of software used to generate them are reported in the figure.

The graph generated (Figure 3.1) allowed us to group the different homology models and to select 9 models to use for the docking studies.

3.2.2 Molecular docking into CXCR2 homology model

The molecular docking of the NAMs in the selected models was performed using Maestro from the Schrödinger suite. The grid used had its centroid between Ala249$^{6.33}$ and Lys320$^{8.49}$ and it comprised all the residues involved in the binding according to the mutagenesis studies. The compounds were docked both selecting bonding with Lys320$^{8.49}$ as a constraint or without any constraint. This residue was chosen as a constraint as it is reported to be crucial for NAMs binding to the receptor[139] and the constraint was removed

to verify if the docked compounds were in effect interacting with Lys320$^{8.49}$. The binding poses of the compounds docked into the homology models were evaluated considering several factors. Firstly, how deeply the furan ring was inserted into the binding pocket, then the number of interactions that the compounds were making with crucial residues of the receptor present in the mutagenesis studies, the binding score of the most selective compound, *R*-navarixin (**2**), compared to the other NAMs and the presence of a distinction between the *R* and *S*-navarixin (**2**, **24**) enantiomers, reported to have notably different affinity for CXCR2.[166] Considering all the above parameters, the model that most accurately represented *R*-navarixin (**2**) binding CXCR2 was the one built using CCR9 (PDB: 5LWE) as template.

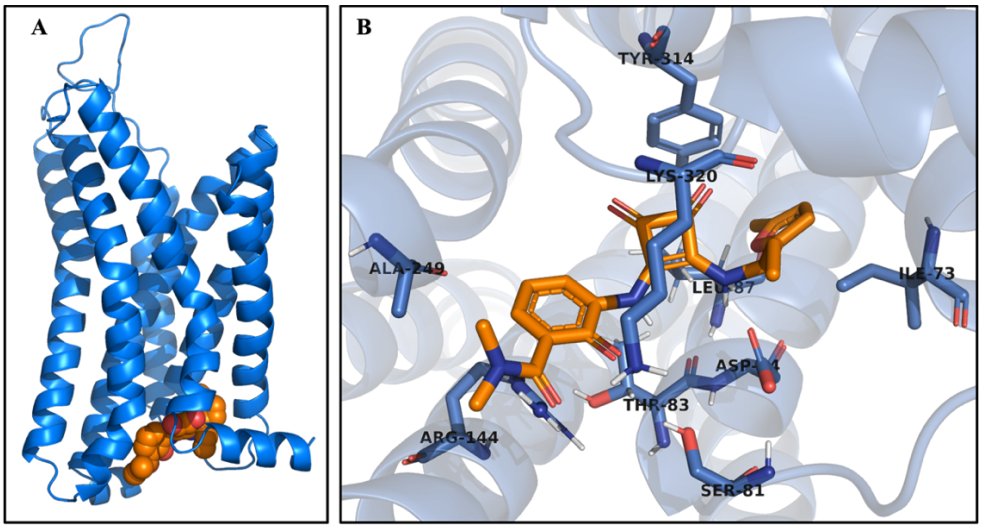

Figure 3.2: (A) Side view of CXCR2 homology model built using CCR9 (PDB: 5LWE) as template with *R*-Navarixin (**2**) (orange). (B) View from the bottom of the receptor of *R*-Navarixin docked pose (**2**) (orange). Crucial receptor residues lining the pocket are shown as blue sticks. Image generated with PyMOL.

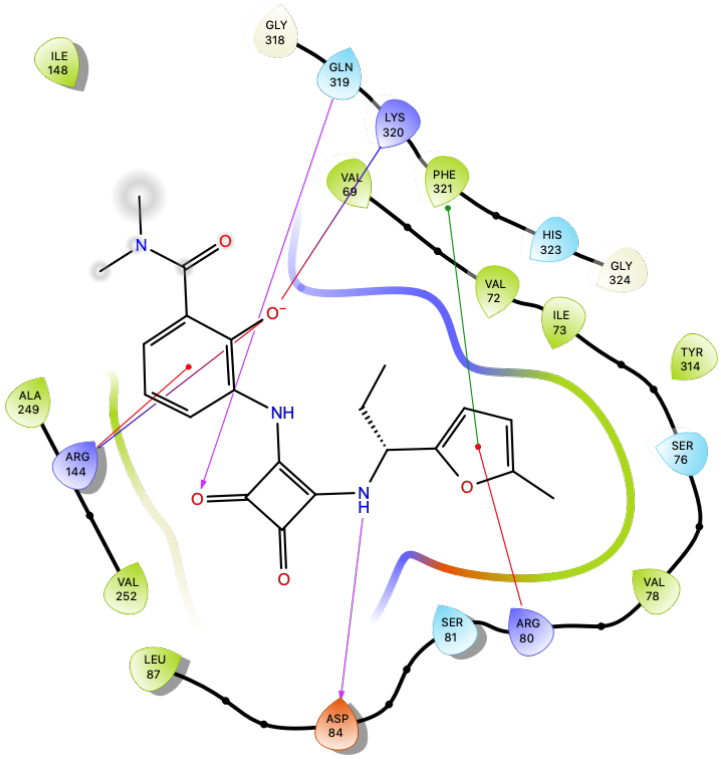

Figure 3.3: *R*-Navarixin (**2**) interactions with CXCR2 homology model built using CCR9 (PDB: 5LWE) as template. Image generated with Maestro from the Schrödinger suite.

The chosen homology model of CXCR2 exhibited several of the features crucial for *R*-navarixin (**2**) binding. As shown in figure 3.2 and 3.3, the methyl-furan part of the molecule is deeply inserted into the binding pocket and *R*-navarixin (**2**) formed interactions with all the crucial amino acid residues reported in the mutagenesis studies such as Phe321$^{8.50}$, Lys320$^{8.49}$, Gln319$^{8.48}$, Arg144$^{3.50}$ and Asp84$^{2.40}$ and the pocket where it binds is lined with other residues present in the mutagenesis studies including Tyr314$^{8.43}$, Ser81$^{2.37}$, Val78$^{2.34}$ and Ser76$^{2.32}$.^{139} Additionally, the docking score of *R*-navarixin (**2**), generated by the docking software, is adequate and, crucially, the compound is ranked first between the docked compounds (**2**, **8**, **11**, **24**, data not shown), indicating that its binding to the receptor is stronger than the one of the other compounds docked into this model. On the negative side, this model could not provide rationale which could justify the significant diversity

in potency between the enantiomers, not showing any differences in their binding poses.

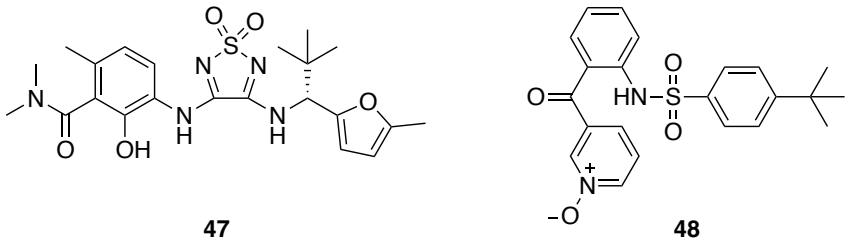

47 **48**

Figure 3.4: Structures of Cmp2105 (**47**) on the left and structure of Vercirnon (**48**) on the right, intracellular allosteric modulators of CCR7 and CCR9 respectively.

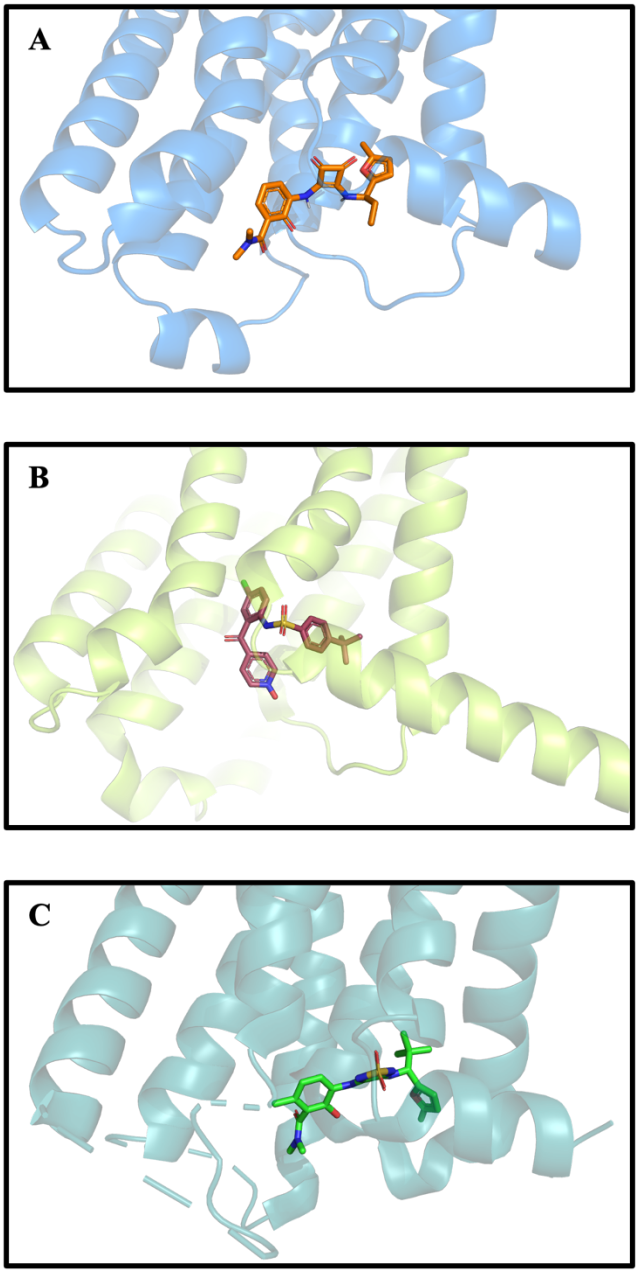

Figure 3.5: Homology modelling of the binding. Side view of (A) CXCR2 homology model built using CCR9 (PDB: 5LWE) as template with *R*-Navarixin (**2**) (orange), (B) CCR9 (PDB: 5LWE) with vercirnon (**48**) (pink) and (C) CCR7 (PDB: 6QZH) with Cmp2105 (**47**) (green). Image generated with PyMOL.

To further evaluate the CXCR2 homology model selected, the binding pose of *R*-navarixin (**2**) in the homology model was compared to the one of Cmp2105 (**47**) in CCR7 (PDB: 6QZH)[145] (Figure 3.5.C) and the one of

vercirnon (**48**) in CCR9 (PDB: 5LWE)[142] (Figure 3.5.B), both published structures with a modulator crystallized in. Cmp2105 (**47**) and vercirnon (**48**) are intracellular allosteric modulators of their respective receptors, that bind in intracellular pockets near the *C*-terminal region of their receptor, similar to the one where *R*-navarixin (**2**) binds. Cmp2105 (**47**) possess a thiadiazole dioxide core, vercirnon (**48**) a sulfonamide core while *R*-navarixin (**2**) has a cyclobutenedione core.[145] As shown in figure 3.5 the three NAMs (**2**, **47**, **48**) present comparable binding poses into their respective receptors, and this further supports the choice of the CXCR2 model chosen since homology modelling of the binding can be seen for receptors with intracellular allosteric modulators.

The chosen homology model, built using CCR9 as template, has contributed profoundly to the initial design of the fluorescent ligand series in the absence of a published X-ray crystal structure. The docking studies of *R*-navarixin (**2**) in the homology model of CXCR2 showed the presence of crucial functional groups in the compound that cannot be modified or removed without a loss in binding and activity. The groups essential for binding are the methyl-furan arm, the vinylogous amides and the ketone oxygens of the central cyclobutene-dione core, the phenol hydroxyl group and the ketone oxygen of the dimethylamide side of the molecule. On the other hand, the dimethyl-amide part of *R*-navarixin (**2**) could be modified and elongated with the attachment of a linker, since it is shown to protrude from the binding pocket, not establishing any crucial interaction with the receptor.

3.3 Comparison between molecular docking into CXCR2 crystal structure (6LFL) and into CXCR2 homology model

In 2020, the crystal structure of CXCR2 with a NAM (00767013, **5**) bound (PDB: 6LFL) was published.[45] This allowed us to compare the generated docking of *R*-navarixin (**2**) in the homology model of CXCR2 with the crystal

structure of the receptor. It must be pointed out that although 00767013 (**5**) and *R*-navarixin (**2**) possesses a very similar structure having both a 3,4-diamino-cyclobutenedione core, they have two major differences. Firstly, 00767013 (**5**) possess a 3-hydroxypyridine while *R*-navarixin (**2**) has a phenol moiety, secondly, the substituents on the furan ring are a 4-isopropyl in 00767013 (**5**) and a 5-methyl in *R*-navarixin (**2**). These variations in the two compounds should be considered as they may generate some changes in the relative binding poses into the receptor.

Firstly, the structures of 6LFL with compound **5** bound and the homology model of CXCR2 with compound **2** docked in were superimposed (Figure 3.6).

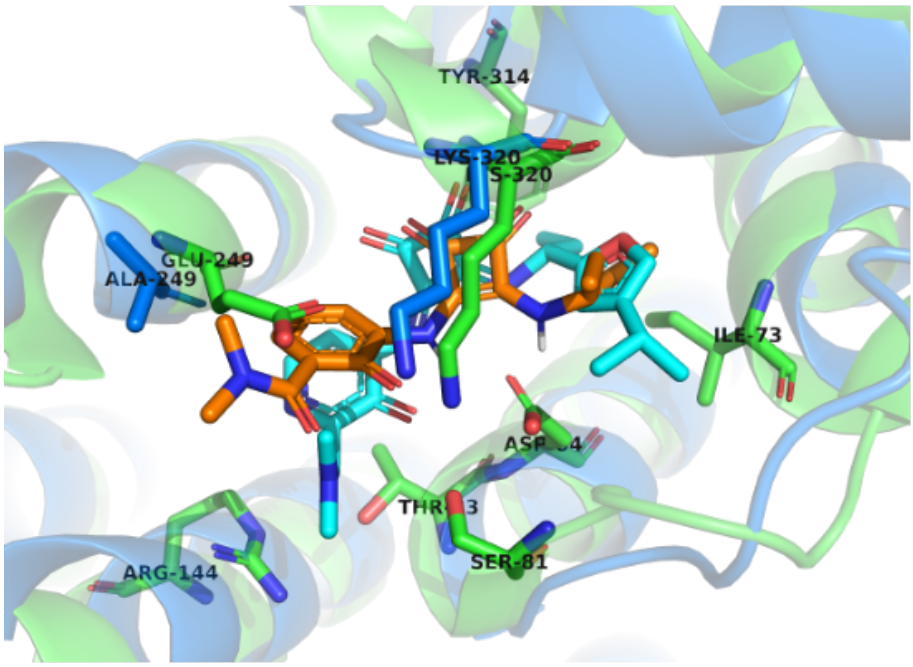

Figure 3.6: View from the bottom of the receptor of the superimposition of CXCR2 crystal structure (PDB: 6LFL) (green ribbons) with 00767013 (**5**) (cyan) and CXCR2 homology model with CCR9 as template (blue ribbons) with docked *R*-navarixin (**2**) (orange). Crucial receptor residues lining the pocket are shown as green sticks. Residues that differ between 6LFL and CXCR2 homology model are shown as green and blue sticks respectively for 6LFL and CXCR2 homology model (Glu249$^{6.33}$, Ala249$^{6.33}$ and Lys320$^{8.49}$). Image generated with PyMOL.

The superimposition of CXCR2 (PDB: 6LFL) and the selected homology model of CXCR2 with their respective ligands was performed to assess how different the two structures were and how the ligands were positioned in the respective binding pockets. From figure 3.6, it can be appreciated that the two receptor structures are nicely overlapped, and the binding poses of the two NAMs are overall similar. They differ in the positioning of the hydroxyl group respectively of the 3-hydroxypyridine in compound **5** and of the phenol in *R*-navarixin (**2**) (Figure 3.6). This may be due to the slightly different positioning of residue Lys320$^{8.49}$ in the two structures, closer to TM7 in CXCR2 crystal structure than in the homology model, since this residue makes a hydrogen-bond with the hydroxyl group of both compounds. Moreover, the orientation of the furan ring is dissimilar, even though the interactions made with the amino acid residues lining the pocket, such as Ile73$^{2.29}$, are comparable. This may be explained considering the different substituents on the furan ring, 4-isopropyl in 00767013 (**5**) and 5-methyl in *R*-navarixin (**2**), which may sterically influence the binding in a dissimilar way for the two compounds. It must be noticed that, in order to crystallize CXCR2 (PDB: 6LFL), three mutations were introduced into the sequence, including A249E[45]. The change of Ala249$^{6.33}$ into Glu249$^{6.33}$ may influence the interaction of the modulator with the receptor since this residue is lining the binding pocket, although it does not make any interaction with the ligand (Figure 3.6).

To validate the docking methodology previously reported employed with the homology model, compound 00767013 (**5**) was redocked with no constraints selected, using Maestro from the Schrödinger suite, into the original CXCR2 x-ray crystal structure (PDB: 6LFL), in essentially exactly the same binding pose (Figure 3.7). The grid used had its centroid between Glu249$^{6.33}$, reported mutation of Ala249$^{6.33}$, and Lys320$^{8.49}$.

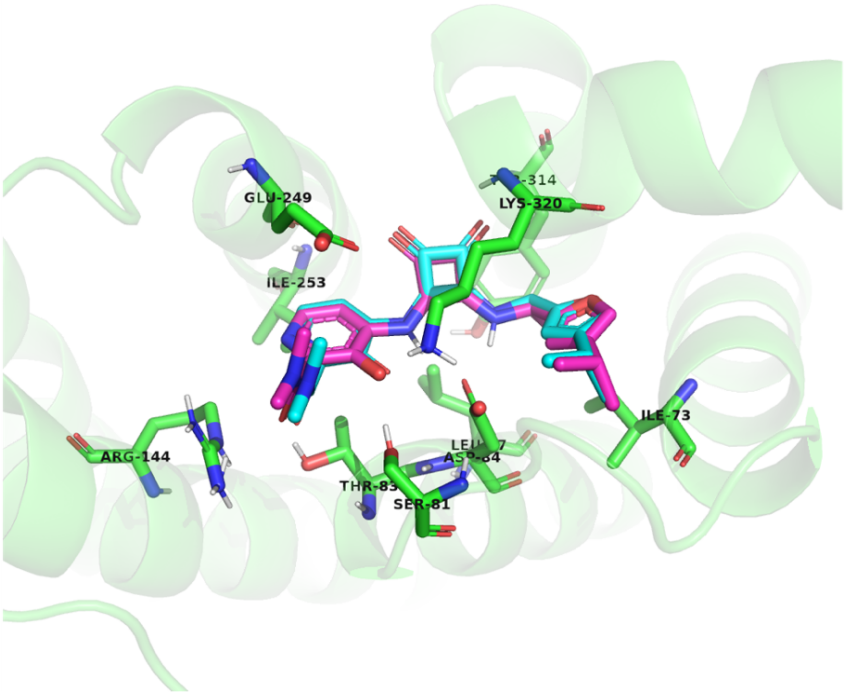

Figure 3.7: View from the bottom of the receptor of crystallographically determined (cyan) and redocked (magenta) poses of 00767013 (**5**) in the crystal structure of CXCR2 (PDB ID: 6LFL). Crucial residues lining the pocket are shown as green sticks. Image generated with PyMOL.

This validated docking method was then used to dock *R*-Navarixin (**2**) in CXCR2 crystal structure (PDB: 6LFL). The docking was performed with and without selecting interaction with Lys320$^{8.49}$ as a constraint. This did not make any difference in the binding pose or in the interactions with the receptor, meaning that the bond with Lys320$^{8.49}$ would be present even without its selection as constraint.

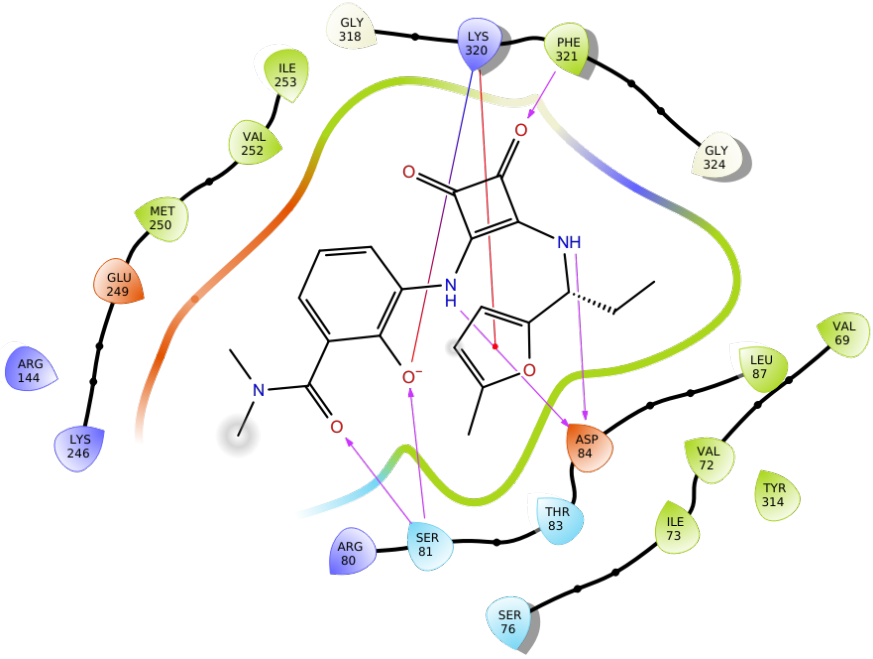

Figure 3.8: Key interactions between *R*-navarixin (**2**) and CXCR2 (PDB: 6LFL). Image generated with Maestro from the Schrödinger suite.

As shown in figure 3.8, *R*-navarixin (**2**) establishes a large number of interactions with CXCR2. The amino groups of the cyclobutene-dione core form hydrogen bonds with Asp84$^{2.40}$, the squaramide ketone oxygens form hydrogen bonds with Phe321$^{8.50}$ which interacts as well with the *R*-ethyl group, the furan ring establishes hydrophobic interactions with Arg80$^{2.36}$, Ile73$^{2.29}$, Val72$^{2.28}$ and Lys320$^{8.49}$. The hydroxyl group in the phenol moiety forms hydrogen bonds with Lys320$^{8.49}$ and Ser81$^{2.37}$ and the ketone oxygen of the left arm of the molecule makes hydrogen bond with Ser81$^{2.37}$. The comparison between the interactions of *R*-navarixin (**2**) with CXCR2 (PDB: 6LFL) (Figure 3.8) and the interactions formed between **2** and the homology model of the receptor generated (Figure 3.3) show several similarities and some differences. The hydrogen bond that Asp84$^{2.40}$ forms with the squaramide amino groups, the hydrophobic interactions between the furan ring and the residues lining the pocket and the interaction of Lys320$^{8.49}$ and the phenol moiety are maintained in both crystal structure and homology modelling docking poses. Differently, Phe321$^{8.50}$ hydrogen bond with the squaramide ketone oxygen of *R*-navarixin (**2**) in CXCR2 crystal structure

(PDB: 6LFL) while it interacts with the furan ring in the homology model. Ser81$^{2.37}$ shows interactions with **2** only in CXCR2 crystal structure and, conversely, Arg144$^{3.50}$ interacts with the phenol ring of *R*-navarixin (**2**) in CXCR2 homology model. On the whole, the binding poses of *R*-navarixin (**2**) in CXCR2 crystal structure and in the homology model are similar and the residues lining both binding pockets are identical.

To further evaluate the binding of the NAMs, *R*-navarixin (**2**) and 00767013 (**5**) both bound to CXCR2 (PDB: 6LFL) were superimposed (figure 3.9.A).

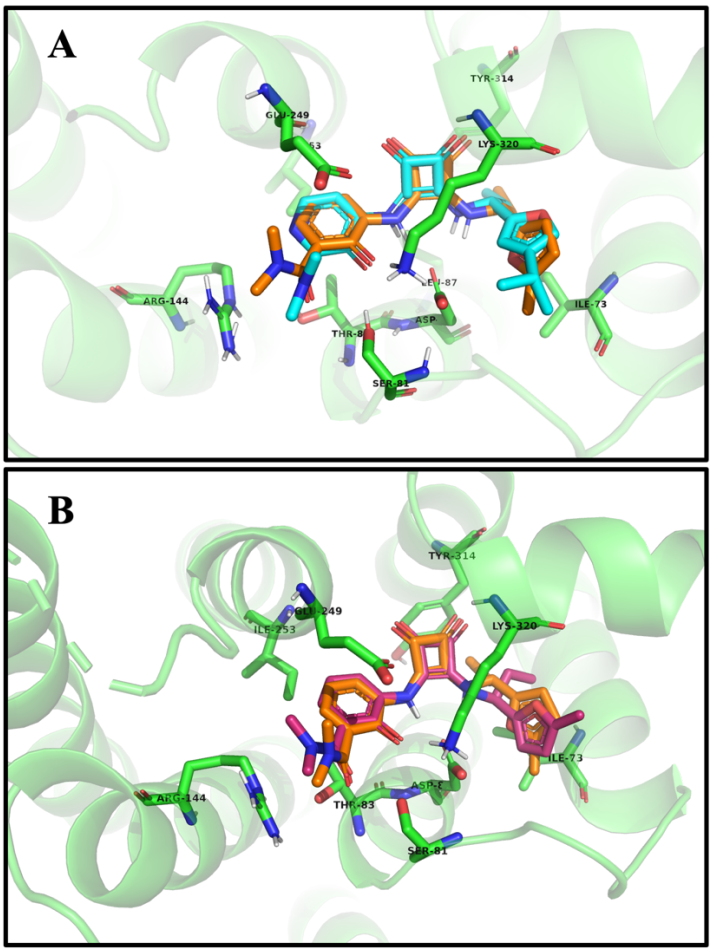

Figure 3.9: View from the bottom of the receptor of (A) docked pose of *R*-Navarixin (**2**) (orange) and crystallographically determined pose 00767013 (**5**) (cyan) in the the crystal structure of CXCR2 (PDB ID: 6LFL) and (B) docked poses of *R*-Navarixin (**2**) (orange) and *S*-Navarixin (**24**) (pink) in the the crystal structure of CXCR2 (PDB ID: 6LFL). Crucial residues lining the pocket are shown as green sticks. Image generated with PyMOL.

The 3,4-diamino-3-cyclobutene-1,2-dione core of the two compounds is positioned in CXCR2 in a similar manner. The differences in binding mainly reside in the parts of the molecules that possess different groups. Firstly, the substituents on the furan ring, 4-isopropyl in 00767013 (**5**) and 5-methyl in *R*-navarixin (**2**), may be the reason why the ring is flipped since they have a different steric influence. Secondly, the positioning of the dimethyl-amide left arm of the molecule may differ due to the different nature of 3-hydroxypyridine and phenol moieties. Overall, through the generation and evaluation of the homology model of CXCR2 and its comparison with the recently published crystal structure (PDB: 6LFL), it has been shown that a carefully, but artificially constructed receptor model could be remarkably similar to the actual real structure.

S-navarixin (**24**) was also docked in CXCR2 crystal structure (PDB: 6LFL) to try to elucidate the difference in potency and binding affinities between the navarixin enantiomers that the homology model could not predict. As shown in figure 3.9.B, the binding pose of the two compounds is comparable but the docking score calculated by the docking software (Glide in Maestro from the Schrödinger suite)[284–286], on the contrary, is dissimilar. The docking score is a predicted value of the free energy of protein-ligand binding. The score function is used to rank compounds in order of binding strength, identifying a more negative score with a stronger receptor binding and vice-versa. In particular the GlideScore function is an empirical scoring function that accounts for the physics of the binding process including terms such as hydrogen bonds, liphophilic interactions, rotatable bond penalties, contributions from protein-ligand coulomb-vdW energies[284] and terms that accounts for the displacement of water molecules by a ligand with many lipophilic protein atoms in close proximity, known as hydrophobic enclosure.[286] The docking score is equal to the Glide score with applied Epik state penalties, therefore the first one is more accurate to assess ligand docking.

The docking score for *R* and *S*-navarixin (**2, 24**) are -8.6 kcal/mol and -7.3 kcal/mol respectively. A log difference in docking score could be considered significant to provide a reason for the higher binding affinity of *R*-navarixin

(**2**). In fact, for the *S* enantiomer (**24**), assuming a conformation convenient for binding results in an energy loss, reflected in a higher docking score (the lower the docking score, the strongest the binding) and this energy penalty could explain the different binding affinities of the two compounds.

3.4 Molecular docking into humanized CXCR2 crystal structure (6LFL)

The previously presented mutation of Ala249$^{6.33}$ to Glu249$^{6.33}$, inserted to make the crystallization of CXCR2 possible[45], may influence the binding of the NAMs to the receptor. This residue is close to the binding site, and it lines the pocket where the ligands bind. Moreover, since the mutation of Ala249$^{6.33}$ to Leu during mutagenesis studies resulted in a 280-fold loss in affinity of *R*-navarixin (**2**)[139], the impact of this mutation must be further evaluated to understand if the mutated receptor can be used for accurate docking studies. To understand the impact of this mutation, residue 249 of CXCR2 crystal structure (PDB: 6LFL) was mutated back to alanine, using Maestro from the Schrödinger suite. *R*-navarixin (**2**) was then docked into a this more humanized sequence of the receptor following the same docking methodology described and applied for the previous docking studies. The binding pose of *R*-navarixin (**2**) and its interaction with CXCR2 did not change with the presence of Ala249$^{6.33}$. This further validate the docking methodology used and confirmed that the mutation A249E does not influence the binding of the NAMs to the receptor. Moreover, the humanized CXCR2 structure can be used for future docking studies as a more accurate representation of the native receptor.

3.5 Conclusions and molecular docking of modified CXCR2 intracellular allosteric antagonists

In this chapter was presented the generation and evaluation of the homology model of CXCR2, its comparison with the recently published crystal structure (PDB: 6LFL) and the molecular docking of a potent CXCR2 NAM, *R*-navarixin (**2**) into both structures. The aim of the docking studies was to understand which parts of *R*-navarixin (**2**) could be modified to be able to synthesize fluorescent probes for the study of this receptor. The binding pose and interactions of *R*-navarixin (**2**) with the receptor were practically identical in all the receptor model used for binding, which included the CXCR2 homology model, the published CXCR2 X-ray crystal structure (PDB: 6LFL) and its humanized version with Ala249$^{6.33}$. The furan moiety, squaramide moiety, phenol group and the carbonyl oxygen of the *N*-*N*-dimethyl amide part of the molecule show interactions with different amino acid residues in the binding pocket such as Phe321$^{8.50}$, Lys320$^{8.49}$, Gln319$^{8.48}$, Arg144$^{3.50}$ and Asp84$^{2.40}$ presented as important residues for NAM binding in mutagenesis studies[139]. These crucial groups could therefore not be removed or modified without a significant loss in binding affinity. Conversely, in all models employed for docking, the *N*-*N*-dimethyl amide moiety does not appear critical for receptor binding as it is shown to protrude from the pocket towards the cytosol without establishing any crucial interactions with CXCR2. This side can therefore be a suitable side for attachment of a linker moiety and associated fluorophore.

The *N*-*N*-dimethylamide side of *R*-navarixin (**2**) has been identified as an appropriate point alterable with linker attachment. Therefore, the following step consisted in the molecular docking of modified versions of the congener into the humanized CXCR2 crystal structure (Ala249$^{6.33}$), employing the docking methodology described and validated previously in this chapter.

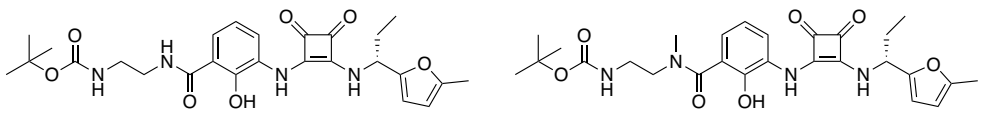

49a 49b

Figure 3.10: Structures of docked congeners compound **49a,b**.

The compounds chosen (Figure 3.10) had a short Boc-protected ethylenediamine linker instead of the *N*-*N*-dimethylamide of *R*-navarixin (**2**). The two compounds differ for the amide methylation as compound **49a** is unmethylated while compound **49b** is the methylated version. The amide methyl group will be kept in a series of congener in order to check whether a tertiary amide may influence the compounds interaction with the receptor and their activity the with respect to a secondary amide, considering that *R*-navarixin (**2**) presents a tertiary amide, which may have a beneficial effect on receptor binding.

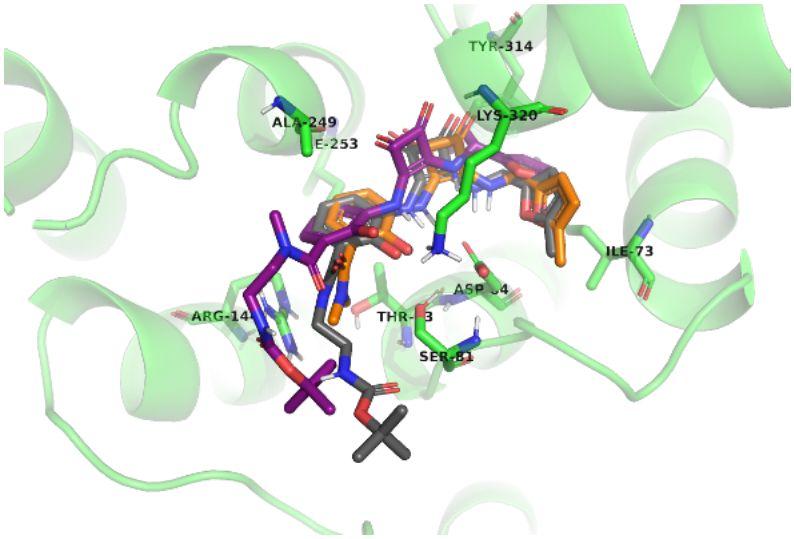

Figure 3.11: View from the bottom of the receptor of docked poses of *R*-navarixin (**2**) (orange), **49a** (grey) and **49b** (purple) in the crystal structure of CXCR2 (PDB ID: 6LFL). Crucial residues lining the pocket are shown as green sticks. Image generated with PyMOL.

As shown in figures 3.11 and predicted from the previous docking studies performed, the linker coupled amide side of the molecules extends in the

cytosol, not interfering or preventing receptor binding. This confirmed this point of *R*-navarixin (**2**) as ideal for modification and corroborate the idea that the addition of longer linkers and a fluorophore moiety to this side of the congener should not interfere with receptor binding. It would not be beneficial trying to perform molecular docking with the final fluorescent probes because the modelling of a long and excessively flexible linker is extremely complex and could result in an inaccurate view of the binding. The two linker-coupled congeners docked show a similar binding pose (Figure 3.11) but a difference in docking score -7.4 kcal/mol and -8.2 kcal/mol for compound **49a** and **49b** respectively. This may be a result of a dissimilar molecular conformation of the two compounds. The methyl group could indeed introduce a conformational restriction in the *N*-methylated analogue that may result in a substantial molecular rigidity, forcing the molecule in a specific conformation more favorable for receptor binding, while the unmethylated analogues, on the contrary, may be more flexible and could require to spend energy to reach the correct binding conformation. These data are not adequate to evaluate the real binding affinity of a compound as there are more properties to take into account and, ultimately, it can be accurately evaluated only through pharmacological testing, presented in the next chapters.

Chapter 4. Design and synthesis of novel fluorescent CXCR2 intracellular allosteric antagonists based on *R*-navarixin

The initial chemical synthesis and functional pharmacological evaluation of the selected literature compounds, presented in chapter 2 of this thesis, identified *R*-navarixin (**2**) as a potent CXCR2 NAM, clearly corroborating what was reported in previous literature studies.[41,166] Its potency at CXCR2 and its moderate selectivity for CXCR2 over CXCR1, were properties that made *R*-navarixin (**2**) ideal as a congener to build a library of fluorescent probes. Subsequently, the molecular modelling studies presented in the previous chapter, allowed prediction of *R*-navarixin (**2**) binding to the intracellular allosteric pocket of CXCR2. This allowed identification of a suitable region of the molecule that was not crucial for receptor binding and could therefore be modified with linker and fluorophore attachment. The docking studies of *R*-navarixin (**2**), showed that the dimethylamide moiety of the molecule protrudes from the binding pocket and is not predicted to participate in any critical interactions with any amino acid residues in the binding pocket. The other functional groups present on *R*-navarixin (**2**) such as the phenol, the squaramide moiety and the methyl furan, on the other hand, could not be removed or modified without a loss in binding. We therefore decided to use the dimethylamide side of the molecule as anchor point to initially add linkers of different lengths to which the fluorophore would be coupled at a later stage. Fluorescent ligands are composed of three parts: the congener, which contains the pharmacophoric region of the ligand, the fluorophore, and the linker, which connects the two parts together (Figure 1.14, Chapter 1). For the generation of the desired library of CXCR2 intracellular allosteric fluorescent ligands, *R*-navarixin (**2**) was chosen as the parent pharmacophore to which different linkers are coupled, prior to fluorophore attachment.

The initial synthetic plan was designed around the generation of a common precursor, containing a free carboxylic acid moiety instead of the dimethylamide present in *R*-navarixin (**2**), to which all the different linkers would then be coupled at a later stage. This was intended to make the synthesis more efficient, minimizing the number of synthetic steps. In order to achieve this 3-nitrosalycilic acid (**26**), was employed as the starting point in this synthesis.

Scheme 4.1 Synthesis of common precursor 52

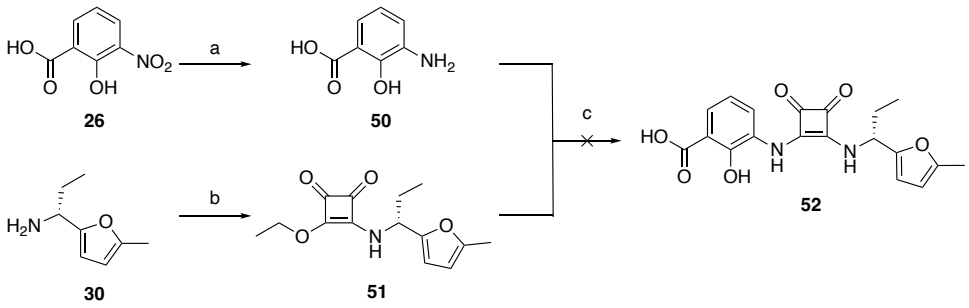

Reagents and conditions:(a) 10% Pd/C, H_2, tetrahydrofuran (THF), RT, 47%; (b) diethyl squarate, EtOH, RT, 61%; (c) (*R*)-1-(5-methylfuran-2-yl)propan-1-amine (**30**), EtOH, RT.

Initially a procedure present in patent US2004/0106794 A1 by Taveras *et al.* was followed (Scheme 4.1). 3-Nitrosalycilic acid (**26**) was reduced to the corresponding aniline (**50**) through a Pd/C catalysed hydrogenation in tetrahydrofuran (THF) and, separately, (*R*)-1-(5-methylfuran-2-yl)propan-1-amine (**30**) was reacted with diethyl squarate in ethanol to afford compound **51**. Compounds **50** and **51** were then combined in ethanol to generate the desired common precursor **52,** which contains a free carboxylic acid moiety. The last step of this synthetic route did not result in the formation of any product. This is probably due to the fact that aniline **50** is not reactive enough to perform the second displacement of the squaric acid monoamide monoester. The second displacement is more difficult to happen with respect

to the first one, which, in this synthetic route, was performed using the more nucleophilic chiral primary amine **30**. The mono-squaramide is deactivated compared to diethyl squarate and this may be rationalised by the increased resonance stabilization of mono-squaramides compared to diethyl squarates.[287] This decreased reactivity can also be exploited to allow the reaction to be controlled such that the mono-squaramide generated does not easily react further to give symmetrical bis-squaramides.[287] Moreover, the reduced nucleophilicity of aromatic amines compared with aliphatic amines, results in longer reaction times in displacement reactions with diethyl squarates.[287]

Compared to *R*-navarixin (**2**) synthesis (Scheme 2.1, Chapter 2), where the first displacement on the diethyl squarate is done using the dimethylamide phenolic aniline and the second one with the chiral amine **30**, in this tried approach (Scheme 4.1) the displacements on the diethyl squarate are reversed and are done firstly with the amine and secondly with aniline **50**. Having pointed out that the second displacement on the squarate is more challenging with respect to the first one, the difference in reactivity between anilines and amine should also be considered in order to clarify why the final step in the synthesis did not succeed. Anilines are less reactive than amines because the nitrogen lone pair can be delocalized into the benzene ring and because the nitrogen is attached to a sp^2 carbon although the lone pair of the nitrogen is not fully conjugated to the benzene ring, as the plane of the NH_2 group is about 40° away from the plane of the ring.[288]

Moreover, it should be pointed out that aniline **50** is also less reactive than aniline **28** used in *R*-navarixin (**2**) synthesis, having a carboxylic acid instead of an amide in meta position to the aniline. A carboxylate is inductively electron-withdrawing and could therefore reduce the reactivity of the aniline.

Having established that this synthetic pathway was not a viable option, it was decided to modify it, removing the established problematic steps explained in this section, which lead to the synthesis presented in scheme 4.2.

Scheme 4.2 Alternative synthesis of common precursor 52

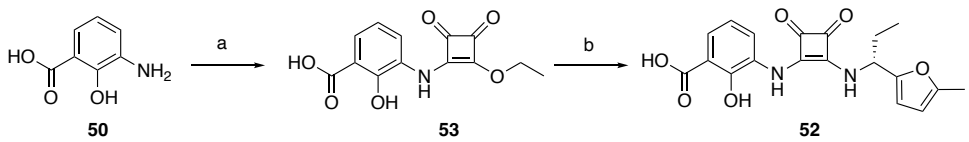

50 53 52

Reagents and conditions: (a) Diethyl squarate, *N,N*-diisopropylethylamine (DIPEA), 1,4-dioxane, microwave (MW) 120 °C, 78%; (b) (*R*)-1-(5-methylfuran-2-yl)propan-1-amine (**30**), EtOH, RT, 29%.

As pointed out previously, the order of the displacement reactions performed on the diethyl squarate is crucial for a positive outcome of the synthetic route. It was therefore decided to react the diethyl squarate firstly with aniline **35** and secondly with (*R*)-1-(5-methylfuran-2-yl)propan-1-amine (**30**). Interestingly, the conditions of the first squarate displacement had to be optimized in order for the reaction to proceed and to obtain an acceptable yield. The initial conditions used for step (a) in scheme 4.2 were those employed for the same step during *R*-navarixin (**2**) synthesis (Scheme 2.1, Chapter 2)[166], in which the reaction was performed at room temperature using ethanol as solvent. Interestingly, the ethoxy displacement with aniline **50** did not happen at room temperature but did proceed on heating (microwave 120 °C). It was also necessary to change the solvent from ethanol to 1,4-dioxane. It is probable that ethanol gave problem as reaction solvent, in this particular case, because it may have acted as a nucleophile, regenerating the starting material. In addition, protic solvents are able to form hydrogen bonds and may have a cage effect on the nucleophile, thus making it weaker.[289–291] Moreover, compound **50** is a hindered aniline with a phenol in the ortho position and a carboxylic acid meta substituent, which may make the aniline less reactive. Taking into consideration all these observations, it is clear that the squarate displacement in scheme 4.2 is markedly different from the one performed during *R*-navarixin (**2**) synthesis. Aniline **28** presents an amide group in meta position to the aniline, which has a lower electron-withdrawing effect and is less involved in potential intramolecular hydrogen bonding,

resulting in being a more reactive aniline than **50**.

The common precursor **52** was generated but presented challenges during the purification step. The clean product partially precipitated during the reaction workup but, since the yield was low, the residual product, extracted in the organic phase, needed to be purified. The free carboxylic acid present in the compound posed significant complications during this step in both reverse phase and normal phase conditions probably due to its instability in aqueous environment, and it was therefore not possible to purify the product without experiencing a loss in yield.

Subsequently, coupling reactions of amine linkers with compound **52** were attempted but were not successful, maybe due to the difficulty to activate the acid with a coupling agent[292].

Overall, the free carboxylic acid compounds were complex to handle during the synthesis, not only in the reactions themselves but also during their purification.

A new, more efficient synthetic strategy involving simpler purification steps was needed and this required the removal of the free carboxylic acid group. It was therefore decided to start the synthetic route with the incorporation of two different short Boc protected linkers, *N*-(2-aminoethyl)amide or *N*-methyl-*N*-(2-aminoethyl)amide linker, acting as handles for subsequent linker couplings, and to conduct the synthesis of each compound series separately (Scheme 4.3). These initial linkers were chosen to assess the importance of the *N,N*-dialkylamide moiety present on *R*-navarixin (**2**). Therefore, two series of linker-coupled compounds were generated through the addition of an initial *N*-(2-aminoethyl)amide or *N*-methyl-*N*-(2-aminoethyl)amide spacer. Once *N*-Boc protection has been removed, the terminal primary amine functionality present on this spacer will allow either direct reaction with a suitable *N*-reactive fluorescent dye, or further elongation of the linker through incorporation of a glycyl or β-alanyl moiety. Short simple amino acids were chosen as additional linkers to assess whether a small elongation of the linker length could have a considerable influence on the activity of the fluorescent probes. Moreover, the fluorophore chosen (BODIPY 630/650-X) for the final coupling and generation of fluorescent probes already contains an aminohexanoyl linker.

Scheme 4.3 Synthesis of common precursors 49a and 49b

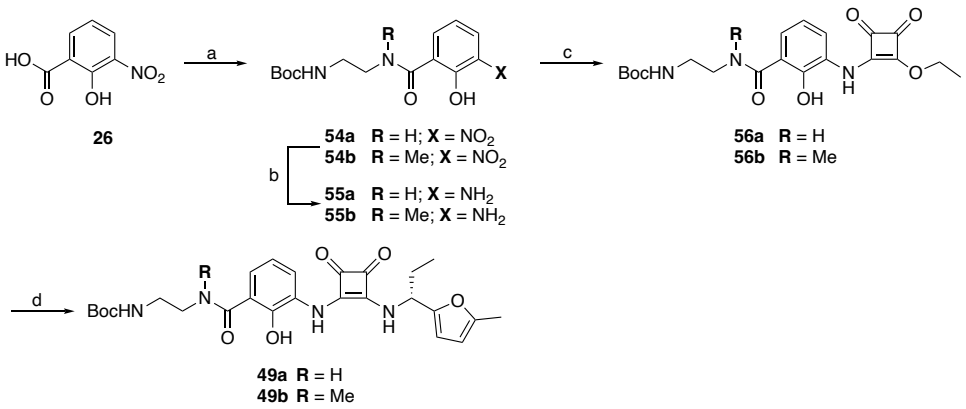

Reagents and conditions: (a)(i) $(COCl)_2$, DMF, CH_2Cl_2, RT; (ii) BocNH-$(CH_2)_2$-NHR, CH_2Cl_2, 0 °C, 50-70%; (b) 10% Pd/C, H_2, EtOH, RT, 90%; (c) diethyl squarate, EtOH, RT, 40-70%; (d) (*R*)-1-(5-methylfuran-2-yl)propan-1-amine hydrochloride (**30**), Et_3N EtOH, RT, 50-60%.

3-Nitrosalicilic acid (**26**) was initially converted to the amides **54a-b**. This was achieved firstly by the formation of the corresponding acyl chloride via a modified Vilsmeier-Haack reaction, which was then reacted with *tert*-butyl *N*-(2-aminoethyl)carbamate or *tert*-butyl (2-(methylamino)ethyl)carbamate at 0 °C. The nitro moiety of compounds **54a-b** was reduced, through catalytic hydrogenation over 10% Pd/C, to afford the corresponding anilines **55a-b**. These were then reacted with diethyl squarate in ethanol to afford the corresponding squaric acid monoamide monoesters **56a-b** which were subsequently treated with (*R*)-1-(5-methylfuran-2-yl)propan-1-amine (**30**) to afford compounds **49a-b**. Interestingly, the generation of amides **54a-b** via acyl chloride formation is a more efficient approach compared to any previously attempted amide couplings involving the use of a coupling agent. This may be due to a difficulty in the carboxylic acid activation step with a coupling agent, which is overcome in the acyl chloride approach, and this may be the reason why *R*-navarixin (**2**) synthesis employs this method instead of a coupling agent for amide formation. The common precursors **49a-b** were generated and, in order to perform coupling

reactions with additional linkers or fluorophores, the terminal amine required *N*-Boc deprotection (Scheme 4.4).

Scheme 4.4 Attempted *N*-Boc deprotection of compounds 49a-b

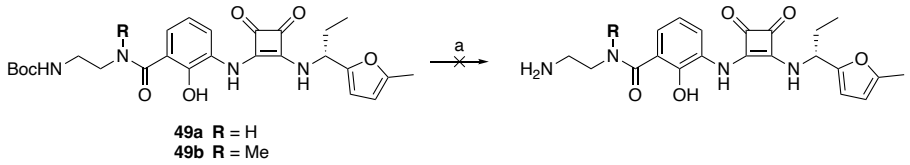

Reagents and conditions: (a) 4M HCl/1,4-dioxane, RT or TFA/CH_2Cl_2, RT or 85% aq H_3PO_4/CH_2Cl_2, RT.

N-Boc deprotection was initially attempted using 4M HCl in 1,4-dioxane at room temperature, but unexpectedly the straightforward *N*-Boc deprotection was found not to occur. Further analysis of the reaction mixture revealed that the compounds were cleaving, generating first an amino squarate (**57a,b**) and then they were Boc deprotecting (**58a,b**) (Figure 4.1). In order to avoid the degradation of the starting material, several other conditions were attempted to effect *N*-Boc removal. Initially different acidic conditions were explored in order to understand if the molecules were sensitive to any conditions involving acid or if the usage of other acids may have been tolerated. 2,2,2-Trifluoroacetic acid (TFA) in dichloromethane and 85% aq. H_3PO_4 in dichloromethane were tried as alternative conditions but both resulted in the same as outcome in terms of molecular degradation. It was therefore clear that the molecules were sensitive to acidic environments and that this could be due to the presence of the squarate next to the furan ring, which could open in these conditions[293]. The potential mechanism happening to compounds **49a-b** in acidic conditions is shown in figure 4.1.

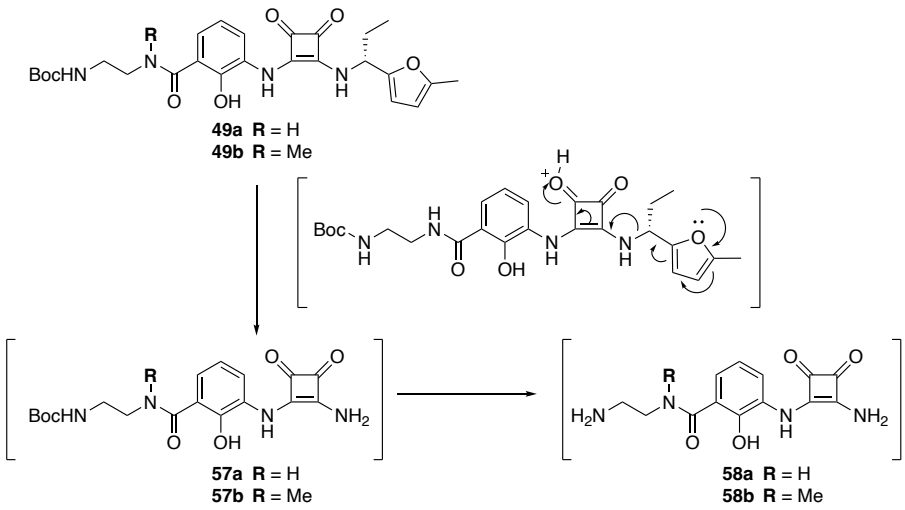

Figure 4.1: Proposed mechanism for *N*-Boc deprotection of compounds **49a-b** under acidic conditions for observed mass spectrometry data obtained.

Having established that acidic conditions needed to be avoided, *N*-Boc deprotection of compounds **49a-b** was attempted employing alternative methods such as treatment with tetra-*N*-butylammonium fluoride (TBAF) in THF, with potassium *ter*t-butoxide in THF[294] both at room temperature and at reflux conditions, with $FeCl_3$ in dichloromethane[295,296] at room temperature and with $(Cu(OTf)_2)$[297] in dichloromethane at room temperature. No product generation was observed with any of these conditions, and the starting material appeared to remain unreacted. It was subsequently decided to exploit high temperature as a method to thermolytically *N*-Boc deprotect the compounds.[298–302] Compounds **49a-b** were dissolved both in water only and in a mixture of *N*-methyl-2-pyrrolidone (NMP) and water and heated in the microwave up to 150 °C and 160 °C for up to 1 hour but no reaction was observed. The compounds were also dissolved in methanol and treated with K_3PO_4 H_2O in the microwave at 120 °C[303] but also this approach did not result in any product formation. Overall, all the *N*-Boc deprotection methods involving acidic conditions resulted in the decomposition of the compounds while the milder methods which involved either basic or high temperature conditions did not give any product formation, leaving unreacted starting materials (Table 4.1).

Table 4.1 49a-b *N*-Boc deprotection conditions

N) Conditions	Temperature	Outcome
1) 4M HCl/ 1,4-dioxane	RT	Molecule degradation
2) TFA/ CH_2Cl_2	RT	Molecule degradation
3) aq H_3PO_4/ CH_2Cl_2	RT	Molecule degradation
4) TBAF/ THF	RT or reflux	No reaction
5) KO*t*Bu/ THF	RT or reflux	No reaction
6) $FeCl_3$/ CH_2Cl_2	RT	No reaction
7) $(Cu(OTf)_2)$/ CH_2Cl_2	RT	No reaction
8) H_2O or NMP/ H_2O	150-160 °C (MW)	No reaction
9) K_3PO_4/ H_2O	120 °C (MW)	No reaction

To confirm that the acid sensitive portion of the molecule was the furan ring, it was decided to attempt to *N*-Boc deprotect the previous intermediates in the synthesis, **56a-b**, which would also allow us to save a valuable intermediate of the synthesis. The deprotection of compounds **56a-b** was achieved with acidic conditions, 4 M HCl in dioxane and TFA in dichloromethane respectively, that did not result in any compound decomposition and gave clean unprotected intermediates **59a-b**. Interestingly, for the methylated compound **56b**, the use of HCl/dioxane for deprotection resulted firstly in the hydrolysis of the squarate ethyl ester and subsequently Boc deprotection of the compound, not seen with the unmethylated analogue, and this did not happen with the use of TFA. This difference between the compounds may be due to the different intramolecular hydrogen bonding pattern that they possess (explained in more details in Chapter 6) which may leave, in the case of the methylated compound, the ethyl group more susceptible to leave, not being

involved in any intramolecular interaction. A protecting group for the generated unprotected amines and for the new amine linkers that would be added, was still necessary, since the final chiral amine addition step still needed to be performed to afford the final congeners. The fluorenylmethoxycarbonyl protecting group (Fmoc) was therefore identified as a suitable protecting group since it is removed under basic conditions, under which the molecule is stable.

Scheme 4.5 Synthesis of linker-coupled compounds

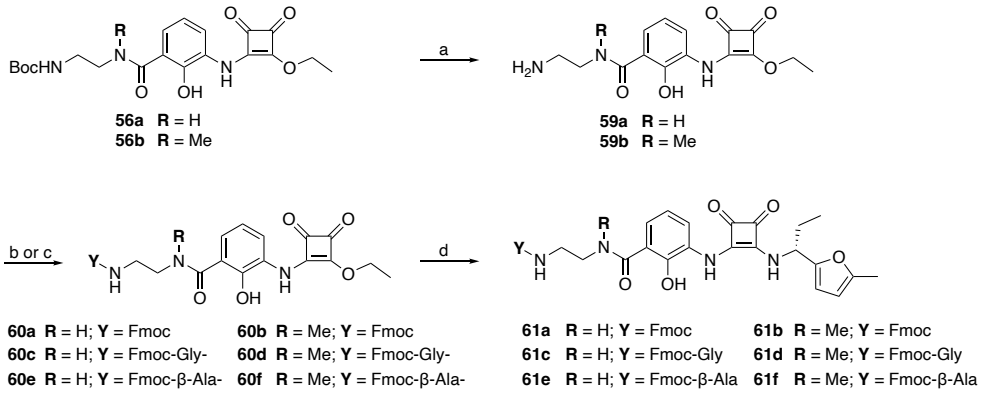

Reagents and conditions: (a) 4M HCl/1,4-dioxane or TFA/CH_2Cl_2, RT, 100%; (b) (9*H*-fluoren-9-yl)methyl (2,5-dioxopyrrolidin-1-yl) carbonate (Fmoc-OSu), *N,N*-diisopropylethylamine (DIPEA), CH_2Cl_2, 0 °C, 39-58%; (c) Fmoc-Gly-OH or Fmoc-β-Ala-OH, 1-ethyl-3-(3-dimethylaminopropyl) carbodiimide (EDCI), 1-hydroxybenzotriazole (HOBt), CH_2Cl_2, 0 °C, 11-42%; (d) (*R*)-1-(5-methylfuran-2-yl)propan-1-amine hydrochloride (**30**), Et_3N EtOH, RT, 50-60%;

As previously explained and as shown in scheme 4.5, the *N*-Boc deprotection of **56a-b** was achieved by treatment with either 4M HCl/1,4-dioxane or TFA/CH_2Cl_2. The deprotected compounds were subsequently either Fmoc protected using Fmoc-OSu and *N,N*-diisopropylethylamine (DIPEA) in dimethylformamide (DMF) to give **60a-b** or coupled to Fmoc-Gly-OH or

Fmoc- β-Ala-OH using 1-etyl-3 (3-dimetylaminopropyl) carbodiimide (EDCI), hydroxybenzotriazole (HOBt), DIPEA in CH_2Cl_2 to afford **60c-f** respectively. Compounds **60a-f** were subsequently stirred at room temperature in the presence of (*R*)-1-(5-methylfuran-2-yl)propan-1-amine (**30**) to afford protected congeners **61a-f**.

Scheme 4.6 Fmoc deprotection and fluorophore coupling

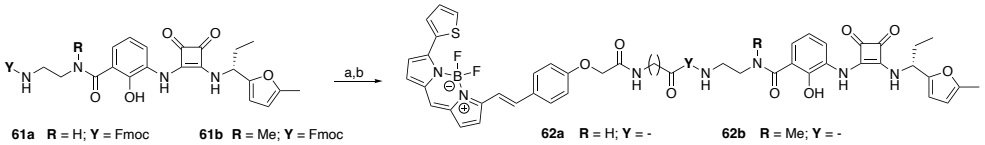

61a **R** = H; **Y** = Fmoc **61b** **R** = Me; **Y** = Fmoc
61c **R** = H; **Y** = Fmoc-Gly **61d** **R** = Me; **Y** = Fmoc-Gly
61e **R** = H; **Y** = Fmoc-β-Ala **61f** **R** = Me; **Y** = Fmoc-β-Ala

62a **R** = H; **Y** = - **62b** **R** = Me; **Y** = -
62c **R** = H; **Y** = Gly **62d** **R** = Me; **Y** = Gly
62e **R** = H; **Y** = β-Ala **62f** **R** = Me; **Y** = β-Ala

Reagents and conditions: (a) 20% piperidine/DMF, RT; (b) BODIPY 630/650-X NHS ester, DMF, RT, 34-69%.

Base-mediated *N*-Fmoc cleavage of **61a,c-f** in the presence of piperidine/DMF afforded the corresponding free amines, which were not isolated, but directly acylated with BODIPY 630/650-X NHS ester to afford the desired fluorescent probes **62a,c-f** (Scheme 4.6). Unfortunately, compound **61b** was found to be chemically unstable thus the corresponding fluorescent probe **62b** was found not to be synthetically accessible, despite multiple attempts at purification it was not pure enough for pharmacological testing.

Chapter 5. Pharmacological evaluation and application of novel fluorescent CXCR2 allosteric antagonists

5.1 Pharmacological evaluation of linker coupled congeners

The previous chapter described the synthesis of compounds based on *R*-navarixin (**2**), modified through the addition of different linkers on the dimethylamide side of the molecule, which were employed as congeners for the generation of the fluorescent ligand library. The modification that the parent congener, *R*-navarixin (**2)** underwent could have an influence on receptor binding and, overall, on the potency of the compounds. For this reason, the activity of protected congeners **49a-b**, **61a**, **61c** was evaluated in order to determine any functional effect that may be a result of linker addition. To assess the activity of the compounds, the NanoBiT complementation assay previously presented in Chapter 2.2, measuring CXCL8 stimulated recruitment of β-arrestin2 to the human CXCR2 receptor[244], was used (Figure 2.3, Chapter 2).[244]

To assess the initial pharmacological activity of the synthesized protected congeners, the HEK293 CXCR2/β-arrestin2 NanoBiT cell line was pre-treated with **2**, **49a-b**, **61a**, **61c** in a concentration dependent manner (10 μM - 0.1 nM) for 30 minutes prior to furimazine addition and $CXCL8_{28-99}$ stimulation. 10 nM $CXCL8_{28-99}$ was used as the stimulus for determination of the NAM IC_{50}, as this represents an EC_{80} concentration of the $CXCL8_{28-99}$. The luminescence represents basal and agonist stimulated β-arrestin2 recruitment by the CXCR2 receptor, and it was recorded for up to 60 minutes after agonist activation. The data at 60 min are presented in Figure 5.1 and pIC_{50} values of the tested compounds are summarized in Table 5.1.

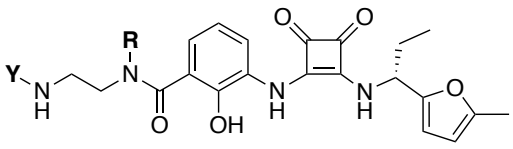

49a **R** = H; **Y** = Boc **61a** **R** = H; **Y** = Fmoc
49b **R** = Me; **Y** = Boc **61c** **R** = H; **Y** = Fmoc-Gly

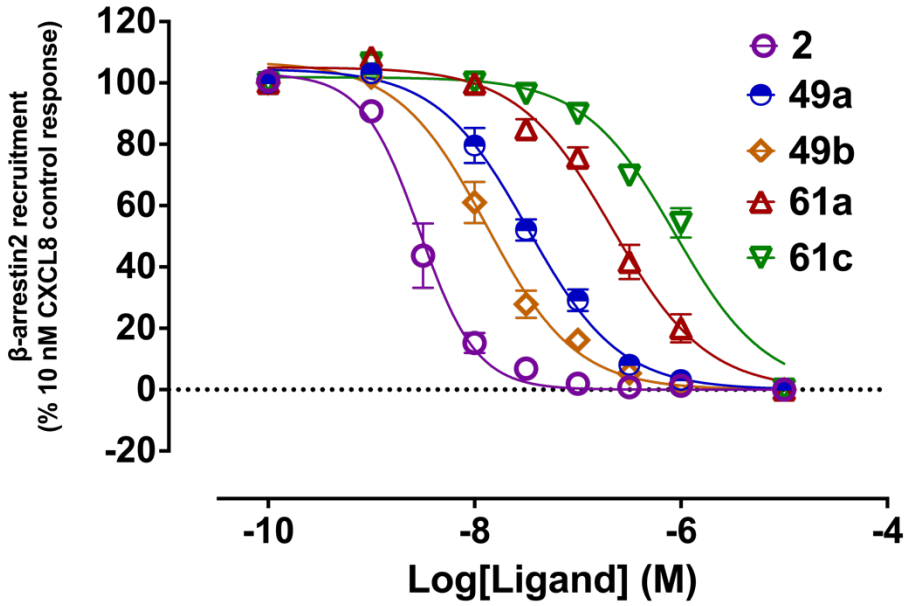

Figure 5.1: Concentration inhibition curves for compounds **2, 49a-b**, **61a**, **61c**, demonstrating the effect on 10 nM CXCL8 responses in the CXCR2-βarrestin2 NanoBiT assay. Cells were pretreated for 30 min with test compounds, followed by 60 min CXCL8 stimulation. The data shown represent are pooled from three individual experiments (mean ± SEM) with each experiment performed in technical duplicate.

Table 5.1. Functional inhibition of CXCR2 employing the NanoBiT assay (pIC_{50}) for protected congeners (**49a-b, 61a, 61c**) compared to *R*-navarixin (**2**).

Compound	pIC_{50} ± SEM*
2	8.54 ± 0.04
49a	7.54 ± 0.10
49b	7.93 ± 0.11
61a	6.67 ± 0.09
61c	5.95 ± 0.15

*All data are mean ± SEM of individual estimates from n = 3 separate experiments.

R-Navarixin (**2**), was used as reference for the assay and it showed the highest potency overall, in line with previously published data.[304] The following order of inhibitor potency for the linker congeners **2**>**49b** > **49a** > **61a** > **61c** was observed, with a 3 fold loss of potency between **2** and **49b**, and approximately 400 fold between **2** and **61c**. Compounds **49a** and **49b** differ only through the *N*-methyl status of the salicylamide moiety, in which the *N*-methylated analogue (**49b**) had 2.5-fold higher potency compared to the corresponding unmethylated analogue (**49a**). The influence of linker length and nature of the protecting group present on the congener can be observed when comparing **49a**, **61a** and **61c**. Compounds **49a** and **61a**, comprise only the initial ethylenediamine spacer with different protecting groups, *N*-Boc and *N*-Fmoc respectively, whereas **61c** additionally incorporates an *N*-Fmoc protected glycyl linker. These analogues demonstrated an association between decreased functional potency and the larger Fmoc protecting group. Overall linker addition to *R*-navarixin (**2**) via the amide moiety identified in the docking studies performed and described previously in chapter 3, appeared tolerated, and activity of the modified analogues as antagonists /

NAMs appeared retained in the functional NanoBiT assay. Furthermore, this assessment was performed in a whole cell assay, which also requires the designed NAMs to cross the plasma membrane and bind at the intracellular CXCR2 binding site. Therefore, the difference in potency observed in this assay may reflect not only an influence on CXCR2 binding affinity and kinetics, but different physicochemical properties of the linker-coupled compounds that influence their cellular permeabilities.

5.2 Introduction to NanoBRET detection of ligand binding

To evaluate the binding affinities of the fluorescent probes **62a**, **62c-f** at CXCR2, a bioluminescence resonance energy transfer (NanoBRET) assay was generated and performed both in CXCR2 membranes and whole cells. In this technique a bioluminescent donor is attached to the protein of interest and the second interacting molecule, protein or ligand, is labelled with a fluorescent molecule which acts as the acceptor molecule.[200] BRET takes advantage of a enzymatic reaction to generate donor luminescence in the presence of a substrate, and therefore does not require external fluorescence excitation, unlike in the case of Förster resonance energy transfer (FRET) techniques.[200,305] This represents an advantage since it results in minimization of photobleaching, decreased background noise, and simplified analysis of the BRET signal.[306] The donor luciferase oxidises its substrate, resulting in light emission. The nonradiative transfer of this light energy occurs when the donor and acceptor-tagged proteins are in close proximity.[200] This results in the excitation of the acceptor fluorescent moiety, which emits light of a longer wavelength. In order for this energy transfer process to occur, the two proteins need to be within 10 nm of each other, in the right orientation and there must be an overlap of the donor emission and acceptor excitation spectra.[200,307] NanoLuc is especially useful in BRET assays since its increased brightness of emission results in a substantial light emitted over a range of wavelengths which allows it to be used in conjunction with a range of acceptor fluorophores[200], including those at the red end of the spectrum used here in the designed fluorescence ligands. This also improves specificity of

the signal as the emission measurement is less affected by issues such as cellular autofluorescence.

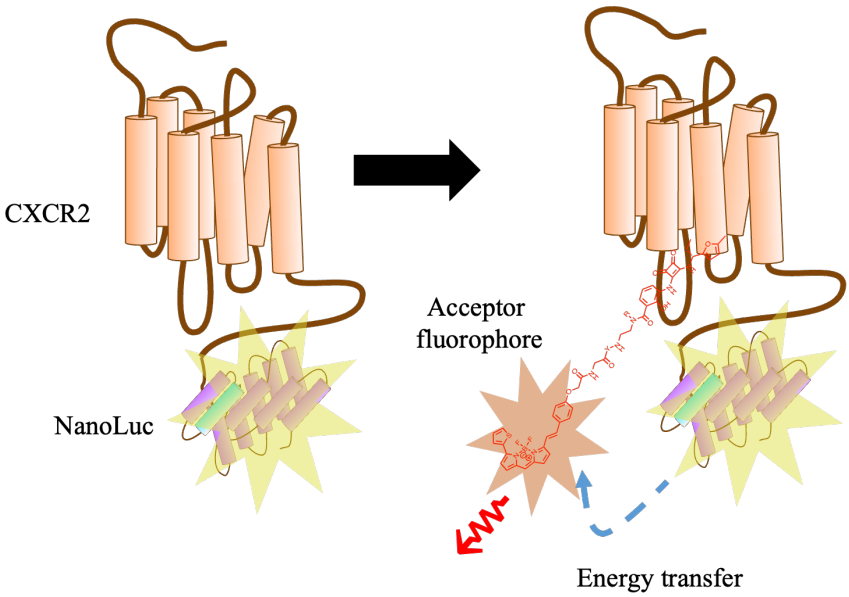

Figure 5.2: Representation of the CXCR2 NanoBRET binding assay. BRET occurs upon co-localization of the Nanoluciferase and the intracellular fluorescent ligand, allowing dual readout of donor luminescence at 450 nm and acceptor fluorescence at 630 nm to generate a BRET ratio (acceptor / donor).

The initial step in developing a BRET-based ligand binding assay consists in labelling the receptor with a luciferase.[200] In our assay, HEK 293 cells expressed CXCR2 fused with full length NanoLuc at the intracellular *C*-terminus, as shown in figure 5.2. This is in contrast to the majority of GPCR ligand binding assays reported to date, involving a transmembrane or extracellular ligand binding site, in which the Nanoluc is located extracellularly on the *N* terminus. The NanoLuc acts as the donor bioluminescent enzyme from which the energy transfer occurs in the presence of membrane permeant furimazine[308], and the fluorescent ligand is the

acceptor fluorophore. Since the energy transfer only occurs when there is close proximity (<10 nm) between the donor and the acceptor[308], it is possible to monitor specific, homogeneous, measurements of fluorescent ligand binding to the receptor of interest through the increase in BRET ratio (acceptor emission 630 nm/donor emission 450 nm) in real time, without removal of free ligand.[308] BRET-based binding assays allowed the studies of receptor signalling, receptor-protein interactions, protein recruitment and trafficking. There are extensive reviews presenting the use of fluorescently labelled compounds in BRET assays to investigate protein-protein interactions in real time[200,306,309,310] with applications to multiple GPCRs and tyrosine kinase receptors (RTKs).[200,201,206,311–313]

5.3 Investigation of novel fluorescent ligands as suitable probes for CXCR2 NanoBRET binding assays

The binding of the generated fluorescent ligands (**62a**, **62c-f**), which synthesis was previously described in chapter 4, was initially tested in a cell free NanoBRET assay using HEK-CXCR2-NanoLuc membranes or whole cells (Figure 5.3), using a saturation assay format comparing increasing concentrations of fluorescent probe with or without 10 μM *R*-navarixin (**2**) to determine non-specific binding (NSB). The CXCR2-NanoLuc construct behaves like wild type. Based on comparison with pharmacological assays performed previously, the addition of the NanoLuc luciferase does not modify the potency of CXCL8.[41,182]

Membrane binding assays used a HEPES based binding buffer at pH7.4 containing $MgCl_2$ and 0.1 % BSA, in the absence of NaCl, while cell based assays used HBSS / 0.1 % BSA (Chapter 8). Endpoint saturation data were generated from 60 min incubations at 37 °C, confirmed as equilibrium conditions in later kinetic data (see Figure 5.3).

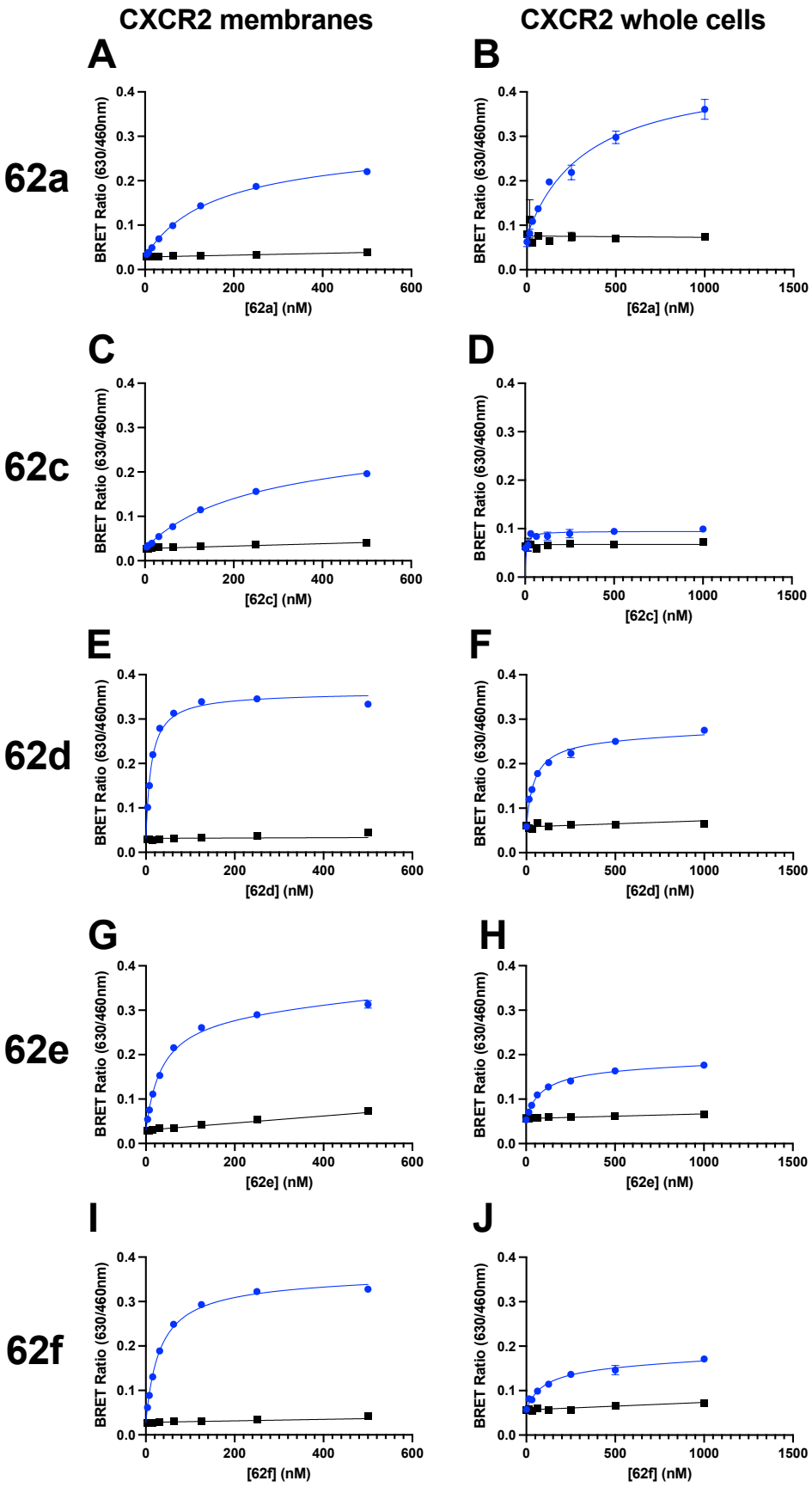
CXCR2 membranes
CXCR2 whole cells
A
B
C
D
E
F
G
H
I
J
62a
62c
62d
62e
62f
BRET Ratio (630/460nm)
[62a] (nM)
[62c] (nM)
[62d] (nM)
[62e] (nM)
[62f] (nM)

Figure 5.3: Fluorescent ligand (**62a**, **62c-f**) NanoBRET saturation binding studies in CXCR2 membranes (left column, A, C, E, G, I), CXCR2 whole cells (central column, B, D, F, H, J) in the absence (blue) or presence (black) of 100 nM (membranes) or 10 μM (whole cells) *R*-navarixin (**2**) used to measure non-specific binding (NSB). Data are representative experiments from n = 5 individual experiments performed in duplicates.

Table 5.2 Binding affinities of the fluorescent ligands in CXCR2 membranes or CXCR2 whole cells determined by saturation binding assays.

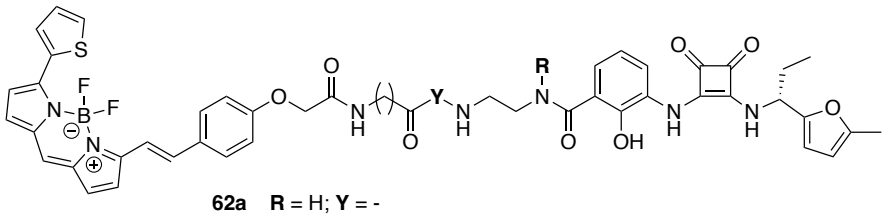

62a **R** = H; **Y** = -
62c **R** = H; **Y** = Gly **62d** **R** = Me; **Y** = Gly
62e **R** = H; **Y** = β-Ala **62f** **R** = Me; **Y** = β-Ala

Compound	K_D ± SEM* (nM)	
	CXCR2 membranes	CXCR2 whole cells
62a	137 ± 12	549 ± 83
62c	301 ± 31	-
62d	9.0 ± 4.9	52 ± 7
62e	45 ± 4	82 ± 14
62f	27 ± 3	88 ± 23

*All values represent mean ± SEM of n=5 separate experiments.

All the ligands showed saturable binding and low NSB (with the exception of **62c** in whole cells), from which affinities could be determined (Table 5.2). The *N*-methylated ligands **62d** and **62f** showed the highest CXCR2 binding affinities (K_D 10 – 27 nM; Table 5.2), indicating that the *N*-methyl group substituent improves binding affinity, as predicted in the earlier functional congener study (Table 5.1). The linker composition also influenced probe

binding affinity, as evident in the comparison of non-methylated analogues with the order of K_D for **62e > 62a** > **62c** (10 fold change in total; Table 5.2). A longer β-alanine linker (**62e**) improved binding affinity compared to glycine linker (**62c**) and to no additional linker (**62a**). This may be due to the ability of a longer linker to form more interaction or to its effect on the lipophilicity of the compound. Conversely, only a glycine linker (**62c**) decreased binding affinity with respect to the absence of linker (**62a**), as previously seen with the linker coupled compounds **61a** and **61c** (Table 5.1).

Additionally, the use of fluorescent ligands within a homogeneous real-time NanoBRET system facilitated characterization of ligand binding kinetics. As an example, the association rate of different concentrations of tracer **62a** (in the absence and presence of 10 μM *R*-navarixin (**2**) to define non-specific binding) was measured over 60 minutes (Figure 5.4). By fitting a one site association model for probe binding to these data, the association rate constant k_{on} ($1.9 \pm 0.2 \times 10^5$ $M^{-1}min^{-1}$), and dissociation rate constant k_{off} (0.013 ± 0.005 min^{-1}) for **62a** could be estimated. From this a kinetically derived pK_D 7.3 ± 0.2 (n=4) of compound **62a** could be derived (as the ratio of k_{off} / k_{on}) which was in line with endpoint derived K_D from saturation binding (Table 5.2). Additional plotting of determined k_{obs} determined within these kinetic assays validates the use of a one-site association model through derivation of a linear relationship between k_{obs} and ligand concentration (Figure 5.4 E-F).

Furthermore, saturation binding and kinetic association experiments were also carried out in the presence of 10 nM CXCL8 for comparison, a concentration predicted to be substantially higher than CXCL8 K_D for CXCR2 (Figure 5.4). The rationale for this study was the potential ability of the orthosteric bound chemokine to influence the NAM binding site and the affinity of the intracellular directed probe. Interestingly, it was observed that, under agonist conditions, the affinity and kinetic parameters of **62a** displayed no significant difference to that determined in the absence of CXCL8 (**62a** + 10 nM CXCL8, $K_D = 149 \pm 16$ nM, p = 0.45, n=4, Student's paired t-test; $k_{on} = 1.7 \pm 0.2 \times 10^5$ $M^{-1}min^{-1}$, $k_{off} = 0.014 \pm 0.005$ min^{-1}, n = 4). This observation

is consistent with [^{3}H]navarixin binding studies performed by Gonsiorek et al[41], in which CXCL8 at high concentrations failed to compete for [^{3}H]navarixin binding.[41,139] Together these data suggest that orthosteric chemokine does not modulate the CXCR2 affinity of navarixin based probes.

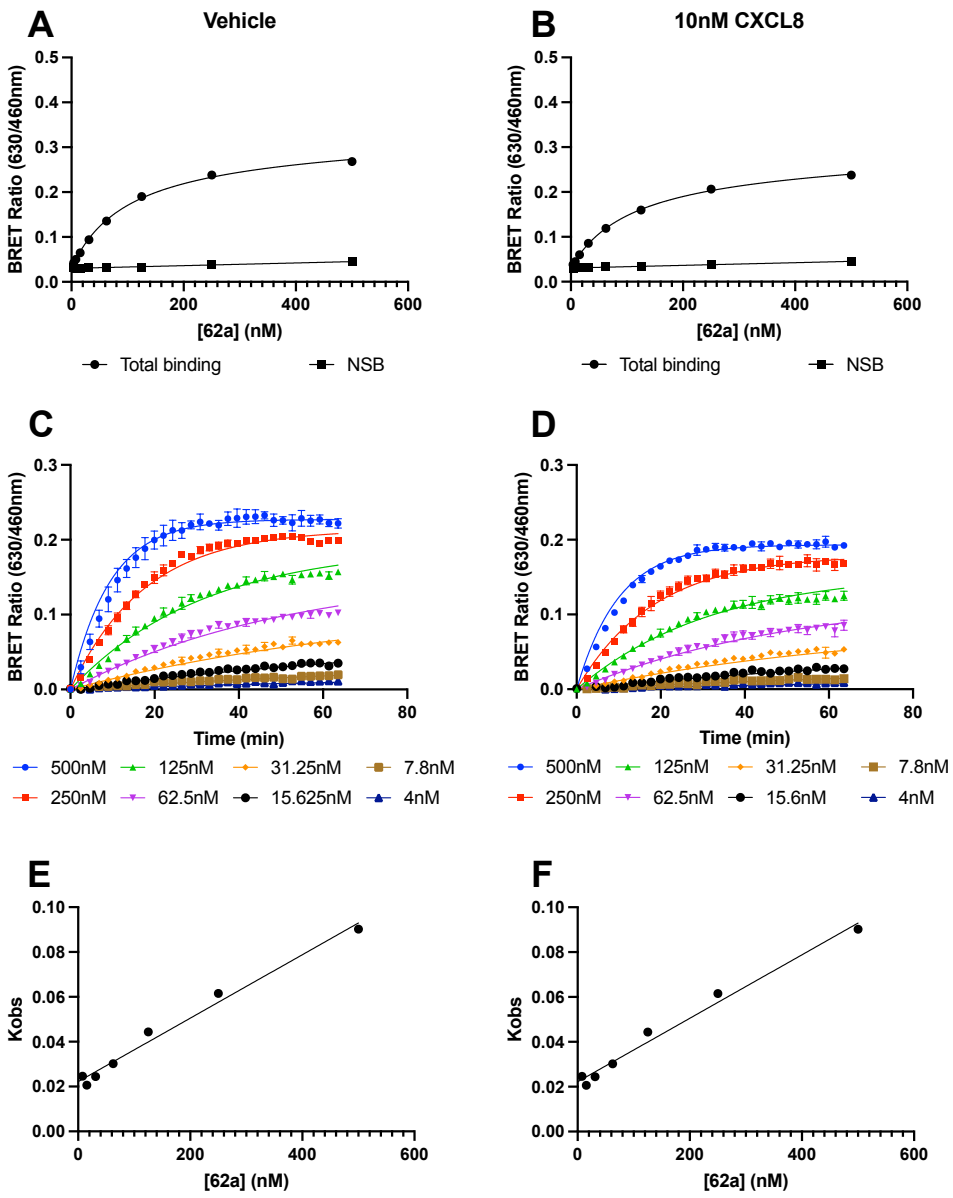

Figure 5.4: Endpoint and association kinetic analysis for **62a** in CXCR2 membranes in the absence and presence of the orthosteric $CXCL8_{28-99}$ agonist**. 62a** NanoBRET saturation binding and association kinetic studies were performed in CXCR2 membranes in the absence of CXCL8 (A, C) and in the presence of 10 nM CXCL8 (B, D). Data are representative experiments from 4 performed. Plot of [**62a**] concentration against k_{obs} in the absence (E) and in the presence (F) of 10 nM CXCL8 showing binding following a simple law of mass action model with k_{obs} increasing with concentration in a linear manner. Plot is linear if binding to a single affinity site in the receptor population.

Having determined fluorescent ligand binding affinities in membranes we sought to employ these ligands within a cellular setting. Whole cell studies would provide an idea of whether the ligands could cross the cell membrane as well as receptor binding, since the navarixin allosteric binding site is on the intracellular side.[42,45,139] **62a**, **62c**-**f** were tested in the whole cell format of the CXCR2 NanoBRET assay previously described in this chapter. As shown in figure 5.3. B, D, F, H, J, we were able to measure saturable binding and determine K_D values for all compounds except for **62c**, with the same rank order of affinity as seen in the membrane assay, and a drop in apparent K_D of 1.8 – 5.8-fold compared to membranes. The *N*-methylated fluorescent ligands **62d**-**f** and compound **62e** again possessed the highest affinity in the whole cell system as seen in the cell free environment, with K_D values of 52 – 88 nM. These experiments demonstrate the applicability of these fluorescent probes in both membrane and cell based CXCR2 binding assays. Moreover, cell accessibility of the probes was also confirmed by direct fluorescent imaging of the CXCR2 cell line, co-labelled with the SNAPtag receptor fluorophore SNAPlabel-AF-488 to identify the SNAP-CXCR2 protein, and **62a** (Figure 5.5). The CXCR2-SNAPtag construct behaves like wild type. Based on comparison with pharmacological assays performed previously, the addition of the SNAPtag does not modify the potency of CXCL8.[41,182] The data generated demonstrated predominantly cell surface and some intracellular endosomal fluorescent labelling of the cells by **62a**. **62a** labelling was competitively displaced by a high concentration of unlabelled *R*-navarixin (**2**).

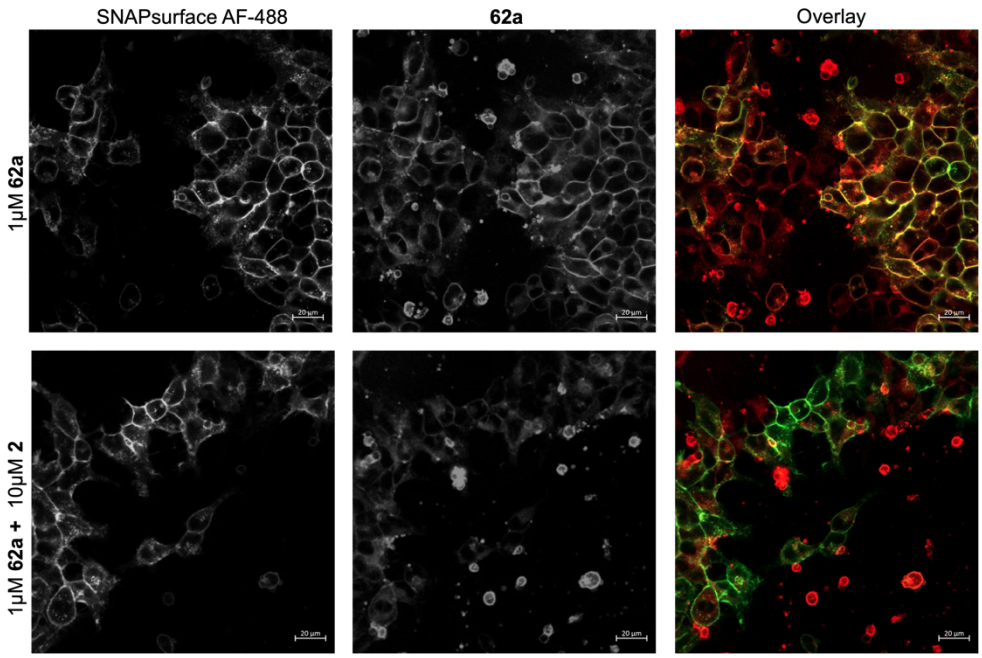

Figure 5.5: Live cell imaging of **62a** binding to SNAP-tagged CXCR2-NanoLuc HEK293. Cells were pre-labelled for 30 min with SNAPsurface-AF488 to identify the SNAP-tagged receptors (green), prior to incubation of **62a** (red) in the absence or presence of 10 μM **2** to define non-specific binding (10 min at 37 °C), prior to fluorescence imaging. Scale indicates 20μm.

5.4 Selectivity studies: CXCR1

Given the reported 100-fold CXCR2:CXCR1 functional selectivity for the parent NAM *R*-navarixin (**2**)[41], the selectivity of probes **62a**, **62c-f** for the related chemokine receptor CXCR1 compared to CXCR2 was assessed. This was performed in a cell free NanoBRET assay using HEK-CXCR1-NanoLuc membranes.

CXCR1 membranes

62a

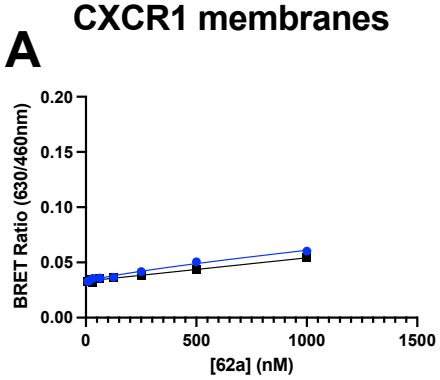

62c

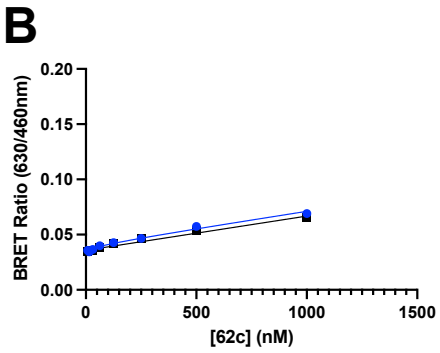

62d

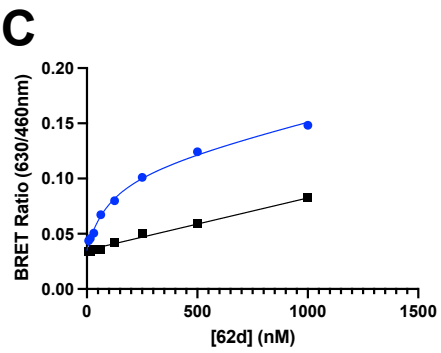

62e

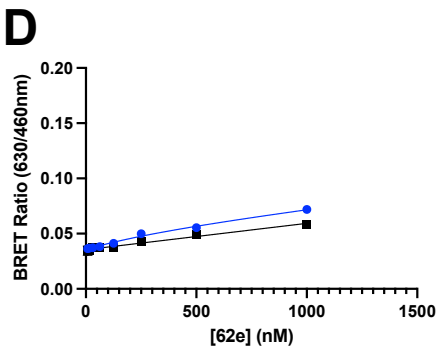

62f

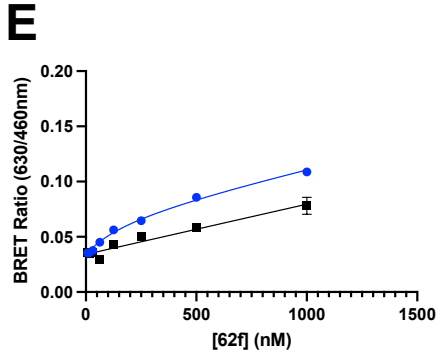

Figure 5.6: Fluorescent ligands (**62a**, **62c-f**) NanoBRET saturation binding studies in CXCR1 membranes (A, B, C, D, E) in the absence (blue) or presence (black) of 10 μM navarixin (**2**) used to measure non-specific binding (NSB). Data are representative experiments from n = 5 individual experiments performed in duplicates.

Table 5.3 Binding affinities of the fluorescent ligands in CXCR2 and CXCR1 membranes determined by saturation binding assays.

Compound	K_D ± SEM* (nM)	
	CXCR2 membranes	CXCR1 membranes
62a	137 ± 12	-
62c	301 ± 31	-
62d	9.0 ± 4.9	101 ± 21
62e	45 ± 4	-
62f	27 ± 3	372 ± 107

*All values represent mean ± SEM of n=5 separate experiments.

As shown in figure 5.6 compounds **62a**, **62c** and **62e** showed no CXCR1 specific binding. However, saturable CXCR1 binding was observed for the *N*-methyl compounds **62d** and **62f**, with respectively 11-fold and 14-fold reductions in affinity at CXCR1 compared to CXCR2 (Table 5.3). These data demonstrate that the selectivity of the fluorescent probes for CXCR2 over CXCR1 is retained. However, **62d** and **62f** possess sufficient affinity to be used in a CXCR1 NanoBRET assay probing for the corresponding intracellular binding site. **62d** also demonstrated a higher Bmax BRET ratio than **62f** to enhance the assay window for the binding assay, potentially arising from a reduced distance and / or improved origination of the fluorescent ligand pharmacophore relative to the donor luciferase tag in the CXCR1 fusion protein.

Overall, the generated fluorescent ligands **62a, c-f** all bind CXCR2 both in membranes with affinities of 9 – 300 nM. In particular, the *N*-methyl fluorescent ligands **62d** and **62f** were found to have the highest affinities in both CXCR2 membranes and whole cells. Interestingly, this also translated to the ability of **62d** and **62f** to bind CXCR1 with sufficient affinity, although CXCR2 selectivity characteristic of the navarixin pharmacophore was retained. Thus, the use of **62d** in particular could be extended to development of CXCR1 binding assays exploring NAM receptor pharmacology as well as CXCR2. Having a library of fluorescent probes with a range of binding affinities could prove to be beneficial in terms of fluorescent ligand-based assay development to determine ligand binding to the receptor. For example, theoretically, a fluorescent probe possessing fast kinetics (and lower receptor affinity) extends the range and accuracy of determination of unlabelled ligand kinetic parameters in competition kinetic NanoBRET assay development.[250] Moreover, compounds **62a, d-f** were able to cross the cell membrane and reach their intracellular binding site. They showed similar orders of affinity to CXCR2 membrane data and the 4-6 fold reduced binding affinity observed in cells compared to membranes may be due to membrane permeability and reduced intracellular concentration of the probes in a whole cell receptor context. Membrane permeability of the generated fluorescent probes is a key consideration, given the intracellular nature of the modulator binding site, since this allows the use of in cell target engagement binding assays, with the receptors in a native context, in addition to cell free membrane assays. The presented cell-permeable probes could therefore have a potential utility in future cell-based assays, as well as probes for CXCR2 expression and localization in native cells (e.g. neutrophils). Overall, the development of fluorescent probes and associated NanoBRET binding assays outlined in this study represents one of the first demonstrations of the applicability of this approach to GPCR intracellular allosteric modulator binding sites, together with very recent reports describing fluorescent CCR9 NAMs[238], CCR2 NAMS[239] and G protein peptidomimetic probes for G_s GPCRs that target a similar intracellular binding site.[203]

5.5 Fluorescent probes application

5.5.1 CXCR2 NanoBRET competition binding assays to assess unlabelled ligand affinities

Having shown that the fluorescent ligands **62a, c-f** bind CXCR2, they were used as tools to directly measure the affinity of unlabeled NAMs acting at the intracellular binding site of CXCR2 (structures shown in Figures 1.7, 1.8, 1.11 and Table 2.1).

To perform NanoBRET competition binding experiments in membranes from HEK293 CXCR2-NanoLuc cells, **62a** was chosen to be employed as the probe to measure the affinity of a variety of competing unlabelled CXCR2 NAMs, including both known literature compounds and previously presented protected congeners (Figure 5.7).[41,58,141,166,182,314] Unlabeled NAMs fully displaced the fluorescent ligand in a competitive manner, enabling the calculation of pK_i values (see Table 5.4) through application of Cheng-Prusoff correction. The values generated were in good agreement with previously reported CXCR2 affinity measurements for literature compounds[41,58,141,166,182,314], as well as the NanoBiT assay potencies established for *R*-navarixin (**2**) and its protected congeners in Table 5.1.

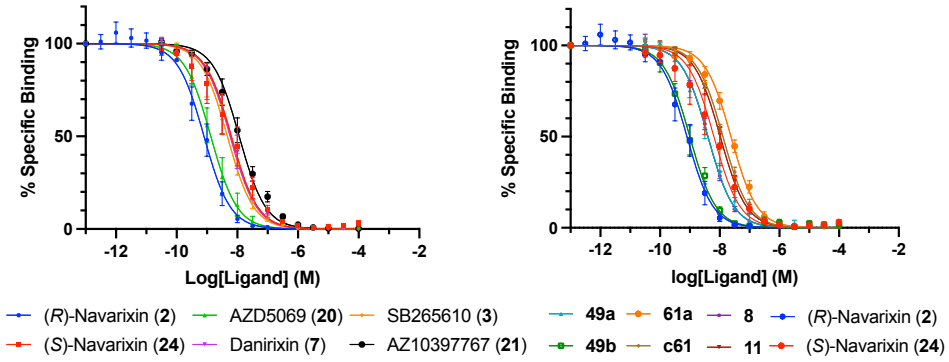

Figure 5.7: NanoBRET competition binding studies CXCR2 allosteric modulators in CXCR2 membranes. Membranes were incubated with 100 nM **62a** and increasing concentrations of unlabeled ligands for 3-hours at 37°C. The data shown represent the combined mean ± SEM of n = 5 experiments where each experiment was performed in duplicate.

Table 5.4 Measured binding affinities of CXCR2 NAMs using the **62a** NanoBRET assay and literature values[41,58,166,182,314]

Compound	pK_i ± SEM*	Literature pK_D
R-Navarixin (**2**)	9.19 ± 0.17	10.3[41,166]
49a	8.16 ± 0.16	-
49b	8.87 ± 0.06	-
61a	7.62 ± 0.05	-
61c	7.97 ± 0.04	-
SB265610 (**3**)	8.68 ± 0.21	8.5[58]
8	8.48 ± 0.06	-
Danirixin (**7**)	8.71 ± 0.12	8.2[314]
11	8.06 ± 0.08	-
AZD5069 (**20**)	9.61 ± 0.33	9.4[182]
AZ10397767 (**21**)	8.32 ± 0.12	8.7[182**]
S-Navarixin (**24**)	8.31 ± 0.28	-

*All values represent mean ± SEM of n=5 separate experiments. ** indicates pA_2 parameters derived from functional data

Furthermore, we performed NanoBRET competition binding experiments in membranes derived from a HEK293 CXCR1-NanoLuc cell line, employing **62d** as fluorescent probe and two competing CXCR1/2 NAMs, *R*- and *S*-navarixin (**2** and **24**). Membranes were incubated with 100 nM **62d** and increasing concentrations of unlabelled ligands for 1-hour at 37°C.

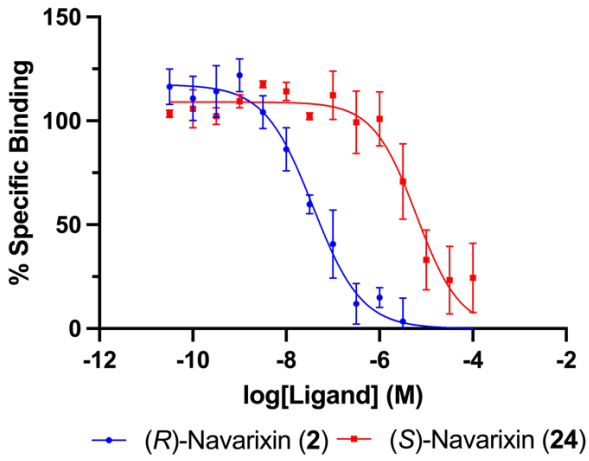

Figure 5.8: NanoBRET competition binding studies CXCR1 allosteric modulators in CXCR1 membranes. Membranes were incubated with 100 nM **62d** and increasing concentrations of unlabelled ligands for 1 hour at 37°C. The data shown represent the combined mean ± SEM of n = 3 experiments where each experiment was performed in duplicates. The error bars observed appear increased compared to those observed in CXCR2 assays as the BRET ratio window is smaller in CXCR1 compared to CXCR2.

Similarly to what was observed in the CXCR2 competition binding studies, the NAMs displayed full displacement of the fluorescent probe **62d** in a competitive manner at CXCR1 (Figure 5.8). It was therefore possible to calculate pK_i values through application of the Cheng-Prusoff correction, as previously described, for *R*-navarixin (**2**) ($pK_i = 7.66 \pm 0.15$) and *S*-navarixin (**24**) ($pK_i = 5.59 \pm 0.18$). Our data corroborate previous literature findings, indicating both enantiomers display reduced affinity for CXCR1.[166] They demonstrate the capabilities of our allosteric site fluorescent probe NanoBRET assay for direct assessment of binding affinity for novel CXCR1 and CXCR2 NAMs in future.

5.5.2 Kinetic studies

The characterised fluorescent probes can be employed not only to directly measure binding affinity of CXCR2 NAMs, but also to study the binding kinetics of the NAMs. Previous studies reported *R*-navarixin (**2**) to possess a slow dissociation rate from the receptor ($t_{1/2}$ ~22h)[41,139], a crucial characteristic which may have a strong influence on the potency of the molecule itself. Ultimately, the difference in affinity between the different CXCR2 NAMs may be explained in terms of different kinetics of receptor binding and different dissociation rates from the receptor.

According to the law of mass action ($D + R \rightleftharpoons DR$), the rates of association (k_{on}) and dissociation (k_{off}) are governed by the concentrations of the participants. K_{off} describes the rate of drug-target dissociation, is independent from the local drug concentration and it is expressed in time (e.g. min^{-1}). It is a first order or unimolecular rate constant, and can be viewed as the proportion of drug that dissociates from the receptor complex in unit time.[251] K_{on} is a second order or bimolecular rate constant (e.g M^{-1} min^{-1}), describing the rate at which the drug and the receptor (two molecules) associate.[251] However in a binding assay, the observed rate of drug association to equilibrium binding is defined as k_{obs} and is dependent on drug concentration, k_{on} and k_{off} . For single site binding $k_{obs} = k_{on}.[ligand] + k_{off}$. It is resulting from both dissociation and association rates, and it is highly dependent on drug concentration as a higher concentration of ligand results in a faster $k_{on(obs)}$. Therefore, k_{on} is equal to $(k_{obs} – k_{off})/[ligand]$ and it is expressed in M^{-1} min^{-1}.[251] In considering molecular interactions between drugs and their target binding sites, k_{on} may more sensitive to electrostatic interactions while k_{off} is influenced more by hydrogen bonds, salt bridges and Van der Waals interactions.[315,316] Extracellular water molecules could also influence the binding kinetics interrupting ligand-receptor hydrogen bonding. Therefore, hydrogen bonds that are shielded from the extracellular water molecules may be responsible for slow dissociation rates, forming more kinetically stable contacts[317] which increase the stability of the drug-receptor complex.[251,318] In addition, the dissociation and association rates are thought to be influenced

by the physicochemical properties of the binding ligand such as lipophilicity (logP), molecular weight and rotational bonds.[251,319] For example, lipophilic drugs possessing several non-polar substituents, should easily displace water on entry to the binding pocket and this may explain an increased on-rate with the receptor.[251,320] High molecular weight ligands, on the other hand, may result in reduced rates of receptor association, depending on the specific target, due to limited access to the binding pocket, if the passage to access it is narrow.[251,315]

The equilibrium dissociation constant (K_D) is a crucial pharmacological parameter which describes the drug concentration required to occupy 50% of the target receptor at equilibrium, or, if derived from saturation binding assays, as the concentration of ligand producing 50% of the maximal specific binding.[251] When measured in a closed system, K_D is an equilibrium parameter derived from the two kinetics parameters, association rate constant (k_{on}) and dissociation rate constant (k_{off}). At equilibrium k_{on} [DR] = k_{off} [D] [R] and K_D is defined as a ratio of these rate constants ($K_D = k_{off}/k_{on}$).[251,321]

The binding kinetic constants (k_{off} and k_{on}) have been recognized as key indicators of drug properties such as drug onset and duration of action[322], drug efficacy and side effect profiles.[323,324] Most focus on the impact of binding kinetics on drug discovery has concentrated on the influence of the dissociation rate constant (k_{off}), often referred to as its inverse residence time ($=1/k_{off}$).[325,326] Initially the benefits of slow k_{off} ligands have been considered in terms of prolonging target occupancy to extend the duration of pharmacological effect.[325]

Ligands with slower dissociation kinetics show an increase in potency over time which can be attributed to an increase in receptor occupancy over time[327] and increased receptor activation which promotes prolonged signalling[328,329]. The prolonged residence time is thought to be linked to an increased duration of action in *in vivo* studies.[330] A slow k_{off} can increase duration of action or change the observed mode of action.[30] The extent to which this occurs *in vivo* depends on the balance between k_{off} at the target, and the pharmacokinetic rate of elimination of the drug (k_{el}). For the k_{off} to be the determinant of the

duration of target occupancy, its value should be higher than k_{el}, if, on the contrary, $k_{off} << k_{el}$ the target becomes closer to get saturated and the k_{off} value is not the determinant.[326] As an example, the long duration of action of tiotropium, muscarinic receptor antagonist employed for respiratory diseases such as COPD, is the result of its long receptor residency time. Interestingly, it was found that in physiological conditions the dissociation half-life was shorter compared to nonphysiological conditions, therefore the duration of action was not solely the result of the slow dissociation of the receptor.[330] Secondly, kinetic properties of compounds may influence their selectivity for different targets and ligands with similar receptor affinities but different dissociation rates from the receptor, can result in markedly different target engagement, due to prolonged receptor occupancy[330], leading to an improved safety profile resulting from the avoidance of off target effect. An example of kinetics influencing selectivity has been reported for the muscarinic receptor M3 antagonist for which lower M2 receptor blockage, resulting from different k_{off} from the receptor, resulted in avoidance of cardiovascular side effect.[331] K_{off} differences are also capable of altering pharmacological behaviour of the ligands in a manner which may be beneficial for the desired therapeutic response, in systems which are not at equilibrium. Insurmountable inhibition can be advantageous for an effective antagonist profile, particularly in context where the concentration of stimulating messenger is high, for example in tumour microenvironments, in neuronal synapses or during inflammation flare ups.[332,333] Under these conditions, slow dissociation rates can contribute to insurmountable inhibition (reduction in maximal response even in the presence of high concentrations of agonist or substrate) of the receptor at early timepoints[334] that is resistant to variations in stimulating agonist concentrations.[31] This behaviour can improve the clinical effect of the antagonist during acute inflammation.[31] For agonists, k_{off} also determines the time to equilibrium, and differences in agonist kinetics can also dictate distinct time dependent signalling profiles across different assays, and be a factor in considering biased pathway dependent signalling of receptor agonists.[327]

The additional importance of k_{on} for pharmacology has only recently become apparent. When the target is within a region of restricted diffusion (for example a neurotransmitter synapse), the drug molecules may re-associate with nearby receptors.[30] This process, known as rebinding, is promoted by more rapid association rates. This causes the elevation of local effective drug concentration within the restricted reservoir, providing a mechanism to prolong target occupancy and improve apparent potency. This relationship has recently been proposed between the association rates of D2 targeting antipsychotics, and the risk of extrapyramidal side effects elicited via D2 containing synapses in the nigrostriatal pathway.[30,335]

Kinetic parameters of different CXCR2 NAMs, in addition to the allosteric mode of action, may therefore have an effect on their functional effects at the receptor. For this reason, it was decided to employ the generated fluorescent ligands and establish a competition association binding assay methodology [250,336] to determine the binding kinetic properties of different CXCR2 NAMs present in the literature.

In the Motulsky-Mahan approach, the receptor preparation is mixed with the fluorescent probe at a single concentration, and a range of concentrations of unlabelled ligand acting as competitor. The profiles of the association kinetic curves are dependent on the relative kinetics of the tracer and unlabelled ligand. For example, a peak-plateau behaviour is observed for unlabelled ligands with slower kinetics than the tracer, because in this case the tracer binds first, and then re-equilibrates with unlabelled ligand binding at later timepoints. These sets of curves can be fitted globally to a model of competitive binding to provide k_{on} / k_{off} estimates for the unlabelled ligand, as well as the probe. The homogenous BRET format we established is highly advantageous for these kinetic studies since high resolution kinetic data can be obtained over time from a single assay well. Moreover, a condition of the competitive-association model is that the probe and unlabelled ligand compete for the same binding site, therefore the generation of fluorescent probes for the CXCR2 allosteric binding site was essential for its application to the unlabelled NAM series.

Compound **62e** was selected as more optimal fluorescent probe to use for kinetics studies as it possesses a moderate-high affinity for the receptor, but lower compared to the *N*-methyl fluorescent ligands (Table 5.2), together with a fast off rate (0.022 ± 0.002 min^{-1}) (Figure 5.10). The use of a fast off, lower affinity probe retaining suitable selectivity extends the dynamic range of unlabelled ligand kinetic parameters that can be estimated using the methodology[250], and in this instance was preferable to the *N*-methyl derivatives. Association kinetic curves for the fluorescent ligand were generated on the same day as the competition association binding assays were performed and the k_{off} and k_{on} of the fluorescent probe estimated in this manner were used as constants in the Motulsky-Mahan fitting to obtain unlabelled ligand kinetics form the experiment. This helped control for experiment to experiment variation influencing the parameters, for example small changes in temperature.

Further optimisation for the analysis of the binding kinetics of unlabelled CXCR2 NAMs focused on the choice of assay buffer. The optimization was performed employing *R*-navarixin (**2**) as the unlabelled ligand competing with the chosen fluorescent probe **62e**. Initially, the assay was performed in the same conditions used for the competition binding studies shown previously in this chapter, which did not include Na^+ in the assay buffer (Figure 5.9 A). Employing these conditions, we were unable to obtain kinetics data for the unlabelled ligand as the k_{on} and k_{off} values were unstable since the data did not fit the model adequately (Figure 5.9 A). Potentially this may reflect a mixed population of receptor conformations within the assay. It was therefore decided to add Na^+ into the buffer (chapter 8.2), to concentrations equivalent to the extracellular concentration. For many GPCRs, the addition of Na^+ shifts the conformational equilibrium towards the inactive state.[337,338] It might be predicted that this is the conformation with higher affinity for negative allosteric modulators such as *R*-navarixin (**2**)[45]. This change alone was not sufficient to allow the measurement of k_{on} and k_{off} for the unlabelled compound tested since the data still did not adequately fit the model, resulting in unstable kinetics parameters generation (Figure 5.9 B). Subsequently, Gpp(NH)p, a non-hydrolysable GTP analogue, was added to the Na^+ buffer,

to ensure that the G-protein is uncoupled (and remains uncoupled)from the receptor[327,339–341]. In combination with high sodium concentrations, this also reduces the availability of high affinity active complex stabilized by Gαβγ binding. Gpp(NH)p forces the G-protein to remain dissociated as Gα-Gpp(NH)p and Gβγ subunits, therefore not free to bind the receptor allosterically as the heterotrimer.[339,340] Association kinetics were also followed for an increased timecourse of 120 min. Overall, the addition of Gpp(NH)p to the high sodium buffer generated high quality association kinetics tracers and allowed accurate fitting and measurement of k_{on} and k_{off} and kinetically derived pK_D for the unlabelled compounds (Figure 5.9 C). It was therefore decided to use a 136 mM Na^+ buffer with the addition of 100 µM of Gpp(NH)p in the future competition binding assays performed to study binding kinetics of the unlabelled CXCR2 NAMs.

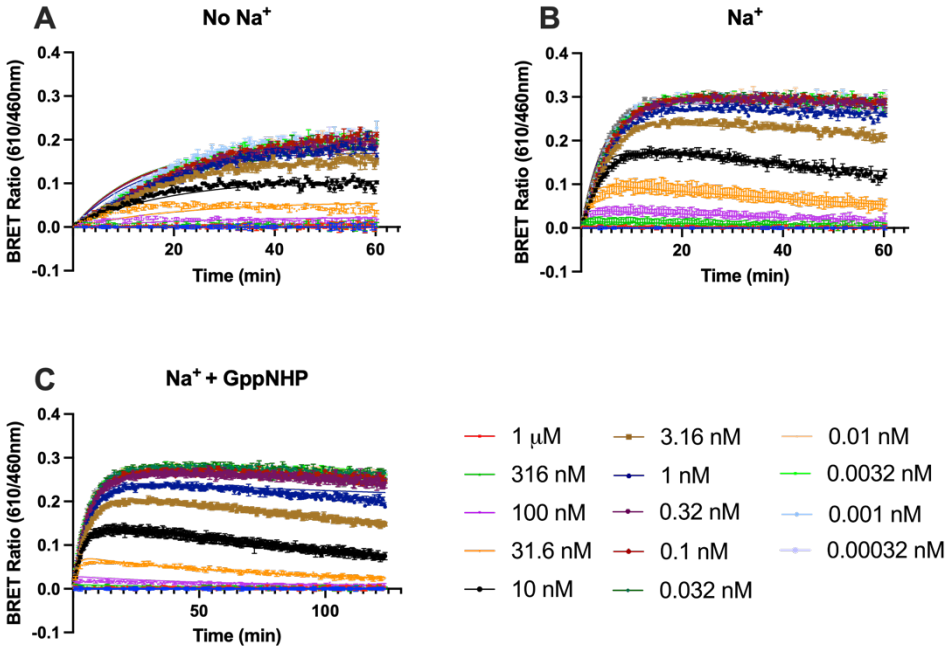

Figure 5.9: Optimisation of the assay buffer for competition kinetics of **62e** in the presence of increasing concentrations of unlabelled *R*-navarixin (**2**). A) No Na^+ buffer; B) Na^+ buffer; C) Na^+ + 100 µM of Gpp(NH)p. Data shown are representative experiments (of 5 performed) fitted to a global model of competition association kinetics for single site binding.

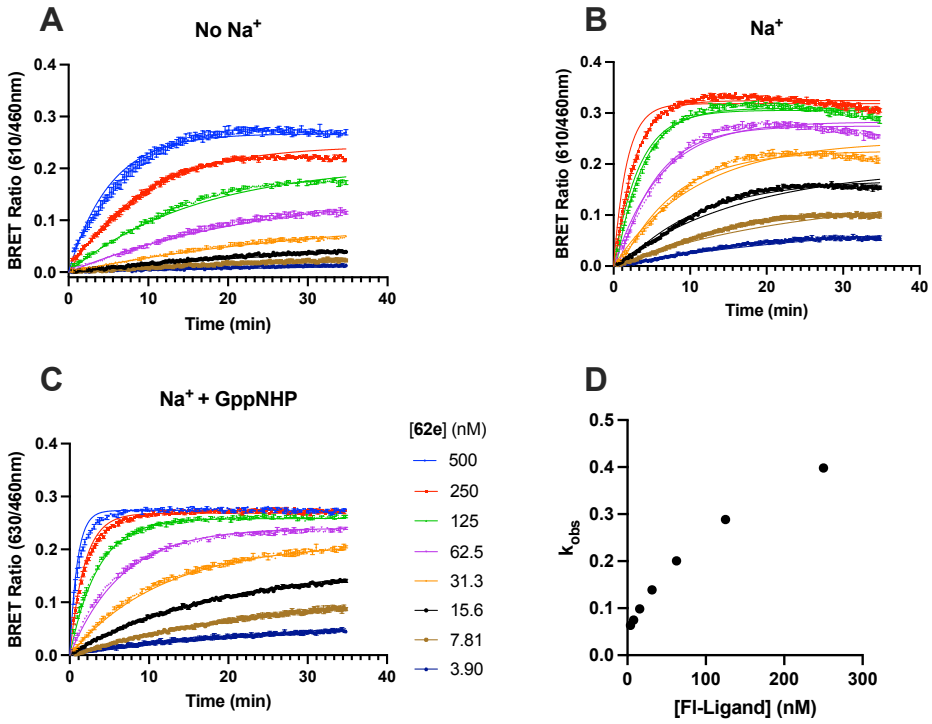

Figure 5.10: Association binding kinetics of **62e** at CXCR2-NanoLuc membranes. A) No Na^+ buffer; B) Na^+ buffer; C) Na^+ + 100 µM of Gpp(NH)p. Membranes were incubated with increasing concentration of fluorescent ligand and 10 µM of *R*-navarixin (**2**) to determine NSB. Dual emission wavelengths were monitored for 60 min and binding was represented by the BRET ratio. Data points show the specific binding (total - NSB) for a representative experiment fitted to a global model of association kinetics for single site binding. D) Plot of [**62e**] concentration (as displayed in 5.10B) against k_{obs} showing binding following a simple law of mass action model with k_{obs} increasing with concentration. The non-linear trend displayed suggests a multi-site binding relationship.

Graph 5.10 B did not adequately fit the model suggesting multi-site binding. This was then confirmed by the plotting of k_{obs} against ligand concentration, displaying a non-linear relationship. This observation is likely due to the presence of native G-protein proteins driving conformational change of a small population of receptors within the system into a high-affinity state which is in contrast to the negative modulation (towards the inactive

conformation) promoted by the inclusion of sodium. This hypothesis is further strengthened upon the inclusion of Gpp(NH)p which results in a much more reliable fit with the one-site binding model.

Fluorescent compound **62e** was employed to probe binding kinetics of some of the previously presented CXCR2 NAMs present in the literature. Through competition binding NanoBRET assays performed in CXCR2-NanoLuc membranes it was possible to obtain a clearer picture of the kinetic profiles of the unlabelled NAMs, with a particular interest to the compounds which were reported to have a very slow dissociation rate from the receptor.[41,139,182]

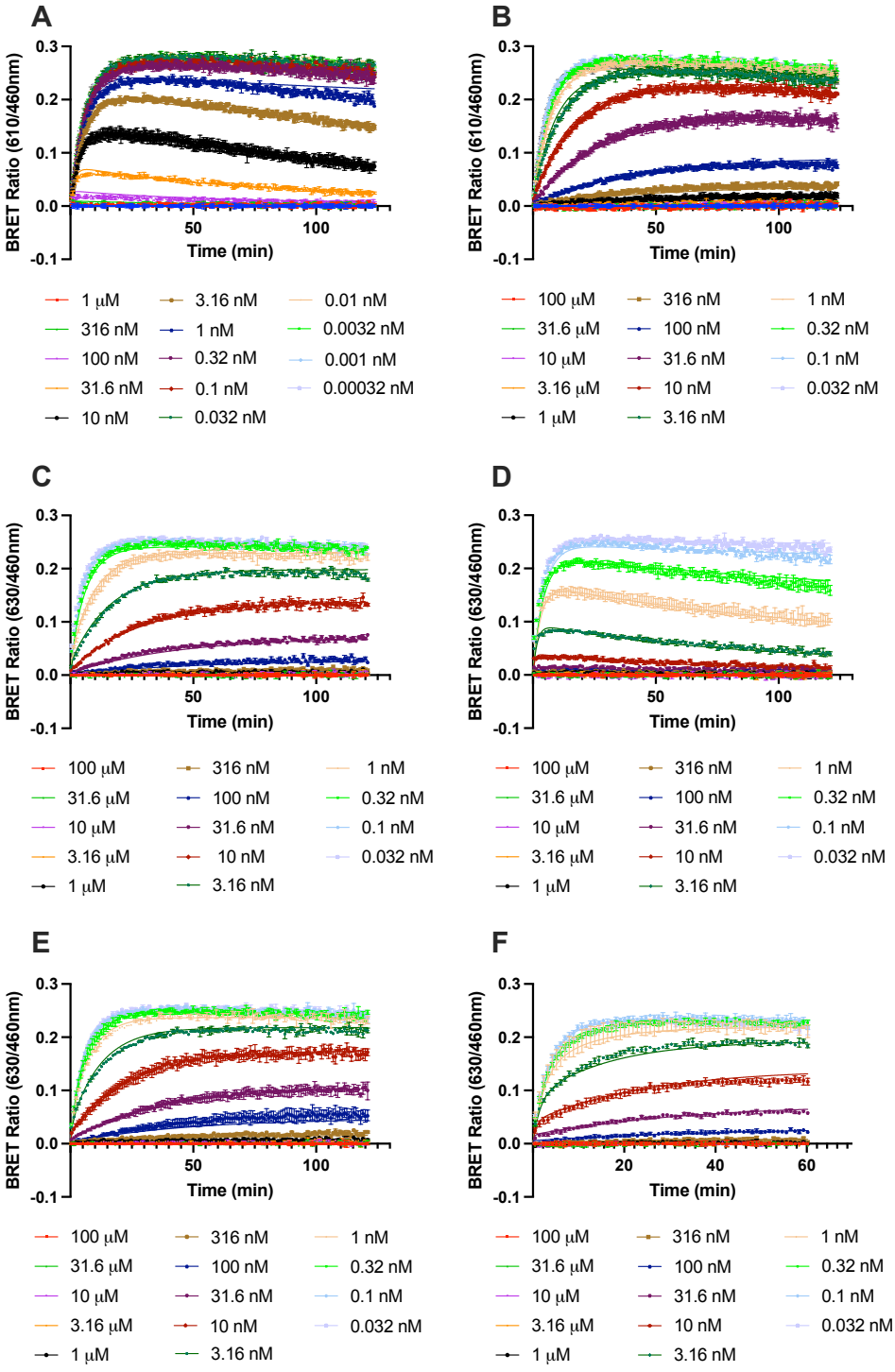

Figure 5.11: Competition kinetics curves of 100 nM **62e** at CXCR2-NanoLuc membranes in the presence of increasing concentrations of unlabelled NAMs. A) *R*-navarixin (**2**); B) *S*-navarixin (**24**); C) SB265610 (**3**); D) AZD5069 (**20**); E) Danirixin (**7**); F) AZ10397767 (**21**). The fluorescent tracer binding was recorded kinetically over 120 min or 60 min. Buffer containing Na^+ + 100 µM of Gpp(NH)p. Data are representative experiments from n = 5 individual experiments performed in duplicates.

Table 5.5 Kinetic binding parameters of the fluorescent probe **62e** and of unlabelled CXCR2 NAMs from global association fits and the Motulsky-Mahan model of competitive binding.

Labelled ligand	**k_{on} (M^{-1} min^{-1}) ± SEM**	**k_{off} (min^{-1}) ± SEM**	**Kinetic pK_D ± SEM**
62e	1.9 ± 0.2 x 10^6	0.022 ± 0.002	1.67 ± 0.04
Unlabelled ligands			
R-navarixin (**2**)	0.48 ± 0.14 x 10^8	0.0039 ± 0.0007	10.1 ± 0.13
S-navarixin (**24**)	5.5 ± 3.8 x 10^8	1.7 ± 0.7	8.22 ± 0.13
SB265610 (**3**)	5.2 ± 1.5 x 10^8	0.55 ± 0.1	8.94 ± 0.04
AZD5069 (**20**)	0.68 ± 0.18 x 10^8	0.0042 ± 0.0006	10.1 ± 0.16
Danirixin (**7**)	1.0 ± 0.3 x 10^8	0.2 ± 0.05	8.65 ± 0.07
AZ10397767 (**21**)	1.8 ± 0.5 x 10^8	0.1 ± 0.02	9.14 ± 0.11

* Kinetically derived K_D values were derived from a ratio of dissociation and association rates ($K_D = k_{off}/k_{on}$). All values represent mean ± SEM of n=5 separate experiments. Values were in good agreement with measured binding affinities reported in table 5.4.

As shown in figure 5.11 A and D, *R*-navarixin (**2**) and AZD5069 (**20**) present very slow dissociation rates from the receptor, as predicted from previous studies[41,182], with k_{off} values of 0.0039 ± 0.0007 min^{-1} and 0.0042 ± 0.0006 min^{-1} respectively (Table 5.5). They both produced a rise-and-fall to steady-state type of curve[342], generally observed for unlabelled competitors that possess slower k_{off} compared to the fluorescent probe.[321] The other NAMs tested, AZ10397767 (**21**), danirixin (**7**) SB265610 (**3**) and *S*-navarixin (**24**) in order of increasing k_{off}, showed lower affinities and faster dissociation rates from the receptor.

Both allosteric mechanisms and slow off rate (non-equilibrium) effects can lead to insurmountable antagonist behaviour. The data presented in chapter 2.2 showed that, from functional assays, *S*-navarixin (**24**) and *R*-navarixin (**2**) exhibit a surmountable antagonist and non-surmountable antagonist profile respectively, despite both binding the same allosteric site. The kinetics data presented (Table 5.5) show that the observation of insurmountability in this series is driven by a slow k_{off}, rather than the allosteric mechanism. On the other hand, rapidly dissociating compounds display surmountable properties in which high levels of competing agonist can overcome the inhibitory effect of the ligand[31,330], in accordance with previous functional studies findings (Chapter 2.2) for *S*-navarixin (**24**).

In a more extended study of the literature NAMs (performed by Dr Desislava Nesheva, University of Nottingham; Figure 5.12), this correlation was observed for all the NAMs tested. As an example, AZD5069 (**20**) was found to have an insurmountable behaviour, similarly to *R*-navarixin (**2**)**.**

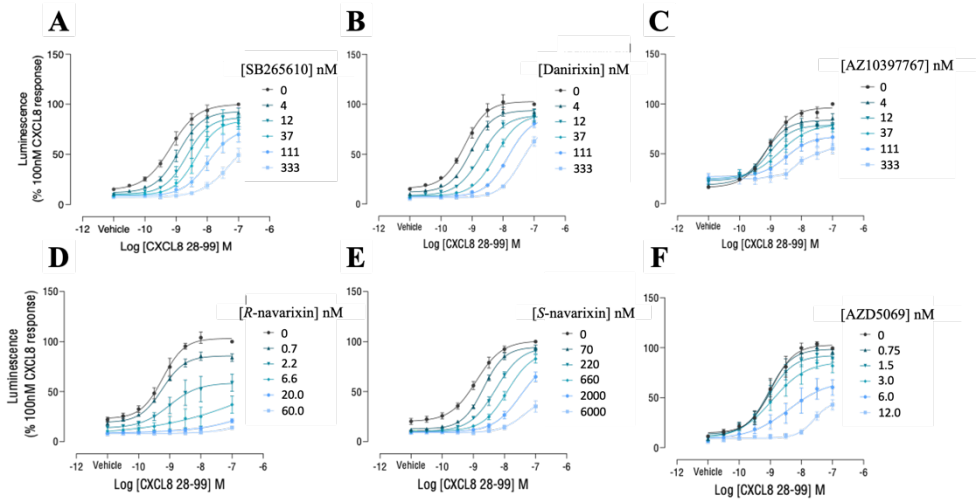

Figure 5.12: Effect of NAMs on CXCR2 - βarrestin2 interactions measured with the NanoBiT complementation system (Chapter 2.2). Concentration-response curves (30-minute time-point) of $CXCL8_{28-99}$ with a range of concentration of the NAMs A) SB265610 (**3**); B) danirixin (**7**); C)AZ10397767 (**21**); D) *R*-navarixin (**2**); E) *S*-navarixin (**24**); F) AZD5069 (**20**). Cell line was pre-treated (1 hour at 37 °C) with the compounds prior to furimazine substrate loading and $CXCL8_{28-99}$ stimulation. Graphs represent pooled data from 5 individual experiments; error bars = S.E.M. Data and figure generated by Dr Desislava Nesheva (University of Nottingham).

Slow k_{off} NAMs also show equivalent insurmountability in further functional assays.[100,166,182] Therefore, a slow k_{off} can be a valuable property for a potential therapeutic drug. For CXCR2 NAMs optimizing the k_{off} could be a crucial step of an effective allosteric antagonist design that generates insurmountability and effective inhibition, for example against transiently high levels of chemokine in inflammatory storms.

Together, this data highlights the binding capabilities of synthesized novel fluorescent ligands. It presents a diverse toolkit applicable in both highly selective CXCR2 targeted or CXCR1 related assays within both membrane and whole cell systems and demonstrates efficient derivation of unlabelled ligand binding parameters, including the successful and novel application of kinetic binding methodology to an intracellular allosteric binding site.

Chapter 6. Conformational analysis of methylated and unmethylated ligands

An interesting and recurrent observation in the pharmacological data, shown in chapter 5, is the enhanced potency of *N*-methylated ligands over their unmethylated analogues. This is seen, for example, in the difference in affinity between fluorescent ligand **62d** and **62f** compared to **62c** and **62e** respectively. The original docking studies presented in chapter 3, upon which the ligand designs were based on, could not predict this finding. In fact, they suggested that the *N,N*-dimethylamide portion of *R*-navarixin (**2**) was protruding from the binding pocket and it was not involved in significant interactions with the receptor. Therefore, to rationalize the pharmacological data, it was decided to perform some additional studies, with a particular focus to the *N*-methylamide portion of the congeners, analyzing some intermediates made during the synthesis of the fluorescent probes. Compounds **49a** and **49b** were initially chosen for the analysis, as they include a short *N*-Boc protected ethylenediamine linker, with or without *N*-methylation of the amide, more convenient for docking purposes, being not excessively long and flexible. Moreover, these two analogues showed a notable difference in potency when tested in the NanoBiT assay previously described in chapter 5 (**49b** > **49a**). The compounds were docked in CXCR2 crystal structure (PDB:6LFL) humanized with Ala249$^{6.33}$ following the methodology previously described in chapter 3. The binding poses of both compounds mimic that for *R*-navarixin (**2**) and no significant difference was shown in the interaction with the receptor or in docking score between the *N*-methylated (**49b**) and the unmethylated (**49a**) analogues. Since docking studies did not provide sufficient data which could explain the difference in potency between the analogues, we decided to focus on their potential difference in structural conformation. Initial evidence for this arose from the observation of broadened signals in the ^{1}H-NMR spectra of the methylated compounds with respect to the corresponding unmethylated analogues, suggesting that methylation could affect the conformational preference of the

ligands. To perform more detailed structural NMR studies, we selected two previous intermediates in the synthesis, compounds **56a** and **56b**. These compounds can be considered as "minimal ligands" as they retain either a methylated or unmethylated amide moiety, the phenol moiety and a mixed squarate moiety, lacking the chiral furanylalkylamino moiety, which is replaced with an ethoxy group. In addition, the lack of chirality of analogues **56a** and **56b** facilitated more straightforward acquisition and analysis of ^{1}H-NMR spectra with a focus on the conformational nature of the benzamide region. Firstly, ^{1}H- NMR spectra for each compound in d_6-DMSO were fully assigned using two-dimensional NMR spectroscopy experiments (Correlation spectroscopy (COSY), Heteronuclear single-quantum correlation spectroscopy (HSQC) and Heteronuclear multiple-bond correlation spectroscopy (HMBC)). In addition, variable temperature NMR (VT-NMR) experiments in deuterated dimethyl sulfoxide (d_6-DMSO) on both compounds were performed to analyse the effect of the temperature on the chemical shifts (Figure 6.2, 6.3). NMR chemical shifts, in fact, are sensitive probes of structure and dynamics[343] of molecules and can sometimes be temperature dependents. Therefore, VT-NMR experiments could be useful to offer structural insights and to facilitate resolution of overlapping peaks which may separate due to different temperature dependence.[343] Hydrogen bonding protons chemical shift could vary with temperature. As the temperature rises the amount of hydrogen bonding diminishes[344] as higher temperatures could weaken the hydrogen bonds and could therefore reduce the electron withdrawing effect of the hydrogen bond acceptor on the proton resulting in a more shielded proton with a change in chemical shift which moves upfield.[343,345–347]

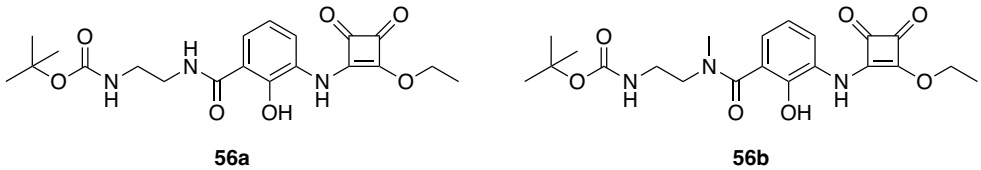

Figure 6.1: Structures of compounds **56a** and **56b**.

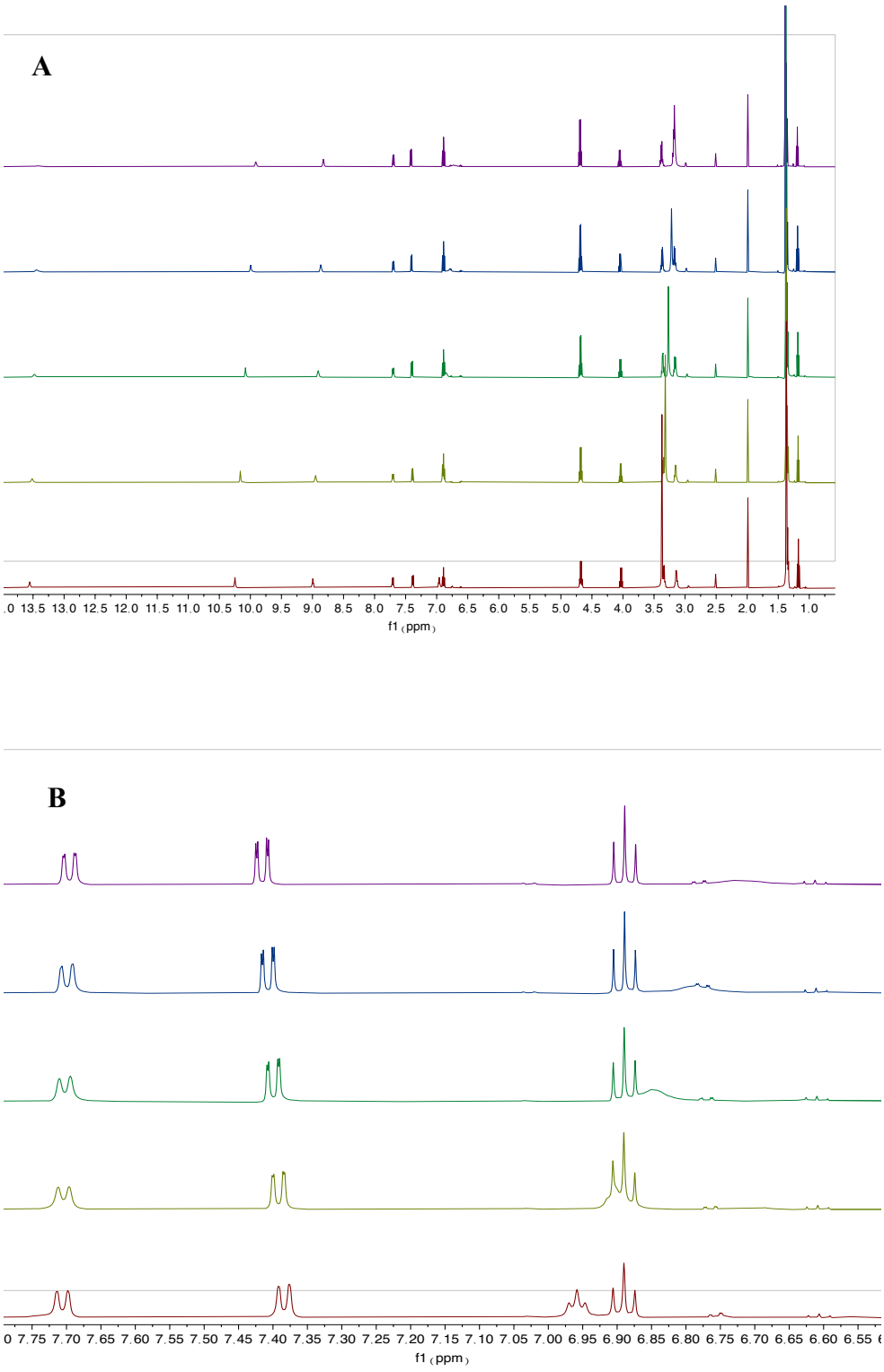

Figure 6.2: Variable temperature (VT) ^{1}H- nuclear magnetic resonance spectroscopy (NMR) experiments of compound **56a** in d_6-DMSO. A) View of the whole spectra and B) magnification of the aromatic region. Red spectrum recorded at 25 °C, yellow spectrum at 35 °C, green spectrum at 45 °C, blue spectrum at 55 °C, violet spectrum at 65 °C.

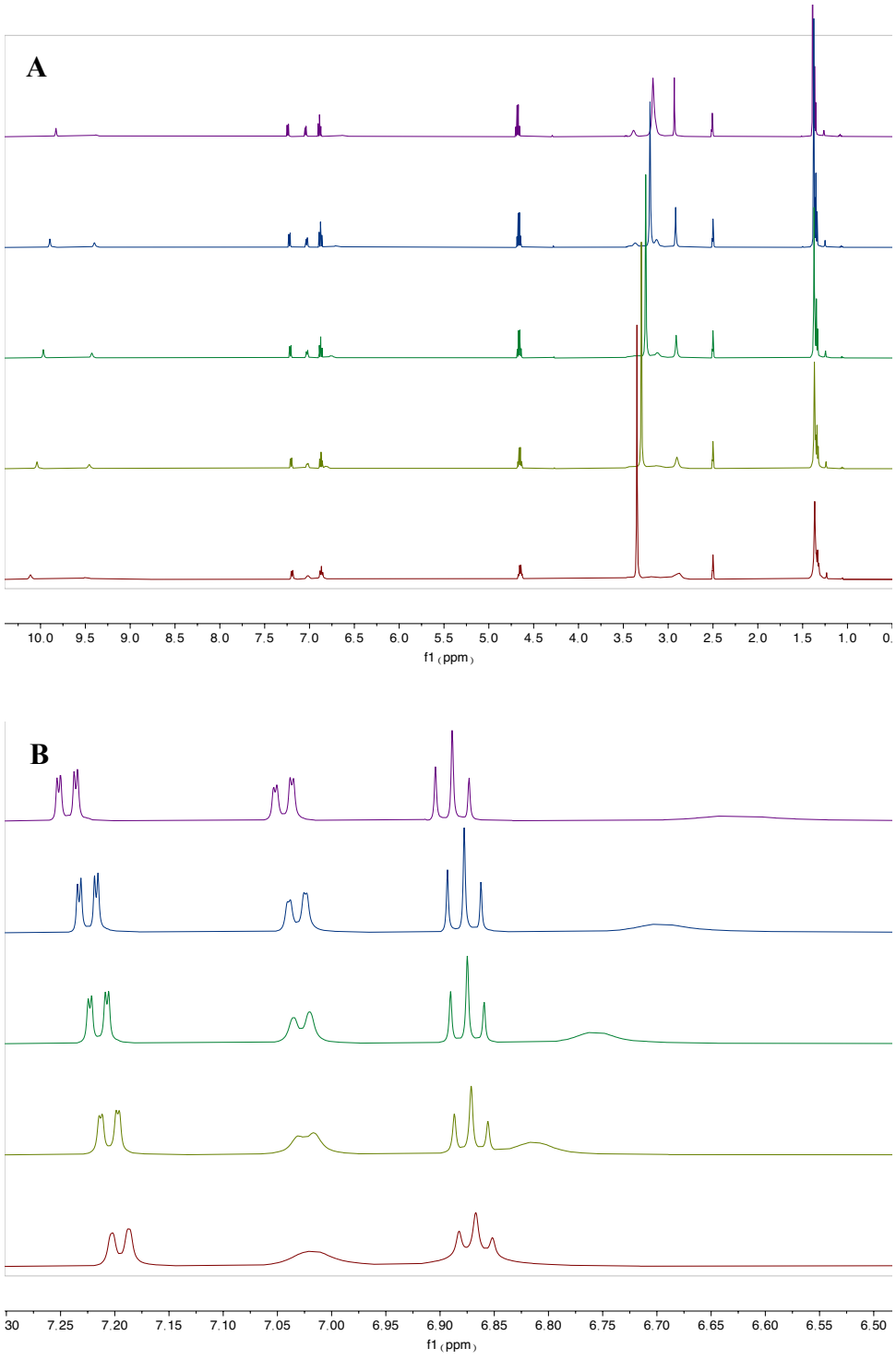

Figure 6.3: Variable temperature (VT) ^{1}H-NMR experiments of compound **56b** in d_6-DMSO. A) View of the whole spectra and B) magnification of the aromatic region. Red spectrum recorded at 25 °C, yellow spectrum at 35 °C, green spectrum at 45 °C, blue spectrum at 55 °C, violet spectrum at 65 °C.

^{1}H-NMR spectra for compounds **56a** and **56b** were acquired at variable temperature, starting from room temperature (25 °C) and rising the temperature of 10 °C each time up to 65 °C. Temperatures higher than 65 °C were evaluated but the spectra of both compounds did not change above this temperature. Therefore, it was decided to report data up to 65 °C. As seen in Figure 6.1 and 6.2, the only proton that varies its chemical shift with temperature is the N**H**-Boc proton. In both compounds the chemical shift of this carbamate proton moves upfield and becomes broader. For compound **56a** its signal changes from a triplet at 6.95 ppm at 25 °C to a broad singlet at 6.70 ppm at 65 °C (Figure 6.2). Similarly, for compound **56b**, the amide proton signal moves from overlapping with aromatic proton-5 at 6.87 ppm at room temperature to a broad singlet at 6.62 ppm at 65 °C (Figure 6.3). Interestingly, for both compounds, the signals of the aromatic protons 4 and 6 (7.38 and 7.70 ppm respectively for compound **56a** and 7.19 and 7.02 ppm respectively for compound **56b**) resolve at higher temperature from a doublet to a doublet of doublets (Figure 6.2 and 6.3). Notably, also the water peak moves upfield as the temperature increase (3.35 ppm at room temperature). From VT-NMR experiments it was not possible to obtain information about the structure of the molecules. Subsequently, to obtain structural information, we employed Rotating-frame nuclear Overhauser effect spectroscopy (ROESY), as suggested by the NMR specialist in the university department who provided precious advice in performing the experiments and in the analysis of the spectra. This NMR technique, used to establish through-space correlation between nuclei physically near to each other[348,349], allowed to visualize the interactions of the protons in the molecule that are close in space rather than through chemical bonds.

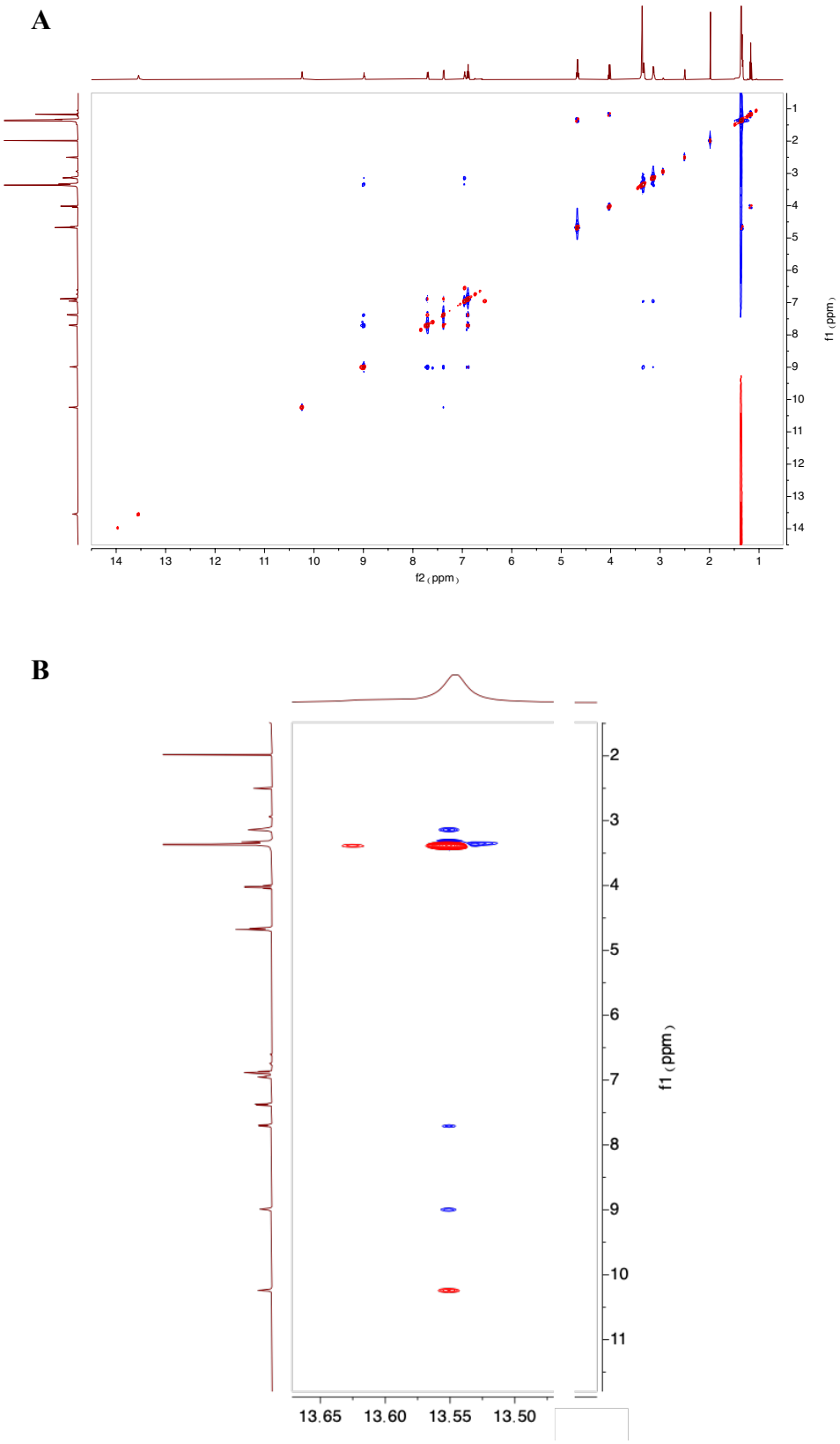

Figure 6.4: A) Full ^{1}H-^{1}H Rotating-frame nuclear Overhauser effect spectroscopy (ROESY) NMR experiment for compound **56a** in d_6-DMSO at 25 °C and B) magnification of the phenol interactions. The relevant ^{1}H proton

experiments are displayed on the x- and y-axes. ROE cross peaks (representing through-space interactions) are shown in blue and exchange cross peaks are shown in red.

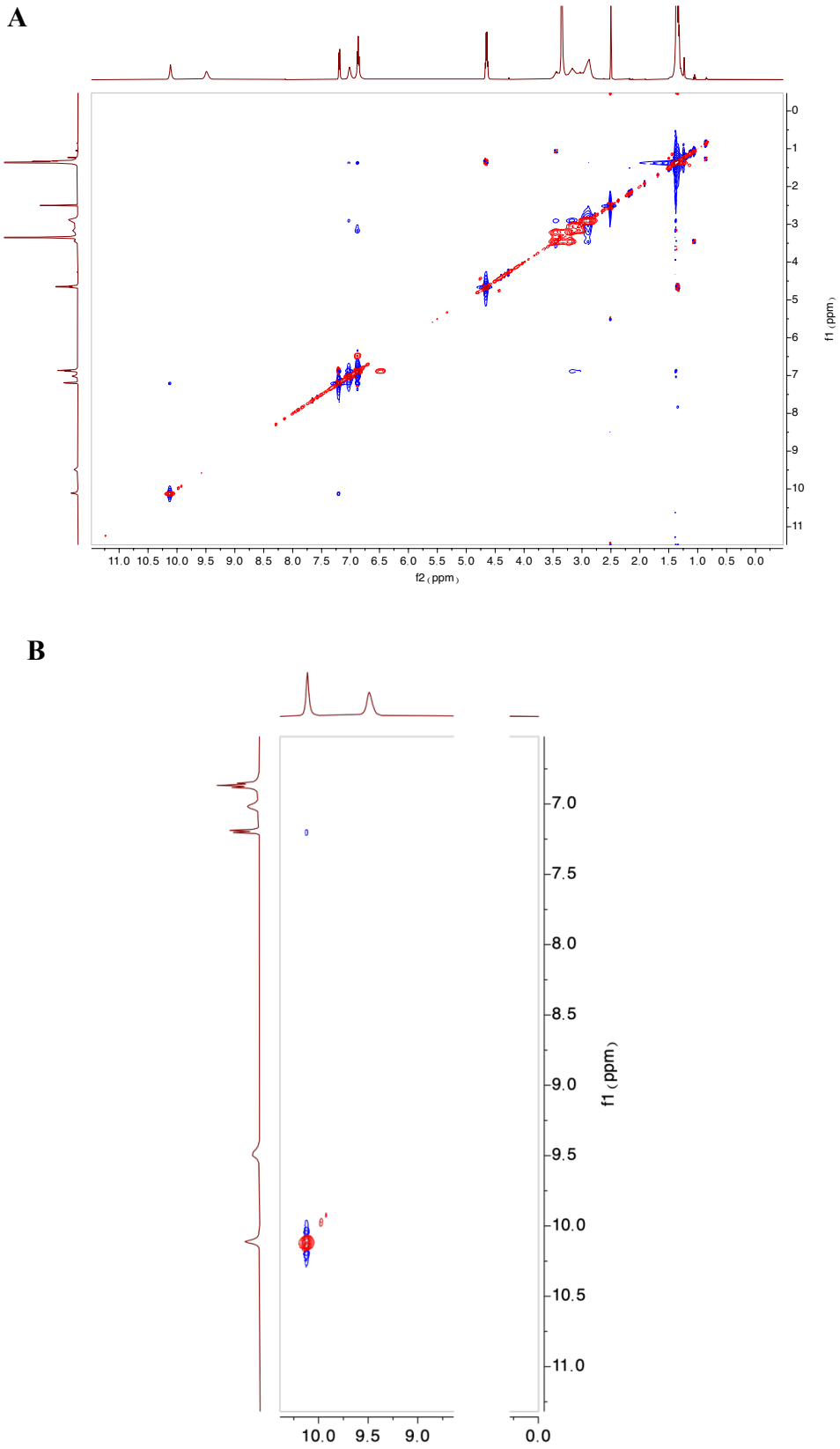

Figure 6.5: A) Full ^{1}H-^{1}H ROESY NMR experiment for compound **56b** in d_6-DMSO at 25 °C and B) magnification of the phenol interactions. The

relevant ^{1}H proton experiments are displayed on the x- and y-axes. ROE cross peaks (representing through-space interactions) are shown in blue and exchange cross peaks are shown in red.

Overall, the through-space interactions formed were similar for both methylated and unmethylated analogues. Figures 6.4 and 6.5 show through-space interactions (blue dots) between the aromatic protons, the aromatic protons and the benzylic amide proton or the *N*-methyl protons, the amide protons (both N**H**-Boc and benzylic amide N**H**) and both the adjacent ethylene CH_2 protons, the squaramide proton and the ethyl ester protons. Moreover, the Boc group was spatially interacting with the ethylenediamine linker protons and weakly interacting with the aromatic protons, probably transiently. Interestingly, compounds **56a** and **56b** differ particularly in their phenolic OH signal. Notably, the phenolic OH peak is shifted downfield in the unmethylated compound **56a** with respect to the *N*-methylated analogue **56b** (13.5 ppm and 9.4 ppm respectively). Moreover, for the phenolic OH of compound **56a**, several through-space interactions with other protons of the molecule, such as the benzamide NH and adjacent CH_2 protons of the ethylene region and the aromatic protons, were detected (Figure 6.4.B). Conversely, no through-space interactions were detected for the phenolic OH in the *N*-methylated compound **56b**. These data suggest that the *N*-methyl group could introduce a conformational restriction in compound **56b** and consequently in the other *N,N*-dialkylamide analogues, preventing intramolecular hydrogen bonding between the phenol and benzamide moieties. On the other hand, the absence of the *N*-methyl group allows the above intramolecular hydrogen bond to form, making phenol less available for receptor interaction. Furthermore, the need to disrupt the intramolecular hydrogen bond would confer an energetic penalty. This could explain the difference in potency between unmethylated and methylated analogues, as previous studies[162] suggest the interaction between the phenol and the receptor is crucial. Additionally, the rotational restriction present in the *N*-

methylated analogue **56b**, could promote a conformation of the molecule that favours receptor binding.

Alongside the NMR experiments, molecular dynamics simulations of **56a** and **56b** in DMSO were performed by Professor Charles Laughton.

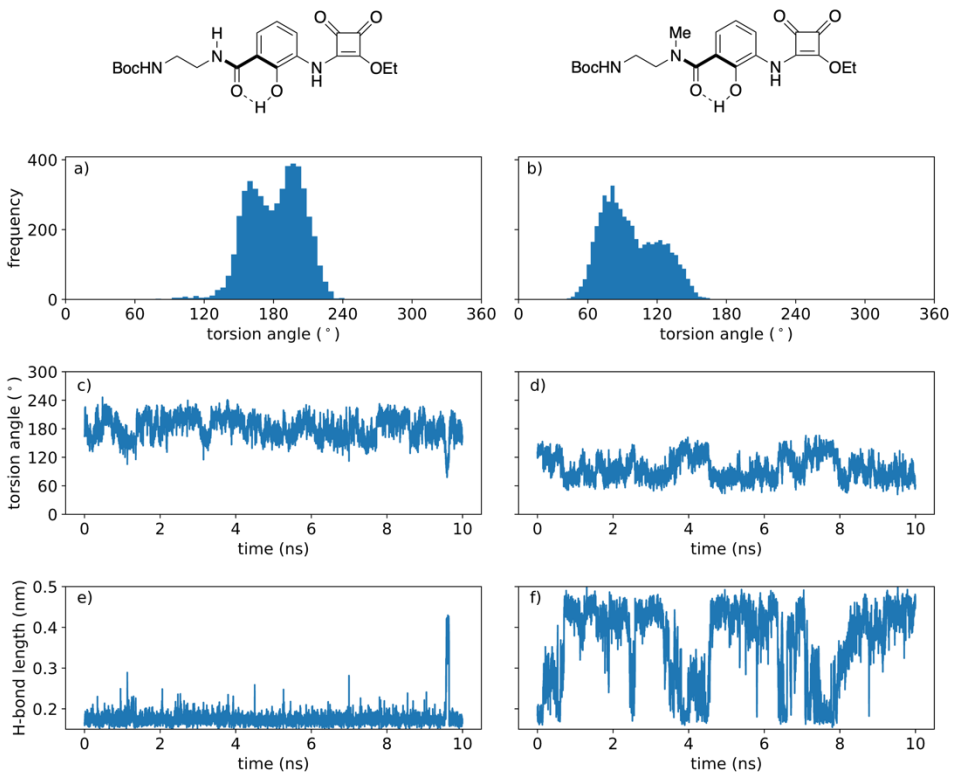

Figure 6.6: Conformational analysis of molecular dynamics simulations of **56a** and **56b** in DMSO. Panels a) and b): torsion angle distributions for the highlighted bond in **56a** and **56b** respectively. Panels c) and d): time courses for the selected torsion angle. In **56a** the angle rapidly and repeatedly passes through the planar (180 degrees) conformation, while for **56b** it is restricted (atropisomerism, at least on this timescale). Panels e) and f): time courses for the distance between the carbonyl oxygen and phenolic hydrogen atoms in **56a** and **56b** respectively). In **56a** a strong H-bond is maintained, whilst in **56b** it is present or absent depending on whether the high or low twist conformation of the torsion angle is adopted. Image generated and analysed by Professor Charles Laughton.

These predict that the key amide bond maintains a strict *trans*-geometry in both molecules, but that the neighboring bond connecting to the phenolic ring (torsion angle highlighted in Figure 6.6) behaves very differently in **56b** compared to **56a**. In the unmethylated compound **56a**, we observe the torsion angle distribution (Figure 6.6.a) shows a bifurcated maximum ~20 degrees either side of 180 degrees, with a low barrier between the two states that is crossed rapidly and repeatedly over the 10ns simulation (Figure 6.6.c). Throughout this time a hydrogen bond between the amide oxygen and phenolic OH is highly conserved (Figure 6.6.e). In contrast, for the methylated compound **56b**, we observe the torsion angle distribution (Figure 6.6.b) shows a bimodal distribution with maxima at 80 degrees and 120 degrees. Transitions between the two states are rapid and frequent (Figure 6.6.d) and correlate with the formation (120 degrees) and breakage (80 degrees) of the hydrogen bond with the phenolic OH (Figure 6.6.f). There is a symmetry-related conformation when the torsion angle lies in the -80 to -120 range. This can be generated by the application of torsion angle restraints to the simulation to drive it through the planar state, but the increased steric hinderance provided by the *N*-methyl group means that, in contrast to **56a**, we observe no spontaneous transitions, at least on the 10 ns timescale (results not shown).

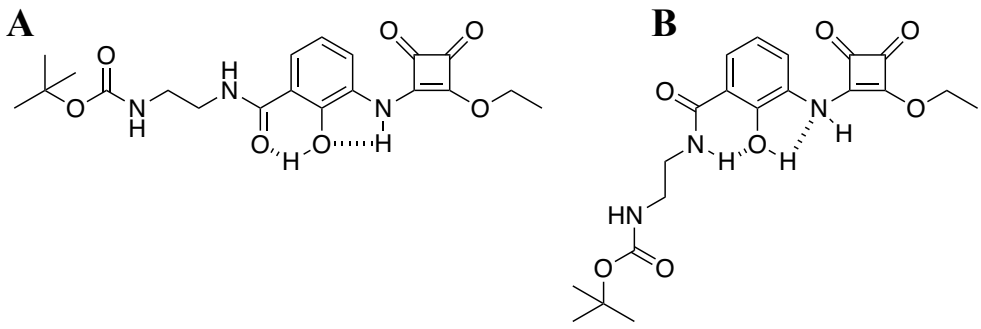

Figure 6.7: Possible intramolecular hydrogen bonding pattern for compound **56a**.

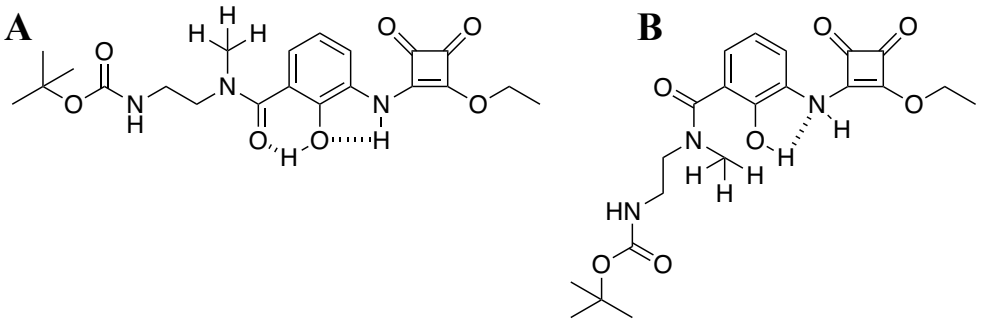

Figure 6.8: Possible intramolecular hydrogen bonding pattern for compound **56b**. Notably, in 6.8.B no intramolecular hydrogen bonds are shown.

The simulations thus are in full agreement with the NMR analysis, supporting the hypothesis that a considerable portion of the enhanced activity of *N*-methylated analogues could come from the effects that this modification has on the structure of the free ligand. Methylation favors a less planar conformation and a weaker intramolecular hydrogen bond, both of which would be expected to contribute to a more favorable binding free energy, ultimately resulting in the increased potency of the *N*-methylated analogues.

Chapter 7. General conclusions and future work

CXCR2 is a member of G protein-coupled receptor family and a key mediator of inflammation. It regulates neutrophil chemotaxis, integrin expression and activation, cell motility, polarization, respiratory burst, phagocytosis, proliferation, apoptosis, calcium mobilization and angiogenesis.[8,42] Playing a critical role in the regulation of neutrophil homeostasis and release from the bone marrow[8,49,50], CXCR2 is involved in a variety of diseases with inflammatory components[8,42] including pulmonary diseases[9], such as COPD, asthma and cystic fibrosis.[8,9] Moreover, CXCR2 plays a crucial role in tumour growth.[52,53] Its effect on migration, invasion and angiogenesis implicates CXCR2 with the progression of several cancers such as of lung cancer[111,112], breast cancer[115–117], pancreatic cancer[108], ovarian cancer[121,122], prostate cancer[114] and melanoma.[110,113] Subsequently, CXCR2 inhibition may have important potential therapeutic applications, due to the involvement of this receptor in the pathologic conditions presented in Chapter 1. For this reason, there has been an extensive search for selective CXCR2 antagonists.[58,134–136] The interaction between the native chemokine ligand and CXCR2 is complex[44] and it consists in a two-step process[43], elucidated by Liu *et al.* through the release of two cryo-electron microscopy structures.[45] The binding at the orthosteric binding site is therefore highly complex and difficult to mimic with a small molecule interventions, however, an alternative intracellular allosteric binding site, located near the *C*-terminus of the receptor, has been discovered. Exploitation of this intracellular site has been hypothesized to provide greater therapeutic selectivity, bypassing the complexity of the orthosteric site. Therefore, different classes of negative allosteric modulators, acting at this intracellular site, have been develop to block CXCR2 signalling.[137] The different classes of NAMs, including urea-based compounds[134,160], 3,4-diamino-cyclobutenediones compounds[161,162] and pyrimidine-based compounds[181,182], have been presented in Chapter 1. Some promising compounds reached clinical trials for the treatment of

COPD, asthma and some types of cancer.[137] Unfortunately, the clinical evaluation of some compounds have been stopped for undisclosed reasons, presumably involving the reported reduction in neutrophil counts.[137,169]

The mechanism of action of CXCR2 NAMs has been elucidated by Liu *et al.* through the release of the X-ray crystal structure of CXCR2 bound to the NAM 00767013 (**5**) (PDB ID: 6LFL).[45] The NAMs sterically interfere with the binding of the G-protein to the receptor, since their binding sites are overlapping, and restrict the conformational changes required for receptor activation.[45] *R*-navarixin (**2**)[166] is a particularly interesting compound belonging to the 3,4-diamino-3-cyclobutene-1,2-dione-based series of CXCR2 NAMs. It possesses excellent potency at CXCR2, which is believed to be related to its binding kinetic profile, since it has been reported to have a slow dissociation rate from the receptor.[41,139] In order to directly explore these binding relationships, a molecular tool able to bind at the intracellular allosteric binding site of CXCR2 was needed to be able to directly determine the binding affinity and to study the binding kinetics of the NAMs acting at this binding site. High affinity fluorescent ligands are ideal for this purpose, having diverse functionality in several GPCR binding techniques such as BRET[198–203] and can therefore be used in real time, homogenous, analysis of ligand binding.

The work presented in this thesis has focused on the design, synthesis, pharmacological characterisation and application of a novel series of fluorescent ligands targeting the intracellular allosteric binding site of CXCR2.

The aim of this thesis was the design of CXCR2 fluorescent ligands. It was therefore essential to identify a congener for the series, which would then be modified with linker and fluorophore attachment. **Chapter 2** reports the synthesis and pharmacological activity evaluation of small molecules belonging to the 3,4-diaminocyclobutenediones class of CXCR2 NAMs. The purpose of these initial studies was to confirm the reported potency of a series of literature compounds at CXCR2 to find a suitable potent congener for the library of fluorescent ligands. The synthesis of *R*-navarixin (**2**), compound **8**,

compound **11** and *S*-navarixin (**24**) was performed following the procedure reported by Dwyer *et al.* [166] (Scheme 2.1). The activities of the synthesised compounds were evaluated in a NanoBiT Luciferase complementation assay[244] (Figure 2.3) that allowed measurements of the effects of the NAMs on agonist-induced (CXCL8) CXCR2 recruitment of effector proteins (mini Gα protein[245,246] or β-arrestin2) to CXCR2. The data reported in Figures 2.4 and 2.5, showed that the treatment with the NAMs inhibited CXCL8 stimulated recruitment of effector proteins, with a similar response in both cell lines. Moreover, the NAMs produced a rightwards shift of the CXCL8 concentration response curve and a decrease in the maximal response. These data were consistent with a non-competitive mode of action of the compounds. An interesting observation presented in Chapter 2 is the difference between the two navarixin enantiomers. *R*-navarixin (**2**), possessing subnanomolar potency, was found to be the most potent compound tested, producing pronounced insurmountable antagonism at CXCR2 (Figure 2.4 A,B). In comparison, *S*-navarixin (**24**) required 100 times the concentration of the *R* enantiomer (**2**) to exert a similar effect and it presented a more surmountable profile (Figure 2.4 C,D). The findings reported were in accordance with previous literature reports[41,139,166] and they confirmed the importance of the *R* stereochemistry for high affinity antagonism. The difference between navarixin enantiomers, both targeting the same binding site, could derive from the different binding kinetics of two compounds. As suggested from previous studies[41,139], *R*-navarixin (**2**) slow dissociation rate (k_{off}) from the receptor could have an effect on the high affinity and non-surmountable behaviour of the compound. The use of fluorescent probes allows investigation of the kinetics of CXCR2 NAMs in more depth and to directly measure the k_{off} of the compounds. Among the compounds tested in Chapter 2, *R*-navarixin (**2**) possessed suitable high potency to be an ideal choice of congener for the library of fluorescent ligands.

The structure of the chosen congener, *R*-navarixin (**2**), needed to be evaluated in order to identify a suitable point for linker and fluorophore attachment. Moreover, it was crucial to have a visualisation of the binding pose of

compound **2** to understand which functional groups present on the compound are actively involved in receptor binding, and therefore essential for activity and which can be modified without a loss in binding affinity. The computational studies performed are presented in **Chapter 3**. The initial absence of a crystal structure of CXCR2 made it necessary to build an homology model[255,256] of the receptor, based on available crystal structures of homologous proteins. The homology models generated were then evaluated (Chapter 3.2.1) and used for molecular docking (Chapter 3.2.2). This process led to the identification of a suitable model to evaluate *R*-navarixin (**2**) binding (model based on CCR9, PDB: 5LWE)[142] which contributed profoundly to the initial design of the fluorescent ligand series. The *N,N*-dimethyl-amide part of **2** was found to protrude from the binding pocket, not establishing crucial interactions with CXCR2 and could therefore be modified and elongated with liker attachment. The X-ray crystal structure of CXCR2 with a NAM (00767013, **5**) bound (PDB: 6LFL) was published in 2020 by Liu et al[45], allowing the comparison with the generated homology model. The overlay of this CXCR2 crystal structure and the homology model with their respective ligands bound (00767013, **5** and *R*-navarixin, **2** respectively) (Figure 3.8) revealed a nice overlap between the two receptor structures and a similar binding pose of the two ligands. Additional docking studies of *R*-navarixin (**2**) in 6LFL (Chapter 3.3) and humanised 6LFL (with residue $249^{6.33}$ mutated back to Ala, Chapter 3.4) confirmed the *N,N*-dimethyl-amide part of **2** an appropriate point for linker attachment. In Chapter 3.5, modified versions of *R*-navarixin (**2**) were docked into the receptor and their binding poses (Figure 3.18) corroborated the previous finding that the addition of linker and fluorophore to this side of the congener should not interfere with receptor binding.

The findings presented in Chapter 2 and 3 allowed the design of a library of fluorescent ligands, the synthesis of which is presented in **Chapter 4** of this thesis. The *N,N*-dimethyl-amide side was initially elongated with the incorporation of two short spacers (*N*-(2-aminoethyl)amide or *N*-methyl-*N*-(2-aminoethyl)amide linker), acting as handles for subsequent linker couplings (Scheme 4.3). This also allowed assessment of the importance of

the *N,N*-dialkylamide moiety present on *R*-navarixin (**2**), through the comparison between the two series (*N*-methylated and non-methylated). Subsequent reaction, either directly with a suitable *N*-reactive fluorescent dye or further elongation of the linker through incorporation of a glycyl or β-alanyl moiety and then reaction with the fluorescent dye (Schemes 4.5 and 4.6), allowed the generation of the library of fluorescent ligands (**62a, c-f**).

Chapter 5 reports the evaluation of the activity of protected congeners (**49a-b**, **61a**, **61c**) in the NanoBiT complementation assay (described in Chapter 2.2) in order to determine any functional effect resulting from linker addition. The activity of the modified analogues appeared retained in the functional NanoBiT assay, although reduced compared to the parent compound **2**. This confirmed that the linker addition to *R*-navarixin (**2**) via the amide moiety identified in the docking studies, is tolerated. Chapter 5.3 reports the evaluation of the binding affinities of the fluorescent probes **62a**, **62c-f** at CXCR2 through a NanoBRET binding assay (Figure 5.2) performed both in membranes and whole cells. All the ligands showed saturable binding and low NSB (with the exception of **62c** in whole cells) at CXCR2, from which affinities (K_D) could be determined. (Figure 5.3, Table 5.2). Interestingly, the *N*-methylated fluorescent ligands **62d-f** possessed the highest affinity in both whole cell system and cell free (membrane) environment. In addition, cell accessibility of the probes was confirmed by direct fluorescent imaging of the CXCR2 cell line, co-labelled with the SNAP-tag receptor fluorophore SNAPlabel-AF-488 to identify the SNAP-CXCR2 protein, and **62a** (Figure 5.5). These data demonstrate the applicability of these novel fluorescent ligands in both membrane and cell based CXCR2 binding assays.

Selectivity of the probes for the related receptor CXCR1 was also assessed (Chapter 5.4). Saturable CXCR1 binding was observed for the *N*-methyl fluorescent probes **62d** and **62f**, with reductions in affinity at CXCR1 compared to CXCR2, while compounds **62a**, **62c** and **62e** showed no CXCR1 specific binding (Figure 5.6, Table 5.3). Overall, the selectivity for CXCR2 over CXCR1 is retained, however **62d** and **62f** possess sufficient affinity to be used in a CXCR1 NanoBRET competition binding assay. Chapter 5.5

presents the application of compound **62a** in NanoBRET competition binding experiments in CXCR2 membranes to measure the affinity of a variety of competing, unlabelled, CXCR2 NAMs, including literature compounds. Unlabeled NAMs were shown to fully displace fluorescent ligand **62a** in a competitive manner (Figure 5.7). This enabled the calculation of pK_i values (Table 5.4) through application of Cheng-Prusoff correction, and the values generated were in good agreement with previously reported CXCR2 affinity measurements for the tested literature compounds.[41,58,141,166,182,314] Moreover, NanoBRET competition binding experiments in CXCR1 membranes were performed, employing compound **62d** and, similarly to CXCR2, the NAMs tested displayed full displacement of the fluorescent probe in a competitive manner, again allowing calculation of pK_i values for the unlabelled ligands. Finally, the characterised fluorescent probes were employed to study the binding kinetics of the NAMs acting at the intracellular site of CXCR2, to assess if their kinetic parameters have an effect of their functional effect (Chapter 5.5.2). Compound **62e** was employed to probe binding kinetics of some CXCR2 NAMs present in the literature. Through competition binding NanoBRET assays performed in CXCR2 membranes it was possible to obtain the kinetic parameters of the unlabelled NAMs (Figure 5.12, Table 5.5). In particular, it was possible to confirm the reported very slow dissociation rate from the receptor of *R*-navarixin (**2**)[41,139,182] which is conferring its insurmountable profile in functional studies. On the other hand, rapidly dissociating compounds, such as *S*-navarixin (**24**), displayed surmountable properties, confirming previous findings.

A recurrent observation in the pharmacological data presented in Chapter 5, was the enhanced potency of *N*-methylated ligands over their unmethylated congeners. **Chapter 6** reports the structural NMR studies performed to rationalise the pharmacological data. From the NMR analysis of compounds **56a** and **56b** arise the hypothesis that the enhanced activity of *N*-methylated analogues could come from the effects that this modification has on the structure of the ligand. Methylation favors a less planar conformation that could favour receptor binding and a weaker intramolecular hydrogen bond, ultimately resulting in increased potency of the *N*-methylated analogues.

Furthermore, molecular dynamics simulations were performed, and they were in full agreement with the NMR analysis. These corroborated the findings emerged from the structural NMR studies which identified *N*-methylation as a crucial characteristic for enhanced potency.

Overall, the work presented in this thesis has resulted in the development of a series of fluorescent probes targeting the intracellular allosteric binding site of CXCR2. These ligands can be applied in both CXCR2 or CXCR1 assays within both membrane and whole cell systems. Their application in competition binding assays demonstrated efficient derivation of unlabelled ligand binding parameters, including kinetic parameters, with the successful and novel application of kinetic binding methodology to an intracellular allosteric binding site. Additionally, the fluorescent nature of these ligands provides them with functionality beyond unlabelled ligand characterisation, as presented in this thesis. The high employment of fluorescent ligands within the field of advanced microscopy provides these ligands with potential future uses for furthering our understanding of receptor biology. In particular, the fluorescent ligands described could be employed as tools to monitor receptor trafficking, particularly in relation to receptor internalisation and endosomal localisation.[350] This would allow for future exploration of receptor interactions at subcellular compartments, such as endosomes, potentially identifying novel signalling pathways for future therapeutic exploitation. Additionally, the high selectivity of the presented ligands also facilitates their use in labelling receptors within physiologically relevant systems[351], such as primary cell lines. This allows for more translational pharmacological studies to be performed, including characterisation of receptor localisation within particular cell types, as well as allowing exploration of unlabelled ligands able to compete with tracer binding within disease relevant systems.

In conclusion, this work provides the scientific community with a set of new pharmacological tools which can contribute to a better understanding of allosteric modulation of chemokine receptors and, potentially, of other related GPCRs. It has the potential to drive the discovery of new, more selective, CXCR2 antagonists which could result in the identification of novel clinical

pharmacological entities for safer and improved treatment of several pathological conditions.

Chapter 8. Methods

8.1 Chemistry

8.1.1 Materials and General methods

Chemicals and solvents were purchased from standard suppliers and used without further purification. BODIPY 630/650-X NHS was purchased from Lumiprobe (Hunt Valley, MD). Unless otherwise stated, reactions were carried out at ambient temperature and monitored by thin layer chromatography (TLC) on commercially available precoated aluminum-backed plates (Merck Kieselgel TLC Silica gel 60 Å F_{254}). Visualization was by examination under UV light (254 and 366 nm) followed by staining with ninhydrin. Organic solvents were evaporated under reduced pressure at ≤ 40°C (water bath temperature). Flash column chromatography was carried out using technical grade silica gel from Aldrich, pore size 60Å, 230–400 mesh and particle size 40–63 μm. Automated flash column chromatography was performed on a Interchim Puriflash 4100 system (PF4100-250) equipped with a dual wavelength DAD UV detector (200-600 nm) using silica high performance (HP) 50 μm cartriges. Preparative layer chromatography (PTLC) was performed using precoated glass plates (Analtech uniplate silica gel GF, 20 x 20 cm, 2000 μm). Analytical RP-HPLC was performed using a Waters 996 HPLC machine and a YMC-Pack C8 column (150 mm x 4.6 mm x 5 μm) at a flow rate of 1.0 mL/min over a 30 min period (gradient method of 10%-90% solvent B; solvent A = 0.01% formic acid in H_2O, solvent B = 0.01% formic acid in CH_3CN), UV detection at 425 nm and spectra were analyzed using Millennium 32 software. ^{1}H NMR and ^{13}C NMR spectra were recorded on a Bruker-AV 400 respectively at 400.13 MHz and at 101.62 MHz. Chemical shifts (δ) are quoted in parts per million (ppm) with calibration to the residual undeuterated solvent signal. Solvents used for NMR analysis were $CDCl_3$ supplied by Cambridge Isotope Laboratories Inc., (δ_H = 7.26 ppm, δ_C = 77.16 ppm), DMSO-*d*$_6$ supplied by Sigma Aldrich (δ_H = 2.50 ppm, δ_C = 39.52 ppm) and CD_3OD supplied by Sigma Aldrich (δ_H = 3.31 ppm, δ_C = 49.00 ppm). The spectra were analyzed using MestReNova (v14.2.0-26256)

NMR software. Coupling constants (*J*) are recorded in Hz and the significant multiplicities described by singlet (s), doublet (d), triplet (t), quartet (q), broad (br), multiplet (m) doublet of doublets (dd). LC/MS was carried out using a Phenomenex Gemini-NX C18 110Å, column (50 mm × 2 mm x 3 μm) at a flow rate 0.5mL/min over a 5 min period (gradient method of 5%-95% solvent B; solvent A = 0.01% formic acid in H_2O, solvent B = 0.01% formic acid in CH_3CN). LC/MS spectra were recorded on a Shimadzu UFLCXR system combined with an Applied Biosystems API2000 electrospray ionization mass spectrometer and visualized at 254 nm (channel 1) and 220 nm (channel 2). High resolution mass spectra (HRMS) were recorded on a Bruker microTOF mass spectrometer using electrospray ionization (ESI-TOF) operating in positive or negative ion mode. All pharmacologically tested compounds are >95% pure by HPLC analysis. Optical rotations were measured using a ADP200 polarimeter (Bellingham + Stanley Ltd). For crystallization of compound **24**: a suitable single crystal of the compound was selected and acquired on a SuperNova, Titan S2 diffractometer. The crystal was kept at 120 K during data collection. Using Olex2, the structure was solved with the ShelXT structure solution program using Intrinsic Phasing and refined with the ShelXL refinement package using Least Squares minimisation. Crystallisation was performed by Stephen Argent (Chrystallography department, University of Nottingham).

General procedure 1: Conversion of mixed squarates to chiral squaramides 49a-b, 61a-f. To a solution of the required squaric acid monoamide monoesters compound (**56a-b**, **60a-f**) in 1.5 mL EtOH were added (*R*)-1-5-methylfuran-2-yl-propan-1- amine hydrochloride (1.1 equiv) and Et_3N (1.1 equiv). The mixture was stirred at RT for 144 h, concentrated under reduced pressure and purified by PTLC (Si).

General procedure 2: Amide coupling for 60c-f. To a solution of the Fmoc protected amino acid (1 equiv) in anhydrous CH_2Cl_2 at 0 °C were added EDCI (1.2 equiv) and HOBt (1.1 equiv). The solution was stirred for 30 min prior to the addition of the required amine (**59a-59b**) (1.1 equiv) and DIPEA (2.1

equiv). The mixture was stirred at RT for 72 h, evaporated to dryness and purified by PTLC (Si).

General procedure 3: Fluorophore ligation via amide bond formation for 62a, 62c-f. The desired Fmoc protected amine congener (**61a**, **61c-f**) (1 equiv) was dissolved in DMF and treated with 20 % piperidine in DMF. The solution was stirred at RT for 3h and concentrated under reduced pressure to generate the desired amine congener. The compound was then dissolved in DMF (1 mL) and treated with BODIPY 630/650-X NHS ester (0.9 equiv). The solution was stirred at RT for 18h in the dark and concentrated under reduced pressure. The reaction mixture was purified using PTLC (Si, MeOH/CH_2Cl_2, 5:95).

8.1.2 Methods Chapter 2

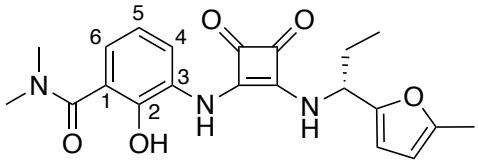

(*R*)-2-Hydroxy-*N*,*N*-dimethyl-3-((2-((1-(5-methylfuran-2-yl)propyl)amino)-3,4-dioxocyclobut- 1-en-1-yl)amino)benzamide (*R*-navarixin, 2). To a solution of (*R*)-1-5-methylfuran-2-yl-propan-1- amine (**30**) (20 µL, 0.14 mmol) in EtOH (1.1 mL) was added 3-((2-ethoxy-3,4-dioxocyclobut-1-en- 1-yl)amino)-2-hydroxy-*N*,*N*-dimethylbenzamide (**29**) (36mg, 0.12mmol) at RT. The reaction mixture was stirred at RT for 16h and then concentrated under reduced pressure. Purification (PTLC, MeOH/CH_2Cl_2, 3:97) gave the title compound (35 mg, 74%) as a pink solid. Mp 118–120 °C; ^{1}H NMR (400 MHz, DMSO-d_6) δ 9.94 (s, 1H, O**H**), 9.29 (s, 1H, ar-N**H**), 8.66 (d, J = 9.0 Hz, 1H, ar-C**H**-6), 7.79 (dd, J = 7.2, 2.4 Hz, 1H, ar-C**H**-4), 6.98–6.76 (m, 2H, N**H**CH + ar-C**H**-5), 6.26 (d, J = 3.1 Hz, 1H, furan-C**H**), 6.05 (dd, J = 3.1, 1.3 Hz, 1H, furan-C**H**CHCH$_3$), 5.14 (q, J = 7.8 Hz, 1H, NHC**H**), 2.93 (s, 6H, N(C**H$_3$**)$_2$), 2.26 (s, 3H, furan-C**H$_3$**), 2.03-1.78

(m, 2H, C**H2**CH_3), 0.92 (t, *J* = 7.3 Hz, 3H, CH_2C**H₃**); ^{13}C NMR (101 MHz, DMSO- d_6) δ 184.4 (**C** squaramide), 180.6 (**C** squaramide), 169.0 (**C** squaramide), 168.7 (**C** squaramide), 163.9 (**C**=O), 152.5 (furan-**C**), 151.8 (furan-**C**), 129.1 (ar-**C**), 124.9 (ar-**C**), 122.6 (ar-**C**), 121.2 (ar-**C**), 120.2 (ar-**C**), 108.0 (furan-**C**H), 106.9 (furan-**C**H), 55.3 (NH**C**H) 53.2 ((N**C**$H_3)_2$), 27.6 (**C**H_2CH_3), 13.8 (furan-**C**H_3), 10.7 (CH_2**C**H_3) (ar-**C** not observed); LC/MS *m/z* calculated for $C_{21}H_{24}N_3O_5$ $[M+H]^+$: 398.1, found 397.9, t_R = 4.61 min; HRMS (TOF ES$^+$) calculated for $C_{21}H_{24}N_3O_5$ $[M+H]^+$: 398.1710 , found 398.1703, $[\alpha]^{32.4\ °C}_D$ = +64 (1; MeOH).

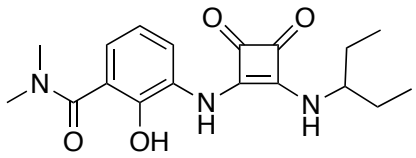

3-((3,4-Dioxo-2-(pentan-3-ylamino)cyclobut-1-en-1-yl)amino)-2-hydroxy-*N,N*- dimethylbenzamide (8). To a solution of 3-aminopentane (**31**) (76 µL, 0.66 mmol) in EtOH (3 mL) was added 3-((2-ethoxy-3,4-dioxocyclobut-1-en-1-yl)amino)-2-hydroxy-*N*,*N*-dimethylbenzamide (**29**) (100 mg, 0.33 mmol) at RT. The reaction mixture was stirred at RT for 16h. It was concentrated under reduced pressure. Purification by flash column chromatography (MeOH/CH_2Cl_2, 3:97) gave 99 mg (87%) of the title compound as a pink solid. Mp 200–202 °C; ^{1}H NMR (400 MHz, DMSO-d_6) δ 9.95 (s, 1H, O**H**), 9.23 (s, 1H, ar-N**H**), 8.19 (d, *J* = 9.1 Hz, 1H, ar-C**H**-6), 7.83 (dd, *J* = 7.6, 2.0 Hz, 1H, ar-C**H**-4), 6.91–6.83 (m, 2H, N**H**CH + ar-C**H**-5), 3.90 (qt, *J* = 8.8, 4.7 Hz, 1H), 2.94 (s, 6H, N(C**H₃)₂**), 1.56-1.41 (m, 5H, 2C**H₂** + NHC**H**), 0.90 (t, *J* = 7.4 Hz, 6H, 2C**H₃**); ^{13}C NMR (101 MHz, DMSO- d_6) δ 184.6 (**C** squaramide), 180.3 (**C** squaramide), 169.9 (**C** squaramide), 168.8 (**C** squaramide), 163.5 (**C**=O), 129.3 (ar-**C**), 124.8 (ar-**C**), 122.5 (ar-**C**), 121.1 (ar-**C**), 120.3 (ar-**C**), 57.5((N**C**$H_3)_2$), 28.4 (2**C**H_2), 10.5 (2**C**H_3) (1ar-**C** and NH**C**H not observed); LC/MS *m/z* calculated for $C_{18}H_{24}N_3O_4$ $[M+H]^+$: 346.1, found 346.0, t_R = 4.02 min; HRMS (TOF ES$^+$) calculated for $C_{18}H_{24}N_3O_4$ $[M+H]^+$: 346.1761, found 346.1760.

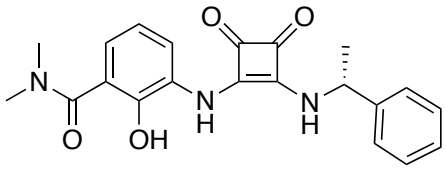

(*R*)-3-((3,4-Dioxo-2-((1-phenylethyl)amino)cyclobut-1-en-1-yl)amino)-2-hydroxy-*N*,*N*- dimethylbenzamide (11). To a solution of (*R*)-a-methylbenzylamine (170 µL, 1.32 mmol) (**32**) in EtOH (6 mL) was added 3-((2-ethoxy-3,4-dioxocyclobut-1-en-1-yl)amino)-2-hydroxy-*N*,*N*-dimethylbenzamide (**29**) (200 mg, 0.66 mmol) at RT. The reaction mixture was stirred at RT for 16h and then concentrated under reduced pressure. Purification by flash column chromatography ($MeOH/CH_2Cl_2$, 3:97) gave 157 mg (63%) of the title compound as a pink foamy solid. Mp 130–132 °C; ^{1}H NMR (400 MHz, DMSO- d_6) δ 9.95 (s, 1H, O**H**), 9.28 (s, 1H, ar-N**H**), 8.71 (d, J = 8.5 Hz, 1H, ar-C**H**-6), 7.78 (dd, J = 7.1, 2.5 Hz, 1H, ar-C**H**-4), 7.47– 7.36 (m, 4H, N**H**CH + ar-C**H**-5 + 2 ar'-C**H**), 7.31 (ddd, J = 8.6, 5.3, 3.2 Hz, 1H, ar'-C**H**), 6.93–6.82 (m, 2H, 2 ar'-C**H**), 5.34 (p, J = 7.2 Hz, 1H, NHC**H**), 2.94 (s, 6H, N(C**H₃**)**₂**), 1.59 (d, J = 6.9 Hz, 3H, C**H₃**); ^{13}C NMR (101 MHz, DMSO-d_6) δ 184.4 (**C** squaramide), 180.6 (**C** squaramide), 168.9 (**C** squaramide), 168.8 (**C** squaramide), 164.0 (**C**=O), 143.8 (ar-**C**), 143.7 (ar-**C**), 129.2 (ar-**C**), 128.9 (ar-**C**), 128.0 (ar-**C**), 126.4 (ar-**C**), 124.8 (ar-**C**), 122.8 (ar-**C**), 121.4 (ar-**C**), 120.3 (ar-**C**), 53.5 ((N**C**H_3)$_2$), 23.4 (**C**H_3) (ar-**C** and NH**C**H not observed); LC/MS *m/z* calculated for $C_{21}H_{22}N_3O_4$ $[M+H]^+$: 380.1, found 379.9, t_R = 4.34 min; HRMS (TOF ES$^+$) calculated for $C_{21}H_{22}N_3O_4$ $[M+H]^+$: 380.1605, found 380.1602; $[\alpha]^{28.6\ °C}_D$ = -72 (1; MeOH).

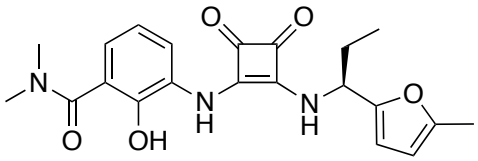

(*S*)-2-Hydroxy-*N,N*-dimethyl-3-((2-((1-(5-methylfuran-2-yl)propyl)amino)-3,4-dioxocyclobut- 1-en-1-yl)amino)benzamide (24). To a solution of (*S*)-1-5-methylfuran-2-yl-propan-1-amine (**33**) hydrochloride (24.6 mg, 0.14 mmol) in EtOH (1.1 mL) was added triethylamine (19.5 μL, 0.14mmol). To the mixture was added 3-((2-ethoxy-3,4-dioxocyclobut-1-en-1-yl)amino)-2-hydroxy-*N*,*N*-dimethylbenzamide (**29**) (36 mg, 0.12 mmol) at RT. The reaction mixture was stirred at RT for 16h and then concentrated under reduced pressure. Purification (PTLC, MeOH/CH_2Cl_2, 3:97) gave the title compound (25 mg, 53%) as a pink solid. Mp 118–120 °C; ^{1}H NMR (400 MHz, DMSO-d_6) δ 9.93 (s, 1H, O**H**), 9.28 (s, 1H, ar-N**H**), 8.66 (d, J = 9.1 Hz, 1H, ar-C**H**-6), 7.79 (dd, J = 7.3, 2.3 Hz, 1H, ar-C**H**-4), 6.97– 6.73 (m, 2H, N**H**CH + ar-C**H**-5), 6.26 (d, J = 3.1 Hz, 1H, furan-C**H**), 6.05 (dd, J = 3.1, 1.3 Hz, 1H, furan-C**H**CHCH$_3$), 5.14 (q, J = 7.8 Hz, 1H, NHC**H**), 2.93 (s, 6H, N(C**H$_3$**)$_2$), 2.26 (s, 3H, furan-C**H$_3$**), 2.02-1.77 (m, 2H, C**H$_2$**CH$_3$), 0.92 (t, J = 7.3 Hz, 3H, CH$_2$C**H$_3$**) ^{13}C NMR (101 MHz, DMSO-d_6) δ 184.4 (**C** squaramide), 180.6 (**C** squaramide), 169.0 (**C** squaramide), 168.7 (**C** squaramide), 163.9 (**C**=O), 152.5 (furan-**C**), 151.8 (furan-**C**), 143.7 (ar-**C**), 129.1 (ar-**C**), 124.9 (ar-**C**), 122.6 (ar-**C**), 121.2 (ar-**C**), 120.2 (ar-**C**), 108.0 (furan-**C**H), 106.9 (furan-**C**H), 53.2 ((N**C**H$_3$)$_2$), 27.6 (**C**H$_2$CH$_3$), 13.8 (furan-**C**H$_3$), 10.7 (CH$_2$**C**H$_3$) (NH**C**H not observed); LC/MS *m/z* calculated for $C_{21}H_{24}N_3O_5$ [M+H]$^+$: 398.1, found 397.9, t_R = 4.61 min; HRMS (TOF ES$^+$) calculated for $C_{21}H_{24}N_3O_5$ [M+H]$^+$: 398.1710 , found 398.1707; $[\alpha]^{33\ °C}_D$ = -76 (1; MeOH).

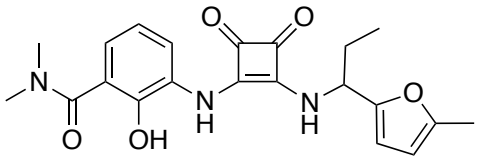

(*RS*)-2-Hydroxy-*N*,*N*-dimethyl-3-((2-((1-(5-methylfuran-2-yl)propyl)amino)-3,4-dioxocyclobut-1- en-1-yl)amino)benzamide (25). To a solution of (*RS*)-1-(5-methylfuran-2-yl)propan-1-amine (**34**) (10 mg, 0.036mmol) in EtOH (0.5mL) was added 3-((2-ethoxy-3,4-dioxocyclobut-1-en-1-yl)amino)-2- hydroxy-*N*,*N*-dimethylbenzamide (**29**) (6 mg, 0.043 mmol) at rt. The reaction mixture was stirred at RT for 48h and then concentrated under reduced pressure. Purification (PTLC, MeOH/CH_2Cl_2, 3:97) gave 4 mg (30%) of the title compound as a pink solid. Mp 118–120 °C; ^{1}H NMR (400 MHz, DMSO-d_6) δ 8.66 (s, 1H, N**H**), 7.77 (dd, J = 6.8, 2.8 Hz, 1H, ar-C**H**-6), 6.91-6.79 (m, 2H, ar-C**H**-4,5), 6.24 (d, J = 3.1 Hz, 1H, furan-C**H**), 6.04 (d, J = 3.0 Hz, 1H, furan-C**H**CHCH$_3$), 5.12 (t, J = 7.3 Hz, 1H, NHC**H**), 2.92 (s, 6H, N(C**H$_3$**)$_2$), 2.25 (s, 3H, furan-C**H$_3$**), 1.99-1.79 (m, 2H, C**H$_2$**CH$_3$), 0.91 (t, J = 7.3 Hz, 3H, CH$_2$C**H$_3$**) (O**H** and N**H** not observed); LC/MS *m/z* calculated for $C_{21}H_{24}N_3O_5$ $[M+H]^+$: 398.1, found 397.9, t_R = 4.61 min.

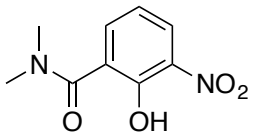

2-Hydroxy-*N*,*N*-dimethyl-3-nitrobenzamide (27). To a solution of 3-nitrosalicylic acid (**26**) (2.0 g, 10.9 mmol) in anhydrous CH_2Cl_2 (100 mL) at RT were added oxalyl chloride (2.8 mL, 32.7 mmol) and DMF (2 drops) under N_2 atmosphere. The mixture was stirred for 16 h at RT and then concentrated under reduced pressure to give a yellow solid. To the solid was added anhydrous CH_2Cl_2 (35 mL) under N_2 atmosphere. The mixture was cooled to 0 °C and dimethylamine in THF (2 M, 16.4 mL) was added dropwise. The mixture was stirred at RT for 1 h and concentrated under reduced pressure to afford an orange solid. It was recrystallized from ethyl

acetate and hexane to afford 1.5 g (65%) of yellow crystals. Mp 115–117 °C; ^{1}H NMR (400 MHz, $CDCl_3$) δ 10.86 (s, 1H, O**H**), 8.16 (dd, *J* = 8.5, 1.7 Hz, 1H, ar-C**H**-6), 7.62 (dd, *J* = 7.4, 1.7 Hz, 1H, ar-C**H**-4), 7.06 (dd, *J* = 8.5, 7.4 Hz, 1H, ar-C**H**-5), 3.04 (s, 6H, N(C**H**$_3$)$_2$); LC/MS *m/z* calculated for $C_9H_{11}N_2O_4$ $[M+H]^+$: 211.0, found 211.0, t_R = 2.17 min.

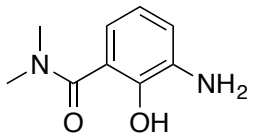

3-Amino-2-hydroxy-*N*,*N*-dimethylbenzamide (28). To 2-hydroxy-*N*,*N*-dimethyl-3-nitrobenzamide (**27**) (2.0 g, 9.5 mmol) in EtOH (100 mL) at RT was added 10% Pd/C (200 mg). The mixture was stirred under H_2 atmosphere at RT for 2 h. The mixture was filtered through a pad of Celite and concentrated under reduced pressure to give 1.5 g (72%) of an orange viscous solid. ^{1}H NMR (400 MHz, $CDCl_3$) δ 6.88–6.55 (m, 3H, 3 ar-C**H**), 3.14 (s, 6H, N(C**H**$_3$)$_2$) (N**H**$_2$ and O**H** not observed); LC/MS *m/z* calculated for $C_9H_{13}N_2O_2$ $[M+H]^+$: 181.1, found 181.0, t_R = 2.07 min.

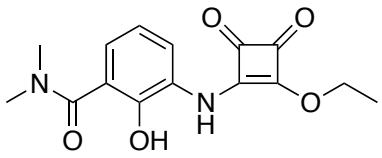

3-((2-Ethoxy-3,4-dioxocyclobut-1-en-1-yl)amino)-2-hydroxy-*N*,*N*-dimethylbenzamide (29). To a solution of 3-amino-2-hydroxy-*N*,*N*-dimethylbenzamide (**28**) (1.5 g, 8.3 mmol) in EtOH (60 mL) was added diethoxysquarate (1.7 mL, 11.4 mmol) dropwise at 0 °C. The mixture was stirred for 64 h. It was filtered, the precipitate was washed with cold EtOH and dried under vacuum. Purification by flash column chromatography (MeOH/CH_2Cl_2, 2:98) gave 1.1 g (45 %) of the title compound as a pink solid. Mp 166–168 °C; ^{1}H NMR (400 MHz, $CDCl_3$) δ 11.0 (br s, 1H, O**H**), 7.79 (s, 1H, ar-C**H**-6), 7.11 (dd, *J* = 8.0, 1.4 Hz, 1H, ar-C**H**-4), 6.89 (t, *J* = 8.0 Hz, 1H, ar-C**H**-5), 4.88 (q, *J* = 7.1 Hz, 2H, C**H**$_2$CH$_3$), 3.19 (s, 6H, N(C**H**$_3$)$_2$), 1.53

(t, J = 7.1 Hz, 3H, $CH_2C\mathbf{H_3}$) (N**H** not observed); LC/MS *m/z* calculated for $C_{15}H_{17}N_2O_2$ $[M+H]^+$: 305.1, found 305.0, t_R = 2.30 min.

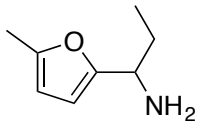

(*RS*)-1-(5-Methylfuran-2-yl)propan-1-amine (34). To (*E*)-*N*-benzhydryl-1-(5-methylfuran-2-yl)methanimine (**41**) (500 mg, 1.82 mmol) in anhydrous DMF (9.1 mL) under N_2 atmosphere at 0 °C was added *t*-BuOK (245 mg, 2.18 mmol). The deep red solution was stirred for 5 min and then EtBr (0.2 mL, 2.73 mmol) was added and it was stirred for 5.30 h. Changing of colour from deep red to yellow was observed. To the reaction mixture were added H_2O (5.5 mL) and sat $NaHCO_3$ solution (10 mL). It was extracted with Et_2O (3 x 15 mL), washed with brine (1 x 10 mL) and concentrated under reduced pressure. The residue was dissolved in MeOH (5 mL), 1 M HCl (5 mL) was added and the mixture was stirred for 5 h. The aqueous layer was washed with Et_2O and concentrated under reduced pressure. Purification by flash column chromatography (1 M NH_3 in MeOH/CH_2Cl_2, 5:95) gave 6 mg (3%) of the title compound as a brown oil. ^{1}H NMR (400 MHz, $CDCl_3$) δ 6.02 (d, J = 3.0 Hz, 1H, furan-C**H**), 5.87 (dd, J = 3.0, 1.1 Hz, 1H, furan-C**H**), 3.81 (t, J = 6.8 Hz, 1H, C**H**NH_2), 2.26 (s, 3H, furan-$C\mathbf{H_3}$), 1.85-1.68 (m, 2H, C**H2**CH_3), 0.93 (t, J = 7.4 Hz, 3H, $CH_2C\mathbf{H_3}$); LC/MS *m/z* calculated for $C_8H_{14}NO$ $[M+H]^+$: 140.1, found 140.1, t_R = 0.57 min.

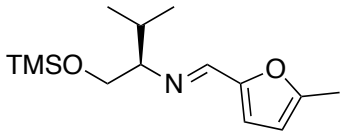

(*R*,*E*)-*N*-(3-Methyl-1-((trimethylsilyl)oxy)butan-2-yl)-1-(5-methylfuran-2-yl)methanimine (38). To (*D*)-Valinol (**35**) (900 mg, 8.7 mmol) in CH_2Cl_2 (15 mL) at 0 °C and under N_2 atmosphere were added $MgSO_4$ (4.3 mg) and 5-methylfuraldehyde (**36**) (860 μL, 8.7 mmol) dropwise. The mixture was stirred at 0 °C for 2h and then at RT for 40h. It was filtered, the drying agent was washed with CH_2Cl_2 and the filtrate was concentrated under reduced pressure. The crude imine was used for the next step without further purification. To the solution of the imine in CH_2Cl_2 (15 mL) at RT and under N_2 atmosphere were added Et_3N (1.34 mL, 9.57 mmol) and TMSCl (1.04 mL, 9.57 mmol) dropwise. The mixture was stirred for 18h. It was filtered and the precipitate was washed with CH_2Cl_2. The filtrate was concentrated under reduced pressure and taken up in Et_2O/Hexane (1:1, 150 mL). The precipitate was filtered off and the filtrate was concentrated under reduced pressure giving 974 mg (42%) of the title compound as a brown oil used for the subsequent step without further purification. ^{1}H NMR (400 MHz, $CDCl_3$) δ 7.90 (s, 1H, N=C**H**), 6.59 (d, *J* = 3.2 Hz, 1H, furan-C**H**), 6.06 (dq, *J* = 3.1, 1.0 Hz, 1H, furan-C**H**), 3.89 (dd, *J* = 10.3, 4.1 Hz, 1H, C**H**), 3.63 (dd, *J* = 10.3, 8.0 Hz, 1H, 1/2C**H₂**), 2.82 (td, *J* = 7.6, 4.1 Hz, 1H, 1/2C**H₂**), 2.36 (s, 3H, furan-C**H₃**), 1.95 (hept, *J* = 6.8 Hz, 1H, C**H**), 0.94 (d, *J* = 6.8 Hz, 3H, CHC**H₃**), 0.89 (d, *J* = 6.8 Hz, 3H, CHC**H₃**), 0.05 (s, 9H, **TMS**); LC/MS *m/z* calculated for $C_{14}H_{26}NO_2Si$ $[M+H]^+$: 268.2 , found 268.1, t_R = 3.51 min.

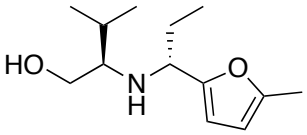

(*R*)-3-Methyl-2-(((*S*)-1-(5-methylfuran-2-yl)propyl)amino)butan-1-ol (39). To an oven dried flask under N_2 atmosphere were added EtI (346 μL, 4.31 mmol) and dry Et_2O (9.6 mL). At -78 °C *t*-BuLi (6.13 mL, 8.58 mmol) was added to the mixture, it was stirred for 10 min at -78 °C and then warmed to RT over 1h and recooled to -40 °C. A solution of (*R*,*E*)-*N*-(3-methyl-1-

((trimethylsilyl)oxy)butan-2-yl)-1-(5-methylfuran-2-yl)methanimine (**38**) (960 mg, 3.59 mmol) in Et_2O (7.2 mL) was added dropwise to the reaction mixture and it was stirred for 2.5h at -40 °C. To the mixture was added 2M HCl (12 mL) and it was warmed to RT. H_2O (12 mL) was added, the aqueous layer was extracted with Et_2O (2 x 8 mL) and the organic layers were combined and discarded. The aqueous layer was cooled to 0 °C and basified (pH=12) with the addition of 2M NaOH. The aqueous layer was extracted with Et_2O (3 x 10 mL), the combined organic layers were washed with brine (1 x 10 mL), dried (Na_2SO_4), filtered and concentrated under reduced pressure to afford 424 mg (52%) of the title amine as a yellow oil. ^{1}H NMR (400 MHz, $CDCl_3$) δ 5.96 (d, *J* = 3.0 Hz, 1H, furan-C**H**), 5.85 (dq, *J* = 2.9, 1.0 Hz, 1H, furan-C**H**), 3.55 (dd, *J* = 10.7, 4.1 Hz, 1H, NHC**H**), 3.45 (dd, *J* = 7.9, 6.4 Hz, 1H, N**H**), 3.37 (dd, *J* = 10.7, 4.2 Hz, 1H, C**H**), 2.99 (br, 1H, O**H**), 2.30–2.23 (m, 1H, C**H**), 2.29-2.22 (m, 4H, furan-C**H₃** + 1/2C**H₂**), 1.85–1.55 (m, 3H, C**H₂**CH_3 + 1/2C**H₂**), 0.88 (t, *J* = 7.4 Hz, 3H, CH_2C**H₃**), 0.84 (dd, *J* = 6.8, 1.0 Hz, 6H, 2CHC**H₃**); LC/MS *m/z* calculated for $C13H_{24}NO_2$ $[M+H]^+$: 226.2 , found 226.1 , t_R = 1.90 min.

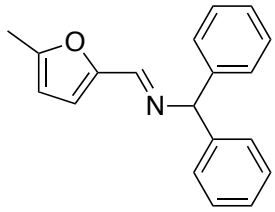

(*E*)-*N*-Benzhydryl-1-(5-methylfuran-2-yl)methanimine (41). To a solution of 5-methylfuraldehyde (**36**) (0.54 mL, 5.46 mmol) in EtOH (22 mL) at RT under N_2 atmosphere was added benzhydrylamine (**40**) (0.94 mL, 5.46 mmol). The mixture was stirred at RT for 24h. The precipitate was filtered off, washed with cold Et_2O and recrystallized from EtOH giving 852 mg (57%) of colourless crystals of the title compound. Mp 98–100 °C; ^{1}H NMR (400 MHz, $CDCl_3$) δ 8.08 (d, *J* = 0.9 Hz, 1H, N=C**H**), 7.40–7.18 (m, 10H, 10ar-C**H**), 6.68 (d, *J* = 3.2 Hz, 1H, furan-C**H**), 6.08 (dd, *J* = 3.3, 1.0 Hz, 1H, furan-C**H**), 5.58 (s, 1H, C**H**), 2.37 (s, 3H, furan-C**H₃**); LC/MS *m/z* calculated for $C_{19}H_{18}NO$ $[M+H]^+$: 276.1 , found 275.9, t_R = 2.50 min.

8.1.3 Methods Chapter 4

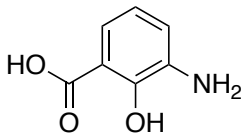

3-Amino-2-hydroxybenzoic acid (50). To a solution of 2-hydroxy-3-nitrobenzoic acid (**26**) (2.0 g, 10.9 mmol) in THF (100 mL) at RT was added 10% Pd/C (200 mg). The mixture was stirred under H_2 atmosphere at RT for 24 h. The mixture was filtered through a pad of Celite and concentrated under reduced pressure. The precipitate obtained was then dissolved in MeOH and precipitated with the addition of cold Et_2O to give 770 mg (47%) of the title compound as a brown viscous solid. ^{1}H NMR (400 MHz, DMSO) δ 8.01 (br s, 1H, O**H**), 7.05 (dd, *J* = 8.0, 1.6 Hz, 1H, ar-C**H**-6), 6.87 (dd, *J* = 7.7, 1.6 Hz, 1H, ar-C**H**-4), 6.64 (t, *J* = 7.8 Hz, 1H, ar-C**H**-5), 2.51 (p, *J* = 1.9 Hz, 2H, N**H₂**) (COO**H** not observed); LC/MS *m/z* calculated for $C_7H_8NO_3$ $[M+H]^+$: 154.1 , found 154.2 , t_R = 0.49 min.

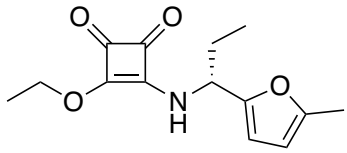

(*R*)-3-Ethoxy-4-((1-(5-methylfuran-2-yl)propyl)amino)cyclobut-3-ene-1,2-dione (51). To a solution of diethoxysquarate (20.7 µL, 0.14 mmol) in EtOH (0.8 mL) was added a solution of (*R*)-1-5-methylfuran-2-yl-propan-1-amine hydrochloride (25 mg, 0.14 mmol) and Et_3N (19.5 µL, 0.14mmol) in EtOH (0.7 mL) dropwise at 0 °C. The mixture was stirred at RT for 20 h, concentrated under reduced pressure and purified (PTLC, MeOH/CH_2Cl_2, 0.5:95.5) to give 22 mg (61%) of the title compound as a yellow viscous solid. ^{1}H NMR (400 MHz, $CDCl_3$) δ 6.10 (s, 1H, furan-C**H**), 5.89 (dd, *J* = 3.0, 1.3 Hz, 1H, furan-C**H**CHCH$_3$), 4.88 – 4.54 (m, 3H, NHC**H** + ethyl-C**H2**CH$_3$), 2.26 (s, 3H, furan-C**H₃**), 2.05-1.82 (m, 2H, C**H2**CH$_3$), 1.46 (t, *J* = 7.1 Hz, 3H, ethyl-C**H₃**), 0.97 (t, *J* = 7.4 Hz, 3H, CH$_2$C**H₃**) (N**H** not observed); LC/MS *m/z* calculated for $C_{14}H_{18}NO_4$ $[M+H]^+$: 264.1 , found 264.2 , t_R = 2.56 min.

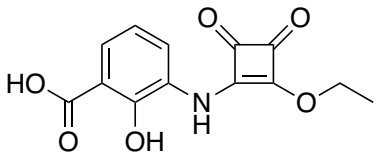

3-((2-Ethoxy-3,4-dioxocyclobut-1-en-1-yl)amino)-2-hydroxybenzoic acid (53). To a solution of 3-amino-2-hydroxybenzoic acid (**50**) (400 mg, 2.61 mmol) in dioxane (3 mL), were added diethylsquarate (460 µL, 3.13 mmol) and DIPEA (455 µL, 2.61 mmol). The mixture was reacted in the microwave at 120 °C for 15 min and concentrated under reduced pressure. H_2O (20 mL) was added, the aqueous layer was washed with Et_2O (3 x 20 mL) and the organic layers were combined and discarded. The aqueous layer was acidified (pH=2) with the addition of 2M HCl. The aqueous layer was extracted with EtOAc (3 x 20 mL) and the combined organic layers were concentrated under reduced pressure. Purification by flash column chromatography ($MeOH/CH_2Cl_2$, 10:90) gave 450 mg (62%) of the title compound as a yellow viscous solid. ^{1}H NMR (400 MHz, DMSO-d_6) δ 10.32 (s, 1H, O**H**), 7.66 (dd, J = 8.0, 1.6 Hz, 1H, ar-C**H**-6), 7.44 (dd, J = 7.8, 1.6 Hz, 1H, ar-C**H**-4), 6.90 (t, J = 7.9 Hz, 1H, ar-C**H**-5), 4.67 (q, J = 7.1 Hz, 2H, ethyl-C**H₂**), 1.34 (t, J = 7.0 Hz, 3H, ethyl-C**H₃**) (N**H** and COO**H** not observed); LC/MS *m/z* calculated for $C_{13}H_{12}NO_6$ $[M+H]^+$: 278.1 , found 278.1 , t_R = 2.65 min.

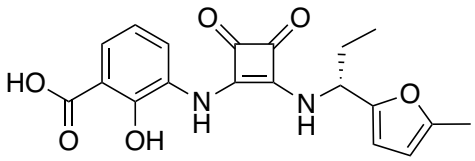

(*R*)-2-Hydroxy-3-((2-((1-(5-methylfuran-2-yl)propyl)amino)-3,4-dioxocyclobut-1-en-1-yl)amino)benzoic acid (52). To a solution of 3-((2-ethoxy-3,4-dioxocyclobut-1-en-1-yl)amino)-2-hydroxybenzoic acid (**53**) (400 mg, 1.44 mmol) and DIPEA (250 µL, 1.44 mmol) in EtOH (5 mL) was added a solution of (*R*)-1-5-methylfuran-2-yl-propan-1- amine hydrochloride (**30**) (200 mg, 1.44 mmol) and DIPEA (250 µL, 1.44 mmol) in EtOH (5 mL). The mixture was stirred at RT for 144 h and concentrated under reduced pressure. H_2O (5 mL) was added, the aqueous layer was washed with Et_2O (3 x 5 mL) and the organic layers were combined and discarded. The aqueous layer was acidified (pH=2) with the addition of 2M HCl and the viscous

precipitated title product (86 mg, 16%) was collected and used without further purification. ^{1}H NMR (400 MHz, DMSO-d_6) δ 9.38 (s, 1H, O**H**), 8.68 (d, J = 9.0 Hz, 1H, ar-N**H**), 8.02 (dd, J = 7.9, 1.5 Hz, 1H, ar-C**H**-6), 7.47 (dd, J = 8.0, 1.5 Hz, 1H, ar-C**H**-4), 6.91 (t, J = 8.0 Hz, 1H, ar-C**H**-5), 6.27 (d, J = 3.1 Hz, 1H, furan-C**H**), 6.05 (d, J = 3.1 Hz, 1H, furan-C**H**CHCH$_3$), 5.13 (q, J = 7.8 Hz, 1H, NHC**H**), 2.27 (s, 3H, furan-C**H$_3$**), 2.03-1.79 (m, 2H, C**H2**CH$_3$), 0.92 (t, J = 7.3 Hz, 3H, CH$_2$C**H$_3$**) (N**H** and COO**H** not observed); ^{13}C NMR (101 MHz, DMSO-d_6) δ 185.5 (**C**-squarate), 184.6 (**C**-squarate), 181.5 (**C**-squarate), 180.6(**C**-squarate), 172.8 (**C**=O), 152.4 (furan-**C**), 151.8 (furan-**C**), 128.0(ar-**C**), 125.4(ar-**C**), 124.3(ar-**C**), 119.3(ar-**C**), 113.2(ar-**C**), 108.0 (furan-**C**), 106.9 (furan-**C**), 53.3 (NH**C**H), 27.7 (**C**H$_2$CH$_3$), 13.7 (furan-**C**H$_3$), 10.73 (CH$_2$**C**H$_3$) (ar-**C** not observed); LC/MS *m/z* calculated for $C_{19}H_{19}N_2O_6$ $[M+H]^+$: 371.1 , found 371.2 , t_R = 3.15 min.

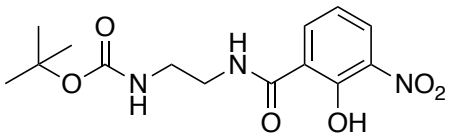

***tert*-Butyl (2-(2-hydroxy-3-nitrobenzamido)ethyl)carbamate (54a).** To a solution of 3-nitrosalicylic acid (**26**) (2.0 g, 10.9 mmol) in anhydrous CH_2Cl_2 (25 mL) at 0 °C were added oxalyl chloride (2.8 mL, 32.7 mmol) and DMF (2 drops) under N2 atmosphere. The mixture was stirred for 1.5 h at RT and then concentrated under reduced pressure to give a yellow solid. To the solid was added anhydrous CH_2Cl_2 (25 mL) under N2 atmosphere and *tert*-butyl (2-aminoethyl)carbamate (5.1 mL, 32.7 mmol) dropwise. The mixture was stirred at RT for 24 h and concentrated under reduced pressure to give a yellow solid. The solid was dissolved in CH_2Cl_2 and the organic layer was washed with $KHSO_4$ and H_2O and concentrated under reduced pressure. Purification by flash column chromatography (EtOAc/CH2Cl2, 50:50) gave 2.1 g (58 %) of the title compound as a yellow solid. Mp 103-105 °C; ^{1}H NMR (400 MHz, $CDCl_3$) δ 12.95 (s, 1H, O**H**), 8.33 – 8.11 (m, 3H, ar-(C=O)N**H** + ar-C**H**-6 + ar-C**H**-4), 7.05 (t, J = 8.1 Hz, 1H, ar-C**H**-5), 5.01 (s, 1H, BocN**H**), 3.58 (q, J = 5.3 Hz, 2H, BocNHCH$_2$C**H$_2$**), 3.42 (s, 2H, BocNHC**H$_2$**CH$_2$), 1.43 (s, 9H, Boc); ^{13}C NMR (101 MHz, $CDCl_3$) δ 166.1

(ar-**C**=ONH), 157.3(Boc-**C**=O), 154.5 (ar-**C**), 136.4 (ar-**C**), 136.1(ar-**C**), 129.1(ar-**C**), 120.6 (ar-**C**), 118.9 (ar-**C**), 80.1 (Boc-**C**), 41.7 (BocNHCH$_2$**C**H$_2$), 39.9 (BocNH**C**H$_2$CH$_2$), 28.3 (Boc-(**C**H$_3$)$_3$); LC/MS *m/z* calculated for $C_{14}H_{20}N_3O_6$ $[M+H]^+$: 326.1, found 326.2, t_R = 3.02 min.

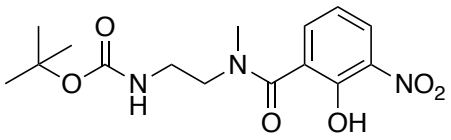

***tert*-Butyl (2-(2-hydroxy-*N*-methyl-3-nitrobenzamido)ethyl)carbamate (54b).** To a solution of 3-nitrosalicylic acid (**26**) (1.5 g, 8.2 mmol) in anhydrous CH_2Cl_2 (20 mL) at 0 °C were added oxalyl chloride (2.1 mL, 24.6 mmol) and DMF (2 drops) under N_2 atmosphere. The mixture was stirred for 1.5 h at RT and then concentrated under reduced pressure to give a yellow solid. To the solid was added anhydrous CH_2Cl_2 (20 mL) under N_2 atmosphere and *tert*-butyl (2-(methylamino)ethyl) carbamate (4.2 mL, 24.6 mmol) dropwise. The mixture was stirred at RT for 24 h and concentrated under reduced pressure to give a yellow solid. The solid was dissolved in CH_2Cl_2 and the organic layer was washed with $KHSO_4$ and H_2O and concentrated under reduced pressure Purification by flash column chromatography (EtOAc/CH_2Cl_2, 50:50) gave 1.9 g (70 %) of the title compound as a yellow oil. ^{1}H NMR (400 MHz, $CDCl_3$) δ 10.85 (s, 1H, O**H**) 8.14 (d, *J* = 8.5 Hz, 1H, ar-C**H**-4), 7.66 – 7.50 (m, 1H, ar-C**H**-6), 7.05 (t, *J* = 7.9 Hz, 1H, ar-C**H**-5), 5.03 (s, 1H, BocN**H**), 3.79 – 2.82 (m, 7H, BocNHCH$_2$C**H$_2$** + BocNHC**H$_2$**CH$_2$ + C**H$_3$**), 1.49 – 1.31 (m, 9H, Boc); ^{13}C NMR (101 MHz, $CDCl_3$) δ 167.2 (ar-**C**=ONH), 156.2 (Boc-**C**=O), 150.9 (ar-**C**), 136.0 (ar-**C**), 133.8 (ar-**C**), 128.5 (ar-**C**), 126.0 (ar-**C**), 120.4 (ar-**C**), 79.4 (Boc-**C**), 47.1 (BocNHCH$_2$**C**H$_2$), 38.1 (BocNH**C**H$_2$CH$_2$), 36.8 (**C**H$_3$), 28.4 (Boc-(**C**H$_3$)$_3$); LC/MS *m/z* calculated for $C_{15}H_{22}N_3O_6$ $[M+H]^+$: 340.1, found 340.1, t_R = 2.79 min.

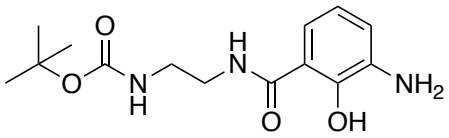

***tert*-Butyl (2-(3-amino-2-hydroxybenzamido)ethyl)carbamate (55a).** To *tert*-butyl (2-(2-hydroxy-3-nitrobenzamido)ethyl)carbamate (**54a**) (2.0 g, 6.1 mmol) in EtOH (50 mL) at RT was added 10% Pd/C (200 mg). The mixture was stirred under H_2 atmosphere at RT for 2.5 h. The mixture was filtered through a pad of Celite and concentrated under reduced pressure to give 1.8 g (99%) of a brown viscous solid. ^{1}H NMR (400 MHz, $CDCl_3$) δ 12.66 (s, 1H, O**H**), 7.65 (s, 1H, ar-(C=O)N**H**), 6.87 (dd, *J* = 8.0, 1.4 Hz, 1H, ar-C**H**-6), 6.79 (dd, *J* = 7.7, 1.4 Hz, 1H, ar-C**H**-4), 6.64 (t, *J* = 7.9 Hz, 1H, ar-C**H**-5), 5.12 (d, *J* = 7.2 Hz, 1H, BocN**H**), 3.57 – 3.26 (m, 6H, N**H₂** + BocNHCH$_2$C**H₂** + BocNHC**H₂**CH$_2$), 1.42 (s, 9H, Boc); ^{13}C NMR (101 MHz, $CDCl_3$) δ 171.0 (ar-**C**=ONH), 157.8 (Boc-**C**=O), 149.7 (ar-**C**), 136.4 (ar-**C**), 118.5 (ar-**C**), 118.0 (ar-**C**), 114.9 (ar-**C**), 113.3 (ar-**C**), 80.2 (Boc-**C**), 42.0 (BocNHCH$_2$**C**H$_2$), 39.5 (BocNH**C**H$_2$CH$_2$), 28.3 (Boc-(**C**H$_3$)$_3$); LC/MS *m/z* calculated for $C_{14}H_{22}N_3O_4$ $[M+H]^+$: 296.1, found 296.3 , t_R = 2.68 min.

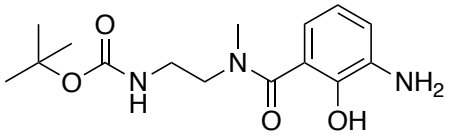

***tert*-Butyl (2-(3-amino-2-hydroxy-N-methylbenzamido)ethyl)carbamate (55b)**. To *tert*-butyl (2-(2-hydroxy-*N*-methyl-3-nitrobenzamido) ethyl)carbamate (**54b**) (1.8 g, 5.3 mmol) in EtOH (30 mL) at RT was added 10% Pd/C (180 mg). The mixture was stirred under H_2 atmosphere at RT for 3.5 h. The mixture was filtered through a pad of Celite and concentrated under reduced pressure to give 1.6 g (81%) of a brown viscous solid. ^{1}H NMR (400 MHz, $CDCl_3$) δ 6.80 – 6.63 (m, 3H, ar-C**H**-6 + ar-C**H**-4 + ar-C**H**-5), 5.00 (s, 1H, , BocN**H**), 3.64 (t, *J* = 6.1 Hz, 2H, BocNHCH$_2$C**H₂**), 3.40 (q, *J* = 6.2 Hz, 2H, BocNHC**H₂**CH$_2$), 3.18 (s, 3H, C**H₃**), 1.41 (s, 9H, Boc) (O**H** and aniline N**H₂** not observed);^{13}C NMR (101 MHz, $CDCl_3$) δ 172.5 (ar-**C**=ONH), 156.2 (Boc-**C**=O), 146.2 (ar-**C**), 136.0 (ar-**C**), 118.7 (ar-**C**), 118.0 (ar-**C**), 117.5 (ar-

C), 79.6 (Boc-**C**), 58.4 (BocNHCH$_2$**C**H$_2$), 50.7 (BocNH**C**H$_2$CH$_2$), 38.1 (**C**H$_3$), 28.3 (Boc-(**C**H$_3$)$_3$) (ar-**C** not observed); LC/MS *m/z* calculated for $C_{15}H_{24}N_3O_4$ $[M+H]^+$: 310.1, found 310.2 , t_R = 2.37 min.

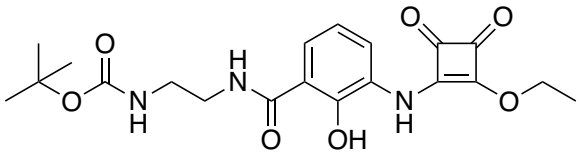

***tert*-Butyl(2-(3-((2-ethoxy-3,4-dioxocyclobut-1-en-1-yl)amino)-2-hydroxybenzamido)ethyl) carbamate (56a).** To a solution of *tert*-butyl (2-(3-amino-2-hydroxybenzamido)ethyl)carbamate (**55a**) (1.7 g, 5.7 mmol) in EtOH (30 mL) was added diethoxysquarate (0.89 mL, 6.1 mmol) dropwise. The mixture was stirred at RT for 24 h and concentrated under reduced pressure. Purification by flash column chromatography (EtOAc/CH_2Cl_2, 30:70) gave 1.7 g (71 %) of the title compound as a pink solid. Mp 88-90 °C; ^{1}H NMR (500 MHz, DMSO-d_6) δ 13.55 (s, 1H, O**H**), 10.24 (s, 1H, ar-N**H**), 8.99 (t, *J* = 5.7 Hz, 1H, ar-(C=O)N**H**), 7.70 (dd, *J* = 8.2, 1.5 Hz, 1H, ar-C**H**-6), 7.38 (dd, *J* = 7.8, 1.4 Hz, 1H, ar-C**H**-4), 6.95 (t, *J* = 6.0 Hz, 1H, BocN**H**), 6.88 (t, *J* = 8.0 Hz, 1H, ar-C**H**-5), 4.67 (q, *J* = 7.0 Hz, 2H, C**H$_2$**CH$_3$), 3.37 – 3.29 (m, 2H + H_2O, BocNHCH$_2$C**H$_2$**), 3.13 (q, *J* = 6.2 Hz, 2H, BocNHC**H$_2$**CH$_2$), 1.26-1.40 (m, 12H, Boc + CH$_2$**CH$_3$**); ^{13}C NMR (101 MHz, DMSO-d_6) δ 188.0 (**C** squaramide), 184.1 (**C** squaramide), 178.1 (**C** squaramide), 170.9 (**C** squaramide), 169.8 (ar-**C**=ONH), 155.7 (Boc-**C**=O), 154.4 (ar-**C**-2), 128.1 (ar-**C**-4), 125.9 (ar-**C**-3), 124.3 (ar-**C**-6), 117.4 (ar-**C**-5), 114.6 (ar-**C**-1), 77.7 (Boc-**C**), 69.1 (**C**H$_2$CH$_3$), 39.1 (BocNHCH$_2$**C**H$_2$), 38.8 (BocNH**C**H$_2$CH$_2$), 28.2 (Boc-(**C**H$_3$)$_3$), 15.5 (CH$_2$**C**H$_3$); LC/MS *m/z* calculated for $C_{20}H_{26}N_3O_7$ $[M+H]^+$: 420.1, found 420.1 , t_R = 2.90 min.

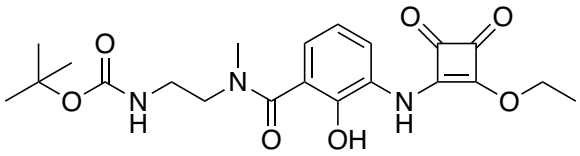

***tert*-Butyl(2-(3-((2-ethoxy-3,4-dioxocyclobut-1-en-1-yl)amino)-2-hydroxy-N-methylbenzamido)ethyl) carbamate (56b).** To a solution of *tert*-butyl (2-(3-amino-2-hydroxy-*N*-methylbenzamido)ethyl)carbamate (**55b**) (1.3 g, 4.2 mmol) in EtOH (15 mL) was added diethoxysquarate (0.65 mL, 4.4 mmol) dropwise. The mixture was stirred at RT for 40 h and concentrated under reduced pressure. Purification by flash column chromatography (MeOH/CH_2Cl_2, 4:96) gave 0.7 g (39 %) of the title compound as a pink solid. Mp 75-77 °C; ^{1}H NMR (500 MHz, DMSO-d_6) δ 10.11 (s, 1H, ar-N**H**), 9.49 (s, 1H, O**H**), 7.19 (dd, J = 7.8, 1.7 Hz, 1H, ar-C**H**-4), 7.02 (s, 1H, ar-C**H**-6), 6.87 (t, J = 7.7 Hz, 2H, ar-C**H**-5 + BocN**H**), 4.65 (q, J = 7.1 Hz, 2H, C**H$_2$**CH$_3$), 3.43 (t, J = 7.0 Hz, 2H + H_2O, BocNHCH$_2$C**H$_2$**), 3.17 (s, 2H, BocNHC**H$_2$**CH$_2$), 2.89 (s, 3H, C**H$_3$**), 1.30-1.42 (m, 12H, Boc + CH$_2$C**H$_3$**); ^{13}C NMR (126 MHz, DMSO-d_6) δ 188.2 (**C** squaramide), 184.1 (**C** squaramide), 178.0 (**C** squaramide), 171.2 (**C** squaramide), 168.2 (ar-**C**=ONH), 155.6 (Boc-**C**=O), 146.7 (ar-**C**-2), 126.0 (ar-**C**-3), 125.9 (ar-**C**-1),125.6 (ar-**C**-6), 125.2 (ar-**C**-4), 119.3 (ar-**C**-5), 77.7 (Boc-**C**), 69.1 (**C**H$_2$CH$_3$), 46.8 (BocNHCH$_2$**C**H$_2$), 37.5 (BocNH**C**H$_2$CH$_2$), 36.8 (**C**H$_3$) 28.2 (Boc-(**C**H$_3$)$_3$), 15.6 (CH$_2$**C**H$_3$); LC/MS *m/z* calculated for $C_{21}H_{28}N_3O_7$ $[M+H]^+$: 434.1, found 434.2, t_R= 2.56 min.

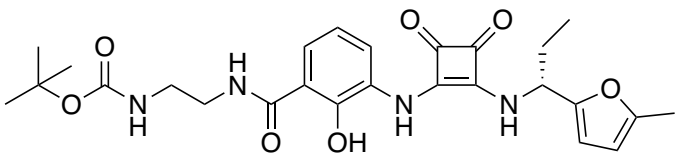

***tert*-Butyl-(*R*)-(2-(2-hydroxy-3-((2-((1-(5-methylfuran-2-yl)propyl)amino)-3,4-dioxocyclobut-1-en-1-yl)amino) benzamido)ethyl)carbamate (49a).** The title compound was synthesized following general procedure 1 using *tert*-butyl (2-(3-((2-ethoxy-3,4-dioxocyclobut-1-en-1-yl)amino)-2-hydroxybenzamido)ethyl)carbamate (**56a**) (600mg, 1.43 mmol). Purification by flash column chromatography (MeOH/CH_2Cl_2, 3:97) gave the title compound (410 mg, 56%) as a pink solid.

Mp 128-130 °C; ^{1}H NMR (400 MHz, DMSO-d_6) δ 13.96 (s, 1H, O**H**), 9.34 (s, 1H, ar-N**H**), 9.00 (t, *J* = 5.7 Hz, 1H, ar-(C=O)N**H**), 8.70 (d, *J* = 9.0 Hz, 1H, ar-C**H**-6), 7.99 (d, *J* = 8.0 Hz, 1H, ar-C**H**-4), 7.52 (d, *J* = 8.1 Hz, 1H, ar-C**H**-5), 7.02 – 6.80 (m, 2H, BocN**H** + N**H**CH), 6.26 (d, *J* = 3.1 Hz, 1H, furan-C**H**), 6.05 (dd, *J* = 3.1, 1.2 Hz, 1H, furan-C**H**CHCH$_3$), 5.13 (q, *J* = 7.8 Hz, 1H, NHC**H**), 3.33 (q, *J* = 6.5 Hz, 2H, BocNHCH$_2$C**H$_2$**), 3.13 (q, *J* = 6.2 Hz, 2H, BocNHC**H$_2$**CH$_2$), 2.26 (d, *J* = 1.0 Hz, 3H, furan-C**H$_3$**), 2.03 – 1.77 (m, 2H, C**H2**CH$_3$), 1.36 (s, 9H, Boc), 0.92 (t, *J* = 7.3 Hz, 3H, CH$_2$C**H$_3$**); ^{13}C NMR (101 MHz, DMSO-d_6) δ 184.5 (**C** squaramide), 180.6 (**C** squaramide), 170.6 (**C** squaramide), 169.0 (**C** squaramide), 163.6 (**C**=ONH), 156.2 (Boc-**C**=O), 152.5 (furan-**C**), 151.8 (furan-**C**), 151.4 (ar-**C**), 128.4 (ar-**C**), 123.5 (ar-**C**), 121.2 (ar-**C**), 118.4 (ar-**C**), 114.3(ar-**C**), 108.0 (furan-**C**H), 106.9(furan-**C**H), 78.2 (Boc-**C**), 63.2 (NH**C**H) 55.3 (**C**H$_2$), 53.3 (**C**H$_2$), 28.6 (Boc-(**C**H$_3$)$_3$), 27.7 (**C**H$_2$), 13.8 (furan-**C**H$_3$), 10.7 (CH$_2$**C**H$_3$) (**C**=O not observed); LC/MS *m/z* calculated for $C_{26}H_{33}N_4O_7$ $[M+H]^+$: 513.2, found 513.2 , t_R = 6.36 min; HRMS (TOF ES$^+$) calculated for $C_{26}H_{33}N_4O_7$ $[M+H]^+$: 513.2344, found 513.2315; $[\alpha]^{24.5\ °C}_D$ = +72 (0.5; MeOH).

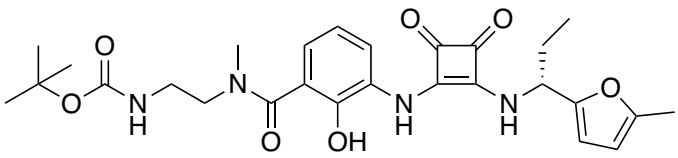

***tert*-Butyl(*R*)-(2-(2-hydroxy-N-methyl-3-((2-((1-(5-methylfuran-2-yl)propyl)amino)-3,4-dioxocyclobut-1-en-1-yl)amino)benzamido)ethyl)carbamate (49b).** The title compound was synthesized following general procedure 1 using *tert*-butyl(2-(3-((2-ethoxy-3,4-dioxocyclobut-1-en-1-yl)amino)-2-hydroxy-*N*-methylbenzamido)ethyl) carbamate (**56b**) (10mg, 0.02 mmol). Purification by flash column chromatography (MeOH/CH_2Cl_2, 3:97) gave the title compound (5 mg, 50%) as a pink oil. ^{1}H NMR (400 MHz, DMSO-d_6) δ 10.07 – 8.75 (m, 2H, ar-N**H** + O**H**), 8.49 (s, 1H, N**H**CH), 7.79 (dd, *J* = 7.6, 1.9 Hz, 1H, ar-C**H**-4), 6.97 – 6.79 (m, 2H, ar-C**H**-6 + ar-C**H**-5), 6.62 (s, 1H, BocN**H**), 6.24 (d, *J* = 3.1 Hz, 1H, furan-C**H**), 6.04 (d, *J* = 3.1 Hz, 1H, furan-C**H**CHCH$_3$), 5.17 (s, 1H, NHC**H**), 3.42 (t, *J* = 6.4 Hz, 2H, BocNHCH$_2$C**H$_2$**), 3.17 (t, *J* = 6.2 Hz, 2H,

BocNHC**H₂**CH₂), 2.98 (s, 3H, C**H₃**), 2.28 (s, 3H, furan-C**H₃**), 2.05 – 1.83 (m, 2H, C**H2**CH₃), 1.38 (s, 9H, Boc), 0.96 (t, *J* = 7.3 Hz, 3H, CH₂C**H₃**); ^{13}C NMR (101 MHz, DMSO-*d*₆) δ 184.3 (**C** squaramide), 180.6 (**C** squaramide), 169.0 (**C** squaramide), 168.4 (**C** squaramide), 163.9 (**C**=ONH), 156.1 (Boc-**C**=O), 152.5 (furan-**C**), 151.8 (furan-**C**), 132.9 (ar-**C**), 129.2(ar-**C**), 122.7 (ar-**C**), 116.3(ar-**C**), 108.0 (furan-**C**H), 106.9 (furan-**C**H), 83.3 (NH**C**H), 78.2 (Boc-**C**), 75.6 (**C**H₂), 53.2 (**C**H₂), 28.7 (Boc-(**C**H₃)₃), 27.6 (**C**H₂), 13.8 (furan-**C**H₃), 10.7 (CH₂**C**H₃) (**C**H₃ under DMSO-*d*₆, ar-**C** not observed); LC/MS *m/z* calculated for $C_{27}H_{35}N_4O_7$ $[M+H]^+$: 527.2, found: 527.2, t_R = 2.74 min; HRMS (TOF ES$^+$) calculated for $C_{27}H_{35}N_4O_7$ $[M+H]^+$: 527.2500, found 527.2485; $[\alpha]^{24.5\ °C}_D$ = +200 (0.1; MeOH).

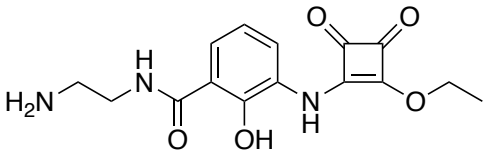

***N*-(2-Aminoethyl)-3-((2-ethoxy-3,4-dioxocyclobut-1-en-1-yl)amino)-2-hydroxybenzamide (59a)**. *Tert*-butyl(2-(3-((2-ethoxy-3,4-dioxocyclobut-1-en-1-yl)amino)-2-hydroxybenzamido)ethyl) carbamate (**56a**) (100 mg, 0.2 mmol) was dissolved in dioxane (2 mL) and it was treated with a solution of HCl in dioxane (4 M, 2mL). The solution was stirred at RT for 18h and concentrated under reduced pressure to afford 70 mg (100%) of the hydrochloride salt of the title compound as a white gum that was used without further purification. ^{1}H NMR (400 MHz, DMSO-*d*₆) δ 13.28 (s, 1H, O**H**), 10.28 (s, 1H, ar-N**H**), 9.25 (t, *J* = 5.6 Hz, 1H, ar-(C=O)N**H**), 7.99 (s, 3H, N**H₃**$^+$), 7.81 (dd, *J* = 8.2, 1.5 Hz, 1H, ar-C**H**-6), 7.40 (dd, *J* = 7.9, 1.4 Hz, 1H, ar-C**H**-4), 6.91 (td, *J* = 8.0, 3.0 Hz, 1H, ar-C**H**-5), 4.67 (q, *J* = 7.0 Hz, 2H, C**H₂**CH₃), 3.62-3.48 (m, 2H + H₂O, NH₂CH₂C**H₂**), 3.04 (dq, *J* = 11.9, 5.9 Hz, 2H, NH₂C**H₂**CH₂), 1.34 (t, *J* = 7.1 Hz, 3H, CH₂C**H₃**); ^{13}C NMR (101 MHz, DMSO-*d*₆) δ 184.6 (**C** squaramide), 178.6 (**C** squaramide), 171.4 (**C** squaramide), 170.7 (**C** squaramide), 154.8 (ar-**C**), 128.9 (ar-**C**), 126.4 (ar-**C**), 125.3 (ar-**C**), 118.0 (ar-**C**), 115.1 (ar-**C**), 69.6 (**C**H₂CH₃), 38.7 (NH₂CH₂**C**H₂), 37.3 (NH₂**C**H₂CH₂), 16.0 (CH₂**C**H₃) (**C**=O not observed); LC/MS *m/z* calculated for $C_{15}H_{18}N_3O_5$ $[M+H]^+$: 320.1, found 320.1, t_R = 2.13 min.

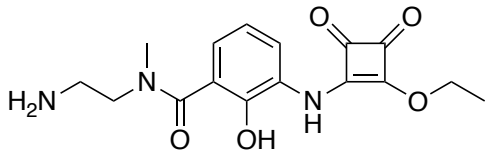

***N*-(2-Aminoethyl)-3-((2-ethoxy-3,4-dioxocyclobut-1-en-1-yl)amino)-2-hydroxy-*N*-methylbenzamide (59b).** To a solution of *tert*-butyl(2-(3-((2-ethoxy-3,4-dioxocyclobut-1-en-1-yl)amino)-2-hydroxy-*N*-methylbenzamido)ethyl) carbamate (**56b**) (50 mg, 0.1 mmol) in CH_2Cl_2 (2 mL) was added TFA (0.6 mL, 8 mmol). The solution was stirred at RT for 18 h and concentrated under reduced pressure to afford 40 mg (100%) of the TFA salt of the title compound as a white gum that was used without further purification. ^{1}H NMR (400 MHz, DMSO-d_6) δ 9.82 (s, 1H, ar-N**H**), 7.80 (s, 3H, N**H₂** + O**H**), 7.28 (d, J = 7.8 Hz, 1H, ar-C**H**-4), 7.11 (d, J = 7.5 Hz, 1H, ar-C**H**-6), 6.92 (t, J = 7.7 Hz, 1H, ar-C**H**-5), 4.69 (q, J = 7.0 Hz, 2H, C**H₂**CH$_3$), 3.63 (t, J = 6.6 Hz, 2H, NH$_2$CH$_2$C**H₂**), 3.07 (t, J = 6.5 Hz, 2H, NH$_2$C**H₂**CH$_2$), 2.91 (s, 3H, C**H₃**), 1.38 (t, J = 7.0 Hz, 3H, CH$_2$C**H₃**); ^{13}C NMR (101 MHz, DMSO-d_6) δ 184.5 (**C** squaramide), 178.5 (**C** squaramide), 169.6 (**C** squaramide), 161.0 (**C**=O), 158.8 (ar-**C**), 158.4 (ar-**C**), 126.5 (ar-**C**), 118.2(ar-**C**), 115.3 (ar-**C**), 69.6 (**C**H$_2$CH$_3$), 55.3 (NH$_2$CH$_2$**C**H$_2$), 45.1 (NH$_2$**C**H$_2$CH$_2$), 37.1 (**C**H$_3$), 16.0 (CH$_2$**C**H$_3$) (**C** squaramide and ar-**C** not observed); LC/MS *m/z* calculated for $C_{16}H_{20}N_3O_5$ $[M+H]^+$: 334.1, found 334.2, t_R = 0.96 min.

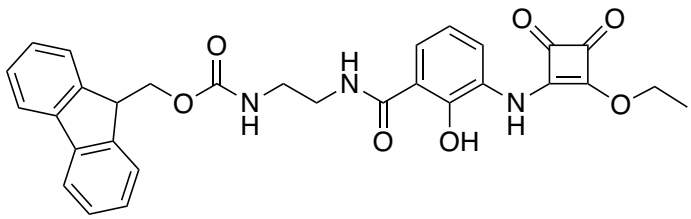

(9H-Fluoren-9-yl)methyl(2-(3-((2-ethoxy-3,4-dioxocyclobut-1-en-1-yl)amino)-2-hydroxybenzamido)ethyl)carbamate (60a). To a solution of *N*-(2-aminoethyl)-3-((2-ethoxy-3,4-dioxocyclobut-1-en-1-yl)amino)-2-hydroxybenzamide (**59a**) (30 mg, 0.1 mmol) in DMF (1.5 mL) were added DIPEA (37 µL, 0.21 mmol) and Fmoc-OSU (37 mg, 0.11 mmol). The solution was stirred for 72 h at RT and it was concentrated under reduced pressure. Purification (PTLC, MeOH/CH_2Cl_2, 1:99) gave the title compound (22 mg,

39%) as a yellow oil. ^{1}H NMR (400 MHz, DMSO-d_6) δ 13.53 (s, 1H, O**H**), 10.24 (s, 1H, ar-N**H**), 9.06 (s, 1H, ar-(C=O)N**H**), 7.88 (d, J = 7.5 Hz, 2H, 2**H**-Fmoc), 7.69 (dd, J = 11.5, 8.0 Hz, 3H, 2**H**-Fmoc + FmocN**H**), 7.50 – 7.26 (m, 6H, 4**H**-Fmoc + ar-C**H**-6 + ar-C**H**-4), 6.87 (t, J = 7.9 Hz, 1H, ar-C**H**-5), 4.67 (q, J = 7.1 Hz, 2H, C**H₂**CH₃), 4.38 – 4.18 (m, 3H, Fmoc-C**H₂** + Fmoc-C**H**), 3.34-3.23 (q, J = 6.4 Hz, 2H, FmocNHCH₂C**H₂**), 3.21 (t, J = 6.1 Hz, 2H, FmocNHC**H₂**CH₂), 1.34 (t, J = 7.1 Hz, 3H, CH₂C**H₃**); ^{13}C NMR (101 MHz, DMSO-d_6) δ 184.5 (**C** squaramide), 178.6 (**C** squaramide), 171.2 (**C** squaramide), 170.3 (**C** squaramide), 162.7 (**C**=O), 156.7 (**C**=O), 144.3 (ar-**C**), 141.2 (ar-**C**), 128.0 (ar-**C**), 127.5 (ar-**C**), 126.5 (ar-**C**), 125.6 (ar-**C**), 124.7 (ar-**C**), 120.5 (ar-**C**), 115.1 (ar-**C**), 69.6 (**C**H₂CH₃), 55.3 (**C**H₂), 49.0 (**C**H₂), 36.2 (**C**H₂), 31.2(Fmoc-**C**H), 16.0 (CH₂**C**H₃); LC/MS *m/z* calculated for $C_{30}H_{28}N_3O_7$ $[M+H]^+$: 542.1, found 542.2, t_R = 3.03 min.

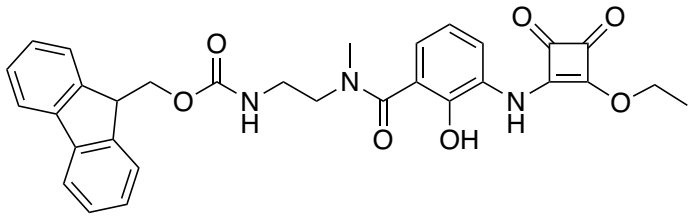

(9*H*-Fluoren-9-yl)methyl (2-(3-((2-ethoxy-3,4-dioxocyclobut-1-en-1-yl)amino)-2-hydroxy-N-methylbenzamido)ethyl)carbamate (60b). To a solution of *N*-(2-aminoethyl)-3-((2-ethoxy-3,4-dioxocyclobut-1-en-1-yl)amino)-2-hydroxy-*N*-methylbenzamide (**59b**) (25 mg, 0.075 mmol) in DMF (1.5 mL) were added DIPEA (28 µL, 0.16 mmol) and Fmoc-OSU (28 mg, 0.083 mmol). The solution was stirred for 96 h at RT and it was concentrated under reduced pressure. Purification (PTLC, MeOH/CH_2Cl_2, 3:97) gave the title compound (24 mg, 58%) as a yellow oil. ^{1}H NMR (400 MHz, DMSO-d_6) δ 7.89 (d, J = 7.5 Hz, 2H, 2**H**-Fmoc), 7.69 (d, J = 7.5 Hz, 2H, 2**H**-Fmoc), 7.46 – 7.26 (m, 5H, 4**H**-Fmoc + N**H**), 7.19 (s, 1H, ar-C**H**-4), 7.08 – 6.55 (m, 3H, ar-C**H**-6 + ar-C**H**-5 + N**H**), 4.63 (q, J = 7.0 Hz, 2H, C**H₂**CH₃), 4.41 – 4.08 (m, 3H, Fmoc-C**H₂** + Fmoc-C**H**), 3.57 – 2.74 (m, 7H + H20, FmocNHCH₂C**H₂** + FmocNHC**H₂**CH₂ + C**H₃**), 1.31 (t, J = 7.1 Hz, 3H, CH₂C**H₃**) (O**H** not observed); ^{13}C NMR (101 MHz, DMSO-d_6) δ 188.8 (**C** squaramide), 184.4 (**C** squaramide), 178.5 (**C** squaramide), 171.5 (**C**

squaramide), 168.7 (**C**=O), 144.3 (ar-**C**), 141.2 (ar-**C**), 128.0 (ar-**C**), 127.5 (ar-**C**), 126.5 (ar-**C**), 125.9 (ar-**C**), 125.6 (ar-**C**), 125.2 (ar-**C**), 120.5 (ar-**C**), 119.4 (ar-**C**), 69.5 (**C**H_2), 65.8 (**C**H_2), 49.8 (**C**H_2), 47.1 (**C**H_2), 29.4 (**C**H_3) , 16.0 (CH_2**C**H_3) (**C**=O, **C**H and ar-**C** not observed); LC/MS *m/z* calculated for $C_{31}H_{30}N_3O_7$ $[M+H]^+$: 556.2, found 556.1, t_R = 2.82 min.

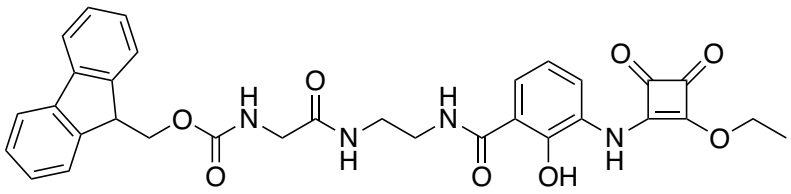

(9*H*-Fluoren-9-yl)methyl(2-((2-(3-((2-ethoxy-3,4-dioxocyclobut-1-en-1-yl)amino)-2-hydroxybenzamido)ethyl)amino)-2-oxoethyl)carbamate (60c). The title compound was synthesized following general procedure 2 using (((9*H*-fluoren-9-yl)methoxy)carbonyl)glycine (27 mg, 0.09 mmol) and *N*-(2-aminoethyl)-3-((2-ethoxy-3,4-dioxocyclobut-1-en-1-yl)amino)-2-hydroxybenzamide (**59a**) (30 mg, 0.1 mmol). Purification (PTLC, MeOH/ CH_2Cl_2, 3:97 + 1% acetic acid) gave the title compound (25 mg, 42%) as a yellow oil. ^{1}H NMR (400 MHz, DMSO-d_6) δ 13.49 (s, 1H, O**H**), 10.23 (s, 1H, ar-N**H**), 9.07 (s, 1H, ar-(C=O)N**H**), 8.04 (t, *J* = 5.7 Hz, 1H, FmocN**H**), 7.89 (d, *J* = 7.5 Hz, 2H, 2**H**-Fmoc), 7.76 – 7.64 (m, 3H, 2**H**-Fmoc + FmocN**H**), 7.52 (q, *J* = 7.1 Hz, 1H, ar-C**H**-6), 7.46 – 7.26 (m, 5H, 4**H**-Fmoc + ar-C**H**-4), 6.85 (t, *J* = 7.9 Hz, 1H, ar-C**H**-5), 4.67 (q, *J* = 7.1 Hz, 2H, C**H₂**CH_3), 4.35 – 4.01 (m, 4H, Fmoc-C**H₂** + FmocNHCH_2C**H₂**), 3.59 (d, *J* = 6.0 Hz, 2H, FmocNHC**H₂**CH_2), 3.17 (s, 2H, C**H₂**), 1.34 (t, *J* = 7.0 Hz, 3H, CH_2C**H₃**) (1**H**, under H_2O peak); ^{13}C NMR (101 MHz, DMSO-d_6) δ 184.5 (**C** squaramide), 178.6 (**C** squaramide), 172.4 (**C** squaramide), 170.2 (**C** squaramide), 169.9 (**C**=O), 156.9 (**C**=O), 144.3 (ar-**C**), 141.2 (ar-**C**), 128.1 (ar-**C**), 127.5 (ar-**C**), 126.5 (ar-**C**), 125.7 (ar-**C**), 124.7 (ar-**C**), 120.5 (ar-**C**), 115.1 (ar-**C**), 69.6 (**C**H_2), 66.1 (**C**H_2), 55.3 (**C**H_2), 47.1 (**C**H_2), 44.0 (**C**H_2), 21.5 (**C**H), 16.0 (CH_2**C**H_3) (**C**=O not observed); LC/MS *m/z* calculated for $C_{32}H_{31}N_4O_8$ $[M+H]^+$: 599.2, found 599.1 , t_R = 2.81 min.

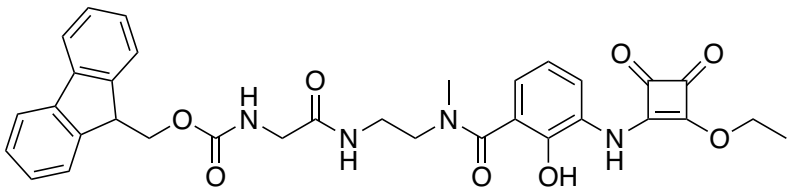

(9*H*-Fluoren-9-yl)methyl(2-((2-(3-((2-ethoxy-3,4-dioxocyclobut-1-en-1-yl)amino)-2-hydroxy-*N*-methylbenzamido)ethyl)amino)-2-oxoethyl)carbamate (**60d**). The title compound was synthesized following general procedure 2 using (((9*H*-fluoren-9-yl)methoxy)carbonyl)glycine (33 mg, 0.11 mmol) and *N*-(2-aminoethyl)-3-((2-ethoxy-3,4-dioxocyclobut-1-en-1-yl)amino)-2-hydroxybenzamide (**59b**) (40 mg, 0.1 mmol). Purification by flash column chromatography ((3:1, EtOAc:IMS)/cyclohexane 60:40 + 0.1% acetic acid) gave the title compound (8 mg, 11%) as a yellow oil. ^{1}H NMR (400 MHz, CD_3OD) δ 7.78 (d, *J* = 7.6 Hz, 2H, 2**H**-Fmoc), 7.64 (d, *J* = 7.5 Hz, 2H, 2**H**-Fmoc), 7.44 – 7.18 (m, 6H, 4**H**-Fmoc + ar-C**H** + FmocN**H**), 7.10 (d, *J* = 7.7 Hz, 1H, , ar-C**H**), 6.90 (t, *J* = 7.8 Hz, 1H, , ar-C**H**-5), 4.70 (q, *J* = 7.1 Hz, 2H, C**H₂**CH_3), 4.34 (t, *J* = 7.6 Hz, 2H, Fmoc-C**H₂**), 4.19 (t, *J* = 6.9 Hz, 1H, Fmoc-C**H**), 3.74 (m, 6H, FmocNHCH_2C**H₂** + FmocNHC**H₂**CH_2 + C**H₂**), 3.05 (s, 3H, C**H₃**), 2.01 (s, 1H, N**H**), 1.39 (t, *J* = 7.1 Hz, 3H, CH_2C**H₃**) (OH and NH not observed); ^{13}C NMR (101 MHz, MeOD) δ 184.8 (**C** squaramide), 171.1 (**C** squaramide), 170.5 (**C** squaramide), 157.6 (**C**=O), 146.3 (ar-**C**), 143.8 (ar-**C**), 141.1 (ar-**C**), 127.4 (ar-**C**), 126.7 (ar-**C**), 126.3 (ar-**C**), 125.1 (ar-**C**), 124.8 (ar-**C**), 124.6 (ar-**C**), 119.6 (ar-**C**), 119.5 (ar-**C**), 69.7 (**C**H_2), 66.7 (**C**H_2), 43.6 (**C**H_2), 36.8 (**C**H_2), 19.4 (**C**H_2 or **C**H), 14.6 (CH_2**C**H_3) (**C**H_2 or **C**H and **C**H_3 under MeOD peak, **C** squaramide, ar-**C** and **C**=O not observed); LC/MS *m/z* calculated for $C_{33}H_{33}N_4O_8[M+H]^+$: 613.2 , found 613.1, t_R = 2.73 min.

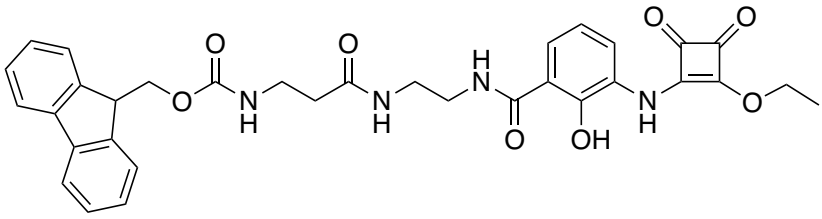

(9*H*-Fluoren-9-yl)methyl (3-((2-(3-((2-ethoxy-3,4-dioxocyclobut-1-en-1-yl)amino)-2-hydroxybenzamido)ethyl)amino)-3-oxopropyl)carbamate (60e). The title compound was synthesized following general procedure 2 using 3-((((9*H*-fluoren-9-yl)methoxy)carbonyl)amino)propanoic acid (28 mg, 0.09 mmol) and *N*-(2-aminoethyl)-3-((2-ethoxy-3,4-dioxocyclobut-1-en-1-yl)amino)-2-hydroxybenzamide (**59a**) (30 mg, 0.1 mmol). Purification by flash column chromatography (MeOH/CH_2Cl_2, 3:97 + 1% acetic acid) gave the title compound (25 mg, 40%) as a yellow oil. ^{1}H NMR (400 MHz, DMSO-d_6) δ 12.31 (s, 2H, O**H** + N**H**), 9.54 (s, 1H, N**H**), 8.07 (t, *J* = 5.6 Hz, 1H, N**H**), 7.88 (d, *J* = 7.5 Hz, 2H, 2**H**-Fmoc), 7.66 (t, *J* = 8.0 Hz, 3H, 2**H**-Fmoc + N**H**), 7.49 – 7.18 (m, 6H, 4**H**-Fmoc + 2ar-**H**), 6.72 (t, *J* = 7.9 Hz, 1H, ar-C**H**-5), 4.68 (q, *J* = 7.0 Hz, 2H, C**H₂**CH₃), 4.27 (d, *J* = 6.6 Hz, 2H, Fmoc-C**H₂**), 4.19 (t, *J* = 7.0 Hz, 1H, Fmoc-C**H**), 3.40 – 3.16 (m, 6H, 3C**H₂**), 2.27 (t, *J* = 7.2 Hz, 2H, C**H₂**), 1.34 (t, *J* = 7.0 Hz, 3H, CH₂C**H₃**); ^{13}C NMR (101 MHz, DMSO-d_6) δ 188.6 (**C** squaramide), 184.2 (**C** squaramide), 178.4 (**C** squaramide), 172.5 (**C** squaramide), 171.0 (**C**=O), 170.6 (**C**=O), 169.9 (ar-**C**), 156.5 (ar-**C**), 144.3 (ar-**C**), 141.1 (ar-**C**), 128.0 (ar-**C**), 127.5 (ar-**C**), 127.1 (ar-**C**), 125.6 (ar-**C**), 124.9 (ar-**C**), 120.5 (ar-**C**), 115.7 (ar-**C**), 69.6 (**C**H₂), 65.8 (**C**H₂), 47.1 (**C**H₂), 38.5 (**C**H₂), 37.5 (**C**H₂), 36.2 (**C**H₂), 21.5 (**C**H), 16.0 (CH₂**C**H₃) (ar-**C** and **C**=O not observed); LC/MS *m/z* calculated for $C_{33}H_{33}N_4O_8$ $[M+H]^+$: 613.2, found 613.2, t_R = 1.91 min.

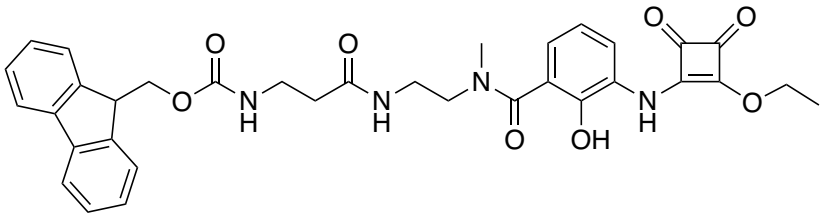

(9*H*-Fluoren-9-yl)methyl(3-((2-(3-((2-ethoxy-3,4-dioxocyclobut-1-en-1-yl)amino)-2-hydroxy-*N*-methylbenzamido)ethyl)amino)-3-oxopropyl)carbamate (60f). The title compound was synthesized following general procedure 2 using 3-((((9*H*-fluoren-9-yl)methoxy)carbonyl)amino)propanoic acid (34 mg, 0.11 mmol) and *N*-(2-aminoethyl)-3-((2-ethoxy-3,4-dioxocyclobut-1-en-1-yl)amino)-2-hydroxybenzamide (**59b**) (40 mg, 0.1 mmol). Purification by flash column chromatography ((3:1, EtOAc:IMS)/cyclohexane 60:40 + 0.1% acetic acid) gave the title compound (18 mg, 24%) as a yellow oil. ^{1}H NMR (400 MHz, CD_3OD) δ7.76 (t, *J* = 5.9 Hz, 2H, 2**H**-Fmoc), 7.63 – 7.55 (m, 2H, 2**H**-Fmoc), 7.44 – 7.19 (m, 6H, , 4**H**-Fmoc + ar-C**H** + FmocN**H**), 7.08 (d, *J* = 7.6 Hz, 1H, ar-C**H**), 6.91 (t, *J* = 7.8 Hz, 1H, ar-C**H**-5), 4.69 (q, *J* = 7.1 Hz, 2H, C**H₂**CH_3), 4.27 (d, *J* = 6.8 Hz, 2H, Fmoc-C**H₂**), 4.13 (d, *J* = 7.5 Hz, 1H, Fmoc-C**H**), 3.71 – 3.34 (m, 6H, 3C**H₂**), 3.03 (d, *J* = 5.8 Hz, 3H, C**H₃**), 2.37 (s, 2H, C**H₂**), 2.01 (s, 1H, N**H**),1.38 (t, *J* = 7.1 Hz, 3H, CH_2C**H₃**) (O**H** and N**H** not observed); ^{13}C NMR (101 MHz, MeOD) δ 184.8 (**C** squaramide), 173.8 (**C** squaramide), 170.4 (**C** squaramide), 157.3 (**C** squaramide), 146.3 (**C**=O), 143.9 (**C**=O), 143.8 (ar-**C**), 141.1 (ar-**C**), 127.3 (ar-**C**), 126.7 (ar-**C**), 126.3 (ar-**C**), 125.0 (ar-**C**), 124.7 (ar-**C**), 124.5 (ar-**C**), 124.1 (ar-**C**), 119.6 (ar-**C**), 119.5 (ar-**C**), 119.5 (ar-**C**), 69.9 (**C**H_2), 69.7 (**C**H_2), 66.4 (**C**H_2), 36.9 (**C**H_2), 36.6 (**C**H_2), 35.8 (**C**H_2), 19.3 (**C**H_3 or **C**H), 14.6 (CH_2**C**H_3) (**C**=O, **C**H_3 or **C**H not observed); LC/MS *m/z* calculated for $C_{34}H_{35}N_4O_8[M+H]^+$: 627.2, found 627.2, t_R = 2.75 min.

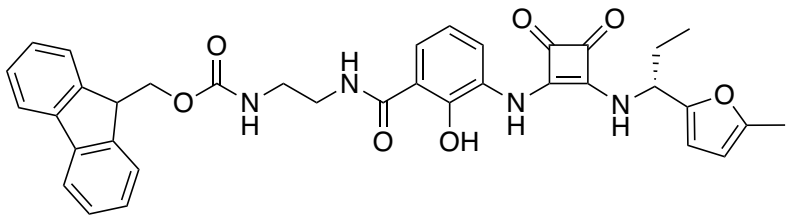

(*R*)-Fluoren-9-yl)methyl (*R*)-(2-(2-hydroxy-3-((2-((1-(5-methylfuran-2-yl)propyl)amino)-3,4-dioxocyclobut-1-en-1-yl)amino)benzamido)ethyl)carbamate (61a). The title compound was synthesized following general procedure 1 using 9*H*-fluoren-9-yl)methyl(2-(3-((2-ethoxy-3,4-dioxocyclobut-1-en-1-yl)amino)-2-hydroxybenzamido)ethyl) carbamate (**60a**)(20 mg, 0.04 mmol). Purification by flash column chromatography ($MeOH/CH_2Cl_2$, 3:97) gave the title compound (8 mg, 35%) as a yellow oil.^{1}H NMR (400 MHz, DMSO-d_6) δ 13.93 (s, 1H, O**H**), 9.34 (s, 1H, ar-N**H**), 9.05 (s, 1H, ar-(C=O)N**H**), 8.70 (d, *J* = 9.0 Hz, 1H, N**H**), 7.99 (d, *J* = 8.0 Hz, 1H, N**H**), 7.88 (d, *J* = 7.5 Hz, 2H, 2**H**-Fmoc), 7.67 (d, *J* = 7.5 Hz, 2H, 2**H**-Fmoc), 7.52 (d, *J* = 8.1 Hz, 1H, ar-C**H**), 7.46 (t, *J* = 5.9 Hz, 1H, ar-C**H**), 7.44 – 7.36 (m, 2H, 2**H**-Fmoc), 7.31 (td, *J* = 7.5, 1.1 Hz, 2H, 2**H**-Fmoc), 6.87 (s, 1H, ar-C**H**), 6.26 (d, *J* = 3.1 Hz, 1H, furan-C**H**), 6.05 (dd, *J* = 3.2, 1.2 Hz, 1H, furan-C**H**), 5.13 (q, *J* = 7.7 Hz, 1H, NHC**H**), 4.30 (d, *J* = 6.9 Hz, 2H, Fmoc-C**H₂**), 4.20 (t, *J* = 6.7 Hz, 1H, Fmoc-C**H**), 3.37 (q, *J* = 6.2 Hz, 2H, C**H₂**), 3.21 (q, *J* = 6.1 Hz, 2H, C**H₂**), 2.26 (d, *J* = 1.0 Hz, 3H, furan-C**H₃**), 2.01 – 1.80 (m, 2H, C**H₂**CH_3), 0.92 (t, *J* = 7.3 Hz, 3H, CH_2C**H₃**); ^{13}C NMR (101 MHz, DMSO-d_6) δ 184.4 (**C** squaramide), 180.6 (**C** squaramide), 170.6 (**C** squaramide), 169.0 (**C** squaramide), 163.6 (**C**=O), 156.7 (ar-**C**), 152.5 (furan-**C**), 151.8 (furan-**C**), 144.3 (ar-**C**), 141.2 (ar-**C**), 128.0 (ar-**C**), 127.5 (ar-**C**), 125.6 (ar-**C**), 123.5 (ar-**C**), 121.2 (ar-**C**), 120.5 (ar-**C**), 114.4 (ar-**C**), 108.0 (furan-**C**H), 106.9 (furan-**C**H), 65.8 (**C**H_2), 53.3 (**C**H_2), 47.1 (**C**H_2 or **C**H), 27.6 (**C**H_2CH_3), 13.8 (furan-**C**H_3), 10.7 (CH_2**C**H_3) (ar-**C**, **C**=O and **C**H not observed); LC/MS *m/z* calculated for $C_{36}H_{34}N_4NaO_7$ $[M+ Na]^+$: 657.2, found 657.2 , t_R = 1.84 min; HRMS (TOF ES$^+$) calculated for $C_{36}H_{34}N_4NaO_7$ $[M+Na]^+$: 657.2320 , found 657.2286; $[\alpha]^{24.5\ °C}_D$ = + 64(0.3; MeOH).

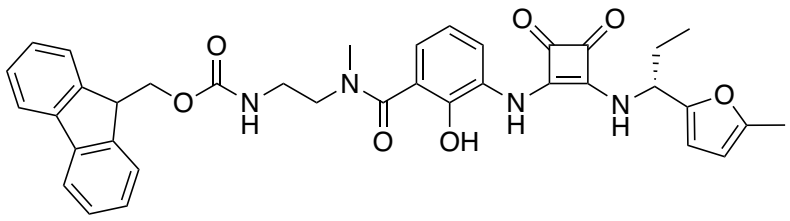

(9*H*-Fluoren-9-yl)methyl(*R*)-(2-(2-hydroxy-N-methyl-3-((2-((1-(5-methylfuran-2-yl)propyl)amino)-3,4-dioxocyclobut-1-en-1-yl)amino)benzamido)ethyl)carbamate (**61b**). The title compound was synthesized following general procedure 1 using (9*H*-Fluoren-9-yl)methyl (2-(3-((2-ethoxy-3,4-dioxocyclobut-1-en-1-yl)amino)-2-hydroxy-*N*-methylbenzamido)ethyl)carbamate **(60b)** (23 mg, 0,04 mmol). Purification (PTLC, MeOH/CH_2Cl_2, 10:90) gave the title compound (12 mg, 48%) as a yellow oil. ^{1}H NMR (400 MHz, DMSO-d_6) δ 9.75 (s, 1H, N**H**), 9.28 (s, 1H, N**H**), 8.65 (d, *J* = 9.0 Hz, 1H, ar-C**H**), 7.88 (d, *J* = 7.5 Hz, 2H, 2**H**-Fmoc), 7.77 (d, *J* = 7.0 Hz, 1H, ar- C**H**), 7.67 (d, *J* = 7.5 Hz, 2H, 2**H**-Fmoc), 7.45 – 7.25 (m, 4H, 4**H**-Fmoc), 6.82 (br s, 2H, 2ar-C**H**),6.24 (d, *J* = 3.1 Hz, 1H, furan-C**H**), 6.04 (d, *J* = 3.1 Hz, 1H, furan-C**H**), 5.13 (q, *J* = 7.7 Hz, 1H, NHC**H**), 4.42 – 4.12 (m, 3H, Fmoc-C**H₂** + Fmoc-C**H**), 3.33 (s, 4H + H_2O, 2C**H₂**), 2.89 (br s, 3H, C**H₃**), 2.25 (s, 3H, furan-C**H₃**), 2.04 – 1.76 (m, 2H, C**H₂**CH_3), 1.23 (s, 1H, N**H**), 0.91 (t, *J* = 7.3 Hz, 3H, CH_2C**H₃**) (O**H** not observed);^{13}C NMR (101 MHz, DMSO-d_6) δ 183.5 (**C** squaramide), 181.1 (**C** squaramide), 170.7 (**C** squaramide), 168.7 (**C** squaramide), 163.7 (**C**=O), 152.9 (furan-**C**), 151.6 (furan-**C**), 143.0 (ar-**C**), 139.8 (ar-**C**), 137.9 (ar-**C**), 130.6 (ar-**C**), 129.4 (ar-**C**), 127.7 (ar-**C**), 124.6 (ar-**C**), 123.4 (ar-**C**), 121.8 (ar-**C**), 120.5 (ar-**C**), 115.7 (ar-**C**), 110.2 (ar-**C**), 107.7 (furan-**C**H), 106.8 (furan-**C**H), 53.1 (**C**H_2), 50.2 (**C**H_2 or **C**H), 36.7 (**C**H_2 or **C**H), 34.0 (**C**H_3), 29.5 (**C**H_2 or **C**H), 27.5 (**C**H_2CH_3), 13.8 (furan-**C**H_3), 10.7 (CH_2**C**H_3) (**C**=O and **C**H not observed); LC/MS *m/z* calculated for $C_{37}H_{36}N_4NaO_7$ $[M+Na]^+$: 671.2, found 671.2, t_R = 3.06 min; $[\alpha]^{24.5\ °C}_D$ = + 266 (0.3; MeOH).

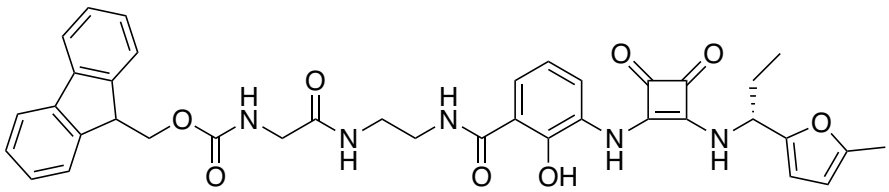

(9*H*-Fluoren-9-yl)methyl(*R*)-(2-((2-(2-hydroxy-3-((2-((1-(5-methylfuran-2-yl)propyl)amino)-3,4-dioxocyclobut-1-en-1-yl)amino)benzamido)ethyl)amino)-2-oxoethyl)carbamate (61c). The title compound was synthesized following general procedure 1 using (9*H*-fluoren-9-yl)methyl (2-((2-(3-((2-ethoxy-3,4-dioxocyclobut-1-en-1-yl)amino)-2-hydroxybenzamido)ethyl)amino)-2-oxoethyl)carbamate (**60c**) (24 mg, 0.04 mmol). Purification (PTLC, MeOH/CH_2Cl_2, 4:96) gave the title compound (11 mg, 40%) as a yellow oil. ^{1}H NMR (400 MHz, DMSO-d_6) δ 13.88 (s, 1H, O**H**), 9.35 (s, 1H, ar-N**H**), 9.04 (s, 1H, ar-(C=O)N**H**), 8.70 (d, J = 9.0 Hz, 1H, N**H**), 8.04 (t, J = 5.7 Hz, 1H, N**H**), 7.98 (d, J = 8.0 Hz, 1H, N**H**), 7.89 (d, J = 7.5 Hz, 2H, 2**H**-Fmoc), 7.70 (d, J = 7.5 Hz, 2H, 2**H**-Fmoc), 7.59 – 7.46 (m, 2H, 2ar-C**H**), 7.41 (t, J = 7.4 Hz, 2H, 2**H**-Fmoc), 7.32 (td, J = 7.4, 1.2 Hz, 2H, 2**H**-Fmoc), 6.84 (s, 1H, ar-C**H**), 6.26 (d, J = 3.1 Hz, 1H, furan-C**H**), 6.05 (dd, J = 3.1, 1.2 Hz, 1H, furan-C**H**), 5.13 (q, J = 7.8 Hz, 1H, NHC**H**), 4.29 – 4.14 (m, 3H, Fmoc-C**H₂** + Fmoc-C**H**), 3.60 (d, J = 6.0 Hz, 2H, C**H₂**), 3.36 (t, J = 5.9 Hz, 2H, C**H₂**), 3.29 (d, J = 6.4 Hz, 2H, C**H₂**), 2.26 (d, J = 1.0 Hz, 3H, furan-C**H₃**), 2.01 – 1.79 (m, 2H, C**H₂**CH_3), 0.92 (t, J = 7.3 Hz, 3H, CH_2C**H₃**); ^{13}C NMR (101 MHz, DMSO-d_6) δ 180.6 (**C** squaramide), 170.5 (**C** squaramide), 169.9 (**C** squaramide), 169.0 (**C** squaramide), 163.6 (**C**=O or ar-**C**), 156.9 (ar-**C**), 152.5 (furan-**C**), 151.8 (furan-**C**), 144.3 (ar-**C**), 141.1 (ar-**C**), 128.1 (ar-**C**), 127.5 (ar-**C**), 125.7 (ar-**C**), 120.5 (ar-**C**), 108.0 (furan-**C**H), 106.9 (furan-**C**H), 66.1 (**C**H_2), 53.3 (**C**H_2), 47.0 (**C**H_2 or **C**H), 44.0 (**C**H_2 or **C**H), 38.4 (**C**H_2 or **C**H), 27.6 (**C**H_2CH_3), 13.8 (furan-**C**H_3), 10.7 (CH_2**C**H_3) (ar-**C**, **C**=O and **C**H not observed); LC/MS *m/z* calculated for $C_{38}H_{37}N_5NaO_8$ $[M+Na]^+$: 714.2, found 714.2 , t_R = 1.94 min; HRMS (TOF ES$^+$) calculated for $C_{38}H_{37}N_5NaO_8$ $[M+Na]^+$: 714.2534, found 714.2519; $[\alpha]^{24.5\ °C}_D$ = +100 (0.2; MeOH).

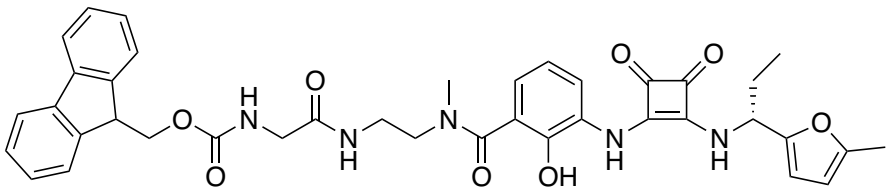

(9*H*-Fluoren-9-yl)methyl(*R*)-(2-((2-(2-hydroxy-*N*-methyl-3-((2-((1-(5-methylfuran-2-yl)propyl)amino)-3,4-dioxocyclobut-1-en-1-yl)amino)benzamido)ethyl)amino)-2-oxoethyl)carbamate (61d). The title compound was synthesized following general procedure 1 using (9H-fluoren-9-yl)methyl(2-((2-(3-((2-ethoxy-3,4-dioxocyclobut-1-en-1-yl)amino)-2-hydroxy-N-methylbenzamido)ethyl)amino)-2-oxoethyl)carbamate (**60d**) (7 mg, 0,01 mmol). Purification by flash column chromatography ($MeOH/CH_2Cl_2$, 3:97) gave the title compound (7 mg, 90%) as a yellow oil (purity 95%). ^{1}H NMR (400 MHz, DMSO-d_6) δ 9.74 (s, 1H, N**H**), 9.29 (s, 1H, N**H**), 8.67 (d, J = 9.0 Hz, 1H, N**H**), 7.89 (d, J = 7.5 Hz, 2H, 2**H**-Fmoc), 7.78 (d, J = 7.9 Hz, 1H, N**H**), 7.70 (d, J = 7.5 Hz, 2H, 2**H**-Fmoc), 7.61 – 7.47 (m, 1H, ar-C**H**), 7.41 (t, J = 7.4 Hz, 2H, 2**H**-Fmoc), 7.36 – 7.25 (m, 2H, 2**H**-Fmoc), 6.84 (s, 2H, 2ar-C**H**), 6.24 (d, J = 3.1 Hz, 1H, furan-C**H**), 6.03 (d, J = 3.3 Hz, 1H, furan-C**H**), 5.13 (q, J = 7.7 Hz, 1H, NHC**H**), 4.27 (d, J = 7.0 Hz, 2H, Fmoc-C**H₂**), 4.24 – 4.15 (m, 1H, Fmoc-C**H**), 3.56 (s, 2H, C**H₂**), 2.92 (s, 2H, C**H₂**), 2.25 (s, 3H, furan-C**H₃**), 1.99 – 1.77 (m, 2H, C**H₂**CH_3), 1.23 (s, 3H, C**H₃**), 0.90 (q, J = 8.2 Hz, 3H, CH_2C**H₃**) (C**H₂**, under H_2O peak, O**H** not observed); ^{13}C NMR (101 MHz, DMSO-d_6) δ ^{13}C NMR (101 MHz, DMSO) δ 180.4 (**C** squaramide), 177.5 (**C** squaramide), 169.0 (**C** squaramide), 163.9 (**C**=O), 161.2 (**C**=O or ar-**C**), 156.9 (ar-**C**), 152.6 (furan-**C**), 151.8 (furan-**C**), 144.3 (ar-**C**), 141.1 (ar-**C**), 128.1 (ar-**C**), 127.5 (ar-**C**), 125.7 (ar-**C**), 120.5 (ar-**C**), 108.0 (furan-**C**H), 106.9 (furan-**C**H), 66.1 (**C**H_2), 56.3 (**C**H_2 or **C**H), 53.2 (**C**H_2), 47.1 (**C**H_2 or **C**H), 29.4 (**C**H_2 or **C**H), 27.6 (**C**H_2CH_3), 13.8 (furan-**C**H_3), 10.7 (CH_2**C**H_3) (**C** squaramide, ar-**C**, **C**H, **C**H_3 not observed); LC/MS *m/z* calculated for $C_{39}H_{39}N_5NaO_8$ $[M+Na]^+$: 728.2, found 728.1, t_R = 2.90 min; $[\alpha]^{24.5\ °C}_D$ = +266 (0.03; MeOH).

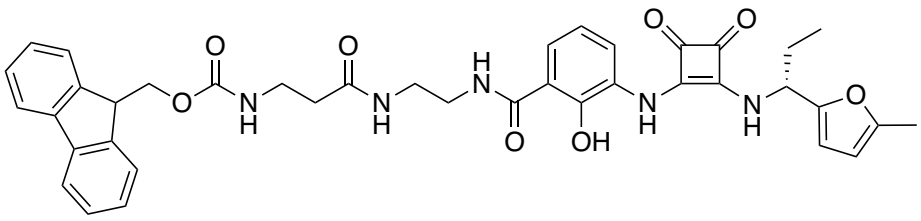

(9*H*-Fluoren-9-yl)methyl(*R*)-(3-((2-(2-hydroxy-3-((2-((1-(5-methylfuran-2-yl)propyl)amino)-3,4-dioxocyclobut-1-en-1-yl)amino)benzamido)ethyl)amino)-3-oxopropyl)carbamate (61e). The title compound was synthesized following general procedure 1 using (9*H*-Fluoren-9-yl)methyl (3-((2-(3-((2-ethoxy-3,4-dioxocyclobut-1-en-1-yl)amino)-2-hydroxybenzamido)ethyl)amino)-3-oxopropyl)carbamate **(60e)** (40 mg, 0,065 mmol). Purification by flash column chromatography ($MeOH/CH_2Cl_2$, 3:97) gave the title compound (11 mg, 24%) as a yellow oil (purity 95%). ^{1}H NMR (400 MHz, DMSO-d_6) δ 13.91 (s, 1H, O**H**), 9.34 (s, 1H, N**H**), 9.05 (t, *J* = 5.5 Hz, 1H, N**H**), 8.69 (d, *J* = 9.0 Hz, 1H, N**H**), 8.06 (t, *J* = 5.8 Hz, 1H, N**H**), 8.02 – 7.94 (m, 1H, N**H**), 7.88 (d, *J* = 7.5 Hz, 2H, 2**H**-Fmoc), 7.67 (d, *J* = 7.7 Hz, 2H, 2**H**-Fmoc), 7.54 – 7.47 (m, 2H, 2ar-C**H**), 7.43 – 7.36 (m, 2H, 2**H**-Fmoc), 7.35 – 7.26 (m, 2H, 2**H**-Fmoc), 6.87 (t, *J* = 8.0 Hz, 1H, ar-C**H**), 6.26 (d, *J* = 3.1 Hz, 1H, furan-C**H**), 6.05 (dd, *J* = 3.1, 1.2 Hz, 1H, furan-C**H**), 5.13 (q, *J* = 7.9 Hz, 1H, NHC**H**), 4.36 – 4.07 (m, 3H, Fmoc-C**H₂** + Fmoc-C**H**), 3.46 – 3.12 (m, 6H + H_2O, 3 C**H₂**), 2.26 (m, 5H, C**H₂**+ furan-C**H₃**), 2.03 – 1.75 (m, 2H, C**H₂**CH_3), 0.92 (t, *J* = 7.3 Hz, 3H, CH_2C**H₃**); ^{13}C NMR (101 MHz, DMSO-d_6) δ 184.5 (**C** squaramide), 180.6 (**C** squaramide), 171.0 (**C** squaramide), 170.5 (**C** squaramide), 169.0 (**C**=O), 163.6 (**C**=O), 156.5 (**C**=O), 152.5 (furan-**C**), 151.8 (furan-**C**), 144.3 (ar-**C**), 141.1 (ar-**C**), 128.4 (ar-**C**), 128.0 (ar-**C**), 127.5 (ar-**C**), 125.6 (ar-**C**), 124.8 (ar-**C**), 123.5 (ar-**C**), 120.5 (ar-**C**), 118.5 (ar-**C**), 114.3 (ar-**C**), 110.1 (ar-**C**), 108.0 (furan-**C**H), 106.9 (furan-**C**H), 65.8 (**C**H_2), 53.3(**C**H_2), 47.1 (**C**H_2 or **C**H), 38.3 (**C**H_2 or **C**H), 37.5 (**C**H_2 or **C**H), 36.2 (**C**H_2 or **C**H), 27.6 (**C**H_2CH_3), 13.8 (furan-**C**H_3), 10.7 (CH_2**C**H_3) (**C**H not observed); LC/MS *m/z* calculated for $C_{39}H_{39}N_5NaO_8$ $[M+Na]^+$: 728.2, found 728.2, t_R = 2.94 min; $[\alpha]^{24.5\ °C}_D$ = +300 (0.03; MeOH).

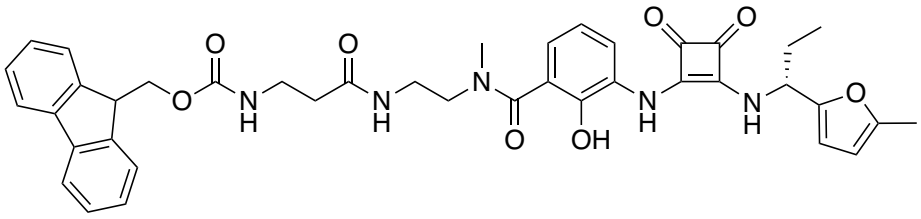

(9*H*-Fluoren-9-yl)methyl(*R*)-(3-((2-(2-hydroxy-N-methyl-3-((2-((1-(5-methylfuran-2-yl)propyl)amino)-3,4-dioxocyclobut-1-en-1-yl)amino)benzamido)ethyl)amino)-3-oxopropyl)carbamate (61f). The title compound was synthesized following general procedure 1 using (9*H*-fluoren-9-yl)methyl(3-((2-(3-((2-ethoxy-3,4-dioxocyclobut-1-en-1-yl)amino)-2-hydroxy-*N*-methylbenzamido)ethyl)amino)-3-oxopropyl)carbamate (**60f)** (17 mg, 0,027 mmol). Purification by flash column chromatography ($MeOH/CH_2Cl_2$, 3:97) gave the title compound (5 mg, 26%) as a yellow oil (purity 95%). ^{1}H NMR (400 MHz, DMSO-d_6) δ 9.76 (s, 1H, N**H**), 9.29 (s, 1H, N**H**), 8.67 (d, J = 9.0 Hz, 1H, N**H**), 7.88 (d, J = 7.5 Hz, 2H, 2**H**-Fmoc), 7.79 (d, J = 8.4 Hz, 1H), 7.66 (d, J = 7.5 Hz, 2H, 2**H**-Fmoc), 7.40 (td, J = 7.5, 1.1 Hz, 2H, 2**H**-Fmoc), 7.35 – 7.23 (m, 3H, 2**H**-Fmoc + ar-C**H**), 6.84 (s, 2H, 2ar-C**H**), 6.25 (d, J = 3.1 Hz, 1H, furan-C**H**), 6.13 – 5.92 (m, 1H, furan-C**H**), 5.14 (q, J = 7.7 Hz, 1H, NHC**H**), 4.32 – 4.12 (m, 3H, Fmoc-C**H₂** + Fmoc-C**H**), 3.17 (br s, 4H, 2C**H₂**), 2.92 (s, 4H, 2C**H₂**), 2.25 (s, 3H, furan-C**H₃**), 2.02 – 1.77 (m, 2H, C**H₂**CH_3), 1.23 (s, 1H, N**H**), 0.91 (t, J = 7.3 Hz, 3H, CH_2**C**H_3) (O**H** not observed); ^{13}C NMR (101 MHz, DMSO-d_6) δ 184.3 (**C** squaramide), 180.7 (**C** squaramide), 169.0 (**C** squaramide), 163.9 (**C**=O), 156.4 (**C**=O), 152.5 (furan-**C**), 151.8 (furan-**C**), 144.3 (ar-**C**), 141.1 (ar-**C**), 129.2 (ar-**C**), 128.0 (ar-**C**), 127.5 (ar-**C**), 125.6 (ar-**C**), 122.6 (ar-**C**), 120.5 (ar-**C**), 117.7 (ar-**C**), 108.0 (furan-**C**H), 106.9 (furan-**C**H), 65.8 (**C**H_2), 53.2 (**C**H_2), 47.1 (**C**H_2 or **C**H), 37.4 (**C**H_2 or **C**H), 36.1 (**C**H_2 or **C**H), 29.4 (**C**H_2 or **C**H), 27.6 (**C**H_2CH_3), 13.8 (furan-**C**H_3), 10.7 (CH_2**C**H_3) (**C** squaramide, **C**=O, ar-**C** and **C**H observed); LC/MS *m/z* calculated for $C_{40}H_{41}N_5NaO_8$ $[M+Na]^+$: 742.2, found 742.1, t_R = 2.87 min; $[\alpha]^{24.5\ °C}_D$ = + 300 (0.04; MeOH).

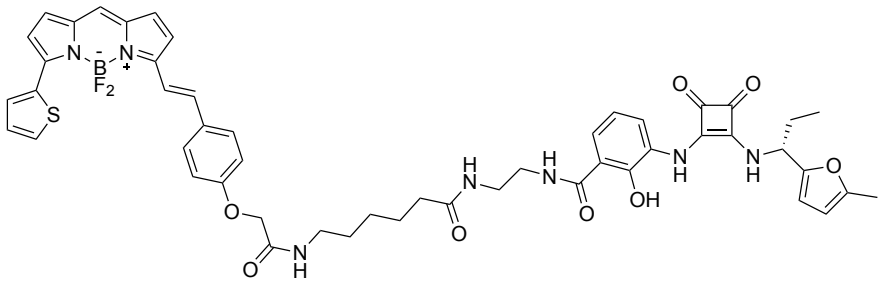

(*R*,*E*)-*N*-(2-(6-(2-(4-(2-(5,5-Difluoro-7-(thiophen-2-yl)-5H-4λ4,5λ4-dipyrrolo[1,2-c:2',1'-f][1,3,2]diazaborinin-3-yl)vinyl)phenoxy)acetamido)hexanamido)ethyl)-2-hydroxy-3-((2-((1-(5-methylfuran-2-yl)propyl)amino)-3,4-dioxocyclobut-1-en-1-yl)amino)benzamide (62a). The title compound was synthesized following general procedure 3 using (9*H*-fluoren-9-yl)methyl (*R*)-(2-(2-hydroxy-3-((2-((1-(5-methylfuran-2-yl)propyl)amino)-3,4-dioxocyclobut-1-en-1-yl)amino)benzamido)ethyl)carbamate **(61a)** (2 mg, 0.0031 mmol). Purification (PTLC, Si, MeOH/CH_2Cl_2 5:95) gave the title compound (2 mg, 69%). HRMS (TOF ES^+) calculated for $C_{50}H_{50}BF_2N_7NaO_8S$ $[M+Na]^+$: 980.3394, found 980.3260.

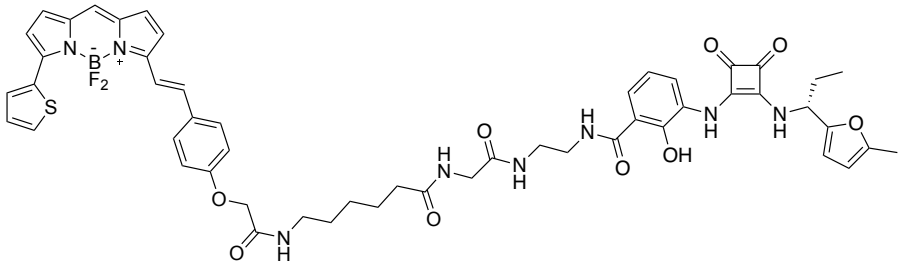

(*R*,*E*)-*N*-(2-(2-(6-(2-(4-(2-(5,5-Difluoro-7-(thiophen-2-yl)-5H-4λ4,5λ4-dipyrrolo[1,2-c:2',1'-f][1,3,2]diazaborinin-3-yl)vinyl)phenoxy)acetamido)hexanamido)acetamido)ethyl)-2-hydroxy-3-((2-((1-(5-methylfuran-2-yl)propyl)amino)-3,4-dioxocyclobut-1-en-1-yl)amino)benzamide (62c). The title compound was synthesized following general procedure 3 using (9*H*-fluoren-9-yl)methyl (*R*)-(2-((2-(2-hydroxy-3-((2-((1-(5-methylfuran-2-yl)propyl)amino)-3,4-dioxocyclobut-1-en-1-yl)amino)benzamido)ethyl)amino)-2-oxoethyl)carbamate **(61c)** (2mg, 0.0029 mmol). Purification (PTLC, Si, MeOH/CH_2Cl_2 5:95) gave the title

compound (2 mg, 69 %). HRMS (TOF ES^+) calculated for $C_{52}H_{53}BF_2N_8NaO_9S$ $[M+Na]^+$: 1037.3609, found 1037.3273.

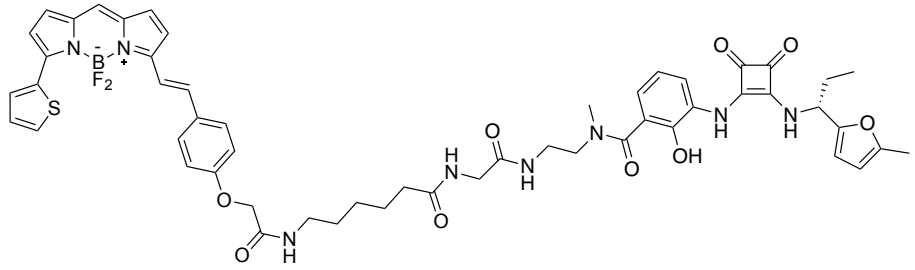

***(R,E)-N*-(2-(2-(6-(2-(4-(2-(5,5-Difluoro-7-(thiophen-2-yl)-5H-4λ4,5λ4-dipyrrolo[1,2-c:2',1'-f][1,3,2]diazaborinin-3-yl)vinyl)phenoxy)acetamido)hexanamido)acetamido)ethyl)-2-hydroxy-*N*-methyl-3-((2-((1-(5-methylfuran-2-yl)propyl)amino)-3,4-dioxocyclobut-1-en-1-yl)amino)benzamide (62d).** The title compound was synthesized following general procedure 3 using (9*H*-fluoren-9-yl)methyl (*R*)-(2-((2-(2-hydroxy-*N*-methyl-3-((2-((1-(5-methylfuran-2-yl)propyl)amino)-3,4-dioxocyclobut-1-en-1-yl)amino)benzamido)ethyl)amino)-2-oxoethyl)carbamate **(61d)** (1.1mg, 0.0015 mmol). Purification (PTLC, Si, MeOH/CH_2Cl_2 5:95) gave the title compound (0.5 mg, 34 %). HRMS (TOF ES^+) calculated for $C_{53}H_{55}BF_2N_8NaO_9S$ $[M+Na]^+$: 1051.3766, found 1051.3648.

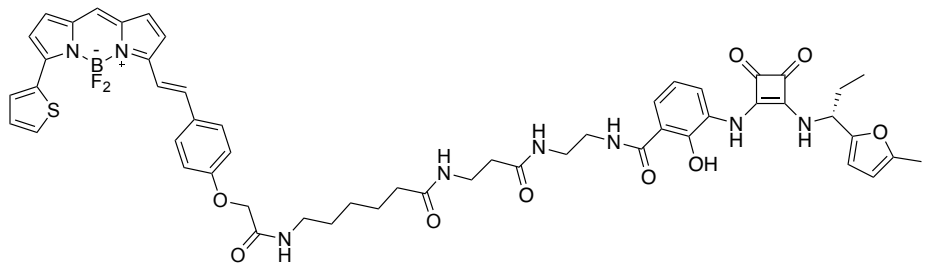

***(R,E)-N*-(2-(3-(6-(2-(4-(2-(5,5-Difluoro-7-(thiophen-2-yl)-5H-4λ4,5λ4-dipyrrolo[1,2-c:2',1'-f][1,3,2]diazaborinin-3-yl)vinyl)phenoxy)acetamido)hexanamido)propanamido)ethyl)-2-hydroxy-3-((2-((1-(5-methylfuran-2-yl)propyl)amino)-3,4-dioxocyclobut-1-en-1-yl)amino)benzamide (62e).** The title compound was

synthesized following general procedure 3 using (9*H*-fluoren-9-yl)methyl (*R*)-(3-((2-(2-hydroxy-3-((2-((1-(5-methylfuran-2-yl)propyl)amino)-3,4-dioxocyclobut-1-en-1-yl)amino)benzamido)ethyl)amino)-3-oxopropyl)carbamate **(61e)** (1mg, 0.0014 mmol). Purification (PTLC, Si, MeOH/CH_2Cl_2 5:95) gave the title compound (0.9 mg, 63 %). HRMS (TOF ES^+) calculated for $C_{53}H_{55}BF_2N_8NaO_9S$ $[M+Na]^+$: 1051.3766, found 1051.3630.

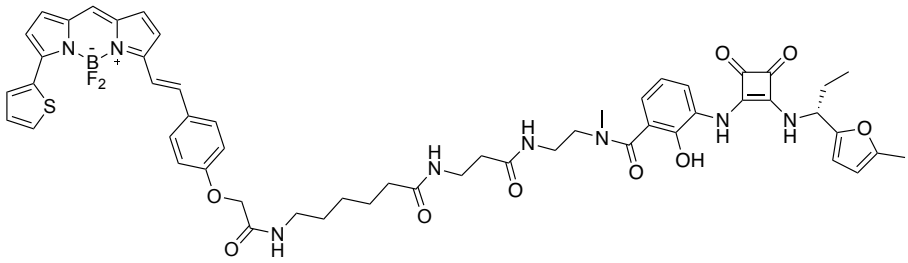

***(R,E)-N*-(2-(3-(6-(2-(4-(2-(5,5-Difluoro-7-(thiophen-2-yl)-5H-4λ4,5λ4-dipyrrolo[1,2-c:2',1'-f][1,3,2]diazaborinin-3-yl)vinyl)phenoxy)acetamido)hexanamido)propanamido)ethyl)-2-hydroxy-*N*-methyl-3-((2-((1-(5-methylfuran-2-yl)propyl)amino)-3,4-dioxocyclobut-1-en-1-yl)amino)benzamide (62f).** The title compound was synthesized following general procedure 3 using (9*H*-fluoren-9-yl)methyl (*R*)-(3-((2-(2-hydroxy-*N*-methyl-3-((2-((1-(5-methylfuran-2-yl)propyl)amino)-3,4-dioxocyclobut-1-en-1-yl)amino)benzamido)ethyl)amino)-3-oxopropyl)carbamate **(61f)** (1mg, 0.0013 mmol). Purification (PTLC, Si, MeOH/CH_2Cl_2 5:95) gave the title compound (0.5 mg, 39 %). HRMS (TOF ES^+) calculated for $C_{54}H_{57}BF_2N_8NaO_9S$ $[M+Na]^+$: 1065.3922, found 1065.3811.

8.2 Pharmacology

8.2.1 Molecular biology, cell culture and membrane preparation

Molecular biology constructs and cell lines were generated by Desislava Nesheva and James Farmer (School of Life Sciences, University of Nottingham). Human CXCR1 (GenBank: NM_000634.3) and CXCR2 (GenBank NM_001557.3) receptor cDNA sequences were amplified via polymerase chain reaction and cloned downstream of a SNAP-tag (New England Biolabs, Hitchin, UK). Each cDNA sequence was inserted between EcoRI and XhoI sites, in the previously generated pcDNA3.1neo(+)-SNAP mammalian expression vector (Invitrogen, Paisley, UK)[335] containing a Kozak sequence (GCCACC) and the 5-HT3 receptor signal sequence (amino acids MRLCIPQVLLALFLSMLTGPGEGSRK) upstream to facilitate membrane insertion and orientation of the extracellular SNAP tag. Addition of either a LgBiT fragment[352] or thermostable Nanoluciferase (tsNanoLuc)[353] at the *C* terminus was achieved through cloning of corresponding sequences, in frame with receptor *C* termini without intervening STOP codon, between XhoI/XbaI restriction sites, generating p3.1neo-SNAP-CXCR1/2-LgBiT and p3.1neo-SNAP-CXCR1/2-tsNanoLuc constructs. Constructs were used to generate HEK 293 stable cell lines through transfection using lipofectamine 3000 (Invitrogen, US) in Opti-MEM media (Sigma Aldrich) with pcDNA3.1 SNAP-CXCR2-LgBit, and pcDNA3.1zeo-β-arrestin2-SmBit (human, GenBank NC_000017.1, as previously described[354]) for NanoBiT complementation or pcDNA3.1neo-SNAP-CXCR1/CXCR2-tsNanoLuc (HEK 293 SNAP-CXCR2-NanoLuc or SNAP-CXCR1-NanoLuc) for NanoBRET binding and imaging assays. Mixed population cell lines were selected through G418 (0.8 mg^{-1}) and Zeocine (200 $\mu g\ ml^{-1}$) resistance.

HEK 293 cells were maintained in Dulbecco's modified Eagle's medium (DMEM) supplemented with 10% foetal bovine serum (FBS; Sigma Aldrich) in a humidified incubator at 37 °C and 5% CO_2 in sterile polystyrene flasks of 25, 75 or 175 cm^2 growing surface (T25, T75 or T175). Cells passaging was done at 70-90% confluency with a split ratio between 1:2 and 1:30. The

media DMEM/10% FCS was aspirated and cells were washed with sterile phosphate buffer saline (PBS) which was then aspirated. Sterile trypsin solution (0.5 mL, 1 mL, 3 mL for T25, T75 and T175 respectively) was added to the flask and incubated at 37 °C for 5 minutes prior to gentle physical agitation by knocking on the flask side. Dissociated cells were then washed off the flask with addition of 5 mL or 10 mL DMEM/10%FCS and collected in 30 mL sterile universal tube, which was subsequently centrifuged (1000 g, 5 minutes) to remove trypsin and pellet cells. The obtained pellet was resuspended in 10 mL DMEM/10%FCS and cells were split according to the required ratio or a sample was counted for seeding plates.

For assays, cells were seeded 24 hours in advance. 96 well white clear-bottomed plates (655098, Greiner Bio-One) were coated with 50 µL poly-D-lysine and incubated for 30 minutes on the day of seeding to ensure cell adherence. Poly-D-lysine was then aspirated and wells were washed with 100 µL of DMEM/10%FCS. Cells were removed from the flask and pelleted with centrifugation described, resuspended in 10 mL DMEM/10%FCS and a cell resuspension sample was added to a haemocytometer for counting within the grid (0.1 mm^3). Cell count was multiplied by 10 000 to scale up to number of cells per mL. Cell density was 32,000 per well using 100 µL seeding volume. The following equation was used to determine volume of cell resuspension required for seeding solution:

$$Volume\ of\ Cell\ Suspension\ Required\ (mL) = \frac{Number\ of\ Cells\ Required\ (per\ mL) x\ Required\ Seeding\ Volume\ (mL)}{Number\ of\ Counted\ Cells\ (per\ mL)}$$

The volume of cell resuspension required was then diluted up to seeding solution volume with DMEM/10%FCS and seeded into poly-D-lysine coated plates using an Eppendorf Multipipette Combitip dispenser.

For NanoBRET binding assays using membranes, cells were allowed to grow to 90% confluency in T175cm^2 flasks prior to membrane preparation. Cells were washed twice with phosphate-buffered saline (PBS, Sigma-Aldrich, Pool, UK) to remove growth medium and removed from the flask by scraping in 10 ml PBS. Cells were pelleted by centrifugation (10 min, 2000rpm) prior

to freezing at -80°C. For membrane homogenization (all steps at 4°C), 20 ml wash buffer (10mM HEPES, 10mM EDTA, pH: 7.4) was added to the pellet before disruption (8 bursts) with an Ultra-Turrax homogenizer (Ika-Werk GmbH & Co. KG, Staufen, Germany), and centrifugation at 48 000*g* at 4 °C using a Beckman Avanti J-251 Ultracentrifuge and JA-25.50 Fixed-Angle Rotor (Beckman Coulter; CA, USA). Supernatant was removed and the pellet was resuspended in 20 ml wash buffer and centrifuged again as above. The final pellet was suspended in cold 10 mM HEPES with 0.1 mM EDTA (pH 7.4). Protein concentration was determined using the bicinchoninic acid assay kit (Sigma-Aldrich, Pool, UK) using bovine serum albumin (BSA) as protein standard, and aliquots were maintained at -80 °C until required.

8.2.2 NanoBiT complementation assays

Stable transfected HEK 293 cells co-expressing SNAP-CXCR2-LgBit and β-arrestin2-SmBit were seeded on white, clear bottom, poly-D-lysine coated 96-well plates (655098, Greiner Bio-One) at a density of 32,000 cells/well and allowed to grow overnight. NanoBit assay buffer consisted of Hepes balanced salt solution (147 mM NaCl, 24 mM KCl, 1.3 mM $CaCl_2$, 1 mM $MgSO_4$, 1 mM Na pyruvate, 1 mM $NaHCO_3$, 10 mM HEPES, pH 7.4) with 0.1% BSA and 10 mM D-Glucose. Cells were washed with assay buffer to remove growth media prior to incubation with respective ligand concentrations (or *R*-navarixin (**2**) control) for one hour. Chosen ligands were first diluted in DMSO to 10 mM and stored at -20°C prior to use. Ligands were diluted in assay buffer to required concentrations (final assay concentration range: 10 μM - 0.1 nM) prior to addition to assay plate. Post incubation furimazine substrate (1/660 dilution in assay buffer from supplier stocks) was added to cells and allowed to equilibrate for five minutes at 37°C. Upon equilibration initial baseline luminescence readings were taken prior to the addition of CXCL8 (aa28-99), either as a single 10 nM concentration or across a range of concentrations (Stratech Scientific, Ely, UK). Luminescence readings were continually monitored over a 60-minute timecourse every 15 minutes at 37°C post agonist addition using a BMG PHERAstar FS (BMG Labtech). Ligand IC_{50} values were obtained using a four-parameter logistic

equation (Response = Control Response · ($IC50^n$/ ($IC50^n$+[Inhibitor]^n) and run including experimental replicates in duplicate. Subsequent data was normalized, presenting data as percentages of the 10 nM CXCL8 response (100%) and vehicle control (0%). IC_{50} values were then subsequently converted to pIC_{50} values via pIC_{50}= $-Log_{10}(IC_{50})$, pooled, and expressed as mean ± standard error margin (SEM). All binding and functional data were analyzed using PRISM 9.0 (GraphPad Software, San Diego).

8.2.3 NanoBRET fluorescent ligand binding assays in membranes and kinetics

NanoBRET endpoint binding assays were carried out in OptiPlate-384 white well microplates (product number: 6007290, PerkinElmer LAS Ltd, UK) and used 25mM HEPES, 1% DMSO, 0.1mg/ml Saponin, 0.02 % Pluronic acid F_{127}, 1mM $MgCl_2$ and 0.1% BSA (pH 7.4). Both saturation and competition assays employed 1μg/well HEK 293 SNAP-CXCR2-NanoLuc or SNAP-CXCR1-NanoLuc cell membranes for characterization of fluorescent ligand binding and employed 100 nM or 10μM *R*-navarixin (**2**) to define non-specific binding (NSB). For saturation binding experiments, used to determine fluorescent ligand affinity, membranes were incubated with increasing concentrations of fluorescent ligand (8 - 1000 nM dilution range in assay buffer) in assays buffer with or without unlabelled *R*-navarixin (**2**) to define NSB, in the additional presence or absence of 10 nM $CXCL8_{28-99}$ (Final assay volume, 40 μL). Membranes were incubated with furimazine at a 1/660 dilution for five minutes prior to addition to assay plate, allowing for equilibration of luminescence output. NanoBRET was monitored every 15 seconds for 60 minutes at 37°C measuring Nanoluciferase output (450nm) and BODIPY 630-650 output (630nm), generating a BRET ratio (630nm/450nm), using a BMG PHERAstar FS (BMG Labtech). Collected data was converted to Specific binding measurements through subtraction of NSB BRET ratios from the total binding data, and analyzed by endpoint

saturation analysis, allowing determination of ligand dissociation constant (K_D) assuming a one site model through:

$$Specific\ binding = Bmax.\frac{[Tracer]}{[Tracer] + K_D}$$

Additionally, specific binding association time-course traces for **62a** (defined as total binding – NSB) were fitted to a one site association model. Global fitting of this model across multiple fluorescent ligand concentrations from the same experiment enabled estimation of ligand association (k_{on}) and dissociation rate constants (k_{off}), together with the kinetically derived K_D (=k_{off}/k_{on}) using the equations:

$$Bound = B_{plateau}.(1 - e^{-k_{obs}.t})$$

Where, the $B_{plateau}$ is the equilibrium level of tracer binding, and the observed association rate constant k_{obs} is related to the binding rate constants for tracer in a single site model by:

$$k_{obs} = [Fl - ligand].k_{on} + k_{off}$$

For competition binding assays, HEK 293 SNAP-CXCR1/CXCR2-tsNanoLuc cell membranes were incubated with 100 nM fluorescent ligand (approximately K_D concentration), ranging concentrations of unlabeled ligands or NSB/vehicle controls, and 1/660 furimazine (final assay volume, 30 μL). Membranes were added to assay plate, post five-minute incubation with furimazine, by online injection using the BMG PHERAstar FS injector. NanoBRET measurements were taken over three hours at 37°C for endpoint assays.

For competition kinetic analysis, Hank's balanced salt solution (136 mM NaCl, 5.1 mM KCl, 0.44 mM KH2PO4, 4.17 mM NaHCO3, 0.34 mM Na2HPO4, 1% DMSO, 0.1mg/mL Saponin, 0.02% Pluronic acid F127, 0.1% bovine serum albumin (BSA) and 20mM HEPES, pH 7.4, supplemented with 100μM Gpp(NH)p) was employed as assay buffer and measurements were taken every 0.93 minutes over a 2-hour time period. Data was normalized

using NSB to define 0% and vehicle controls to define 100% binding and was fit to a three-parameter logistic equation, assuming unit Hill slope to determine unlabeled ligand IC_{50} estimates using:

$$Specific\ Binding = Basal + Total\ Specific\ Binding.\frac{IC_{50}}{[Ligand] + IC_{50}}$$

IC_{50} values were further converted to competing ligand dissociation constants (K_i) values using the Cheng-Prusoff correction:

$$K_i = \frac{IC_{50}}{1 + \frac{[FL]}{K_{FL}}}$$

Where K_{FL} and [FL] represent the fluorescent ligand dissociation constant and concentration respectively.

Competition kinetic data were fitted to a competition kinetic model describing the binding of tracer as a function of time (first derived by Motulsky and Mahan in 1984). This model generates competition association curves to multiple unlabelled compounds with varied association and dissociation rate constants according to:

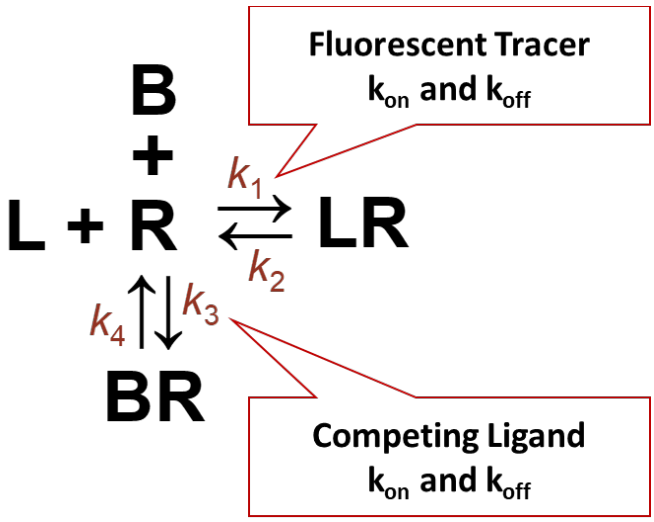

Where L = fluorescente probe, B = competing ligand, R = receptor.

$$K_A = k_1[L] + k_2$$

$$K_B = k_3[I] + k_4$$

$$S = \sqrt{((K_A - K_B)^2 + 4 \cdot k_1 \cdot k_3 \cdot [L] \cdot [I] \cdot 10^{-18})}$$

$$K_F = 0.5 \cdot (K_A + K_B + S)$$

$$K_s = 0.5 \cdot (K_A + K_B - S)$$

$$DIFF = K_F - K_S$$

$$Q = \frac{B_{max} \cdot K_1 \cdot [L] \cdot 10^{-9}}{DIFF}$$

$$Y = Q \cdot \left(\frac{k_4 \cdot DIFF}{K_F \cdot K_s} + \frac{k_4 - F_F}{K_F} \cdot \exp^{(-K_F \cdot X)} - \frac{k_4 - K_s}{K_s} \cdot \exp^{(-K_s \cdot X)}\right)$$

where X = time (minutes), Y = Specific binding, k_1 = k_{on} tracer (molar^{-1} minute^{-1}) , k_2 = k_{off} tracer (minute^{-1}), [L] = tracer ligand concentration (nM) and [I] = unlabelled ligand concentration (nM).

Association kinetics experiments for the tracer were performed on the same day, which derived probe k_{on} and k_{off} separately. These values were then fixed (I.e. k_1, k_2) when globally fitting the Motulsky Mahan model to sets of competition association curves for each unlabelled ligand in Graphpad Prism. This allowed derivation of unlabelled ligand association (k_3) and dissociation (k_4) rate constants.

8.2.4 NanoBRET fluorescent ligand binding assays in whole cells

Cellular based binding assays were carried out in white, clear bottom, 96-well Greiner plates (655098, Greiner Bio-One, Stonehouse, UK). HEK 293 SNAP-CXCR2-NanoLuc cells were seeded at 32,000 cells/well and assay buffer was Hepes balanced salt solution (147 mM NaCl, 5 mM KCl, 1.3 mM $CaCl_2$, 1 mM $MgSO_4$, 1 mM Na pyruvate, 1 mM $NaHCO_3$, 10 mM HEPES, pH 7.4) with 0.1% BSA and 10mM D-Glucose. Growth medium was removed 24 hours after seeding and cells were washed with assay buffer prior to the addition of 20 µl assay buffer per well. Where appropriate, 10 µL vehicle or 10 µM (*R*)-navarixin (**2**) (in assay buffer) was added to wells,

defining total and NSB, and cells were incubated for 30 minutes at 37°C to ensure sufficient binding of the NSB ligand. Chosen fluorescent ligands were diluted in assay buffer to required concentrations (78 nM - 10 μM) and 10 μL added to the assay plate post 30-minute incubation. The plate was then incubated at 37°C for one hour before addition of 1/240 furimazine solution (10 μL per well). Luciferase substrate was allowed to equilibrate for five minutes before measurement of NanoBRET signal using BMG PHERAstar (as per previously described membrane binding assays) with measurements taken every hour over a three-hour period. Fluorescent ligand affinity was derived using saturation analysis as previously described for membrane binding experiments.

8.2.5 Direct imaging of fluorescent ligand binding in the HEK 293 SNAP-CXCR2-tsNanoLuc cell line

HEK 293 cells expressing SNAP-CXCR2-tsNanoLuc were seeded on black, clear bottom, poly-D-lysine coated 96-well plates (Greiner 655097) at a density of 30,000 cells/well and allowed to grow overnight. Post incubation, growth media was replaced with Hepes balances salt solution supplemented with 0.1% BSA (HBSS + 0.1% BSA), 0.1μM SNAP-surface AF488, 2 μg/mL Hoechst 33342 nuclear stain (H33342) and either HBSS + 0.1% BSA or 10 μM (*R*)-navarixin (**2**). The assay plate was incubated for 30 minutes at 37°C prior to addition of 1μM compound **62a** to each well and allowed to equilibrate for 10 minutes before imaging. The maximal concentration of **62a** was employed and equilibration time was chosen from kinetics data in membranes showing equilibrium is reached after 10 minutes. A Zeiss Celldiscoverer 7 microscope was employed to image cells, imaging one site per well using a 20x/0.95 objective and corresponding laser excitatory wavelengths (SNAP-surface AF488: 493nm, BODIPY-630/650: 646nm, H33342: 348nm).

8.3 Molecular Modelling

The Basic Local Alignment Search Tool (BLAST) search was performed with the tool present in the Protein Data Bank (PDB) website. The crystal structures used were retrieved from the Protein Data Bank. Homology models were built using SWISS MODEL and Prime (Schrödinger software suite release 2023-1, Schrödinger, LLC, New York, NY, 2021) and refined using Maestro (Schrödinger software suite release 2020-3 and 2023-1) and the Prime loop refinement module. Docking was carried out using tools from Schrödinger software suite release 2023-1. The structures of the ligands were imported in Maestro in a MOL file format generated from ChemDraw (PerkinElmer Informatics release 19.1) and prepared with LigPrep retaining their specific chirality. The generated homology models and crystal structures were imported and prepared with Maestro's protein preparation wizard, including water removal, H-bonding optimization using PROPKA at pH = 7 and energy minimization using OPLS3 force field. Grids were produced using Glide selecting Ala249$^{6.33}$ or Glu249$^{6.33}$ and Lys320$^{8.49}$ as the centroid of the grid and Lys320$^{8.49}$ hydrogen bonding as a constraint. The docking was performed both without constraints and with the selected constraint. For each ligand 100 poses were minimized post docking and a maximum of 20 poses per output. Default settings were used unless otherwise stated. For all the ligands the highest docking scoring pose was selected. Images were generated using PyMol (The PyMOL Molecular Graphics System, Version 2.0 Schrödinger, LLC). Molecular dynamics simulations were performed using AMBER 20.[355] Molecular models for **56a** and **56b** were built and parameterized using antechamber (gaff2 forcefield) and immersed in a c 43Å^3 box of DMSO.[356] After energy minimization, molecular dynamics simulations were run for a total of 10.3 nanoseconds in the NPT ensemble (Langevin dynamics with a collision frequency of 5 ps-1, temperature regulated to 300K, pressure regulated with a Berendsen barostat, relaxation time 2ps, SHAKE applied to all bonds, long range electrostatic interactions evaluated using the PME method with a real-space cutoff of 8Å). Discarding the first 300ps as equilibration, analysis of the torsion angle and H-bonding data confirmed the simulations were well converged. Simulation analysis was

performed in Jupyter notebooks using tools from the MDTraj Python packagem.[357]

References

(1) Murdoch, C.; Finn, A. Chemokine Receptors and Their Role in Inflammation and Infectious Diseases. *Blood* **2000**, *95* (10), 3032–3043.

(2) Allen, S. J.; Crown, S. E.; Handel, T. M. Chemokine:Receptor Structure, Interactions, and Antagonism. *Annu. Rev. Immunol.* **2007**, *25* (1), 787–820.

(3) Uguccioni, M.; D'Apuzzo, M.; Loetscher, M.; Dewald, B.; Baggiolini, M. Actions of the Chemotactic Cytokines MCP-1, MCP-2, MCP-3, RANTES, MIP-1α and MIP-1β on Human Monocytes. *Eur. J. Immunol.* **1995**, *25* (1), 64–68.

(4) Szekanecz, Z.; Vegvari, A.; Szabo, Z.; Koch, A. E. Chemokines and Chemokine Receptors in Arthritis. *Front. Biosci. - Sch.* **2010**, *2 S* (1), 153–167.

(5) Mantovani, A. The Chemokine System: Redundancy for Robust Outputs. *Immunol. Today* **1999**, *20* (6), 254–257.

(6) Hughes, C. E.; Nibbs, R. J. B. A Guide to Chemokines and Their Receptors. *FEBS J.* **2018**, *285* (16), 2944–2971.

(7) Zlotnik, A.; Yoshie, O.; Nomiyama, H. The Chemokine and Chemokine Receptor Superfamilies and Their Molecular Evolution. *Genome Biol.* **2006**, *7* (12).

(8) Stadtmann, A.; Zarbock, A. CXCR2: From Bench to Bedside. *Front. Immunol.* **2012**, *3*, 263.

(9) Chapman, R. W.; Phillips, J. E.; Hipkin, R. W.; Curran, A. K.; Lundell, D.; Fine, J. S. CXCR2 Antagonists for the Treatment of Pulmonary Disease. *Pharmacol. Ther.* **2009**, *121* (1), 55–68.

(10) Sriram, K.; Insel, P. A. G Protein-Coupled Receptors as Targets for Approved Drugs: How Many Targets and How Many Drugs? *Mol. Pharmacol.* **2018**, *93* (4), 251–258.

(11) Alexander, S. P.; Christopoulos, A.; Davenport, A. P.; Kelly, E.; Mathie, A.; Peters, J. A.; Veale, E. L.; Armstrong, J. F.; Faccenda, E.; Harding, S. D.; Pawson, A. J.; Southan, C.; Davies, J. A.; Abbracchio, M. P.; Alexander, W.; Al-Hosaini, K.; Bäck, M.; Barnes, N. M.; Bathgate, R.; Beaulieu, J.-M.; Bernstein, K. E.; Bettler, B.; Birdsall, N. J. M.; Blaho, V.; Boulay, F.; Bousquet, C.; Bräuner-Osborne, H.; Burnstock, G.; Caló, G.; Castaño, J. P.; Catt, K. J.; Ceruti, S.; Chazot, P.; Chiang, N.; Chini, B.; Chun, J.; Cianciulli, A.; Civelli, O.; Clapp, L. H.; Couture, R.; Csaba, Z.; Dahlgren, C.; Dent, G.; Singh, K. D.; Douglas, S. D.; Dournaud, P.; Eguchi, S.; Escher, E.; Filardo, E. J.; Fong, T.; Fumagalli, M.; Gainetdinov, R. R.; Gasparo, M. de; Gerard, C.; Gershengorn, M.; Gobeil, F.; Goodfriend, T. L.; Goudet, C.; Gregory, K. J.; Gundlach, A. L.; Hamann, J.; Hanson, J.; Hauger, R. L.; Hay, D. L.; Heinemann, A.; Hollenberg, M. D.; Holliday, N. D.; Horiuchi, M.; Hoyer, D.; Hunyady, L.; Husain, A.; IJzerman, A. P.; Inagami, T.; Jacobson, K. A.; Jensen, R. T.; Jockers, R.; Jonnalagadda, D.; Karnik, S.; Kaupmann, K.; Kemp, J.; Kennedy, C.; Kihara, Y.; Kitazawa, T.; Kozielewicz, P.; Kreienkamp, H.-J.; Kukkonen, J. P.; Langenhan, T.; Leach, K.; Lecca, D.; Lee, J. D.; Leeman, S. E.; Leprince, J.; Li, X. X.; Williams, T. L.; Lolait, S. J.; Lupp, A.; Macrae, R.; Maguire, J.; Mazella, J.; McArdle, C. A.; Melmed, S.; Michel, M. C.; Miller, L. J.; Mitolo, V.; Mouillac, B.; Müller, C. E.; Murphy, P.; Nahon, J.-L.; Ngo, T.; Norel, X.; Nyimanu, D.; O'Carroll, A.-M.; Offermanns, S.; Panaro, M. A.; Parmentier, M.; Pertwee, R. G.; Pin, J.-P.; Prossnitz, E. R.; Quinn, M.; Ramachandran, R.; Ray, M.; Reinscheid, R. K.; Rondard, P.; Rovati, G. E.; Ruzza, C.; Sanger, G. J.; Schöneberg, T.; Schulte, G.; Schulz, S.; Segaloff, D. L.; Serhan, C. N.; Stoddart, L. A.; Sugimoto, Y.; Summers, R.; Tan, V. P.;

Thal, D.; Thomas, W. W.; Timmermans, P. B. M. W. M.; Tirupula, K.; Tulipano, G.; Unal, H.; Unger, T.; Valant, C.; Vanderheyden, P.; Vaudry, D.; Vaudry, H.; Vilardaga, J.-P.; Walker, C. S.; Wang, J. M.; Ward, D. T.; Wester, H.-J.; Willars, G. B.; Woodruff, T. M.; Yao, C.; Ye, R. D. THE CONCISE GUIDE TO PHARMACOLOGY 2021/22: G Protein-Coupled Receptors. *Br. J. Pharmacol.* **2021**, *178 Suppl*, S27–S156.

(12) Lagerström, M. C.; Schiöth, H. B. Structural Diversity of G Protein-Coupled Receptors and Significance for Drug Discovery. *Nat. Rev. Drug Discov.* **2008**, *7* (4), 339–357.

(13) Weis, W. I.; Kobilka, B. K. The Molecular Basis of G Protein–Coupled Receptor Activation. *Annu. Rev. Biochem.* **2018**, *87* (1), 897–919.

(14) Legler, D. F.; Thelen, M. New Insights in Chemokine Signaling. *F1000Research* **2018**, *7* (0), 1–8.

(15) Hilger, D.; Masureel, M.; Kobilka, B. K. Structure and Dynamics of GPCR Signaling Complexes. *Nat. Struct. Mol. Biol.* **2018**, *25* (1), 4–12.

(16) Sunahara, R. K.; Dessauer, C. W.; Gilman, A. G. Complexity and Diversity of Mammalian Adenylyl Cyclases. *Annu. Rev. Pharmacol. Toxicol.* **1996**, *36*, 461–480.

(17) Knall, C.; Young, S.; Nick, J. A.; Buhl, A. M.; Worthen, G. S.; Johnson, G. L. Interleukin-8 Regulation of the Ras/Raf/Mitogen-Activated Protein Kinase Pathway in Human Neutrophils. *J. Biol. Chem.* **1996**, *271* (5).

(18) Knall, C.; Worthen, G. S.; Johnson, G. L. Interleukin 8-Stimulated Phosphatidylinositol-3-Kinase Activity Regulates the Migration of Human Neutrophils Independent of Extracellular Signal-Regulated Kinase and P38 Mitogen-Activated Protein Kinases. *Proc. Natl. Acad. Sci. U. S. A.* **1997**, *94* (7).

(19) Vroon, A.; Heijnen, C. J.; Kavelaars, A. GRKs and Arrestins: Regulators of Migration and Inflammation. *J. Leukoc. Biol.* **2006**, *80* (6), 1214–1221.

(20) Wootten, D.; Christopoulos, A.; Marti-Solano, M.; Babu, M. M.; Sexton, P. M. Mechanisms of Signalling and Biased Agonism in G Protein-Coupled Receptors. *Nat. Rev. Mol. Cell Biol.* **2018**, *19* (10), 638–653.

(21) Gurevich, V. V; Gurevich, E. V. GPCR Signaling Regulation: The Role of GRKs and Arrestins. *Front. Pharmacol.* **2019**, *10*, 125.

(22) Williams, J. T.; Ingram, S. L.; Henderson, G.; Chavkin, C.; von Zastrow, M.; Schulz, S.; Koch, T.; Evans, C. J.; Christie, M. J. Regulation of μ-Opioid Receptors: Desensitization, Phosphorylation, Internalization, and Tolerance. *Pharmacol. Rev.* **2013**, *65* (1), 223–254.

(23) Hanson, S. M.; Francis, D. J.; Vishnivetskiy, S. A.; Kolobova, E. A.; Hubbell, W. L.; Klug, C. S.; Gurevich, V. V. Differential Interaction of Spin-Labeled Arrestin with Inactive and Active Phosphorhodopsin. *Proc. Natl. Acad. Sci. U. S. A.* **2006**, *103* (13), 4900–4905.

(24) Peterson, Y. K.; Luttrell, L. M. The Diverse Roles of Arrestin Scaffolds in g Protein–Coupled Receptor Signaling. *Pharmacol. Rev.* **2017**, *69* (3).

(25) Smith, J. S.; Rajagopal, S. The β-Arrestins: Multifunctional Regulators of G Protein-Coupled Receptors. *J. Biol. Chem.* **2016**, *291* (17).

(26) Colquhoun, D. Affinity, Efficacy and Receptor Classification.: Is the Classical Theory Still Useful? *Perspect. Recept. Classif.* **1987**, 103–114.

(27) STEPHENSON, R. P. A Modification of Receptor Theory. *Br. J. Pharmacol. Chemother.* **1956**, *11* (4).

(28) Hill, A. V. The Possible Effects of the Aggregation of the Molecules of Haemoglobin on Its Dissociation Curves. *Proceedings of the Physiological Society*. 1910.

(29) Gesztelyi, R.; Zsuga, J.; Kemeny-Beke, A.; Varga, B.; Juhasz, B.; Tosaki, A. The Hill Equation and the Origin of Quantitative Pharmacology. *Archive for History of Exact Sciences*. 2012.

(30) Vauquelin, G.; Charlton, S. J. Long-Lasting Target Binding and Rebinding as Mechanisms to Prolong in Vivo Drug Action. *Br. J. Pharmacol.* **2010**, *161* (3), 488–508.

(31) Sykes, D. A.; Bradley, M. E.; Riddy, D. M.; Willard, E.; Reilly, J.; Miah, A.; Bauer, C.; Watson, S. J.; Sandham, D. A.; Dubois, G.; Charlton, S. J. Fevipiprant (QAW039), a Slowly Dissociating CRTh2 Antagonist with the Potential for Improved Clinical Efficacy. *Mol. Pharmacol.* **2016**, *89* (5).

(32) Stott, L. A.; Hall, D. A.; Holliday, N. D. Unravelling Intrinsic Efficacy and Ligand Bias at G Protein Coupled Receptors: A Practical Guide to Assessing Functional Data. *Biochemical Pharmacology*. 2016.

(33) Norris, D. O.; Carr, J. A. Synthesis, Metabolism, and Actions of Bioregulators. In *Vertebrate Endocrinology*; 2013.

(34) DEL CASTILLO, J.; KATZ, B. Interaction at End-Plate Receptors between Different Choline Derivatives. *Proc. R. Soc. Lond. B. Biol. Sci.* **1957**, *146* (924).

(35) Buchwald, P. A Receptor Model With Binding Affinity, Activation Efficacy, and Signal Amplification Parameters for Complex Fractional Response Versus Occupancy Data. *Front. Pharmacol.* **2019**, *10*, 605.

(36) De Lean, A.; Stadel, J. M.; Lefkowitz, R. J. A Ternary Complex Model Explains the Agonist-Specific Binding Properties of the Adenylate Cyclase-Coupled β-Adrenergic Receptor. *J. Biol. Chem.* **1980**, *255* (15), 7108–7117.

(37) Costa, T.; Herz, A. Antagonists with Negative Intrinsic Activity at Delta Opioid Receptors Coupled to GTP-Binding Proteins. *Proc. Natl. Acad. Sci. U. S. A.* **1989**, *86* (19), 7321–7325.

(38) Samama, P.; Cotecchia, S.; Costa, T.; Lefkowitz, R. J. A Mutation-Induced Activated State of the Beta 2-Adrenergic Receptor. Extending the Ternary Complex Model. *J. Biol. Chem.* **1993**, *268* (7), 4625–4636.

(39) Weiss, J. M.; Morgan, P. H.; Lutz, M. W.; Kenakin, T. P. The Cubic Ternary Complex Receptor-Occupancy Model I. Model Description. *J. Theor. Biol.* **1996**, *178* (2).

(40) Kenakin, T.; Morgan, P.; Lutz, M.; Weiss, J. The Evolution of Drug-Receptor Models: The Cubic Ternary Complex Model for G Protein-Coupled Receptors; 2000.

(41) Gonsiorek, W.; Fan, X.; Hesk, D.; Fossetta, J.; Qiu, H.; Jakway, J.; Billah, M.; Dwyer, M.; Chao, J.; Deno, G.; Taveras, A.; Lundell, D. J.; Hipkin, R. W. Pharmacological Characterization of Sch527123, a Potent Allosteric CXCR1/CXCR2 Antagonist. *J. Pharmacol. Exp. Ther.* **2007**, *322* (2), 477–485.

(42) Nicholls, D. J.; Tomkinson, N. P.; Wiley, K. E.; Brammall, A.; Bowers, L.; Grahames, C.; Gaw, A.; Meghani, P.; Shelton, P.; Wright, T. J.; Mallinder, P. R. Identification of a Putative Intracellular Allosteric Antagonist Binding-Site in the CXC Chemokine Receptors 1 and 2. *Mol. Pharmacol.* **2008**, *74* (5), 1193–1202.

(43) Scholten, D. J.; Canals, M.; Maussang, D.; Roumen, L.; Smit, M. J.; Wijtmans, M.; De Graaf, C.; Vischer, H. F.; Leurs, R. Pharmacological Modulation of Chemokine Receptor Function. *Br. J. Pharmacol.* **2012**, *165* (6), 1617–1643.

(44) Wu, L.; Ruffing, N.; Shi, X.; Newman, W.; Soler, D.; Mackay, C. R.; Qin, S. Discrete Steps in Binding and Signaling of Interleukin-8 with Its Receptor. *J. Biol. Chem.* **1996**, *271* (49),

31202–31209.

(45) Liu, K.; Wu, L.; Yuan, S.; Wu, M.; Xu, Y.; Sun, Q.; Li, S.; Zhao, S.; Hua, T.; Liu, Z. J. Structural Basis of CXC Chemokine Receptor 2 Activation and Signalling. *Nature* **2020**, *585* (7823), 135–140.

(46) Prado, G. N.; Suetomi, K.; Shumate, D.; Maxwell, C.; Ravindran, A.; Rajarathnam, K.; Navarro, J. Chemokine Signaling Specificity: Essential Role for the N-Terminal Domain of Chemokine Receptor. *Biochemistry* **2007**, *46* (31).

(47) Joseph, P. R. B.; Sawant, K. V.; Isley, A.; Pedroza, M.; Garofalo, R. P.; Richardson, R. M.; Rajarathnam, K. Dynamic Conformational Switching in the Chemokine Ligand Is Essential for G-Protein-Coupled Receptor Activation. *Biochem. J.* **2013**, *456* (2).

(48) Ballesteros, J. A.; Weinstein, H. Integrated Methods for the Construction of Three-Dimensional Models and Computational Probing of Structure-Function Relations in G Protein-Coupled Receptors. *Methods Neurosci.* **1995**, *25* (C).

(49) von Vietinghoff, S.; Asagiri, M.; Azar, D.; Hoffmann, A.; Ley, K. Defective Regulation of CXCR2 Facilitates Neutrophil Release from Bone Marrow Causing Spontaneous Inflammation in Severely NF-KB–Deficient Mice. *J. Immunol.* **2010**, *185* (1), 670–678.

(50) Seitz, M.; Dewald, B.; Gerber, N.; Baggiolini, M. Enhanced Production of Neutrophil-Activating Peptide-1/Interleukin-8 in Rheumatoid Arthritis. *J. Clin. Invest.* **1991**, *87* (2), 463–469.

(51) Cheng, Y.; Ma, X. lei; Wei, Y. quan; Wei, X. W. Potential Roles and Targeted Therapy of the CXCLs/CXCR2 Axis in Cancer and Inflammatory Diseases. *Biochim. Biophys. Acta - Rev. Cancer* **2019**, *1871* (2), 289–312.

(52) Addison, C. L.; Daniel, T. O.; Burdick, M. D.; Liu, H.; Ehlert, J.

E.; Xue, Y. Y.; Buechi, L.; Walz, A.; Richmond, A.; Strieter, R. M. The CXC Chemokine Receptor 2, CXCR2, Is the Putative Receptor for ELR + CXC Chemokine-Induced Angiogenic Activity . *J. Immunol.* **2000**, *165* (9), 5269–5277.

(53) Keane, M. P.; Donnelly, S. C.; Belperio, J. A.; Goodman, R. B.; Dy, M.; Burdick, M. D.; Fishbein, M. C.; Strieter, R. M. Imbalance in the Expression of CXC Chemokines Correlates with Bronchoalveolar Lavage Fluid Angiogenic Activity and Procollagen Levels in Acute Respiratory Distress Syndrome. *J. Immunol.* **2002**, *169* (11), 6515–6521.

(54) Rabe, K. F.; Hurd, S.; Anzueto, A.; Barnes, P. J.; Buist, S. A.; Calverley, P.; Fukuchi, Y.; Jenkins, C.; Rodriguez-Roisin, R.; Van Weel, C.; Zielinski, J. Global Strategy for the Diagnosis, Management, and Prevention of Chronic Obstructive Pulmonary Disease: GOLD Executive Summary. *Am. J. Respir. Crit. Care Med.* **2007**, *176* (6), 532–555.

(55) Vlahos, R.; Bozinovski, S. Recent Advances in Pre-Clinical Mouse Models of COPD. *Clin. Sci. (Lond).* **2014**, *126* (4), 253–265.

(56) Petty, T. L. COPD in Perspective. *Chest* **2002**, *121* (5 Suppl), 116S-120S.

(57) Tiwari, N.; Marudamuthu, A. S.; Tsukasaki, Y.; Ikebe, M.; Fu, J.; Shetty, S. P53-and PAI-1-Mediated Induction of C-X-C Chemokines and CXCR2: Importance in Pulmonary Inflammation Due to Cigarette Smoke Exposure. *Am. J. Physiol. - Lung Cell. Mol. Physiol.* **2016**, *310* (6), L496–L506.

(58) De Kruijf, P.; Van Heteren, J.; Lim, H. D.; Conti, P. G. M.; Van Der Lee, M. M. C.; Bosch, L.; Ho, K. K.; Auld, D.; Ohlmeyer, M.; Smit, M. J.; Wijkmans, J. C. H. M.; Zaman, G. J. R.; Leurs, R. Nonpeptidergic Allosteric Antagonists Differentially Bind to the CXCR2 Chemokine Receptor. *J. Pharmacol. Exp. Ther.*

2009, *329* (2), 783–790.

(59) Mattos, M. S.; Ferrero, M. R.; Kraemer, L.; Lopes, G. A. O.; Reis, D. C.; Cassali, G. D.; Oliveira, F. M. S.; Brandolini, L.; Allegretti, M.; Garcia, C. C.; Martins, M. A.; Teixeira, M. M.; Russo, R. C. CXCR1 and CXCR2 Inhibition by Ladarixin Improves Neutrophil-Dependent Airway Inflammation in Mice. *Front. Immunol.* **2020**, *11*.

(60) Tuder, R. M.; Petrache, I. Pathogenesis of Chronic Obstructive Pulmonary Disease. *Journal of Clinical Investigation*. 2012.

(61) Barnes, P. J. Inflammatory Mechanisms in Patients with Chronic Obstructive Pulmonary Disease. *J. Allergy Clin. Immunol.* **2016**, *138* (1), 16–27.

(62) Qiu, Y.; Zhu, J.; Bandi, V.; Guntupalli, K. K.; Jeffery, P. K. Bronchial Mucosal Inflammation and Upregulation of CXC Chemoattractants and Receptors in Severe Exacerbations of Asthma. *Thorax* **2007**, *62* (6), 475–482.

(63) Qiu, Y.; Zhu, J.; Bandi, V.; Atmar, R. L.; Hattotuwa, K.; Guntupalli, K. K.; Jeffery, P. K. Biopsy Neutrophilia, Neutrophil Chemokine and Receptor Gene Expression in Severe Exacerbations of Chronic Obstructive Pulmonary Disease. *Am. J. Respir. Crit. Care Med.* **2003**, *168* (8), 968–975.

(64) Jeffery, P. K. Comparison of the Structural and Inflammatory Features of COPD and Asthma: Giles F. Filley Lecture. In *Chest*; 2000; Vol. 117.

(65) Traves, S. L.; Smith, S. J.; Barnes, P. J.; Donnelly, L. E. Specific CXC but Not CC Chemokines Cause Elevated Monocyte Migration in COPD: A Role for CXCR2. *J. Leukoc. Biol.* **2004**, *76* (2), 441–450.

(66) Di Stefano, A.; Capelli, A.; Donner, C. F. Role of Interleukin-8 in the Pathogenesis and Treatment of COPD. *Chest* **2004**, *126* (3), 676–678.

(67) Rennard, S. I.; Dale, D. C.; Donohue, J. F.; Kanniess, F.; Magnussen, H.; Sutherland, E. R.; Watz, H.; Lu, S.; Stryszak, P.; Rosenberg, E.; Staudinger, H. CXCR2 Antagonist MK-7123 a Phase 2 Proof-of-Concept Trial for Chronic Obstructive Pulmonary Disease. *Am. J. Respir. Crit. Care Med.* **2015**, *191* (9).

(68) Donnelly, L. E.; Barnes, P. J. Chemokine Receptors as Therapeutic Targets in Chronic Obstructive Pulmonary Disease. *Trends in Pharmacological Sciences*. 2006.

(69) Leaker, B. R.; Barnes, P. J.; O'Connor, B. Inhibition of LPS-Induced Airway Neutrophilic Inflammation in Healthy Volunteers with an Oral CXCR2 Antagonist. *Respir. Res.* **2013**, *14* (1), 137.

(70) Planagumà, A.; Domènech, T.; Pont, M.; Calama, E.; García-González, V.; López, R.; Aulí, M.; López, M.; Fonquerna, S.; Ramos, I.; de Alba, J.; Nueda, A.; Prats, N.; Segarra, V.; Miralpeix, M.; Lehner, M. D. Combined Anti CXC Receptors 1 and 2 Therapy Is a Promising Anti-Inflammatory Treatment for Respiratory Diseases by Reducing Neutrophil Migration and Activation. *Pulm. Pharmacol. Ther.* **2015**, *34*.

(71) Lazaar, A. L.; Miller, B. E.; Tabberer, M.; Yonchuk, J.; Leidy, N.; Ambery, C.; Bloomer, J.; Watz, H.; Tal-Singer, R. Effect of the CXCR2 Antagonist Danirixin on Symptoms and Health Status in COPD. *European Respiratory Journal*. 2018.

(72) Henrot, P.; Prevel, R.; Berger, P.; Dupin, I. Chemokines in COPD: From Implication to Therapeutic Use. *International Journal of Molecular Sciences*. 2019.

(73) Pedersen, F.; Waschki, B.; Marwitz, S.; Goldmann, T.; Kirsten, A.; Malmgren, A.; Rabe, K. F.; Uddin, M.; Watz, H. Neutrophil Extracellular Trap Formation Is Regulated by CXCR2 in COPD Neutrophils. *European Respiratory Journal*. 2018.

(74) Kirsten, A. M.; Förster, K.; Radeczky, E.; Linnhoff, A.; Balint, B.; Watz, H.; Wray, H.; Salkeld, L.; Cullberg, M.; Larsson, B. The Safety and Tolerability of Oral AZD5069, a Selective CXCR2 Antagonist, in Patients with Moderate-to-Severe COPD. *Pulm. Pharmacol. Ther.* **2015**, *31*.

(75) JJ, O.; BE, C.; TC, C.; CH, F. Acute Asthma: The Basics of Assessment and Treatment. *J. Respir. Dis.* **2002**, *23* (3).

(76) Holgate, S. T.; Polosa, R. The Mechanisms, Diagnosis, and Management of Severe Asthma in Adults. *Lancet*. 2006.

(77) Chanez, P.; Wenzel, S. E.; Anderson, G. P.; Anto, J. M.; Bel, E. H.; Boulet, L. P.; Brightling, C. E.; Busse, W. W.; Castro, M.; Dahlen, B.; Dahlen, S. E.; Fabbri, L. M.; Holgate, S. T.; Humbert, M.; Gaga, M.; Joos, G. F.; Levy, B.; Rabe, K. F.; Sterk, P. J.; Wilson, S. J.; Vachier, I. Severe Asthma in Adults: What Are the Important Questions? *J. Allergy Clin. Immunol.* **2007**, *119* (6).

(78) Dockrell, M.; Partridge, M. R.; Valovirta, E. The Limitations of Severe Asthma: The Results of a European Survey. *Allergy Eur. J. Allergy Clin. Immunol.* **2007**, *62* (2).

(79) Mukaida, N. Pathophysiological Roles of Interleukin-8 / CXCL8 in Pulmonary Diseases. **2003**, 566–577.

(80) Yang, T.; Li, Y.; Lyu, Z.; Huang, K.; Corrigan, C. J.; Ying, S.; Wang, W.; Wang, C. Characteristics of Proinflammatory Cytokines and Chemokines in Airways of Asthmatics: Relationships with Disease Severity and Infiltration of Inflammatory Cells. *Chin. Med. J. (Engl).* **2017**, *130* (17).

(81) Schuh, J. M.; Blease, K.; Hogaboam, C. M. CXCR2 Is Necessary for the Development and Persistence of Chronic Fungal Asthma in Mice. *J. Immunol.* **2002**, *168* (3).

(82) Todd, C. M.; Salter, B. M.; Murphy, D. M.; Watson, R. M.; Howie, K. J.; Milot, J.; Sadeh, J.; Boulet, L. P.; O'Byrne, P. M.;

Gauvreau, G. M. The Effects of a CXCR1/CXCR2 Antagonist on Neutrophil Migration in Mild Atopic Asthmatic Subjects. *Pulm. Pharmacol. Ther.* **2016**, *41*.

(83) Watz, H.; Uddin, M.; Pedersen, F.; Kirsten, A.; Goldmann, T.; Stellmacher, F.; Groth, E.; Larsson, B.; Böttcher, G.; Malmgren, A.; Kraan, M.; Rabe, K. F. Effects of the CXCR2 Antagonist AZD5069 on Lung Neutrophil Recruitment in Asthma. *Pulmonary Pharmacology and Therapeutics*. 2017.

(84) Govindaraju, V.; Michoud, M. C.; Al-Chalabi, M.; Ferraro, P.; Powell, W. S.; Martin, J. G. Interleukin-8: Novel Roles in Human Airway Smooth Muscle Cell Contraction and Migration. *Am. J. Physiol. - Cell Physiol.* **2006**, *291* (5), 957–965.

(85) Taylor-Cousar, J. L.; von Kessel, K. A.; Young, R.; Nichols, D. P. Potential of Anti-Inflammatory Treatment for Cystic Fibrosis Lung Disease. *J. Inflamm. Res.* **2010**, *3* (1).

(86) Moss, R. B.; Mistry, S. J.; Konstan, M. W.; Pilewski, J. M.; Kerem, E.; Tal-Singer, R.; Lazaar, A. L. Safety and Early Treatment Effects of the CXCR2 Antagonist SB-656933 in Patients with Cystic Fibrosis. *J. Cyst. Fibros.* **2013**, *12* (3).

(87) Clunes, M. T.; Boucher, R. C. Cystic Fibrosis: The Mechanisms of Pathogenesis of an Inherited Lung Disorder. *Drug Discov. Today Dis. Mech.* **2007**, *4* (2), 63–72.

(88) Elizur, A.; Cannon, C. L.; Ferkol, T. W. Airway Inflammation in Cystic Fibrosis CHEST Translating Basic Research Into Clinical Practice Airway Inflammation in Cystic Fibrosis *. *Chest* **2008**, *133* (2), 489–495.

(89) Chmiel, J. F.; Konstan, M. W. Inflammation and Anti-Inflammatory Therapies for Cystic Fibrosis. *Clinics in Chest Medicine*. 2007.

(90) Konstan, M. W.; Byard, P. J.; Hoppel, C. L.; Davis, P. B. Effect of High-Dose Ibuprofen in Patients with Cystic Fibrosis. *N.*

Engl. J. Med. **1995**, *332* (13).

(91) Auerbach, H. S.; Kirkpatrick, J. A.; Williams, M.; Colten, H. R. ALTERNATE-DAY PREDNISONE REDUCES MORBIDITY AND IMPROVES PULMONARY FUNCTION IN CYSTIC FIBROSIS. *Lancet* **1985**, *326* (8457).

(92) Saiman, L.; Marshall, B. C.; Mayer-Hamblett, N.; Burns, J. L.; Quittner, A. L.; Cibene, D. A.; Coquillette, S.; Fieberg, A. Y.; Accurso, F. J.; Campbell, P. W. Azithromycin in Patients with Cystic Fibrosis Chronically Infected with Pseudomonas Aeruginosa: A Randomized Controlled Trial. *JAMA* **2003**, *290* (13).

(93) Steinkamp, G.; Schmitt-Grohe, S.; Döring, G.; Staab, D.; Pfründer, D.; Beck, G.; Schubert, R.; Zielen, S. Once-Weekly Azithromycin in Cystic Fibrosis with Chronic Pseudomonas Aeruginosa Infection. *Respir. Med.* **2008**, *102* (11).

(94) Sagel, S. D.; Chmiel, J. F.; Konstan, M. W. Sputum Biomarkers of Inflammation in Cystic Fibrosis Lung Disease. *Proc. Am. Thorac. Soc.* **2007**, *4* (4), 406–417.

(95) Mayer-Hamblett, N.; Aitken, M. L.; Accurso, F. J.; Kronmal, R. A.; Konstan, M. W.; Burns, J. L.; Sagel, S. D.; Ramsey, B. W. Association between Pulmonary Function and Sputum Biomarkers in Cystic Fibrosis. *Am. J. Respir. Crit. Care Med.* **2007**, *175* (8).

(96) Eickmeier, O.; Huebner, M.; Herrmann, E.; Zissler, U.; Rosewich, M.; Baer, P. C.; Buhl, R.; Schmitt-Grohé, S.; Zielen, S.; Schubert, R. Sputum Biomarker Profiles in Cystic Fibrosis (CF) and Chronic Obstructive Pulmonary Disease (COPD) and Association between Pulmonary Function. *Cytokine* **2010**, *50* (2).

(97) Kim, J. S.; Okamoto, K.; Rubin, B. K. Pulmonary Function Is Negatively Correlated with Sputum Inflammatory Markers and

Cough Clearability in Subjects with Cystic Fibrosis but Not Those with Chronic Bronchitis. *Chest* **2006**, *129* (5).

(98) Adib-Conquy, M.; Pedron, T.; Petit-Bertron, A. F.; Tabary, O.; Corvol, H.; Jacquot, J.; Clément, A.; Cavaillon, J. M. Neutrophils in Cystic Fibrosis Display a Distinct Gene Expression Pattern. *Mol. Med.* **2008**, *14* (1–2), 36–44.

(99) Hartl, D.; Latzin, P.; Hordijk, P.; Marcos, V.; Rudolph, C.; Woischnik, M.; Krauss-Etschmann, S.; Koller, B.; Reinhardt, D.; Roscher, A. A.; Roos, D.; Griese, M. Cleavage of CXCR1 on Neutrophils Disables Bacterial Killing in Cystic Fibrosis Lung Disease. *Nat. Med.* **2007**, *13* (12), 1423–1430.

(100) Uddin, M.; Betts, C.; Robinson, I.; Malmgren, A.; Humfrey, C. The Chemokine CXCR2 Antagonist (AZD5069) Preserves Neutrophil-Mediated Host Immunity in Non-Human Primates. *Haematologica*. 2017.

(101) Ferlay, J.; Soerjomataram, I.; Dikshit, R.; Eser, S.; Mathers, C.; Rebelo, M.; Parkin, D. M.; Forman, D.; Bray, F. Cancer Incidence and Mortality Worldwide: Sources, Methods and Major Patterns in GLOBOCAN 2012. *Int. J. Cancer* **2015**, *136* (5).

(102) Jaffer, T.; Ma, D. The Emerging Role of Chemokine Receptor CXCR2 in Cancer Progression. *Translational Cancer Research*. 2016.

(103) Bertram, J. S. The Molecular Biology of Cancer. *Molecular Aspects of Medicine*. 2000.

(104) Xiong, X.; Liao, X.; Qiu, S.; Xu, H.; Zhang, S.; Wang, S.; Ai, J.; Yang, L. CXCL8 in Tumor Biology and Its Implications for Clinical Translation. *Frontiers in Molecular Biosciences*. 2022.

(105) Ruffini, P. A. The CXCL8-CXCR1/2 Axis as a Therapeutic Target in Breast Cancer Stem-like Cells. *Frontiers in Oncology*. 2019.

(106) Arenberg, D. A.; Kunkel, S. L.; Polverini, P. J.; Glass, M.; Burdick, M. D.; Strieter, R. M. Inhibition of Interleukin-8 Reduces Tumorigenesis of Human Non-Small Cell Lung Cancer in SCID Mice. *J. Clin. Invest.* **1996**, *97* (12), 2792–2802.

(107) Luppi, F.; Longo, A. M.; de Boer, W. I.; Rabe, K. F.; Hiemstra, P. S. Interleukin-8 Stimulates Cell Proliferation in Non-Small Cell Lung Cancer through Epidermal Growth Factor Receptor Transactivation. *Lung Cancer* **2007**, *56* (1), 25–33.

(108) Matsuo, Y.; Ochi, N.; Sawai, H.; Yasuda, A.; Takahashi, H.; Funahashi, H.; Takeyama, H.; Tong, Z.; Guha, S. CXCL8/IL-8 and CXCL12/SDF-1alpha Co-Operatively Promote Invasiveness and Angiogenesis in Pancreatic Cancer. *Int. J. cancer* **2009**, *124* (4), 853–861.

(109) Liu, Q.; Li, A.; Tian, Y.; Wu, J. D.; Liu, Y.; Li, T.; Chen, Y.; Han, X.; Wu, K.; Carolina, S. The CXCL8-CXCR1/2 Pathways in Cancer. **2018**, 61–71.

(110) Gabellini, C.; Trisciuoglio, D.; Desideri, M.; Candiloro, A.; Ragazzoni, Y.; Orlandi, A.; Zupi, G.; Del Bufalo, D. Functional Activity of CXCL8 Receptors, CXCR1 and CXCR2, on Human Malignant Melanoma Progression. *Eur. J. Cancer* **2009**, *45* (14).

(111) Ohri, C. M.; Shikotra, A.; Green, R. H.; Waller, D. A.; Bradding, P. Chemokine Receptor Expression in Tumour Islets and Stroma in Non-Small Cell Lung Cancer. *BMC Cancer* **2010**, *10*.

(112) Saintigny, P.; Massarelli, E.; Lin, S.; Ahn, Y. H.; Chen, Y.; Goswami, S.; Erez, B.; O'Reilly, M. S.; Liu, D.; Lee, J. J.; Zhang, L.; Ping, Y.; Behrens, C.; Soto, L. M. S.; Heymach, J. V.; Kim, E. S.; Herbst, R. S.; Lippman, S. M.; Wistuba, I. I.; Hong, W. K.; Kurie, J. M.; Koo, J. S. CXCR2 Expression in Tumor Cells Is a Poor Prognostic Factor and Promotes Invasion

and Metastasis in Lung Adenocarcinoma. *Cancer Res.* **2013**, *73* (2).

(113) Singh, S.; Singh, A. P.; Sharma, B.; Owen, L. B.; Singh, R. K. CXCL8 and Its Cognate Receptors in Melanoma Progression and Metastasis. *Future Oncology*. 2010.

(114) Reiland, J.; Furcht, L. T.; McCarthy, J. B. CXC-Chemokines Stimulate Invasion and Chemotaxis in Prostate Carcinoma Cells through the CXCR2 Receptor. *Prostate* **1999**, *41* (2).

(115) Snoussi, K.; Mahfoudh, W.; Bouaouina, N.; Fekih, M.; Khairi, H.; Helal, A. N.; Chouchane, L. Combined Effects of IL-8 and CXCR2 Gene Polymorphisms on Breast Cancer Susceptibility and Aggressiveness. *BMC Cancer* **2010**, *10*.

(116) Nannuru, K.; Sharma, B.; Varney, M.; Singh, R. Role of Chemokine Receptor CXCR2 Expression in Mammary Tumor Growth, Angiogenesis and Metastasis. *J. Carcinog.* **2011**, *10*.

(117) Miller, L. J.; Kurtzman, S. H.; Wang, Y.; Anderson, K. H.; Lindquist, R. R.; Kreutzer, D. L. Expression of Interleukin-8 Receptors on Tumor Cells and Vascular Endothelial Cells in Human Breast Cancer Tissue. *Anticancer Res.* **1998**, *18* (1 A).

(118) Liu, Z.; Yang, L.; Xu, J.; Zhang, X.; Wang, B. Enhanced Expression and Clinical Significance of Chemokine Receptor CXCR2 in Hepatocellular Carcinoma. *J. Surg. Res.* **2011**, *166* (2).

(119) Han, L.; Jiang, B.; Wu, H.; Wang, X.; Tang, X.; Huang, J.; Zhu, J. High Expression of CXCR2 Is Associated with Tumorigenesis, Progression, and Prognosis of Laryngeal Squamous Cell Carcinoma. *Med. Oncol.* **2012**, *29* (4).

(120) Li, A.; Varney, M. L.; Singh, R. K. Expression of Interleukin 8 and Its Receptors in Human Colon Carcinoma Cells with Different Metastatic Potentials. *Clin. Cancer Res.* **2001**, *7* (10).

(121) Yang, G.; Rosen, D. G.; Liu, G.; Yang, F.; Guo, X.; Xiao, X.;

Xue, F.; Mercado-Uribe, I.; Huang, J.; Lin, S. H.; Mills, G. B.; Liu, J. CXCR2 Promotes Ovarian Cancer Growth through Dysregulated Cell Cycle, Diminished Apoptosis, and Enhanced Angiogenesis. *Clin. Cancer Res.* **2010**, *16* (15).

(122) Dong, Y. L.; Kabir, S. M.; Lee, E. S.; Son, D. S. CXCR2-Driven Ovarian Cancer Progression Involves Upregulation of Proinflammatory Chemokines by Potentiating NF-KB Activation via EGFR-Transactivated Akt Signaling. *PLoS One* **2013**, *8* (12).

(123) Bellocq, A.; Antoine, M.; Flahault, A.; Philippe, C.; Crestani, B.; Bernaudin, J. F.; Mayaud, C.; Milleron, B.; Baud, L.; Cadranel, J. Neutrophil Alveolitis in Bronchioloalveolar Carcinoma: Induction by Tumor-Derived Interleukin-8 and Relation to Clinical Outcome. *Am. J. Pathol.* **1998**, *152* (1).

(124) Tazzyman, S.; Barry, S. T.; Ashton, S.; Wood, P.; Blakey, D.; Lewis, C. E.; Murdoch, C. Inhibition of Neutrophil Infiltration into A549 Lung Tumors in Vitro and in Vivo Using a CXCR2-Specific Antagonist Is Associated with Reduced Tumor Growth. *Int. J. Cancer* **2011**, *129* (4).

(125) Murphy, C.; McGurk, M.; Pettigrew, J.; Santinelli, A.; Mazzucchelli, R.; Johnston, P. G.; Montironi, R.; Waugh, D. J. J. Nonapical and Cytoplasmic Expression of Interleukin-8, CXCR1, and CXCR2 Correlates with Cell Proliferation and Microvessel Density in Prostate Cancer. *Clin. Cancer Res.* **2005**, *11* (11).

(126) Halpern, J. L.; Kilbarger, A.; Lynch, C. C. Mesenchymal Stem Cells Promote Mammary Cancer Cell Migration in Vitro via the CXCR2 Receptor. *Cancer Lett.* **2011**, *308* (1).

(127) Wu, W.; Sun, C.; Xu, D.; Zhang, X.; Shen, W.; Lv, Y.; Ma, T. Expression of CXCR2 and Its Clinical Significance in Human Colorectal Cancer. *Int. J. Clin. Exp. Med.* **2015**, *8* (4).

(128) Ginestier, C.; Liu, S.; Diebel, M. E.; Korkaya, H.; Luo, M.; Brown, M.; Wicinski, J.; Cabaud, O.; Charafe-jauffret, E.; Birnbaum, D.; Guan, J.; Dontu, G.; Wicha, M. S. CXCR1 Blockade Selectively Targets Human Breast Cancer Stem Cells in Vivo and in Xenografts. **2010**, *120* (2), 485–497.

(129) Ning, Y.; Labonte, M. J.; Zhang, W.; Bohanes, P. O.; Gerger, A.; Yang, D.; Benhaim, L.; Paez, D.; Rosenberg, D. O.; Nagulapalli Venkata, K. C.; Louie, S. G.; Petasis, N. A.; Ladner, R. D.; Lenz, H. J. The CXCR2 Antagonist, SCH-527123, Shows Antitumor Activity and Sensitizes Cells to Oxaliplatin in Preclinical Colon Cancer Models. *Mol. Cancer Ther.* **2012**, *11* (6), 1353–1364.

(130) Singh, S.; Sadanandam, A.; Nannuru, K. C.; Varney, M. L.; Mayer-Ezel, R.; Bond, R.; Singh, R. K. Small-Molecule Antagonists for CXCR2 and CXCR1 Inhibit Human Melanoma Growth by Decreasing Tumor Cell Proliferation, Survival, and Angiogenesis Seema. *Bone* **2011**, *23* (1), 1–7.

(131) Prajapati, D. R.; Molczyk, C.; Purohit, A.; Saxena, S.; Sturgeon, R.; Dave, B. J.; Kumar, S.; Batra, S. K.; Singh, R. K. Small Molecule Antagonist of CXCR2 and CXCR1 Inhibits Tumor Growth, Angiogenesis, and Metastasis in Pancreatic Cancer. *Cancer Lett.* **2023**, *563*, 216185.

(132) Evans, T. R. J.; Basu, B.; Hubner, R.; Ma, Y. T.; Meyer, T.; Palmer, D. H.; Pinato, D. J. J.; Plummer, E. R.; Ross, P. J.; Samson, A.; Sarker, D.; Kendall, T.; Bellamy, C.; Reeves, H. L.; Thomson, F.; Lawless, C. A.; Stobo, J.; Sansom, O. J.; Mann, D. A.; Bird, T. G. A Phase I/II Study of the CXCR2 Inhibitor, AZD5069, in Combination with Durvalumab, in Patients (Pts) with Advanced Hepatocellular Carcinoma (HCC). *J. Clin. Oncol.* **2023**, *41* (4_suppl).

(133) White, J. R.; Lee, J. M.; Young, P. R.; Hertzberg, R. P.;

Jurewicz, A. J.; Chaikin, M. A.; Widdowson, K.; Foley, J. J.; Martin, L. D.; Griswold, D. E.; Sarau, H. M. Identification of a Potent, Selective Non-Peptide CXCR2 Antagonist That Inhibits Interleukin-8-Induced Neutrophil Migration. *J. Biol. Chem.* **1998**, *273* (17), 10095–10098.

(134) Widdowson, K. L.; Elliott, J. D.; Veber, D. F.; Nie, H.; Rutledge, M. C.; McCleland, B. W.; Xiang, J. N.; Jurewicz, A. J.; Hertzberg, R. P.; Foley, J. J.; Griswold, D. E.; Martin, L.; Lee, J. M.; White, J. R.; Sarau, H. M. Evaluation of Potent and Selective Small-Molecule Antagonists for the CXCR2 Chemokine Receptor. *J. Med. Chem.* **2004**, *47* (6), 1319–1321.

(135) Baxter, A.; Cooper, A.; Kinchin, E.; Moakes, K.; Unitt, J.; Wallace, A. Hit-to-Lead Studies: The Discovery of Potent, Orally Bioavailable Thiazolopyrimidine CXCR2 Receptor Antagonists. *Bioorganic Med. Chem. Lett.* **2006**, *16* (4), 960–963.

(136) Ho, K. K.; Auld, D. S.; Bohnstedt, A. C.; Conti, P.; Dokter, W.; Erickson, S.; Feng, D.; Inglese, J.; Kingsbury, C.; Kultgen, S. G.; Liu, R. Q.; Masterson, C. M.; Ohlmeyer, M.; Rong, Y.; Rooseboom, M.; Roughton, A.; Samama, P.; Smit, M. J.; Son, E.; van der Louw, J.; Vogel, G.; Webb, M.; Wijkmans, J.; You, M. Imidazolylpyrimidine Based CXCR2 Chemokine Receptor Antagonists. *Bioorganic Med. Chem. Lett.* **2006**, *16* (10), 2724–2728.

(137) Dwyer, M.; Yu, Y. CXCR2 Receptor Antagonists: A Medicinal Chemistry Perspective. *Curr. Top. Med. Chem.* **2014**, *14* (13).

(138) Bertini, R.; Allegretti, M.; Bizzarri, C.; Moriconi, A.; Locati, M.; Zampella, G.; Cervellera, M. N.; Di Cioccio, V.; Cesta, M. C.; Galliera, E.; Martinez, F. O.; Di Bitondo, R.; Troiani, G.; Sabbatini, V.; D'Anniballe, G.; Anacardio, R.; Cutrin, J. C.; Cavalieri, B.; Mainiero, F.; Strippoli, R.; Villa, P.; Di Girolamo,

M.; Martin, F.; Gentile, M.; Santoni, A.; Corda, D.; Poli, G.; Mantovani, A.; Ghezzi, P.; Colotta, F. Noncompetitive Allosteric Inhibitors of the Inflammatory Chemokine Receptors CXCR1 and CXCR2: Prevention of Reperfusion Injury. *Proc. Natl. Acad. Sci. U. S. A.* **2004**, *101* (32), 11791–11796.

(139) Salchow, K.; Bond, M. E.; Evans, S. C.; Press, N. J.; Charlton, S. J.; Hunt, P. A.; Bradley, M. E. A Common Intracellular Allosteric Binding Site for Antagonists of the CXCR2 Receptor: Research Paper. *Br. J. Pharmacol.* **2010**, *159* (7), 1429–1439.

(140) De Kruijf, P.; Lim, H. D.; Roumen, L.; Renjaän, V. A.; Zhao, J.; Webb, M. L.; Auld, D. S.; Wijkmans, J. C. H. M.; Zaman, G. J. R.; Smit, M. J.; De Graaf, C.; Leurs, R. Identification of a Novel Allosteric Binding Site in the CXCR2 Chemokine Receptor. *Mol. Pharmacol.* **2011**, *80* (6), 1108–1118.

(141) Bradley, M.; Bond, M.; Manini, J.; Brown, Z.; Charlton, S. SB265610 Is an Allosteric, Inverse Agonist at the Human CXCR2 Receptor. *Br. J. Pharmacol.* **2009**, *158* (1), 328–338.

(142) Oswald, C.; Rappas, M.; Kean, J.; Doré, A. S.; Errey, J. C.; Bennett, K.; Deflorian, F.; Christopher, J. A.; Jazayeri, A.; Mason, J. S.; Congreve, M.; Cooke, R. M.; Marshall, F. H. Intracellular Allosteric Antagonism of the CCR9 Receptor. *Nature* **2016**, *540* (7633), 462–465.

(143) Zheng, Y.; Ortiz Zacarias, N. V.; De Vries, H.; Won Han, G.; Gustavsson, M.; Dabros, M.; Zhao, C.; Cherney, R. J.; Carter, P.; Stamos, D.; Abagyan, R.; Cherezov, V.; Stevens, R. C.; IJzerman, A. P.; Heitman, L. H.; Tebben, A.; Kufareva, I.; Handel, T. M. Structure of CC Chemokine Receptor 2 with Orthosteric and Allosteric Antagonists. *Nature* **2016**, *540* (7633), 458–461.

(144) Liu, X.; Ahn, S.; Kahsai, A. W.; Meng, K. C.; Latorraca, N. R.; Pani, B.; Venkatakrishnan, A. J.; Masoudi, A.; Weis, W. I.;

Dror, R. O.; Chen, X.; Lefkowitz, R. J.; Kobilka, B. K. Mechanism of Intracellular Allosteric β 2 AR Antagonist Revealed by X-Ray Crystal Structure. *Nature* **2017**, *548* (7668), 480–484.

(145) Jaeger, K.; Bruenle, S.; Weinert, T.; Guba, W.; Muehle, J.; Miyazaki, T.; Weber, M.; Furrer, A.; Haenggi, N.; Tetaz, T.; Huang, C. Y.; Mattle, D.; Vonach, J. M.; Gast, A.; Kuglstatter, A.; Rudolph, M. G.; Nogly, P.; Benz, J.; Dawson, R. J. P.; Standfuss, J. Structural Basis for Allosteric Ligand Recognition in the Human CC Chemokine Receptor 7. *Cell* **2019**, *178* (5), 1222-1230.e10.

(146) Jiang, C.; Amaradhi, R.; Ganesh, T.; Dingledine, R. An Agonist Dependent Allosteric Antagonist of Prostaglandin EP2 Receptors. *ACS Chem. Neurosci.* **2020**, *11* (10), 1436–1446.

(147) May, L. T.; Leach, K.; Sexton, P. M.; Christopoulos, A. Allosteric Modulation of G Protein–Coupled Receptors. *Annu. Rev. Pharmacol. Toxicol.* **2007**, *47* (1), 1–51.

(148) Nomiyama, H.; Yoshie, O. Functional Roles of Evolutionary Conserved Motifs and Residues in Vertebrate Chemokine Receptors. *J. Leukoc. Biol.* **2015**, *97* (1), 39–47.

(149) Kalatskaya, I.; Schüssler, S.; Blaukat, A.; Müller-Esterl, W.; Jochum, M.; Proud, D.; Faussner, A. Mutation of Tyrosine in the Conserved NPXXY Sequence Leads to Constitutive Phosphorylation and Internalization, but Not Signaling, of the Human B 2 Bradykinin Receptor. *J. Biol. Chem.* **2004**, *279* (30), 31268–31276.

(150) Galés, C.; Kowalski-Chauvel, A.; Dufour, M. N.; Seva, C.; Moroder, L.; Pradayrol, L.; Vaysse, N.; Fourmy, D.; Silvente-Poirot, S. Mutation of Asn-391 within the Conserved NPXXY Motif of the Cholecystokinin B Receptor Abolishes G(q) Protein Activation without Affecting Its Association with the

Receptor. *J. Biol. Chem.* **2000**, *275* (23), 17321–17327.

(151) Koehl, A.; Hu, H.; Maeda, S.; Zhang, Y.; Qu, Q.; Paggi, J. M.; Latorraca, N. R.; Hilger, D.; Dawson, R.; Matile, H.; Schertler, G. F. X.; Granier, S.; Weis, W. I.; Dror, R. O.; Manglik, A.; Skiniotis, G.; Kobilka, B. K.; Draper-joyce, C. J.; Khoshouei, M.; Thal, D. M.; Liang, Y.; Nguyen, A. T. N.; Furness, S. G. B.; Venugopal, H.; Baltos, J.; Plitzko, J. M.; Danev, R.; Baumeister, W. Structure of the M-Opioid Receptor–G_i Protein Complex. *Nature* **2018**, *558* (7711).

(152) Draper-Joyce, C. J.; Khoshouei, M.; Thal, D. M.; Liang, Y. L.; Nguyen, A. T. N.; Furness, S. G. B.; Venugopal, H.; Baltos, J. A.; Plitzko, J. M.; Danev, R.; Baumeister, W.; May, L. T.; Wootten, D.; Sexton, P. M.; Glukhova, A.; Christopoulos, A. Structure of the Adenosine-Bound Human Adenosine A1 Receptor-Gi Complex. *Nature* **2018**, *558* (7711).

(153) Maeda, S.; Qu, Q.; Robertson, M. J.; Skiniotis, G.; Kobilka, B. K. Structures of the M1 and M2 Muscarinic Acetylcholine Receptor/G-Protein Complexes. *Science (80-.).* **2019**, *364* (6440).

(154) Xing, C.; Zhuang, Y.; Xu, T. H.; Feng, Z.; Zhou, X. E.; Chen, M.; Wang, L.; Meng, X.; Xue, Y.; Wang, J.; Liu, H.; McGuire, T. F.; Zhao, G.; Melcher, K.; Zhang, C.; Xu, H. E.; Xie, X. Q. Cryo-EM Structure of the Human Cannabinoid Receptor CB2-Gi Signaling Complex. *Cell* **2020**, *180* (4).

(155) Widdowson, K.; Nie, H.; Jurewicz, A. J.; Hertzberg, R. P.; Sarau, H. M.; Foley, J. J.; Lee, J.; White, J. R.; Veber, D. F. The Role of the Anionic Groups in the Receptor Binding of Interleukin-8 Antagonists. *Lett. Pept. Sci.* **1998**, *5* (2–3).

(156) Busch-Petersen, J. Small Molecule Antagonists of the CXCR2 and CXCR1 Chemokine Receptors as Therapeutic Agents for the Treatment of Inflammatory Diseases. *Curr. Top. Med.*

Chem. **2012**, *6* (13).

(157) Auten, R. L.; Richardson, R. M.; White, J. R.; Mason, S. N.; Vozzelli, M. A.; Whorton, M. H. Nonpeptide CXCR2 Antagonist Prevents Neutrophil Accumulation in Hyperoxia-Exposed Newborn Rats. *J. Pharmacol. Exp. Ther.* **2001**, *299* (1).

(158) Miller, B. E.; Smart, K.; Mistry, S.; Ambery, C. L.; Bloomer, J. C.; Connolly, P.; Sanderson, D.; Shreeves, T.; Smith, R.; Lazaar, A. L. The Pharmacokinetics of Conventional and Bioenhanced Tablet Formulations of Danirixin (GSK1325756) Following Oral Administration in Healthy, Elderly, Human Volunteers. *Eur. J. Drug Metab. Pharmacokinet.* **2014**, *39* (3).

(159) Bloomer, J. C.; Nash, M.; Webb, A.; Miller, B. E.; Lazaar, A. L.; Beaumont, C.; Guiney, W. J. Assessment of Potential Drug Interactions by Characterization of Human Drug Metabolism Pathways Using Non-Invasive Bile Sampling. *Br. J. Clin. Pharmacol.* **2013**, *75* (2).

(160) Podolin, P. L.; Bolognese, B. J.; Foley, J. J.; Schmidt, D. B.; Buckley, P. T.; Widdowson, K. L.; Jin, Q.; White, J. R.; Lee, J. M.; Goodman, R. B.; Hagen, T. R.; Kajikawa, O.; Marshall, L. A.; Hay, D. W. P.; Sarau, H. M. A Potent and Selective Nonpeptide Antagonist of CXCR2 Inhibits Acute and Chronic Models of Arthritis in the Rabbit. *J. Immunol.* **2002**, *169* (11), 6435–6444.

(161) P. Dwyer, M.; Biju, P. Discovery of 3,4-Diaminocyclobut-3-Ene-1,2-Dione-Based CXCR2 Receptor Antagonists for the Treatment of Inflammatory Disorders. *Curr. Top. Med. Chem.* **2010**, *10* (13).

(162) Merritt, J. R.; Rokosz, L. L.; Nelson, K. H.; Kaiser, B.; Wang, W.; Stauffer, T. M.; Ozgur, L. E.; Schilling, A.; Li, G.; Baldwin, J. J.; Taveras, A. G.; Dwyer, M. P.; Chao, J. Synthesis and

Structure-Activity Relationships of 3,4-Diaminocyclobut-3-Ene-1,2-Dione CXCR2 Antagonists. *Bioorganic Med. Chem. Lett.* **2006**, *16* (15), 4107–4110.

(163) Lai, G.; Merritt, J. R.; He, Z.; Feng, D.; Chao, J.; Czarniecki, M. F.; Rokosz, L. L.; Stauffer, T. M.; Rindgen, D.; Taveras, A. G. Synthesis and Structure-Activity Relationships of New Disubstituted Phenyl-Containing 3,4-Diamino-3-Cyclobutene-1,2-Diones as CXCR2 Receptor Antagonists. *Bioorganic Med. Chem. Lett.* **2008**, *18* (6), 1864–1868.

(164) Yu, Y.; Dwyer, M. P.; Chao, J.; Aki, C.; Chao, J.; Purakkattle, B.; Rindgen, D.; Bond, R.; Mayer-Ezel, R.; Jakway, J.; Qiu, H.; Hipkin, R. W.; Fossetta, J.; Gonsiorek, W.; Bian, H.; Fan, X.; Terminelli, C.; Fine, J.; Lundell, D.; Merritt, J. R.; He, Z.; Lai, G.; Wu, M.; Taveras, A. Synthesis and Structure-Activity Relationships of Heteroaryl Substituted-3,4-Diamino-3-Cyclobut-3-Ene-1,2-Dione CXCR2/CXCR1 Receptor Antagonists. *Bioorganic Med. Chem. Lett.* **2008**, *18* (4), 1318–1322.

(165) Aki, C.; Chao, J.; Ferreira, J. A.; Dwyer, M. P.; Yu, Y.; Chao, J.; Merritt, R. J.; Lai, G.; Wu, M.; Hipkin, R. W.; Fan, X.; Gonsiorek, W.; Fosseta, J.; Rindgen, D.; Fine, J.; Lundell, D.; Taveras, A. G.; Biju, P. Diaminocyclobutenediones as Potent and Orally Bioavailable CXCR2 Receptor Antagonists: SAR in the Phenolic Amide Region. *Bioorganic Med. Chem. Lett.* **2009**, *19* (15), 4446–4449.

(166) Dwyer, M. P.; Yu, Y.; Chao, J. J.; Aki, C.; Chao, J. J.; Biju, P.; Girijavallabhan, V.; Rindgen, D.; Bond, R.; Mayer-Ezel, R.; Jakway, J.; Hipkin, R. W.; Fossetta, J.; Gonsiorek, W.; Bian, H.; Fan, X.; Terminelli, C.; Fine, J.; Lundell, D.; Merritt, J. R.; Rokosz, L. L.; Kaiser, B.; Li, G.; Wang, W.; Stauffer, T.; Ozgur, L.; Baldwin, J.; Taveras, A. G. Discovery of 2-Hydroxy-

N-N-Dimethyl-3-{2-[[(R)-1-(5-Methylfuran-2-Yl)Propyl]Amino]-3,4-Dioxocyclobut-1-Enylamino}benzamide (SCH 527123): A Potent, Orally Bioavailable CXCR2/CXCR1 Receptor Antagonist. *J. Med. Chem.* **2006**, *49* (26), 7603–7606.

(167) Chapman, R. W.; Minnicozzi, M.; Celly, C. S.; Phillips, J. E.; Kung, T. T.; Hipkin, R. W.; Fan, X.; Rindgen, D.; Deno, G.; Bond, R.; Gonsiorek, W.; Billah, M. M.; Fine, J. S.; Hey, J. A. A Novel, Orally Active CXCR1/2 Receptor Antagonist, Sch527123, Inhibits Neutrophil Recruitment, Mucus Production, and Goblet Cell Hyperplasia in Animal Models of Pulmonary Inflammation. *J. Pharmacol. Exp. Ther.* **2007**, *322* (2), 486–493.

(168) Thatcher, T. H.; McHugh, N. A.; Egan, R. W.; Chapman, R. W.; Hey, J. A.; Turner, C. K.; Redonnet, M. R.; Seweryniak, K. E.; Sime, P. J.; Phipps, R. P. Role of CXCR2 in Cigarette Smoke-Induced Lung Inflammation. *Am. J. Physiol. - Lung Cell. Mol. Physiol.* **2005**, *289* (2 33-2).

(169) O., H.; S., K.; A., L.-S.; H., W.; P., S.; P., S.; M., T.; J., S. SCH527123, a Novel CXCR2 Antagonist, Inhibits Ozone-Induced Neutrophilia in Healthy Subjects. *European Respiratory Journal*. 2010.

(170) Holz, O.; Tal-Singer, R.; Kanniess, F.; Simpson, K. J.; Gibson, A.; Vessey, R. S. J.; Janicki, S.; Magnussen, H.; Jörres, R. A.; Richter, K. Validation of the Human Ozone Challenge Model as a Tool for Assessing Anti-Inflammatory Drugs in Early Development. *J. Clin. Pharmacol.* **2005**, *45* (5).

(171) Nair, P.; Gaga, M.; Zervas, E.; Alagha, K.; Hargreave, F. E.; O'Byrne, P. M.; Stryszak, P.; Gann, L.; Sadeh, J.; Chanez, P. Safety and Efficacy of a CXCR2 Antagonist in Patients with Severe Asthma and Sputum Neutrophils: A Randomized, Placebo-Controlled Clinical Trial. *Clin. Exp. Allergy* **2012**, *42*

(7).

(172) Seiberling, M.; Kamtchoua, T.; Stryszak, P.; Ma, X.; Langdon, R. B.; Khalilieh, S. Humoral Immunity and Delayed-Type Hypersensitivity in Healthy Subjects Treated for 30 Days with MK-7123, a Selective CXCR2 Antagonist. *Int. Immunopharmacol.* **2013**, *17* (2).

(173) Singh, S.; Sadanandam, A.; Nannuru, K. C.; Varney, M. L.; Mayer-Ezell, R.; Bond, R.; Singh, R. K. Small-Molecule Antagonists for CXCR2 and CXCR1 Inhibit Human Melanoma Growth by Decreasing Tumor Cell Proliferation, Survival, and Angiogenesis. *Clin. cancer Res. an Off. J. Am. Assoc. Cancer Res.* **2009**, *15* (7), 2380–2386.

(174) Varney, M. L.; Singh, S.; Li, A.; Mayer-Ezell, R.; Bond, R.; Singh, R. K. Small Molecule Antagonists for CXCR2 and CXCR1 Inhibit Human Colon Cancer Liver Metastases. *Cancer Lett.* **2011**, *300* (2).

(175) Chao, J.; Taveras, A. G.; Chao, J.; Aki, C.; Dwyer, M.; Yu, Y.; Purakkattle, B.; Rindgen, D.; Jakway, J.; Hipkin, W.; Fosetta, J.; Fan, X.; Lundell, D.; Fine, J.; Minnicozzi, M.; Phillips, J.; Merritt, J. R. C(4)-Alkyl Substituted Furanyl Cyclobutenediones as Potent, Orally Bioavailable CXCR2 and CXCR1 Receptor Antagonists. *Bioorganic Med. Chem. Lett.* **2007**, *17* (13).

(176) Min, S. H.; Wang, Y.; Gonsiorek, W.; Anilkumar, G.; Kozlowski, J.; Lundell, D.; Fine, J. S.; Grant, E. P. Pharmacological Targeting Reveals Distinct Roles for CXCR2/CXCR1 and CCR2 in a Mouse Model of Arthritis. *Biochem. Biophys. Res. Commun.* **2010**, *391* (1).

(177) Wang, Y.; Busch-Petersen, J.; Wang, F.; Ma, L.; Fu, W.; Kerns, J. K.; Jin, J.; Palovich, M. R.; Shen, J. K.; Burman, M.; Foley, J. J.; Schmidt, D. B.; Hunsberger, G. E.; Sarau, H. M.; Widdowson, K. L. 3-Arylamino-2H-1,2,4-Benzothiadiazin-5-Ol

1,1-Dioxides as Novel and Selective CXCR2 Antagonists. *Bioorganic Med. Chem. Lett.* **2007**, *17* (14).

(178) Nie, H.; Widdowson, K. L.; Palovich, M. R.; Fu, W.; Elliott, J. D.; Bryan, D. L.; Burman, M.; Schmidt, D. B.; Foley, J. J.; Sarau, H. M.; Busch-Petersen, J. N,N′-Diarylcyanoguanidines as Antagonists of the CXCR2 and CXCR1 Chemokine Receptors. *Bioorganic Med. Chem. Lett.* **2006**, *16* (21).

(179) Biju, P.; Taveras, A.; Yu, Y.; Zheng, J.; Chao, J.; Rindgen, D.; Jakway, J.; Hipkin, R. W.; Fossetta, J.; Fan, X.; Fine, J.; Qiu, H.; Merritt, J. R.; Baldwin, J. J. 3,4-Diamino-2,5-Thiadiazole-1-Oxides as Potent CXCR2/CXCR1 Antagonists. *Bioorganic Med. Chem. Lett.* **2008**, *18* (1).

(180) Biju, P.; Taveras, A. G.; Yu, Y.; Zheng, J.; Hipkin, R. W.; Fossetta, J.; Fan, X.; Fine, J.; Lundell, D. 3,4-Diamino-1,2,5-Thiadiazole as Potent and Selective CXCR2 Antagonists. *Bioorganic Med. Chem. Lett.* **2009**, *19* (5).

(181) Norman, P. Evidence on the Identity of the CXCR2 Antagonist AZD-5069. *Expert Opin. Ther. Pat.* **2013**, *23* (1).

(182) Nicholls, D. J.; Wiley, K.; Dainty, I.; MacIntosh, F.; Phillips, C.; Gaw, A.; Mårdh, C. K. Pharmacological Characterization of AZD5069, a Slowly Reversible CXC Chemokine Receptor 2 Antagonist. *J. Pharmacol. Exp. Ther.* **2015**, *353* (2), 340–350.

(183) Jurcevic, S.; Humfrey, C.; Uddin, M.; Warrington, S.; Larsson, B.; Keen, C. The Effect of a Selective CXCR2 Antagonist (AZD5069) on Human Blood Neutrophil Count and Innate Immune Functions. *Br. J. Clin. Pharmacol.* **2015**, *80* (6).

(184) Molfino, N. A. Drugs in Clinical Development for Chronic Obstructive Pulmonary Disease. *Respiration*. 2005.

(185) Fitzgerald, M. F.; Fox, J. C. Emerging Trends in the Therapy of COPD: Novel Anti-Inflammatory Agents in Clinical Development. *Drug Discovery Today*. 2007.

(186) Van Hoof, M.; Boon, K.; Van Loy, T.; Schols, D.; Dehaen, W.; De Jonghe, S. Identification of Novel Chemotypes as CXCR2 Antagonists via a Scaffold Hopping Approach from a Thiazolo[4,5-d]Pyrimidine. *Eur. J. Med. Chem.* **2022**, *235*.

(187) Bizzarri, C.; Pagliei, S.; Brandolini, L.; Mascagni, P.; Caselli, G.; Transidico, P.; Sozzani, S.; Bertini, R. Selective Inhibition of Interleukin-8-Induced Neutrophil Chemotaxis by Ketoprofen Isomers. *Biochem. Pharmacol.* **2001**, *61* (11).

(188) Allegretti, M.; Bertini, R.; Cesta, M. C.; Bizzarri, C.; Di Bitondo, R.; Di Cioccio, V.; Galliera, E.; Berdini, V.; Topai, A.; Zampella, G.; Russo, V.; Di Bello, N.; Nano, G.; Nicolini, L.; Locati, M.; Fantucci, P.; Florio, S.; Colotta, F. 2-Arylpropionic CXC Chemokine Receptor 1 (CXCR1) Ligands as Novel Noncompetitive CXCL8 Inhibitors. *J. Med. Chem.* **2005**, *48* (13).

(189) Casilli, F.; Bianchini, A.; Gloaguen, I.; Biordi, L.; Alesse, E.; Festuccia, C.; Cavalieri, B.; Strippoli, R.; Cervellera, M. N.; Bitondo, R. Di; Ferretti, E.; Mainiero, F.; Bizzarri, C.; Colotta, F.; Bertini, R. Inhibition of Interleukin-8 (CXCL8/IL-8) Responses by Repertaxin, a New Inhibitor of the Chemokine Receptors CXCR1 and CXCR2. *Biochem. Pharmacol.* **2005**, *69* (3).

(190) Cavalieri, B.; Mosca, M.; Ramadori, P.; Perrelli, M. G.; De Simone, L.; Colotta, F.; Bertini, R.; Poli, G.; Cutrìn, J. C. Neutrophil Recruitment in the Reperfused-Injured Rat Liver Was Effectively Attenuated by Repertaxin, a Novel Allosteric Non-Competitive Inhibitor of CXCL8 Receptors: A Therapeutic Approach for the Treatment of Post-Ischemic Hepatic Syndromes. *Int. J. Immunopathol. Pharmacol.* **2005**, *18* (3).

(191) Garau, A.; Bertini, R.; Colotta, F.; Casilli, F.; Bigini, P.; Cagnotto, A.; Mennini, T.; Ghezzi, P.; Villa, P. Neuroprotection

with the CXCL8 Inhibitor Repertaxin in Transient Brain Ischemia. *Cytokine* **2005**, *30* (3).

(192) Leitner, J. M.; Mayr, F. B.; Firbas, C.; Spiel, A. O.; Steinlechner, B.; Novellini, R.; Jilma, B. Reparixin, a Specific Interleukin-8 Inhibitor, Has No Effects on Inflammation during Endotoxemia. *Int. J. Immunopathol. Pharmacol.* **2007**, *20* (1).

(193) Cutshall, N. S.; Ursino, R.; Kucera, K. A.; Latham, J.; Ihle, N. C. Nicotinamide N-Oxides as CXCR2 Antagonists. *Bioorganic Med. Chem. Lett.* **2001**, *11* (14).

(194) Li, J. J.; Carson, K. G.; Trivedi, B. K.; Yue, W. S.; Ye, Q.; Glynn, R. A.; Miller, S. R.; Connor, D. T.; Roth, B. D.; Luly, J. R.; Low, J. E.; Heilig, D. J.; Yang, W.; Qin, S.; Hunt, S. Synthesis and Structure-Activity Relationship of 2-Amino-3-Heteroaryl-Quinoxalines as Non-Peptide, Small-Molecule Antagonists for Interleukin-8 Receptor. *Bioorganic Med. Chem.* **2003**, *11* (17).

(195) Baxter, A.; Bennion, C.; Bent, J.; Boden, K.; Brough, S.; Cooper, A.; Kinchin, E.; Kindon, N.; McInally, T.; Mortimore, M.; Roberts, B.; Unitt, J. Hit-to-Lead Studies: The Discovery of Potent, Orally Bioavailable Triazolethiol CXCR2 Receptor Antagonists. *Bioorganic Med. Chem. Lett.* **2003**, *13* (16).

(196) Dwyer, M. P.; Yu, Y. CXCR2 Modulators: A Patent Review (2009-2013). *Expert Opinion on Therapeutic Patents*. 2014.

(197) Busch-Petersen, J.; Wang, Y. Phenol-Containing Antagonists of the CXCR2 Receptor. *Expert Opinion on Therapeutic Patents*. 2008.

(198) Vernall, A. J.; Hill, S. J.; Kellam, B. The Evolving Small-Molecule Fluorescent-Conjugate Toolbox for Class A GPCRs. *Br. J. Pharmacol.* **2014**, *171* (5), 1073–1084.

(199) Soave, M.; Briddon, S. J.; Hill, S. J.; Stoddart, L. A. Fluorescent Ligands: Bringing Light to Emerging GPCR Paradigms. *Br. J.*

Pharmacol. **2020**, *177* (5), 978–991.

(200) Stoddart, L. A.; Kilpatrick, L. E.; Hill, S. J. NanoBRET Approaches to Study Ligand Binding to GPCRs and RTKs. *Trends Pharmacol. Sci.* **2018**, *39* (2), 136–147.

(201) Stoddart, L. A.; Johnstone, E. K. M.; Wheal, A. J.; Goulding, J.; Robers, M. B.; Machleidt, T.; Wood, K. V; Hill, S. J.; Pfleger, K. D. G. Application of BRET to Monitor Ligand Binding to GPCRs. *Nat. Methods* **2015**, *12* (7), 661–663.

(202) Soave, M.; Stoddart, L. A.; Brown, A.; Woolard, J.; Hill, S. J. Use of a New Proximity Assay (NanoBRET) to Investigate the Ligand-Binding Characteristics of Three Fluorescent Ligands to the Human B1-Adrenoceptor Expressed in HEK-293 Cells. *Pharmacol. Res. Perspect.* **2016**, *4* (5), 1–13.

(203) Farmer, J. P.; Mistry, S. N.; Laughton, C. A.; Holliday, N. D. Development of Fluorescent Peptide G Protein-Coupled Receptor Activation Biosensors for NanoBRET Characterization of Intracellular Allosteric Modulators. *FASEB J. Off. Publ. Fed. Am. Soc. Exp. Biol.* **2022**, *36* (11), e22576.

(204) Stoddart, L. A.; White, C. W.; Nguyen, K.; Hill, S. J.; Pfleger, K. D. G. Fluorescence- and Bioluminescence-Based Approaches to Study GPCR Ligand Binding. *Br. J. Pharmacol.* **2016**, *173* (20).

(205) Hazari, P. P.; Pandey, A.; Chaturvedi, S.; Mishra, A. K. New Trends and Current Status of Positron-Emission Tomography and Single-Photon-Emission Computerized Tomography Radioligands for Neuronal Serotonin Receptors and Serotonin Transporter. *Bioconjugate Chemistry*. 2017.

(206) Stoddart, L. A.; Kilpatrick, L. E.; Briddon, S. J.; Hill, S. J. Probing the Pharmacology of G Protein-Coupled Receptors with Fluorescent Ligands. *Neuropharmacology* **2015**, *98*, 48–57.

(207) Allen, M.; Reeves, J.; Mellor, G. High Throughput

Fluorescence Polarization: A Homogeneous Alternative to Radioligand Binding for Cell Surface Receptors. *J. Biomol. Screen.* **2000**, *5* (2), 63–69.

(208) Valeur, B. *Molecular Fluorescence - Principles and Applications*; 2001; Vol. 8.

(209) Stopel, M. H. W.; Blum, C.; Subramaniam, V. Excitation Spectra and Stokes Shift Measurements of Single Organic Dyes at Room Temperature. *J. Phys. Chem. Lett.* **2014**, *5* (18).

(210) Lakowicz, J. R. *Principles of Fluorescence Spectroscopy*; 2006.

(211) Shaner, N. C.; Steinbach, P. A.; Tsien, R. Y. A Guide to Choosing Fluorescent Proteins. *Nat. Methods* **2005**, *2* (12).

(212) Michel, M. C.; Wieland, T.; Tsujimoto, G. How Reliable Are G-Protein-Coupled Receptor Antibodies? *Naunyn-Schmiedeberg's Archives of Pharmacology*. 2009.

(213) Tian, H.; Furstenberg, A.; Huber, T. Labeling and Single-Molecule Methods to Monitor G Proteincoupled Receptor Dynamics. *Chemical Reviews*. 2017.

(214) Soave, M.; Stoddart, L. A.; White, C. W.; Kilpatrick, L. E.; Goulding, J.; Briddon, S. J.; Hill, S. J. Detection of Genome-Edited and Endogenously Expressed G Protein-Coupled Receptors. *FEBS Journal*. 2021.

(215) Goulding, J.; Mistry, S. J.; Soave, M.; Woolard, J.; Briddon, S. J.; White, C. W.; Kellam, B.; Hill, S. J. Subtype Selective Fluorescent Ligands Based on ICI 118,551 to Study the Human B2-Adrenoceptor in CRISPR/Cas9 Genome-Edited HEK293T Cells at Low Expression Levels. *Pharmacol. Res. Perspect.* **2021**, *9* (3).

(216) Cottet, M.; Faklaris, O.; Falco, A.; Trinquet, E.; Pin, J. P.; Mouillac, B.; Durroux, T. Fluorescent Ligands to Investigate GPCR Binding Properties and Oligomerization. In *Biochemical Society Transactions*; 2013; Vol. 41.

(217) Cottet, M.; Faklaris, O.; Zwier, J. M.; Trinquet, E.; Pin, J. P.; Durroux, T. Original Fluorescent Ligand-Based Assays Open New Perspectives in G-Protein Coupled Receptor Drug Screening. *Pharmaceuticals*. 2011.

(218) Briddon, S. J.; Kilpatrick, L. E.; Hill, S. J. Studying GPCR Pharmacology in Membrane Microdomains: Fluorescence Correlation Spectroscopy Comes of Age. *Trends in Pharmacological Sciences*. 2018.

(219) Hell, S. W. Toward Fluorescence Nanoscopy. *Nature Biotechnology*. 2003.

(220) Sydor, A. M.; Czymmek, K. J.; Puchner, E. M.; Mennella, V. Super-Resolution Microscopy: From Single Molecules to Supramolecular Assemblies. *Trends in Cell Biology*. 2015.

(221) Ciancetta, A.; Jacobson, K. A. Breakthrough in GPCR Crystallography and Its Impact on Computer-Aided Drug Design. In *Methods in Molecular Biology*; 2018; Vol. 1705.

(222) Sridharan, R.; Zuber, J.; Connelly, S. M.; Mathew, E.; Dumont, M. E. Fluorescent Approaches for Understanding Interactions of Ligands with G Protein Coupled Receptors. *Biochimica et Biophysica Acta - Biomembranes*. 2014.

(223) Alcobia, D. C.; Ziegler, A. I.; Kondrashov, A.; Comeo, E.; Mistry, S.; Kellam, B.; Chang, A.; Woolard, J.; Hill, S. J.; Sloan, E. K. Visualizing Ligand Binding to a GPCR In Vivo Using NanoBRET. *iScience* **2018**, *6*, 280–288.

(224) Baker, J. G.; Middleton, R.; Adams, L.; May, L. T.; Briddon, S. J.; Kellam, B.; Hill, S. J. Influence of Fluorophore and Linker Composition on the Pharmacology of Fluorescent Adenosine A1 Receptor Ligands. *Br. J. Pharmacol.* **2010**, *159* (4).

(225) Briddon, S. J.; Kellam, B.; Hill, S. J. Design and Use of Fluorescent Ligands to Study Ligand-Receptor Interactions in Single Living Cells. *Methods Mol. Biol.* **2011**, *746*.

(226) Vernall, A. J.; Stoddart, L. A.; Briddon, S. J.; Ng, H. W.; Laughton, C. A.; Doughty, S. W.; Hill, S. J.; Kellam, B. Conversion of a Non-Selective Adenosine Receptor Antagonist into A3-Selective High Affinity Fluorescent Probes Using Peptide-Based Linkers. *Org. Biomol. Chem.* **2013**, *11* (34), 5673–5682.

(227) Lavis, L. D.; Raines, R. T. Bright Building Blocks for Chemical Biology. *ACS Chem. Biol.* **2014**, *9* (4).

(228) Lavis, L. D.; Raines, R. T. Bright Ideas for Chemical Biology. *ACS Chemical Biology*. 2008.

(229) Hirabayashi, K.; Hanaoka, K.; Takayanagi, T.; Toki, Y.; Egawa, T.; Kamiya, M.; Komatsu, T.; Ueno, T.; Terai, T.; Yoshida, K.; Uchiyama, M.; Nagano, T.; Urano, Y. Analysis of Chemical Equilibrium of Silicon-Substituted Fluorescein and Its Application to Develop a Scaffold for Red Fluorescent Probes. *Anal. Chem.* **2015**, *87* (17), 9061–9069.

(230) Grimm, J. B.; Muthusamy, A. K.; Liang, Y.; Brown, T. A.; Lemon, W. C.; Patel, R.; Lu, R.; Macklin, J. J.; Keller, P. J.; Ji, N.; Lavis, L. D. A General Method to Fine-Tune Fluorophores for Live-Cell and in Vivo Imaging. *Nat. Methods* **2017**, *14* (10).

(231) Grimm, J. B.; English, B. P.; Chen, J.; Slaughter, J. P.; Zhang, Z.; Revyakin, A.; Patel, R.; Macklin, J. J.; Normanno, D.; Singer, R. H.; Lionnet, T.; Lavis, L. D. A General Method to Improve Fluorophores for Live-Cell and Single-Molecule Microscopy. *Nat. Methods* **2015**, *12* (3).

(232) Loudet, A.; Burgess, K. BODIPY Dyes and Their Derivatives: Syntheses and Spectroscopic Properties. *Chemical Reviews*. 2007.

(233) Karolin, J.; Johansson, L. B. A.; Strandberg, L.; Ny, T. Fluorescence and Absorption Spectroscopic Properties of Dipyrrometheneboron Difluoride (BODIPY) Derivatives in

Liquids, Lipid Membranes, and Proteins. *J. Am. Chem. Soc.* **1994**, *116* (17).

(234) Ulrich, G.; Ziessel, R.; Harriman, A. The Chemistry of Fluorescent Bodipy Dyes: Versatility Unsurpassed. *Angew. Chem. Int. Ed. Engl.* **2008**, *47* (7), 1184–1201.

(235) Esteoulle, L.; Daubeuf, F.; Collot, M.; Riché, S.; Durroux, T.; Brasse, D.; Marchand, P.; Karpenko, I. A.; Klymchenko, A. S.; Bonnet, D. A Near-Infrared Fluorogenic Dimer Enables Background-Free Imaging of Endogenous GPCRs in Living Mice. *Chem. Sci.* **2020**, *11* (26).

(236) Pansare, V. J.; Hejazi, S.; Faenza, W. J.; Prud'Homme, R. K. Review of Long-Wavelength Optical and NIR Imaging Materials: Contrast Agents, Fluorophores, and Multifunctional Nano Carriers. *Chemistry of Materials*. 2012.

(237) Ma, Z.; Du, L.; Li, M. Toward Fluorescent Probes for G-Protein-Coupled Receptors (GPCRs). *J. Med. Chem.* **2014**, *57* (20).

(238) Huber, M. E.; Toy, L.; Schmidt, M. F.; Vogt, H.; Budzinski, J.; Wiefhoff, M. F. J.; Merten, N.; Kostenis, E.; Weikert, D.; Schiedel, M. A Chemical Biology Toolbox Targeting the Intracellular Binding Site of CCR9: Fluorescent Ligands, New Drug Leads and PROTACs. *Angew. Chemie - Int. Ed.* **2022**, *61* (12), 1–5.

(239) Toy, L.; Huber, M. E.; Schmidt, M. F.; Weikert, D.; Schiedel, M. Fluorescent Ligands Targeting the Intracellular Allosteric Binding Site of the Chemokine Receptor CCR2. *ACS Chem. Biol.* **2022**, *17* (8), 2142–2152.

(240) Huber, M. E.; Wurnig, S.; Toy, L.; Weiler, C.; Merten, N.; Kostenis, E.; Hansen, F. K.; Schiedel, M. Fluorescent Ligands Enable Target Engagement Studies for the Intracellular Allosteric Binding Site of the Chemokine Receptor CXCR2. *J.*

Med. Chem. **2023**, *66* (14), 9916–9933.

(241) Huber, M. E.; Toy, L.; Schmidt, M. F.; Weikert, D.; Schiedel, M. Small Molecule Tools to Study Cellular Target Engagement for the Intracellular Allosteric Binding Site of GPCRs. *Chemistry* **2023**, *29* (1), e202202565.

(242) Alvaro, G.; Martelli, G.; Savoia, D. Regioselective and Diastereoselective Addition of Organometallic Reagents to (S)-N-[(2-Pyridyl)Methylene]-O-(Trimethylsilyl)Valinol. Synthesis of (S)-1-(2-Pyridyl)Alkylamines. *J. Chem. Soc. - Perkin Trans. 1* **1998**, No. 4, 775–783.

(243) Blume, F.; Albeiruty, M. H.; Deska, J. Alkylative Amination of Biogenic Furans through Imine-to-Azaallyl Anion Umpolung. *Synth.* **2015**, *47* (14), 2093–2099.

(244) Dixon, A. S.; Schwinn, M. K.; Hall, M. P.; Zimmerman, K.; Otto, P.; Lubben, T. H.; Butler, B. L.; Binkowski, B. F.; MacHleidt, T.; Kirkland, T. A.; Wood, M. G.; Eggers, C. T.; Encell, L. P.; Wood, K. V. NanoLuc Complementation Reporter Optimized for Accurate Measurement of Protein Interactions in Cells. *ACS Chem. Biol.* **2016**, *11* (2), 400–408.

(245) Wan, Q.; Okashah, N.; Inoue, A.; Nehme, R.; Carpenter, B.; Tate, C. G.; Lambert, N. A. Mini G Protein Probes for Active G Protein– Coupled Receptors (GPCRs) in Live Cells. *J. Biol. Chem.* **2018**, *293* (19), 7466–7473.

(246) Nehmea, R.; Carpenter, B.; Singhal, A.; Strege, A.; Edwards, P. C.; White, C. F.; Du, H.; Grisshammer, R.; Tate, C. G. Mini-G Proteins: Novel Tools for Studying GPCRs in Their Active Conformation. *PLoS One* **2017**, *12* (4), 1–26.

(247) Hall, M. P.; Unch, J.; Binkowski, B. F.; Valley, M. P.; Butler, B. L.; Wood, M. G.; Otto, P.; Zimmerman, K.; Vidugiris, G.; MacHleidt, T.; Robers, M. B.; Benink, H. A.; Eggers, C. T.; Slater, M. R.; Meisenheimer, P. L.; Klaubert, D. H.; Fan, F.;

Encell, L. P.; Wood, K. V. Engineered Luciferase Reporter from a Deep Sea Shrimp Utilizing a Novel Imidazopyrazinone Substrate. *ACS Chem. Biol.* **2012**, *7* (11), 1848–1857.

(248) Slack, R. J.; Hall, D. A. Development of Operational Models of Receptor Activation Including Constitutive Receptor Activity and Their Use to Determine the Efficacy of the Chemokine CCL17 at the CC Chemokine Receptor CCR4. *Br. J. Pharmacol.* **2012**, *166* (6).

(249) Szczepek, M.; Beyrière, F.; Hofmann, K. P.; Elgeti, M.; Kazmin, R.; Rose, A.; Bartl, F. J.; Von Stetten, D.; Heck, M.; Sommer, M. E.; Hildebrand, P. W.; Scheerer, P. Crystal Structure of a Common GPCR-Binding Interface for G Protein and Arrestin. *Nat. Commun.* **2014**, *5*.

(250) Sykes, D. A.; Jain, P.; Charlton, S. J. Investigating the Influence of Tracer Kinetics on Competition-Kinetic Association Binding Assays: Identifying the Optimal Conditions for Assessing the Kinetics of Low-Affinity Compounds. *Mol. Pharmacol.* **2019**, *96* (3), 378–392.

(251) Sykes, D. A.; Stoddart, L. A.; Kilpatrick, L. E.; Hill, S. J. Binding Kinetics of Ligands Acting at GPCRs. *Mol. Cell. Endocrinol.* **2019**, *485* (October 2018), 9–19.

(252) Burley, S. K.; Berman, H. M.; Bhikadiya, C.; Bi, C.; Chen, L.; Costanzo, L. Di; Christie, C.; Duarte, J. M.; Dutta, S.; Feng, Z.; Ghosh, S.; Goodsell, D. S.; Green, R. K.; Guranovic, V.; Guzenko, D.; Hudson, B. P.; Liang, Y.; Lowe, R.; Peisach, E.; Periskova, I.; Randle, C.; Rose, A.; Sekharan, M.; Shao, C.; Tao, Y. P.; Valasatava, Y.; Voigt, M.; Westbrook, J.; Young, J.; Zardecki, C.; Zhuravleva, M.; Kurisu, G.; Nakamura, H.; Kengaku, Y.; Cho, H.; Sato, J.; Kim, J. Y.; Ikegawa, Y.; Nakagawa, A.; Yamashita, R.; Kudou, T.; Bekker, G. J.; Suzuki, H.; Iwata, T.; Yokochi, M.; Kobayashi, N.; Fujiwara, T.;

Velankar, S.; Kleywegt, G. J.; Anyango, S.; Armstrong, D. R.; Berrisford, J. M.; Conroy, M. J.; Dana, J. M.; Deshpande, M.; Gane, P.; Gáborová, R.; Gupta, D.; Gutmanas, A.; Koča, J.; Mak, L.; Mir, S.; Mukhopadhyay, A.; Nadzirin, N.; Nair, S.; Patwardhan, A.; Paysan-Lafosse, T.; Pravda, L.; Salih, O.; Sehnal, D.; Varadi, M.; Vařeková, R.; Markley, J. L.; Hoch, J. C.; Romero, P. R.; Baskaran, K.; Maziuk, D.; Ulrich, E. L.; Wedell, J. R.; Yao, H.; Livny, M.; Ioannidis, Y. E. Protein Data Bank: The Single Global Archive for 3D Macromolecular Structure Data. *Nucleic Acids Res.* **2019**, *47* (D1), D520–D528.

(253) Berman, H.; Henrick, K.; Nakamura, H.; Markley, J. L. The Worldwide Protein Data Bank (WwPDB): Ensuring a Single, Uniform Archive of PDB Data. *Nucleic Acids Res.* **2007**, *35* (SUPPL. 1), 2006–2008.

(254) Bernstein, F. C.; Koetzle, T. F.; Williams, G. J. B.; Meyer Jr., E. F.; Brice, M. D.; Rodgers, J. R.; Kennard, O.; Shimanouchi, T.; Tasumi, M. The Protein D a t a Bank : A Computer-Based Archival File for Macromolecular Structures The Protein Data Bank Is a Computer-Based Archival File for Macromolecular (a) Scope. *J. Mol. Biol.* **1977**, *112* (3), 535–542.

(255) Kaczanowski, S.; Zielenkiewicz, P. Why Similar Protein Sequences Encode Similar Three-Dimensional Structures? *Theor. Chem. Acc.* **2010**, *125* (3–6), 643–650.

(256) Muhammed, M. T.; Aki-Yalcin, E. Homology Modeling in Drug Discovery: Overview, Current Applications, and Future Perspectives. *Chem. Biol. Drug Des.* **2019**, *93* (1), 12–20.

(257) Vyas, V. K.; Ukawala, R. D.; Ghate, M.; Chintha, C. Homology Modeling a Fast Tool for Drug Discovery: Current Perspectives. *Indian J. Pharm. Sci.* **2012**, *74* (1), 1–17.

(258) Chothia, C.; Lesk, A. M. The Relation between the Divergence of Sequence and Structure in Proteins. *EMBO J.* **1986**, *5* (4),

823–826.

(259) Mart, M. A.; Stuart, A. C.; Roberto, S.; Melo, F.; Andrej, S. Comparative Protein Structure Modeling of Genes and Genomes. *Annu. Rev. Biophys. Biomol. Struct.* **2000**, *29*, 291–325.

(260) Werner, T.; Morris, M. B.; Dastmalchi, S.; Church, W. B. Structural Modelling and Dynamics of Proteins for Insights into Drug Interactions. *Adv. Drug Deliv. Rev.* **2012**, *64* (4), 323–343.

(261) Fiser, A. Template-Based Protein Structure Modeling. *Methods Mol. Biol.* **2010**, *673*, 73–94.

(262) Illergård, K.; Ardell, D. H.; Elofsson, A. Structure Is Three to Ten Times More Conserved than Sequence - A Study of Structural Response in Protein Cores. *Proteins Struct. Funct. Bioinforma.* **2009**, *77* (3), 499–508.

(263) Varadi, M.; Anyango, S.; Deshpande, M.; Nair, S.; Natassia, C.; Yordanova, G.; Yuan, D.; Stroe, O.; Wood, G.; Laydon, A.; Zídek, A.; Green, T.; Tunyasuvunakool, K.; Petersen, S.; Jumper, J.; Clancy, E.; Green, R.; Vora, A.; Lutfi, M.; Figurnov, M.; Cowie, A.; Hobbs, N.; Kohli, P.; Kleywegt, G.; Birney, E.; Hassabis, D.; Velankar, S. AlphaFold Protein Structure Database: Massively Expanding the Structural Coverage of Protein-Sequence Space with High-Accuracy Models. *Nucleic Acids Res.* **2022**, *50* (D1).

(264) Jumper, J.; Evans, R.; Pritzel, A.; Green, T.; Figurnov, M.; Ronneberger, O.; Tunyasuvunakool, K.; Bates, R.; Žídek, A.; Potapenko, A.; Bridgland, A.; Meyer, C.; Kohl, S. A. A.; Ballard, A. J.; Cowie, A.; Romera-Paredes, B.; Nikolov, S.; Jain, R.; Adler, J.; Back, T.; Petersen, S.; Reiman, D.; Clancy, E.; Zielinski, M.; Steinegger, M.; Pacholska, M.; Berghammer, T.; Bodenstein, S.; Silver, D.; Vinyals, O.; Senior, A. W.; Kavukcuoglu, K.; Kohli, P.; Hassabis, D. Highly Accurate

Protein Structure Prediction with AlphaFold. *Nature* **2021**, *596* (7873).

(265) Rose, P. W.; Prlić, A.; Altunkaya, A.; Bi, C.; Bradley, A. R.; Christie, C. H.; Costanzo, L. Di; Duarte, J. M.; Dutta, S.; Feng, Z.; Green, R. K.; Goodsell, D. S.; Hudson, B.; Kalro, T.; Lowe, R.; Peisach, E.; Randle, C.; Rose, A. S.; Shao, C.; Tao, Y.-P.; Valasatava, Y.; Voigt, M.; Westbrook, J. D.; Woo, J.; Yang, H.; Young, J. Y.; Zardecki, C.; Berman, H. M.; Burley, S. K. The RCSB Protein Data Bank: Integrative View of Protein, Gene and 3D Structural Information. *Nucleic Acids Res.* **2017**, *45* (D1), D271–D281.

(266) Altschul, S. F.; Madden, T. L.; Schäffer, A. A.; Zhang, J.; Zhang, Z.; Miller, W.; Lipman, D. J. Gapped BLAST and PSI-BLAST: A New Generation of Protein Database Search Programs. *Nucleic Acids Res.* **1997**, *25* (17), 3389–3402.

(267) Altschul, S. F.; Gish, W.; Miller, W.; Myers, E. W.; Lipman, D. J. Basic Local Alignment Search Tool. *J. Mol. Biol.* **1990**, *215* (3), 403–410.

(268) Fernandez-Fuentes, N.; Rai, B. K.; Madrid-Aliste, C. J.; Eduardo Fajardo, J.; Fiser, A. Comparative Protein Structure Modeling by Combining Multiple Templates and Optimizing Sequence-to-Structure Alignments. *Bioinformatics* **2007**, *23* (19), 2558–2565.

(269) Fernandez-Fuentes, N.; Madrid-Aliste, C. J.; Rai, B. K.; Fajardo, J. E.; Fiser, A. M4T: A Comparative Protein Structure Modeling Server. *Nucleic Acids Res.* **2007**, *35* (SUPPL.2), 363–368.

(270) Dalton, J. A. R.; Jackson, R. M. An Evaluation of Automated Homology Modelling Methods at Low Target-Template Sequence Similarity. *Bioinformatics* **2007**, *23* (15), 1901–1908.

(271) Bates, P. A.; Kelley, L. A.; MacCallum, R. M.; Sternberg, M. J.

E. Enhancement of Protein Modeling by Human Intervention in Applying the Automatic Programs 3D-JIGSAW and 3D-PSSM. *Proteins Struct. Funct. Genet.* **2001**, *45* (June 2001), 39–46.

(272) Bordoli, L.; Kiefer, F.; Arnold, K.; Benkert, P.; Battey, J.; Schwede, T. Protein Structure Homology Modeling Using SWISS-MODEL Workspace. *Nat. Protoc.* **2009**, *4* (1), 1–13.

(273) Kiefer, F.; Arnold, K.; Künzli, M.; Bordoli, L.; Schwede, T. The SWISS-MODEL Repository and Associated Resources. *Nucleic Acids Res.* **2009**, *37* (SUPPL. 1), 387–392.

(274) Laskowski, R. A.; MacArthur, M. W.; Moss, D. S.; Thornton, J. M. PROCHECK: A Program to Check the Stereochemical Quality of Protein Structures. *J. Appl. Crystallogr.* **1993**, *26* (2), 283–291.

(275) Davis, I. W.; Leaver-Fay, A.; Chen, V. B.; Block, J. N.; Kapral, G. J.; Wang, X.; Murray, L. W.; Arendall, W. B.; Snoeyink, J.; Richardson, J. S.; Richardson, D. C. MolProbity: All-Atom Contacts and Structure Validation for Proteins and Nucleic Acids. *Nucleic Acids Res.* **2007**, *35* (SUPPL.2), 375–383.

(276) Hooft, R. W.; Vriend, G.; Sander, C.; Abola, E. E. Errors in Protein Structures. *Nature*. England May 1996, p 272.

(277) Schwede, T.; Kopp, J.; Guex, N.; Peitsch, M. C. SWISS-MODEL: An Automated Protein Homology-Modeling Server. *Nucleic Acids Res.* **2003**, *31* (13), 3381–3385.

(278) Jacobson, M. P.; Pincus, D. L.; Rapp, C. S.; Day, T. J. F.; Honig, B.; Shaw, D. E.; Friesner, R. A. A Hierarchical Approach to All-Atom Protein Loop Prediction. *Proteins Struct. Funct. Genet.* **2004**, *55* (2), 351–367.

(279) Abramyan, T. M.; Snyder, J. A.; Thyparambil, A. A.; Stuart, S. J.; Latour, R. A. Cluster Analysis of Molecular Simulation Trajectories for Systems Where Both Conformation and Orientation of the Sampled States Are Important. *J. Comput.*

Chem. **2016**, *37* (21), 1973–1982.

(280) Xu, R.; Wunsch, D. Survey of Clustering Algorithms. *IEEE Trans. Neural Networks* **2005**, *16* (3), 645–678.

(281) Jain, A. K.; Murty, M. N.; Flynn, P. J. Data Clustering: A Review. *ACM Comput. Surv.* **1999**, *31* (3), 264–323.

(282) Nikolaev, D. M.; Shtyrov, A. A.; Panov, M. S.; Jamal, A.; Chakchir, O. B.; Kochemirovsky, V. A.; Olivucci, M.; Ryazantsev, M. N. A Comparative Study of Modern Homology Modeling Algorithms for Rhodopsin Structure Prediction. *ACS Omega* **2018**, *3* (7), 7555–7566.

(283) Kufareva, I.; Abagyan, R. Methods of Protein Structure Comparison. *Methods Mol. Biol.* **2012**, *857*, 231–257.

(284) Friesner, R. A.; Banks, J. L.; Murphy, R. B.; Halgren, T. A.; Klicic, J. J.; Mainz, D. T.; Repasky, M. P.; Knoll, E. H.; Shelley, M.; Perry, J. K.; Shaw, D. E.; Francis, P.; Shenkin, P. S. Glide: A New Approach for Rapid, Accurate Docking and Scoring. 1. Method and Assessment of Docking Accuracy. *J. Med. Chem.* **2004**, *47* (7), 1739–1749.

(285) Halgren, T. A.; Murphy, R. B.; Friesner, R. A.; Beard, H. S.; Frye, L. L.; Pollard, W. T.; Banks, J. L. Glide: A New Approach for Rapid, Accurate Docking and Scoring. 2. Enrichment Factors in Database Screening. *J. Med. Chem.* **2004**, *47* (7), 1750–1759.

(286) Friesner, R. A.; Murphy, R. B.; Repasky, M. P.; Frye, L. L.; Greenwood, J. R.; Halgren, T. A.; Sanschagrin, P. C.; Mainz, D. T. Extra Precision Glide: Docking and Scoring Incorporating a Model of Hydrophobic Enclosure for Protein-Ligand Complexes. *J. Med. Chem.* **2006**, *49* (21), 6177–6196.

(287) Ian Storer, R.; Aciro, C.; Jones, L. H. Squaramides: Physical Properties, Synthesis and Applications. *Chem. Soc. Rev.* **2011**, *40* (5), 2330–2346.

(288) J. P. Clayden; N. Greeves; S. Warren. *Organic Chemistry*; 2012.

(289) Kim, Y.; Cramer, C. J.; Truhlar, D. G. Steric Effects and Solvent Effects on SN2 Reactions. *J. Phys. Chem. A* **2009**, *113* (32).

(290) Banjoko, O.; Babatunde, I. A. Catalytic Effects of Hydrogen-Bond Acceptor Solvent on Nucleophilic Aromatic Substitution Reactions in Non-Polar Aprotic Solvent: Reactions of Phenyl 2,4,6-Trinitrophenyl Ether with Amines in Benzene-Acetonitrile Mixtures. *Tetrahedron* **2005**, *61* (33).

(291) El Guesmi, N.; Berionni, G.; Asghar, B. H. Electronic and Solvent Effects on Kinetics of SNAr Substitution Reactions of Substituted Anilines with 2,6-Bis(Trifluoromethanesulfonyl)-4-Nitroanisole in MeOH-Me2SO Mixtures of Varying Composition: One Reaction with Two Mechanistic Pathways. *Monatshefte fur Chemie* **2013**, *144* (10).

(292) Leas, D. A.; Wu, J.; Ezell, E. L.; Garrison, J. C.; Vennerstrom, J. L.; Dong, Y. Formation of 2-Imino Benzo[e]-1,3-Oxazin-4-Ones from Reactions of Salicylic Acids and Anilines with HATU: Mechanistic and Synthetic Studies. *ACS Omega* **2018**, *3* (1).

(293) Liang, X.; Haynes, B. S.; Montoya, A. Acid-Catalyzed Ring Opening of Furan in Aqueous Solution. *Energy and Fuels* **2018**, *32* (4).

(294) Tom, N. J.; Simon, W. M.; Frost, H. N.; Ewing, M. Deprotection of a Primary Boc Group under Basic Conditions. *Tetrahedron Lett.* **2004**, *45* (5), 905–906.

(295) López-Soria, J. M.; Pérez, S. J.; Hernández, J. N.; Ramírez, M. A.; Martín, V. S.; Padrón, J. I. A Practical, Catalytic and Selective Deprotection of a Boc Group in N,N′-Diprotected Amines Using Iron(III)-Catalysis. *RSC Adv.* **2015**, *5* (9), 6647–6651.

(296) Giri, R. S.; Roy, S.; Dolai, G.; Manne, S. R.; Mandal, B. FeCl 3 -Mediated Boc Deprotection: Mild Facile Boc-Chemistry in Solution and on Resin . *ChemistrySelect* **2020**, *5* (6), 2050–2056.

(297) Evans, V.; Mahon, M. F.; Webster, R. L. A Mild, Copper-Catalysed Amide Deprotection Strategy: Use of Tert-Butyl as a Protecting Group. *Tetrahedron* **2014**, *70* (41), 7593–7597.

(298) Li, B.; Li, R.; Dorff, P.; McWilliams, J. C.; Guinn, R. M.; Guinness, S. M.; Han, L.; Wang, K.; Yu, S. Deprotection of N-Boc Groups under Continuous-Flow High-Temperature Conditions. *J. Org. Chem.* **2019**, *84* (8), 4846–4855.

(299) Wang, G.; Li, C.; Li, J.; Jia, X. Catalyst-Free Water-Mediated N-Boc Deprotection. *Tetrahedron Lett.* **2009**, *50* (13), 1438–1440.

(300) Cheraiet, Z.; Hessainia, S.; Ouarna, S.; Berredjem, M.; Aouf, N. E. A Simple and Eco-Sustainable Method for the O-Boc Protection/Deprotection of Various Phenolic Structures under Water-Mediated/Catalyst-Free Conditions. *Green Chem. Lett. Rev.* **2013**, *6* (3), 211–216.

(301) Margetić, D.; Đud, M. Solvent-Free Mechanochemical Deprotection of N-Boc Group. *Int. J. Org. Chem.* **2017**, *07* (02), 140–144.

(302) Wang, J.; Liang, Y. L.; Qu, J. Boiling Water-Catalyzed Neutral and Selective N-Boc Deprotection. *Chem. Commun.* **2009**, No. 34, 5144–5146.

(303) Dandepally, S. R.; Williams, A. L. Microwave-Assisted N-Boc Deprotection under Mild Basic Conditions Using K3PO4·H2O in MeOH. *Tetrahedron Lett.* **2009**, *50* (9), 1071–1074.

(304) Dijon, N. C.; Nesheva, D. N.; Holliday, N. D. Luciferase Complementation Approaches to Measure GPCR Signaling Kinetics and Bias. In *G Protein-Coupled Receptor Screening*

Assays: Methods and Protocols; Martins, S. A. M., Prazeres, D. M. F., Eds.; Springer US: New York, NY, 2021; pp 249–274.

(305) Stoddart, L. A.; Johnstone, E. K. M.; Wheal, A. J.; Goulding, J.; Robers, M. B.; Machleidt, T.; Wood, K. V; Hill, S. J.; Pfleger, K. D. G. Application of BRET to Monitor Ligand Binding to GPCRs Europe PMC Funders Group. *Nat Methods* **2015**, *12* (7), 661–663.

(306) Lohse, M. J.; Nuber, S.; Hoffmann, C. Fluorescence/Bioluminescence Resonance Energy Transfer Techniques to Study g-Protein-Coupled Receptor Activation and Signaling. *Pharmacological Reviews*. 2012.

(307) Machleidt, T.; Woodroofe, C. C.; Schwinn, M. K.; Méndez, J.; Robers, M. B.; Zimmerman, K.; Otto, P.; Daniels, D. L.; Kirkland, T. A.; Wood, K. V. NanoBRET-A Novel BRET Platform for the Analysis of Protein-Protein Interactions. *ACS Chem. Biol.* **2015**, *10* (8), 1797–1804.

(308) Dale, N. C.; Johnstone, E. K. M.; White, C. W.; Pfleger, K. D. G. NanoBRET: The Bright Future of Proximity-Based Assays. *Front. Bioeng. Biotechnol.* **2019**, *7* (MAR), 1–13.

(309) Salahpour, A.; Espinoza, S.; Masri, B.; Lam, V.; Barak, L. S.; Gainetdinov, R. R. BRET Biosensors to Study GPCR Biology, Pharmacology, and Signal Transduction. *Frontiers in Endocrinology*. 2012.

(310) Borroto-Escuela, D. O.; Flajolet, M.; Agnati, L. F.; Greengard, P.; Fuxe, K. Bioluminescence Resonance Energy Transfer Methods to Study G Protein-Coupled Receptor-Receptor Tyrosine Kinase Heteroreceptor Complexes. In *Methods in Cell Biology*; 2013; Vol. 117.

(311) Kilpatrick, L. E.; Friedman-Ohana, R.; Alcobia, D. C.; Riching, K.; Peach, C. J.; Wheal, A. J.; Briddon, S. J.; Robers, M. B.; Zimmerman, K.; Machleidt, T.; Wood, K. V.; Woolard, J.; Hill,

S. J. Real-Time Analysis of the Binding of Fluorescent VEGF165a to VEGFR2 in Living Cells: Effect of Receptor Tyrosine Kinase Inhibitors and Fate of Internalized Agonist-Receptor Complexes. *Biochem. Pharmacol.* **2017**, *136*.

(312) Kok, Z. Y.; Stoddart, L. A.; Mistry, S. J.; Mocking, T. A. M.; Vischer, H. F.; Leurs, R.; Hill, S. J.; Mistry, S. N.; Kellam, B. Optimization of Peptide Linker-Based Fluorescent Ligands for the Histamine H1Receptor. *J. Med. Chem.* **2022**, *65* (12).

(313) Comeo, E.; Trinh, P.; Nguyen, A. T.; Nowell, C. J.; Kindon, N. D.; Soave, M.; Stoddart, L. A.; White, J. M.; Hill, S. J.; Kellam, B.; Halls, M. L.; May, L. T.; Scammells, P. J. Development and Application of Subtype-Selective Fluorescent Antagonists for the Study of the Human Adenosine A1Receptor in Living Cells. *J. Med. Chem.* **2021**, *64* (10).

(314) Busch-Petersen, J.; Carpenter, D. C.; Burman, M.; Foley, J.; Hunsberger, G. E.; Kilian, D. J.; Salmon, M.; Mayer, R. J.; Yonchuk, J. G.; Tal-Singer, R. Danirixin: A Reversible and Selective Antagonist of the CXC Chemokine Receptor 2. *J. Pharmacol. Exp. Ther.* **2017**, *362* (2), 338–346.

(315) Pan, A. C.; Borhani, D. W.; Dror, R. O.; Shaw, D. E. Molecular Determinants of Drug-Receptor Binding Kinetics. *Drug Discov. Today* **2013**, *18* (13–14), 667–673.

(316) Fedosova, N. U.; Champeil, P.; Esmann, M. Nucleotide Binding to Na,K-ATPase: The Role of Electrostatic Interactions. *Biochemistry* **2002**, *41* (4).

(317) Schmidtke, P.; Javier Luque, F.; Murray, J. B.; Barril, X. Shielded Hydrogen Bonds as Structural Determinants of Binding Kinetics: Application in Drug Design. *J. Am. Chem. Soc.* **2011**, *133* (46).

(318) Tautermann, C. S. Impact, Determination and Prediction of Drug–Receptor Residence Times for GPCRs. *Current Opinion*

in Pharmacology. 2016.

(319) Miller, D. C.; Lunn, G.; Jones, P.; Sabnis, Y.; Davies, N. L.; Driscoll, P. Investigation of the Effect of Molecular Properties on the Binding Kinetics of a Ligand to Its Biological Target. *Medchemcomm* **2012**, *3* (4).

(320) Sykes, D. A.; Parry, C.; Reilly, J.; Wright, P.; Fairhurst, R. A.; Charlton, S. J. Observed Drug-Receptor Association Rates Are Governed by Membrane Affinity: The Importance of Establishing "Micro-Pharmacokinetic/Pharmacodynamic Relationships" at the B2-Adrenoceptor. *Mol. Pharmacol.* **2014**, *85* (4).

(321) Hoare, S. R. J. The Problems of Applying Classical Pharmacology Analysis to Modern In Vitro Drug Discovery Assays: Slow Binding Kinetics and High Target Concentration. *SLAS Discovery*. 2021.

(322) Dowling, M. R.; Charlton, S. J. Quantifying the Association and Dissociation Rates of Unlabelled Antagonists at the Muscarinic M 3 Receptor. *Br. J. Pharmacol.* **2006**, *148* (7).

(323) De Boer, P.; Anghelescu, I.-G.; Van Iersel, T.; Schmidt, M.; Palumbo, J. M.; Van Nueten, L. Fast Off-Rate Dopamine D2 Receptor Antagonists Are Well Tolerated by Healthy Subjects despite High Levels of Central Dopamine D2 Receptor Occupancy. *Biol. Psychiatry* **2010**, *67* (9).

(324) Jacqmin, P.; McFadyen, L.; Wade, J. R. A Receptor Theory-Based Semimechanistic PD Model for the CCR5 Noncompetitive Antagonist Maraviroc. *Br. J. Clin. Pharmacol.* **2008**, *65* (SUPPL. 1).

(325) Copeland, R. A.; Pompliano, D. L.; Meek, T. D. Drug-Target Residence Time and Its Implications for Lead Optimization. *Nat. Rev. Drug Discov.* **2006**, *5* (9).

(326) de Witte, W. E. A.; Danhof, M.; van der Graaf, P. H.; de Lange,

E. C. M. The Implications of Target Saturation for the Use of Drug-Target Residence Time. *Nature Reviews Drug Discovery*. 2018.

(327) Herenbrink, C. K.; Sykes, D. A.; Donthamsetti, P.; Canals, M.; Coudrat, T.; Shonberg, J.; Scammells, P. J.; Capuano, B.; Sexton, P. M.; Charlton, S. J.; Javitch, J. A.; Christopoulos, A.; Lane, J. R. The Role of Kinetic Context in Apparent Biased Agonism at GPCRs. *Nat. Commun.* **2016**, *7*, 1–14.

(328) Hothersall, J. D.; Brown, A. J.; Dale, I.; Rawlins, P. Can Residence Time Offer a Useful Strategy to Target Agonist Drugs for Sustained GPCR Responses? *Drug Discovery Today*. 2016.

(329) Copeland, R. A. The Dynamics of Drug-Target Interactions: Drug-Target Residence Time and Its Impact on Efficacy and Safety. *Expert Opinion on Drug Discovery*. 2010.

(330) Sykes, D. A.; Dowling, M. R.; Leighton-Davies, J.; Kent, T. C.; Fawcett, L.; Renard, E.; Trifilieff, A.; Charlton, S. J. The Influence of Receptor Kinetics on the Onset and Duration of Action and the Therapeutic Index of NVA237 and Tiotropium. *J. Pharmacol. Exp. Ther.* **2012**, *343* (2).

(331) Trifilieff, A.; Ethell, B. T.; Sykes, D. A.; Watson, K. J.; Collingwood, S.; Charlton, S. J.; Kent, T. C. Comparing the Cardiovascular Therapeutic Indices of Glycopyrronium and Tiotropium in an Integrated Rat Pharmacokinetic, Pharmacodynamic and Safety Model. *Toxicol. Appl. Pharmacol.* **2015**, *287* (1).

(332) Murray, I. A.; Patterson, A. D.; Perdew, G. H. Aryl Hydrocarbon Receptor Ligands in Cancer: Friend and Foe. *Nature Reviews Cancer*. 2014.

(333) Scimemi, A.; Beato, M. Determining the Neurotransmitter Concentration Profile at Active Synapses. *Molecular*

Neurobiology. 2009.

(334) Vauquelin, G. Effects of Target Binding Kinetics on in Vivo Drug Efficacy: Koff , Kon and Rebinding. *Br. J. Pharmacol.* **2016**, *173* (15), 2319–2334.

(335) Sykes, D. A.; Moore, H.; Stott, L.; Holliday, N.; Javitch, J. A.; Robert Lane, J.; Charlton, S. J. Extrapyramidal Side Effects of Antipsychotics Are Linked to Their Association Kinetics at Dopamine D 2 Receptors. *Nat. Commun.* **2017**, *8* (1), 1–11.

(336) Motulsky, H. J.; Mahan, L. C. The Kinetics of Competitive Radioligand Binding Predicted by the Law of Mass Action. *Mol. Pharmacol.* **1984**, *25* (1).

(337) Ferré, G.; Gomes, A. A. S.; Louet, M.; Damian, M.; Bisch, P. M.; Saurel, O.; Floquet, N.; Milon, A.; Banères, J. L. Sodium Is a Negative Allosteric Regulator of the Ghrelin Receptor. *Cell Rep.* **2023**, *42* (4).

(338) Katritch, V.; Fenalti, G.; Abola, E. E.; Roth, B. L.; Cherezov, V.; Stevens, R. C. Allosteric Sodium in Class A GPCR Signaling. *Trends Biochem. Sci.* **2014**, *39* (5), 233–244.

(339) Devree, B. T.; Mahoney, J. P.; Vélez-ruiz, G. A.; Rasmussen, S. G. F.; Kuszak, A. J.; Edwald, E.; Fung, J.; Manglik, A.; Masureel, M.; Du, Y.; Matt, R. A.; Pardon, E.; Steyaert, J.; Kobilka, B. K.; Roger, K. Allosteric Coupling from G Protein to the Agonist Binding Pocket in GPCRs. **2017**, *535* (7610), 182–186.

(340) Janíčková, H.; Rudajev, V.; Zimčík, P.; Jakubík, J.; Tanila, H.; El-Fakahany, E. E.; Doležal, V. Uncoupling of M1 Muscarinic Receptor/G-Protein Interaction by Amyloid B1-42. *Neuropharmacology* **2013**, *67*, 272–283.

(341) Hubner, H.; Schellhorn, T.; Gienger, M.; Schaab, C.; Kaindl, J.; Leeb, L.; Clark, T.; Moller, D.; Gmeiner, P. Structure-Guided Development of Heterodimer-Selective GPCR Ligands. *Nat.*

Commun. **2016**, *7*.

(342) Hoare, S. R. J.; Tewson, P. H.; Quinn, A. M.; Hughes, T. E.; Bridge, L. J. Analyzing Kinetic Signaling Data for G-Protein-Coupled Receptors. *Sci. Rep.* **2020**, *10* (1), 1–23.

(343) Trainor, K.; Palumbo, J. A.; MacKenzie, D. W. S.; Meiering, E. M. Temperature Dependence of NMR Chemical Shifts: Tracking and Statistical Analysis. *Protein Sci.* **2020**, *29* (1), 306–314.

(344) Raiford, D. S.; Fisk, C. L.; Becker, E. D. Calibration of Methanol and Ethylene Glycol Nuclear Magnetic Resonance Thermometers. *Anal. Chem.* **1979**, *51* (12).

(345) Baxter, N. J.; Williamson, M. P. Temperature Dependence of 1H Chemical Shifts in Proteins. *J. Biomol. NMR* **1997**, *9* (4), 359–369.

(346) Cierpicki, T.; Otlewski, J. Amide Proton Temperature Coefficients as Hydrogen Bond Indicators in Proteins. *J. Biomol. NMR* **2001**, *21* (3), 249–261.

(347) Cierpicki, T.; Zhukov, I.; Byrd, R. A.; Otlewski, J. Hydrogen Bonds in Human Ubiquitin Reflected in Temperature Coefficients of Amide Protons. *J. Magn. Reson.* **2002**, *157* (2), 178–180.

(348) Edison, A. S.; Schroeder, F. C. NMR - Small Molecules and Analysis of Complex Mixtures. In *Comprehensive Natural Products II: Chemistry and Biology*; 2010; Vol. 9.

(349) Fattori, J.; Rodrigues, F. H. S.; Pontes, J. G. M.; Paula Espíndola, A.; Tasic, L. Monitoring Intermolecular and Intramolecular Interactions by NMR Spectroscopy. In *Applications of NMR Spectroscopy*; 2015; Vol. 3.

(350) Wright, S. C.; Lukasheva, V.; Gouill, C. Le; Kobayashi, H.; Breton, B.; Mailhot-Larouche, S.; Blondel-Tepaz, É.; Vieira, N. A.; Costa-Neto, C.; Héroux, M.; Lambert, N. A.; Parreiras-E-

Silva, L. T.; Bouvier, M. BRET-Based Effector Membrane Translocation Assay Monitors GPCR-Promoted and Endocytosis-Mediated Gqactivation at Early Endosomes. *Proc. Natl. Acad. Sci. U. S. A.* **2021**, *118* (20).

(351) Stoddart, L. A.; Kindon, N. D.; Otun, O.; Harwood, C. R.; Patera, F.; Veprintsev, D. B.; Woolard, J.; Briddon, S. J.; Franks, H. A.; Hill, S. J.; Kellam, B. Ligand-Directed Covalent Labelling of a GPCR with a Fluorescent Tag in Live Cells. *Commun. Biol.* **2020**, *3* (1).

(352) Dixon, A. S.; Schwinn, M. K.; Hall, M. P.; Zimmerman, K.; Otto, P.; Lubben, T. H.; Butler, B. L.; Binkowski, B. F.; MacHleidt, T.; Kirkland, T. A.; Wood, M. G.; Eggers, C. T.; Encell, L. P.; Wood, K. V. NanoLuc Complementation Reporter Optimized for Accurate Measurement of Protein Interactions in Cells. *ACS Chem. Biol.* **2016**, *11* (2), 400–408.

(353) Hoare, B. L.; Kaur, A.; Harwood, C. R.; Dijon, N. C.; Holliday, N. D.; Sykes, D. A.; Veprintsev, D. B. Measurement of Non-Purified GPCR Thermostability Using the Homogenous ThermoBRET Assay. *bioRxiv* **2020**, 2020.08.05.237982.

(354) Kilpatrick, L. E.; Briddon, S. J.; Holliday, N. D. Fluorescence Correlation Spectroscopy, Combined with Bimolecular Fluorescence Complementation, Reveals the Effects of β-Arrestin Complexes and Endocytic Targeting on the Membrane Mobility of Neuropeptide Y Receptors. *Biochim. Biophys. Acta - Mol. Cell Res.* **2012**, *1823* (6).

(355) Case, D. A.; Aktulga, H. M.; Belfon, K.; Ben-Shalom, I. Y.; Berryman, J. T.; Brozell, S. R.; Cerutti, D. S.; Cheatham III, T. E.; Cisneros, G. A.; Cruzeiro, V. W. D.; Darden, T. A.; Forouzesh, N.; Giambaşu, G.; Giese, T.; Gilson, M. K.; Gohlke, H.; Goetz, A. W.; Harris, J.; Izadi, S.; Kollman, P. A. Amber 2023. *Univ. California, San Fr.*

(356) Fox, T.; Kollman, P. A. Application of the RESP Methodology in the Parametrization of Organic Solvents. *J. Phys. Chem. B* **1998**, *102* (41), 8070–8079.

(357) McGibbon, R. T.; Beauchamp, K. A.; Harrigan, M. P.; Klein, C.; Swails, J. M.; Hernández, C. X.; Schwantes, C. R.; Wang, L. P.; Lane, T. J.; Pande, V. S. MDTraj: A Modern Open Library for the Analysis of Molecular Dynamics Trajectories. *Biophys. J.* **2015**, *109* (8), 1528–1532.